JAERI-M
89-034

BWR LOCA SIMULATION TEST (RUN 992) IN ROSA-III PROGRAM FOR A 10% MAIN STEAM LINE BREAK WITH ECCS DOUBLE FAILURES

March 1989

Mitsuhiro SUZUKI, Yoshinari ANODA, Hiroshige KUMAMARU
Hideo NAKAMURA, Taisuke YONOMOTO, Yasuo KOIZUMI
Hideo MURATA and Kanji TASAKA

日本原子力研究所
Japan Atomic Energy Research Institute

JAERI-Mレポートは、日本原子力研究所が不定期に公刊している研究報告書です。
入手の問合わせは、日本原子力研究所技術情報部情報資料課（〒319－11茨城県那珂郡東海村）あて、お申しこしください。なお、このほかに財団法人原子力弘済会資料センター（〒319-11茨城県那珂郡東海村日本原子力研究所内）で複写による実費頒布をおこなっております。

JAERI-M reports are issued irregularly.
Inquiries about availability of the reports should be addressed to Information Division, Department of Technical Information, Japan Atomic Energy Research Institute, Tokai-mura, Naka-gun, Ibaraki-ken 319-11, Japan.

編集兼発行　日本原子力研究所
印　　刷　日立高速印刷株式会社

BWR LOCA SIMULATION TEST (RUN 992) IN ROSA-III PROGRAM FOR A 10% MAIN STEAM LINE BREAK WITH ECCS DOUBLE FAILURES

Mitsuhiro SUZUKI, Yoshinari ANODA, Hiroshige KUMAMARU
Hideo NAKAMURA, Taisuke YONOMOTO, Yasuo KOIZUMI
Hideo MURATA and Kanji TASAKA

Department of Nuclear Safety Research
Tokai Research Establishment
Japan Atomic Energy Research Institute
Tokai-mura, Naka-gun, Ibaraki-ken

(Received Fabruary 20, 1989)

A loss-of-coolant accident (LOCA) caused by pipe rupture at the high pressure core spray (HPCS) line is equivallent to a LOCA with double failures on the emergency core cooling systems (ECCSs) in a boiling water reactor (BWR) system by assuming single failure on another ECCS. This report presents the ROSA-III experimental results of RUN 992, which simulates a 10% main steam line break (MSLB) LOCA with double failure assumption on the HPCS and the low pressure core spray (LPCS) systems. The ROSA-III test facility simulates a BWR system with volumetric scale of 1/424 and has the principal systems, i.e., four half-length electrically-heated fuel bundles, two active recirculation loops, four types of ECCSs, and steam and feedwater systems.

The report clarifies effectiveness of ECCS even for this double failure assumption in a 10% MSLB LOCA and also clarifies effects of the automatic depressurization system (ADS) on core cooling. In addition to these, mass balance and mass distribution in the system were investigated to clarify the core cooling condition in the small MSLB LOCA test.

Keywords: BWR, LOCA, Steam Line Break, ECCS, ADS, ROSA-III Program
Integral Test, Core Cooling, Mass Inventory, Data Report

ＲＯＳＡ－Ⅲ計画における，ＥＣＣＳ二重故障を仮定したＢＷＲ　ＬＯＣＡ模擬10％主蒸気管破断実験，ＲＵＮ992

日本原子力研究所東海研究所原子炉安全工学部
鈴木　光弘・安濃田良成・熊丸　博滋・中村　秀夫
与能本泰介・小泉　安郎・村田　秀男・田坂　完二

（1989年2月20日受理）

本報告は，高圧及び低圧炉心スプレイ系（ＨＰＣＳ，ＬＰＣＳ）の二重故障を仮定した10％主蒸気管破断（ＭＳＬＢ）冷却材喪失事故（ＬＯＣＡ）を模擬するＲＯＳＡ－Ⅲ実験，ＲＵＮ992の結果をまとめたものである。ＲＯＳＡ－Ⅲ試験装置はＢＷＲを体積比1/424で模擬しており，１／２長さの電気加熱燃料棒集合体４体と，２つの再循環ループ，４つのＥＣＣＳ及び蒸気・給水系統の主要機器を備えている。

本報では，10％ＭＳＬＢ　ＬＯＣＡ時においては二重故障を仮定してもＥＣＣＳは有効であり，自動減圧系（ＡＤＳ）の炉心冷却効果もあることを明らかにしている。また，この主蒸気管小破断ＬＯＣＡ実験における炉心冷却条件を明らかにするために，系内のマスバランスと保有水量分布について検討を行った。

東海研究所：〒319-11 茨城県那珂郡東海村白方字白根２－４

Contents

目　　次

ABBREVIATIONS

ADS	Automatic Depressurization System
AT	Air Tank
AV	Air Actuation Valve
(2)B	(2) inches Pipe of Schedule 80
BN	Boron Nitride
BWR	Boiling Water Reactor
CA	Chromel-Alumel
CCFL	Counter Current Flow Limiting
CHV	Check Valve
CP	Conductivity Prove
CV	Control Valve
CWT	Cooling Water Tank
D	Differential Pressure
d	Diameter
DF	Density of Fluid
DL(+100)	Elevation (+100 mm) from the Bottom of PV
ECCS	Emergency Core Cooling System
ESF	Engineered Safety Features
EX	Heat Exchanger
F	Flow Rate
Fig.	Figure
FS	Full Scale
FW	Feedwater
FWLF	Feedwater Line Flashing
FWP	Feedwater Pump
FWT	Feedwater Tank
HPCS	High Pressure Core Spray
HPCSP	High Pressure Core Spray Pump
HPCST	High Pressure Core Spary Tank
HPWP	High Pressure Water Pump
ID	Inner diameter
INC 600	Inconel 600
JP	Jet Pump
K	Kelvin

kg	Kilogram
kPa	Kilopascal
kW	Kilowatt
L	Liter
LB	Liquid Level in Channel Box
LBWR	Large Boiling Water Reactor
LL	Liquid Level
LOCA	Loss-of-Coolant Accident
LOCE	Loss-of-Coolant Experiment
LP	Lower Plenum
LPCI	Low Pressure Coolant Injection
LPCIP	Low Pressure Coolant Injection Pump
LPCIT	Low Pressure Coolant Injection Tank
LPCS	Low Pressure Core Spray
LPCSP	Low Pressure Core Spary Pump
LPCST	Low Pressure Core Spary Tank
LPF	Lower Plenum Flashing
LTP	Lower Tie Plate
M	Momentum Flux
m	Meter
mm	Milimeter
MLHR	Maximum Linear Heat Rate
MPa	Megapascal
MRP	Main Recirculation Pump
MSIV	Main Steam Isolation Valve
MSL	Main Steam Line
MW	Megawatt
N	Rotation Speed
OR	Orifice
P	Pressure
	Power
PCT	Peak Cladding Temperature
PV	Pressure Vessel
PWT	Pure Water Tank
QOBV	Quick Opening Blowdown Valve
QSV	Quick Shut-off Valve
RCN	Rapid Condencer
ROSA	Rig of Safety Assessment

rpm	Revolution per Minute
S	Signal
s	Second
Sch	Schedule
SUS	Stainless Steel
T	Temperature
T/C	Thermocouple
TC	Temperature of Fluid
TF	Temperature of Fuel
TS	Temperature of Structure Material
UTP	Upper Tie Plate
V	Valve
VF	Void Fraction
W	Watt
WL	Water Level
WSP	Water Supply Pump

List of Tables

List of Figures

1. Introduction

The rig-of-safety assessment (ROSA)-III program[1]-[3] was initiated in 1976 to study the thermal-hydraulic behavior of a boiling water reactor (BWR)[4] during a postulated loss-of-coolant accident (LOCA) with actuation of emergency core cooling system (ECCS), and to provide the data base to evaluate the predictability of computer codes developed for reactor safety analysis. To meet these objectives various kinds of ROSA-III tests have been performed and those results have been published.[5]-[51] The ROSA-III test facility simulates a 1/424 volumetrically scaled primary system of a 3800 MW BWR/6(251-848) with an electrically-heated core, break simulators, steam and feedwater systems, instrumentations and scaled ECCSs.

In the ROSA-III program, six tests of main steam line break (MSLB) LOCA have been performed (references 1, 14, 34, 35, 41 and 46). Clarified are the characteristic features of MSLB LOCA phenomena, such as the high downcomer water level, typical pressure responses and average void fraction in downcomer related with the total steam discharge flow area. However, mass balance and mass distribution in the system are not quantitatively clarified in these studies.

In addition to these, a 10% MSLB LOCA test (RUN 992) was performed in the ROSA-III program to simulate a high pressure core spray (HPCS) line break with an assumption of low pressure core spray (LPCS) failure. This test was initially studied on a view point of break location effects by comparing with the test results of a jet pump drive line break (RUN 991) and two recirculation line breaks (RUNs 927 and 930).[15] However, this test can be studied on another view point of ECCS double failure and ADS actuation trip on L1 level in a 10% MSLB LOCA test.

The primary objectives of this report are to experimentally clarify (1) characteristic features on mass balance and mass distribution related with major events and (2) effects of ECCS double failure and delayed ADS actuation on core cooling conditions in small MSLB LOCA phenomena. The ROSA-III test facility and instrumentations are described in chapters 2 and 3, respectively. Test conditions and test procedures are described in chapter 4. Chapter 5 shows test results of pressure responses, mass balance, mass distribution, and core cooling conditions related with the major events.

2. ROSA-III Test Facility

The ROSA-III test facility[3] is a volumetrically scaled (1/424) BWR system with an electrically-heated core designed to study the response of the primary system, the core and the ECCS during the postulated LOCA. The test facility is instrumented such that various thermal-hydraulic parameters during the test can be investigated.

The test facility consists of four subsystems;(a) the pressure vessel (PV), (b) the steam line and the feedwater line, (c) the recirculation loops and (d) the ECCSs. Figures 2.1, 2.2 and 2.3 illustrate configuration of the test facility, the PV internals and the piping schematics, respectively. Table 2.1 compares the major dimensions of the ROSA-III test facility to the corresponding dimensions of the reference BWR system.

The ROSA-III PV includes various components simulating the internal structures of the reactor pressure vessel (RPV) in the BWR system as shown in Fig.2.4. Interior of the vessel is divided into the core, core bypass, lower plenum, guide tube simulator, upper plenum, downcomer annulus, steam separator, steam dome and the steam dryer simulator.

The core consists of four simulated fuel assemblies of half length and a control rod simulator. Each fuel assembly contains 62 heater rods (Fig.2.5) and 2 water rods spaced in a 8 x 8 square array and supported by spacers and tie plates. The heater rod is heated electrically with chopped cosine power distribution along the axis as shown in Fig.2.6. The effective heated length is 1880 mm, one half of the active length of a BWR fuel rod. A high electric power was supplied to the heater rod bundle "A" with radial peaking factor of 1.4 and another power was supplied to the other three bundles "B", "C" and "D" with radial peaking factor of 1.0. The total electric power is limitted below 4.24 MW. The heater rods in each bundle are divided into three groups with respect to heat generation rate as shown in Fig.2.7. The local peaking factors in each group are 1.1, 1.0 and 0.875. The orifice plate with 44 mm I.D. in one assembly is inserted at each core inlet to control the core inlet flow.

The steam line is connected to top of the steam dome (see Fig.4.1). In the first steam line branch, an orifice and a quick opening air valve (AV165) are installed for break simulation. A control valve (CV-130) is installed in the third branch to control the steam dome pressure in the steady state before the test initiation and to maintain the pressure above

6.7 MPa after the break time as a pressure control system (PCS). The second branch has an air valve (AV169) and an orifice to simulate the automatic depressurization system (ADS). The MSIV closure is simulated by quickly closing an air valve (AV168) in the third line on trip signals. (These valve characteristics and trip conditions are shown in chapter 4.) The feedwater is supplied from the feedwater tank (FWT) through the feedwater line (Fig.2.8) and the feedwater sparger (Fig.2.9) below the steam separator.

Figure 2.10 shows the whole piping schematics including the main steam line (MSL) and two equal recirculation loops. The break is initiated by quickly opening the break valve (break unit B) and the AV-165 in the first branch. The break unit A is isolated both from the steam line and the recirculation loops in this test.

The ROSA-III test facility is furnished with all kinds of the ECCS's available in the BWR system, i.e., the high pressure core spray (HPCS), low pressure core spray (LPCS), low pressure coolant injection (LPCI), and ADS. The HPCS and LPCS spray cooling water onto the core. The LPCI injects cooling water into the core bypass. Each ECCS consists of a pump, a tank, pipings, and a control system. The water level in the upper downcomer, which is measured by a differential pressure transducer between EL 3.90 m (above the PV bottom) and EL 6.04 m, is used for the actuation trips of MSIV and ECCSs (see chapter 4).

3. Instrumentation

Instrumentation of the ROSA-III system is designed to obtain thermal-hydraulic data during a simulated BWR LOCA. Table 3.1 summarizes the instrumentations for No.4 assembly. The measurement list and the core instrumentation list are presented in Appendix I. Instrumentation locations are shown in Fig.3.1 through Fig.3.10. Typical measured parameters in the ROSA-III are pressure, differential pressure, flow rate, electric power, pump speed, fluid and metal temperatures, collapsed liquid level, two-phase mixture level, fluid density, trip signals and so on.

Pressure and differential pressure transducers are two-wire, direct-current type which convert diaphragm displacement to electric capacitance. The pressure lead pipes are either the standard single, cylindrical pipes used in conjunction with condensate pots, or dual concentric cylinders capable of the circulation of cooling water to prevent flashing of the fluid.

The flow rate is measured by four types of instrumentations, i.e., turbine flow meter, orifice type flow meter, Venturi type flow meter and momentum flux measurement equipment depending on the fluid condition and measuring location. The turbine flow meter is used for subcooled water flow such as ECCS injection flow and feedwater flow. The orifice type flow meter is used for both flows, one is steam line flow including ADS flow and another one is jet pump discharge flow in the blowdown loop. The Venturi flow meters are used for recirculation flows in both loops and jet pump discharge flow in the intact loop.

The temperatures of the fluid, structural material and heater rod cladding are measured with chromel-alumel thermocouple (CA T/C) of 1.6, 1.0 or 0.5 mmφ. The thermocouples for heater rod cladding temperatures are imbedded at the surface of the cladding as shown in Fig.2.5. There are seven (maximum) thermocouples for one heater rod along the axial direction.

Liquid levels are measured by either differential pressure transducers, described above or needle type electric conductivity probes (CP) developed in the ROSA-III program. The probes are distributed along the vessel height to detect the existence of water or vapor at different levels.

The electric power supplied to the heater rods is controlled to follow the predetermined power curve with function of time and measured by a fast response electric power meters. The pump speed is measured by a

pulse generator integral of the pump. Trip signals such as selected valve positions and pump coastdown initiations and so on, are detected in order to record the exact actuation times of trip signals.

The fluid density in the pipe is measured by means of gamma densitometers. Preliminary studies indicate that two-beam and three-beam densitometers should be used to determine the flow regime. Figures 3.7 and 3.8 show the beam directions of the three-beam and two-beam gamma densitometers, respectively. The gamma-ray source is ^{137}Cs and the detector is a water cooled NaI(Tl) scintillation counter. The momentum flux is measured by a drag disk as shown in Fig.3.9. The combination of signals from a drag disk and a gamma densitometer is used to determine the two-phase flow rate as shown in Fig.3.10.

The data acquisition system (DATAC 2000B, Iwasaki Tsushinki Co.) scans all of signals with the frequency up to 30 Hz. The data recorded on magnetic tape were processed by the FACOM M200 system computer at JAERI by off-line control. After evaluation, for example by comparing the initial and final pressure values with standard values for the density and momentum flux data, the data were reprocessed using the correct conversion factors as determined from the consistency examination. Reduction of mass balance and mass distribution in the system is shown in chapter 5. More detailed information on the data processing procedure is available in reference (52).

4. Test Conditions and Procedure for RUN 992

The test RUN 992 is a type of 10% main steam line (see Fig.4.1) break LOCA test with double failures on HPCS and LPCS diesel generators. The break orifice area (Fig.4.2, 10.1 mm I.D.) simulates a 1/424 scaled BWR HPCS line flow area and it corresponds to 15% of the scaled BWR recirculation line piping flow area. The test conditions are shown in Table 4.1. The measured initial test conditions were; steam dome pressure of 7.36 MPa, total core power of 3.966 MW (44% of 1/424 scaled BWR rated power), core inlet mass flow of 15.7 kg/s, core inlet subcooling of 10.6 K, main steam flow of 2.07 kg/s, feedwater flow rate of 2.05 kg/s, and pressure vessel water level of 4.82 m above the PV bottom. (Actual downcomer water level was obtained as 4.89 m by taking account of the frictional pressure loss term of 0.07 m.) The initial core inlet flow was lowered to this value in order to establish the same initial enthalpy distribution as in the reference BWR for the ROSA-III system with the limitted initial core power. The initial average fluid quality in the upper plenum was estimated as 13.0%.

RUN 992 was performed by the following procedures (ref. Table 5.1). Break was initiated by quickly opening both the break valve (QOBV) at break unit B and the air valve (AV165) in the first steam line branch (see Fig. 4.1). At the same time, the power supply to both recirculation pumps was terminated and the pump speed rapidly coasted down. The steady state core power was maintained for 7 s after the break and then decreased along the power curve shown in Table 4.2, which was modified from the old MSLB LOCA tests (reference 53) to simulate a heat transfer rate of average-power fuel bundles to coolant during a hypothetical BWR/LOCA.[54]

The steam flow to heat up the feedwater from the third steam line branch was manually stopped immediately after the break by closing the valves CV-1 and CV-2. The feedwater line was closed between 1.5 and 4 s after the break. The MSIV was assumed to close at the steam dome pressure lower than 5.8 MPa or by the L1 level trip (EL 3.9 m) with a time delay of 3 s by quickly closing the control valve (CV-130). The pressure control system (PCS) was initiated at the system pressure of 6.6 MPa by closing the pressure control valve (CV-130). These valve characteristics are shown in Table 4.3 and 4.4. In this test, MSIV closure did not affect

the steam line flow or the pressure responses because the PCS completely closed the steady steam line before the MSIV trip logics were satisfied.

The ADS was actuated by L1 trip level with time delay of 118 s. The ADS orifice (19.0 mm I.D.) was changed from the standard ROSA-III tests (15.5 mm I.D.) to take account of excess steam generation through the structural metal surfaces of the facility in the later blowdown phase. The LPCI was actuated at 720 s after the break (at 1.7 MPa of the system pressure).

The test was performed on March 30, 1983 as the last ROSA-III test. Most of the instruments functioned successfully.

5. Test Results of 10% Steam Line Break LOCA with ECCS Double Failures, RUN 992

Shown in this chapter are typical test results of RUN 992, i.e., system pressure responses with timings of major events, boundary conditions and fluid mass inventory, and core thermal responses related to the fluid mixture level. Timings of major events are listed in Table 5.1. Experimental data are shown in Figs.5.1 through 5.29 and Table 5.2 through 5.11. All of the experimental data and calculated data are included in Appendices I through III with their measuring list and data processing method (see Tables A.1 through A.5 and Figs.A.1 through A.147).

5.1 System Pressure and Major Events in RUN 992

Shown in Fig.5.1 is a representative pressure response in the system measured at the steam dome and timings of major events. The system pressure was mainly controlled by a steam balance as shown in the previous test results[41], i.e., steam generation by the core power generation and in the whole fluid system after the lower plenum flashing (LPF) initiation, and steam discharge through the MSL (initial steady flow, break flow and ADS flow).

After the break initiation, the pressure began to decrease due to the steam discharge both from the break orifice (10.1 mm I.D.) and the steady steam flow line (the third MSL branch), which was fully opened immediately after the break. The steady steam flow was controlled by the pressure control system (PCS) operation between 12 and 18 s at 6.6 MPa. Thereafter steam discharged only through the break orifice until initiation of the ADS opening at 594 s.

The core power (see Fig.5.2) was maintained constant at the initial power (3.966 MW : 44% of the 1/424 scaled BWR power) for 7 s and then started to decrease along the predetermined power curve. The rapid core power decrease resulted in rapid decrease of the steam generation rate in the core. Namely, the steam generation rate of 2.67 kg/s in the initial condition decreased to 0.84 kg/s at 18 s (1.286 MW : 14% of the scaled power) and to 0.35 kg/s at 30 s (0.54 MW : 6% of the scaled power). Reason of the system pressure decrease at 20 s after the break can be asc-

ribable to the decreased steam generation rate lower than the steam discharge flow rate at this time (ref. Fig.5.3).

The downcomer water began to flash at 21 s, which was detected by a decrease of the lower downcomer differential pressure (DP) data. The lower plenum flashing (LPF) started at 29 s, which was confirmed by the conduction probe level detectors and also by a DP increase across the steam separator (PD 22, see Fig.5.13). On the other hand, the recirculation line fluid began to flash at 35 s as shown in the PD 37 (see Fig.5.7) data. Local fluid temperatures at the jet pump outlet and lower plenum bottom showed a little subcooling even after 35 s. Thus system water did not start to flash at once but started gradually within a certain time period more than 14 s. Therefore, the effect of LPF was not so strong in this test as in the large MSLB LOCA tests.(34),(35) The system pressure after the LPF initiation showed a long depressurization as shown in Fig.5.1.

Actuation of the ADS, of which area was 37.6% of the scaled MSL flow area, increased the total steam discharge flow rate to 2.90 times as large as the steam break flow rate at 594 s and it promoted the depressurization. A total steam flow area became 48.2% of the scaled MSL flow area after the ADS actuation (4.55 times as large as the break area). However, the total steam flow rate did not correspond to this total steam flow area probably due to a flow limitation at a narrow air valve (AV169) located upstream the ADS orifice. An effective choking area in the ADS line was derived from the steam flow data as 20.1% of the scaled MSL area because the break area was 10.6% of the scaled MSL flow area.

If the ADS were not actuated or significantly delayed (more than 460 s) in the test of RUN 992, the LPCI would be actuated at approximately 1050 s after the break, which is later than the actual test result by 330 s as shown in Fig.5.1. This indicates an effectiveness of ADS on early LPCI actuation. The LPCI injection started at 720 s (at the system pressure of 1.7 MPa), and contributed to promote the depressurization by condensing steam and vapor mainly in the core bypass region.

5.2 Boundary Fluid Conditions and Mass Balance in System

Shown in Fig.5.3 are the total steam discharge flow rate measured by the low-range orifice flow meter (FM 711) and the volumetric feedwater flow rate. The orifice flow meter can give an accurate mass flow rate

within the nominal accuracy for a single-phase steam flow. The large steam flow rate in the first 18 s was obtained from the middle-range orifice flow meter (FM 713). Although the accuracy of the steam flow measurement was not di- rectly determined by other method, it could be expected to be the same order of the nominal accuracy (±0.92% of full scale, i.e., ±0.016 kg/s) due to the following reasons.

Fluid temperature in the steam line showed super-heated steam temperature in most test period and showed temporarily saturated temperature. Water entrainment into the steam line is expected to be very small in most of the test period in this test because the downcomer mixture level was far below the PV top (see Fig.5.9). And the orifice flow data was accurate even in a 100% MSLB LOCA test (RUN 952, reference (14)) except for a short time period, in which the swelled mixture level reached top of PV. Thus, the steam flow accuracy can be expected as the same order of the nominal value, i.e., ±0.02 kg/s. The data scattering observed was within this range. Therefore, this accuracy can be adopted as a representative for the total steam discharge flow data.

The initial steam flow of 2.07 kg/s increased to 2.32 kg/s at the time of break by full opening of the steady steam line as in other ROSA-III tests. The steam break flow rate was obtained as 1.18 kg/s at the time of break, 0.75 kg/s at 18 s and 0.69 kg/s at 30s, respectively. The steam discharge flow rate became larger than the steam generation rate in the core at approximately 20 s after the break. The steam break flow rate at the time of ADS actuation was 0.30 kg/s and the ADS steam discharge flow rate was 0.58 kg/s. By assuming the same ratio between these two steam flows, the steam break flow rate was obtained even after the ADS actuation time as shown in Table 5.2. On the other hand, the steam break flow was also measured by the drag-disk and densitometer at the break B as shown in Fig.5.4. This flow data agree well to the orifice flow data shown above except for the initial 18 s and the time period after the ADS actuation.

The feedwater supply was terminated between 1.5 and 4 s after the break. Total amount of injected feedwater mass was 6 kg for this period. After flashing initiation in the feedwater piping line (fluid volume is 0.035 m^3) at 2.1 MPa, some amount of remaining water flowed into the downcomer. Approximately a half volume of the remaining feedwater was assumed to flow into the downcomer as shown in Table 5.2. Injected LPCI water flow rate is shown in Fig.5.5.

Mass balance for the total system is shown below by using these mass boundary conditions and an initial system mass (M_o), which was modified from the initial conditions of large MSLB test (RUN 952, reference 14) accoding to the lower initial downcomer water level, as M_o = 651 kg. The remaining fluid mass in the total system (M) is calculated at each time as,

$$M = M_o + M_F - M_D + M_E \qquad (5.1),$$

where M_F, M_D and M_E are the injected feedwater mass, discharged steam mass and injected LPCI water mass, respectively. This results are shown in Table 5.3.

It is shown that the least fluid mass in the total system was 42% of the initial fluid mass at the time of LPCI actuation (720 s). Timings of the major events can be related to this system mass inventory. Namely, the core dryout initiation in the average-power bundle (425 s) started at the mass ratio (M/M_o) of 64%, the ADS actuation at M/M_o = 55% and the final core quech (760 s) at M/M_o = 47%.

The system mass inventory rapidly increased by the LPCI water injection because the LPCI injection flow rate was approximately 7 times as large as the total steam discharge flow rate during 720 and 1000 s after the break. In order to show the effect of LPCI injection on the total mass recovery, an ECC water accumulation efficiency (E_a)[55] was derived as,

$$E_a = (M_E - M_D) / M_E \qquad (5.2),$$

and E_a = 85.5% for the above LPCI injection period in RUN 992. Thus, the system mass recovery was prominent even in the case of double failure on the HPCS and LPCS diesel generators and the LPCI contributed to the complete core cooling as shown later.

5.3 Downcomer Water Level and Fluid Mass Distribution in System

Described below are responses of water level and average void fraction in the downcomer, and fluid mass distribution in the total system. The fluid masses remaining in the downcomer, jet pumps and recirculation loops are derived from their differential pressure data, and that inside the core-shroud and steam dome is obtained by subtracting the other region masses from the total remaining mass. In this chapter, the downcomer region is defined between the bottom (EL 0.50 m) and top of the steam

separator (EL 5.37 m), and it is different from a definition for the large MSLB test analysis (reference 14), in which the downcomer was defined below the normal water level. This analysis result is refered for estimation of the initial total mass inventory.

Shown in Fig.5.6 are the collapsed water levels both in the upper downcomer (EL 3.90 - 6.04 m) and in the lower downcomer (EL 0.94 - 3.90 m). Shown in Figs.5.7 and 5.8 are differential pressures measured in the recirculation loop (between MRP1 discharge side and JP1 drive side, elevation change is 5.80 m) and in the jet pump (between JP1 discharge side and the lower plenum, elevation change is 2.14 m), respectively. These DP data are used for estimation of average void fraction in each region by neglecting the frictional pressure loss.

Average void fraction (α) in the lower downcomer is calculated from the lower downcomer collapsed water level (LM 69 = L_l) by using following relations, as

$$DP = \rho'' g \alpha H + \rho' g (1-\alpha) H \qquad (5.3),$$

$$L_l = DP / (\rho' g) + 0.94 \qquad (5.4),$$

where ρ'', ρ', g and H are saturated steam density, saturated water density, gravity constant and DP measuring height of 2.96 m, respectively. Void fraction in the lower downcomer between 480 and 594 s, in which there was no water level in the upper downcomer region, was assumed to be the same as in the previous time period, because the void fraction was closely related to the total steam discharge flow area (see reference 41), which was kept constant until the ADS actuation time except for the initial 18 s in RUN 992.

A downcomer mixture level (L_m) is calculated from the downcomer collapsed water level (L_u or L_l) by assuming a uniform void distribution in all the downcomer regions. Validity of this assumption, however, is not yet confirmed. As the steam mass contribution to the level is negligiblly small for this test condition,

$$L_m = (L_u - 3.90) / (1.0 - \alpha) + 3.90, \text{ for } L_u > 3.90 \qquad (5.5),$$

$$L_m = (L_l - 0.94) / (1.0 - \alpha) + 0.94, \text{ for } L_u \leq 3.90 \qquad (5.6).$$

Results are shown in Table 5.4 and Fig.5.9. The downcomer void fraction began to increase at 21 s after the break and reached almost constant value of 0.17 - 0.18. This value is consistent with the previous test results for total steam flow area of 10.6% of the scaled MSL area (reference 41). It rapidly increased to 0.35 after the ADS actuation and reached a

maximum value of 0.43 after the LPCI actuation. The void fraction after the ADS actuation is close to an expected value in the previous test results for the total steam flow area of 30.7% of the scaled MSL flow area (see section 5.1). Thus, these downcomer void fraction data are consistent in all the ROSA-III MSLB LOCA tests. Void fraction became zero approximately at 1100 s.

The mixture level was higher than 3.60 m (elevation is just above the core top level) and lower than 5.37 m (top of the steam separator) for most of the test period. The mixture level response is compared with a total downcomer collapsed level (L_d), which is calculated as,

$$L_d = L_l + L_u - 3.90 \qquad (5.7).$$

Difference between L_m and L_d is the level swell caused by void formation. The difference was approximately 0.5 m for the blowdown phase, 1.0 m after the ADS actuation and diminished approximately at 1100 s after the break. Fluid mass remaining in the downcomer (M_{DC}) at each time is calculated by using the mixture level, average void fraction, fluid density and the downcomer configurational data as shown in Table 5.5. The lower and upper downcomer volume are 0.1144 and 0.3560 m^3. The steam mass is included in the total remaining fluid mass of M_{DC}.

Fluid mass remaining in four jet pumps and two recirculation loops (M_L) is calculated as follows. An average void fraction (α_1) in the jet pump discharge line is derived from the corresponding DP data (- PD 41, see Fig.5.8) and is assumed to be a representative of all the jet pump fluid void fraction. Similarly an average void fraction (α_2) in the MRP1 discharge line is derived from PD 37 (see Fig.5.7) and is assumed to be a representative void fraction of all recirculation loop fluid. Namely, the void fractions are calculated as,

$$-PD41 = \rho''gH_1\alpha_1 + \rho'gH_1(1.0 - \alpha_1), \quad H_1 = 2.14 \text{ m} \qquad (5.8),$$

$$PD37 = \rho''gH_2\alpha_2 + \rho'gH_2(1.0 - \alpha_2), \quad H_2 = 5.80 \text{ m} \qquad (5.9).$$

Water mass in the jet pumps (M_1) or recirculation loops (M_2) is calculated by using the void fraction, water density and fluid volume for each region as,

$$M_1 = \rho'(1.0 - \alpha_1)V_1, \quad V_1 = 0.0637 \text{ m}^3 \qquad (5.10),$$

$$M_2 = \rho'(1.0 - \alpha_2)V_2, \quad V_2 = 0.1083 \text{ m}^3 \qquad (5.11).$$

M_1, M_2 and a sum of these (M_L) are shown in Table 5.6. Steam mass is included in the total remaining fluid mass (M_L). By subtracting M_{DC} and M_L from the total system mass (M), remaining fluid mass inside the core-

shroud and steam dome (M_C) is derived as,

$$M_C = M - M_L - M_{DC} \quad (5.12).$$

Fluid mass distribution in the total system is shown in Fig.5.10 and Table 5.7. Following are found from these data analyses.

In the jet pumps and recirculation loops, fluid mass more than 100 kg remained until actuation of ADS at 594 s, and thereafter decreased due to increase of void fraction. The mass recovery after the LPCI actuation was observed in the jet pumps, whereas it was significantly delayed in the recirculation loops. This delay may indicate occurrence of the counter-current flow limiting (CCFL) at the inlets of the recirculation loops.

The downcomer fluid mass decreased rapidly after the flashing initiation and on the contrary, the remaining fluid mass inside the core-shroud slightly increased in the same time. This indicates a mass transfer after the flashing initiation between the downcomer and in-shroud region. After 150 s, fluid masses in these regions decreased similarly due to the steam mass discharge through the MSL.

The ADS actuation caused faster mass decrease inside the core-shroud (62 kg between 594 and 720 s), whereas it caused less mass decrease outside the core-shroud (23 kg for jet pump, recirculation loop and downcomer) in the same period. This indicates a mass transfer from the in-shroud region to the downcomer through the jet pumps, and it is also shown by the net negative flow rates at the core inlet orifices (see Figs.5.18 and 5.20). Thus the ADS actuation changed both the pressure balance and mass distribution in PV.

The LPCI water injection caused rapid mass recovery inside the core-shroud and in the downcomer with a time delay of approximately 80 s. And the LPCI water flowed down into the lower plenum through the core inlet orifice and core bypass holes. Thereafter the LPCI water flowed into the downcomer through the jet pumps.

The transient mass inventory is related with the system pressure responses as shown in Table 5.8 and Fig.5.11. This mass-pressure map shows characteristics of the 10% MSLB LOCA test, RUN 992. It is shown that fluid mass inside the core-shroud was almost a half of the system total mass inventory for all test period before the LPCI actuation. The core dryout initiation in the average-power bundle C started at the mass ratio (M/M_0) of 0.64 and the final core quench was observed at 0.47, respec-

tively as shown previously. Although these two values are much different, the in-shroud mass ratios (M_c/M_o) for these events were similar as, 0.32 and 0.28, respectively. Thus, a critical condition of the core dryout occurrence was observed approximately at M_c/M_o = 0.3 for this 10% MSLB LOCA test.

5.4 Pressure Balance and Internal Flows in Pressure Vessel

Described below is a pressure balance in PV along two steam uprizing flow paths (one is from the lower plenum to steam dome through the core, bypass and separator, and another one is from the lower plenum and recirculation loops to the steam dome through the jet pumps and downcomer). PV internal flow induced by rapid decrease of the core power and actuations of ADS and LPCI is shown later.

Shown in Fig.5.12 are locations of differential pressure (DP) measurements around the PV. There are DP measurements to check the pressure balance between the two steam-uprizing paths. As shown in Table 5.9, a sum of PD 21 and PD 22 (Fig.5.13) agreed well with PD 25 (Fig.5.14) within a discrepancy of 3 kPa, which is much less than a nominal accuracy of ±6.3 kPa for PD 25. This indicates that these DP data are sufficiently accurate for pressure balance estimation. Similarly, PD 25 data was compared with a sum (DP_{out}) of -PD 41, PD 26, -PD 39 and PD 56 (see Fig.5.12) for the steam flow path outside the core-shroud in Table 5.10.

$$DP_{out} = -PD\ 41 + PD\ 26 - PD\ 39 + PD\ 56 \qquad (5.13).$$

A small difference between PD 25 and DP_{out} (less than 6 kPa) was also within the nominal accuracy of PD 25.

The following are derived from these data analyses.

PD 22 in the initial condition included large contribution of frictional pressure loss of approximately 40 kPa across the steam separator, which rapidly decreased immediately after the break due to the rapid core flow coastdown. On the other hand, frictional pressure loss included in the initial condition of PD 21 was less than 15 kPa and became almost zero immediately after the break. It is clear that pressure loss across the separator was significantly larger than that across the core in the initial condition. Rapid decrease of the forced circulation flow changed the pres-

sure distribution in PV so that a natural circulation was established corresponding to a new condition. Rapid decrease of PD 22 immediately after the break largely affected this change. PD 22 increased after the LPF initiation (29 s) upto 7 kPa in maximum.

PD 21 recovered at 7 s after the break due to rapid decrease of void fraction in the core, which was caused by the core power decrease after 7 s. This recovery was promoted after initiation of downcomer fluid flashing (21 s). This increase of PD 21 shows mass transfer from the DC region to the in-shroud region corresponding to the core void decrease and downcomer fluid flashing initiation.

In a later LOCA phase, PD 22 was slightly influenced by the ADS actuation at 594 s. After the LPCI actuation, PD 21 increased rapidly due to mass recovery inside the core-shroud, whereas PD 22 became negative showing reverse flow across the separator probably due to condensation in the bypass and core. PD 22 began to increase after 960 s due to mass recovery also in the separator and steam dome region. PD 25 was nearly the same to PD 21 as PD 22 was very small except for the initial short time and later reflooding phase after the LPCI actuation.

PD 26 rapidly decreased immediately after the break and became almost zero until the LPCI actuation. After 750 s, PD 26 rapidly increased upto approximately 5 kPa, which corresponded to water fulfill in the jet pumps. As there is no elevation change in the PD 39 measurement, PD 39 can be used as a flow direction meter at the jet pump suction line. The flow direction was positive (from DC to JP) between 7 and 31 s after the break. This corresponds to mass recovery time period inside the core-shroud, which was clearly shown in the PD 21 data. On the other hand, PD 39 became slightly negative after the ADS actuation and largely negative after the LPCI actuation with a short time delay of 30 s. These negative responses indicate reverse mass transfer from the in-shroud region to the DC region caused by the ADS and LPCI actuations. These are also described in the system mass distribution in section 5.3.

It is shown from these DP data that mass distribution inside and outside the core-shroud are largely changed by the termination of forced circulation flow, core power change and ECC water injection, and slightly changed by operation of the ADS.

Shown in Figs.5.18 through 5.20 are core inlet flow rates for the four channels, core bypass flow rate through the bypass holes and total core

flow rate of these, respectively. As these data were derived from corresponding DP data, they are adequate only for the water single-phase flow (before the LPF and after the LPCI actuation timings) and can be used for qualitative flow characteristics outside the adequate periods. The mass transfer between outside and inside regions across the core-shroud are also observed in these core flow data. In addition to this internal circulation flow in PV, local circulation flow inside the core-shroud and flow distribution among four channels were obserbed in these flow data as shown below.

Flow distribution were observed between the high-power bundle flow rate and average-power bundle flow rates as shown in Fig.5.18. Namely, a constant uprizing flow was found in bundle A inlet for a long time before the core dryout initiation (455 s). On the other hand, the core inlet flow became almost stagnant after 60 s at inlets of average-power bundles (B, C and D). The bypass flow (see Fig.5.19) showed negative value (downflow at bottom of the guide tube) for the time period of bundle A upflow. This indicates that there was a circulation flow inside the core shroud (from channel A to upper plenum, core bypass, guide tube and to the lower plenum), and it continued as long as the core mixture level covered the top core region. It should be noted that another small circulation flow was possible between the channels and the bypass through the leak holes located at the lower end of each channel box. However, there was no measuring instrumentations for the leak hole flow.

The total core inlet flow was positive as long as the internal circulation flow existed between the core and bypass. These core inlet flows began to oscillate similarly after the ADS actuation and showed a net negative (downward) flow. After the LPCI actuation, the same flow distribution was observed between the channel A and other channels. There was a negative flow rate in the average-power bundles and at the bypass flow holes, but a positive flow at the inlet of high-power bundle. And the net core flow rate was negative after the LPCI actuation as shown in Fig.5.20.

5.5 Heater Rod Temperature Responses Related with Core Mixture Level

Shown in Fig.5.21 are the temperature data at seven axial locations on the A-11 heater rod with the maximum heat flux. These temperature res-

ponses are representative of all the heater rods. Initiation of the heater rod temperature excursion started at 455 s at the top of this heater rod due to decrease of core fluid mass. This dryout region gradually extended to lower part of the core. The ADS actuation at 594 s caused the core mixture level swell (see Fig.5.27) and immediately quenched this heated region.

If the ADS were not actuated or significantly delayed in RUN 992, the first heater rod temperature excursion would continue until the LPCI actuation, which was expected approximately at 1050 s (see section 5.1), and the maximum heater rod surface temperature would exceed 1100 K at A-11 rod Pos.3 as shown in Fig.5.21. Thus, the ADS effect on core cooling is prominent for the small MSLB LOCA.

The heater rod temperature began to rise again as the mixture level decreased. This second core dryout was observed above Position 5 (EL 2.17 m above the PV bottom) and diminished by recovery of the core mass inventory after the LPCI actuation. The peak cladding temperature (PCT) was observed on this A-11 rod Position 3 at 744 s (24 s after the LPCI actuation) as 649 K (Fig.5.22). The PCT in the whole core is listed in Table 5.11.

Heater rod surface temperatures in all the rod bundles showed the similar responses as those of the A-11 rod as shown in Figs.5.23 and 5.24. In the bundle C, the core dryout initiation was the earliest among all of the heater rods as 425 s (30 s earlier than in bundle A). Although there was a little difference of core dryout initiation timings, there was no apparent difference of quench timings between the four bundles. The final core quench was observed at 760 s after the break (40 s after the LPCI actuation).

The dryout and quench timings of heater rods in bundle A and for the four bundles are shown in Figs.5.25 and 5.26, respectively. Shown in Fig. 5.27 are mixture level responses detected by conduction probes located at the same elevations as those of the heater rod thermocouples in the core. It is clear that the mixture level transients agreed well with the trajectories of the dryout and quench timings of the heater rods (dryout and quench fronts). Namely, the heater rod was completely cooled as far as the rod was covered by the mixture level even at the highest heat flux rod.

It is also shown that the mixture level in the high-power bundle was slightly higher than that in the average-power bundle due to difference of their void distribution in the rod bundles. The mixture level was swelled

largely after the ADS actuation and almost covered all of the core (a part of the bundle C top was an exception of the complete quenching). In Fig. 5.27, the collapsed water level inside the core-shroud was compared with the mixture level transient. The collapsed water level corresponded well to the mixture level transients. Difference between them was less than 0.6 m in the blowdown phase except for a short time after the ADS actuation, in which it became approximately 1.0 m. The difference was large in the reflooding phase (less than 1.4 m at 755 s).

It is concluded that the core dryout was temporarily diminished by a core mixture level swell, which was caused by the ADS actuation (169 s after the core dryout initiation), and finally quenched by the LPCI water injection even in a case of double failure assumption on the HPCS and LPCS diesel generators. It was confirmed that the core dryout front agreed well with the core mixture level responses.

Fluid temperatures at the core top region (across the upper tie plate) are shown in Figs.5.28 and 5.29. Detection of the super-heated temperature for the bundles A and C corresponds to core dryout period in each bundle. And large subcooling was observed after 850 s indicating the LPCI water overflow from the core bypass region to the core top region. The lowest fluid temperature above the upper core plate was 336 K (23 K higher than the LPCI water temperature).

6. Conclusions

Characteristic features and effectiveness of ECCSs are investigated for a 10% main steam line break (MSLB) LOCA test (RUN 992) performed in the ROSA-III program. The following are major conclusions.

(1) Total mass inventory and mass distribution in the system were investigated for the whole test period to clarify characteristic features of a small MSLB LOCA in a BWR system.

(1-1) Initial total mass (M_0) including steam mass was estimated as 651 kg for the test of RUN 992 by modifying the initial downcomer water level of the standard MSLB LOCA test (RUN 952[14]). In most of the blowdown phase, fluid mass inside the core-shroud (M_c) was maintained at approximately a half of the total mass inventory (M) and it was slightly larger than in the initial mass ratio of 44%. In the recirculation loops and jetpumps, fluid mass (M_L) remained at M_L/M of 20 - 30%. On the other hand, fluid mass ratio in the downcomer region (M_D/M) gradually decreased from the initial condition (36%) to less than 20% at the ADS actuation time of 594 s.

(1-2) These mass distribution in the system was changed by termination of the forced circulation flow, rapid core power decrease after the reactor scram trip, ADS actuation and ECC water injection. Void diminishing in the core resulted in mass transfer from the downcomer to in-shroud region. On the contrary, the ADS actuation resulted in reverse mass transfer between these regions.

(1-3) A critical condition of core dryout initiation was obtained by the in-shroud mass ratio of $M_c/Mo = 0.3$ for this 10% MSLB LOCA test. The total mass ratio at the core dryout initiation was $M/M_0 = 0.64$.

(2) The LPCI injection flow rate, which was approximately 7 times as large as the total steam discharge flow rate including the ADS flow during the LPCI injection period, was sufficient for the early mass recovery in PV and complete quenching of the heated core. The PCT was observed as 649 K at 24 s after the LPCI actuation. Thus, the double failures on the HPCS and LPCS diesel generators did not result in any severe core heatup in the 10% MSLB LOCA test.

(3) The ADS actuation, which was tripped on L1 level with a time delay of 118 s (169 s after the core dryout initiation), caused not only the fast depressurization for early LPCI actuation but also the temporary core cooling for most of the uncovered region. By extraporating the test results, the maximum heater rod surface temperature was expected to exceed 1100 K at a time of LPCI actuation (1.7 MPa) in a case of no ADS actuation. Thus, effects of the ADS actuation were confirmed in present small MSLB LOCA as in a small main recirculation line break (MRLB) LOCA.

(4) Other characteristic features of the MSLB LOCA phenomena shown previously in reference (41) were also observed in this test. Namely, the system pressure responses, mixture level swell and average void fraction in the downcomer were controlled by the total steam discharge flow area in the MSL.

Acknowledgment

The authors are grateful to Mr.H.ASAHI, T.ODAIRA, T.TAKAYASU, Y.KITANO and T.NUMATA of Nuclear Engineering Corporation for their assistance in conducting the experiment, Mr.K.HIYAMA, E.UMEKI and T.NAKAJIMA of Information System Laboratory Corporation for preparing the data plots and Ms.T.KUROSAWA of Nihon Computer Bureau for type writing.

(3) The ADS actuation, which was tripped on L1 level with a time delay of 118 s (169 s after the core dryout initiation), caused not only the fast depressurization for early LPCI actuation but also the temporary core cooling for most of the uncovered region. By extraporating the test results, the maximum heater rod surface temperature was expected to exceed 1100 K at a time of LPCI actuation (1.7 MPa) in a case of no ADS actuation. Thus, effects of the ADS actuation were confirmed in present small MSLB LOCA as in a small main recirculation line break (MRLB) LOCA.

(4) Other characteristic features of the MSLB LOCA phenomena shown previously in reference (41) were also observed in this test. Namely, the system pressure responses, mixture level swell and average void fraction in the downcomer were controlled by the total steam discharge flow area in the MSL.

Acknowledgment

The authors are grateful to Mr.H.ASAHI, T.ODAIRA, T.TAKAYASU, Y.KITANO and T.NUMATA of Nuclear Engineering Corporation for their assistance in conducting the experiment, Mr.K.HIYAMA, E.UMEKI and T.NAKAJIMA of Information System Laboratory Corporation for preparing the data plots and Ms.T.KUROSAWA of Nihon Computer Bureau for type writing.

References

(1) K.TASAKA, et al., "ROSA-III Experimental Program for BWR LOCA/ECCS Integral Simulation Tests", JAERI 1307 (1987).

(2) K.TASAKA, et al., "Study on the Similarity between ROSA-III Experiment and BWR LOCA", JAERI-M 6703 (1976) (in Japanese).

(3) Y.ANODA, et al.,"ROSA-III System Description for Fuel Assembly No. 4", JAERI-M 9363 (1981) (in Japanese).

(4) General Electric Company, "General Electric Standard Safety Analysis Report, BWR/6", DOCKET-STN-50477 (1978).

(5) K.TASAKA, et al.,"ROSA-III Base Test Series for a Large Break Loss of Coolant Accident in a Boiling Water Reactor", Nucl. Technol. 57, 179-191 (1982).

(6) K.SODA, et al.,"Boiling Water Reactor Loss of Coolant Test (Single Failure Test with ROSA-III)", J. Nucl. Sci. Technol. 20, 537-558 (1983).

(7) K.TASAKA, et al.,"Simulation Experiment of Five Percent Small Break LOCA of BWR", J. Nucl. Sci. Technol. 20, 89-104 (1983).

(8) K.TASAKA, et al.,"ROSA-III Double-Ended Break Test Series for a Loss-of-Coolant Accident in a Boiling Water Reactor", Nucl. Technol. 68, 77-93 (1985).

(9) M.SUZUKI, et al.,"Recirculation Pump Discharge Line Break Tests at ROSA-III for a Boiling Water Reactor", Nucl. Technol. 70, 189-203 (1985).

(10) Y.KOIZUMI, et al., "Experiment Analysis of Power Curve Sensitivity Test Series at ROSA-III", Nucl. Eng. and Design 86, 267-287 (1985)

(11) H.KUMAMARU, et al.,"Five Percent Break BWR LOCA/ECC Test at ROSA-III without HPCS Actuation---Two Dimensional Core Thermal Hydraulic Phenomena", Nucl. Eng. and Design 86, 219-239 (1985).

(12) K.TASAKA, et al.,"Analysis of ROSA-III Break Area Spectrum Experiments on BWR Loss-of-Coolant Accident", Nucl. Technol. 71(3), 628-643 (1985).

(13) T.YONOMOTO, et al.,"Investigation of BWR/LOCA at ROSA-III---Effect of Break Configuration on System Transient---", Nucl. Eng. and Design 92, 195-205 (1986).

(14) M.SUZUKII, et al., "Siumilarity Study of Large Steam Line Break LOCAs in ROSA-III, FIST and BWR/6", Nucl. Eng. and Design 98(1), 39-56 (1986).

(15) Y.KOIZUMI, et al.,"Investigation of Break Location Effects on Thermal-Hydraulics during Intermediate Break Loss-of-Coolant Accident Experiments at ROSA-III", J. Nucl. Sci. Technol., 23(11), 1008-1019 (1986).

(16) H.KUMAMARU, et al.,"Investigation of Effect of Pressure Control System on BWR LOCA Phenomena Using ROSA-III Facility", J. Nucl. Sci. Technol., 24(10), 844-858 (1987).

(17) T.YONOMOTO, et al.,"Core Heat Transfer Analysis during a BWR LOCA Simulation Experiment at ROSA-III", Nucl. Eng. and Design, 103(2), 239-163 (1987).

(18) Y.KOIZUMI, et al., "BWR Small Break LOCA Counterpart Test at ROSA-III and FIST Test Facilities", Nucl. Eng. and Design, 102(2), 151-163 (1987).

(19) H.KUMAMARU, et al.,"BWR Large Break LOCA/ECCS Counterpart Test at ROSA-III and FIST", Nucl. Eng. and Design, 102(2), 223-238 (1987).

(20) K.KOIZUMI, et al.,"Effect of Heat Generation Difference among Fuel Bundles on Core Thermal-Hydraulics during 200% and 5% Loss-of-Coolant Accident Experiments", J. Nucl. Sci. Technol., 24(1), 61-74 (1987).

(21) M.SOBAJIMA, et al.,"Experiment Test Data of ROSA-III Test RUN 701 (Decay Heat Simulation Test with ECCS Actuation)", JAERI-M 8604 (1979).

(22) Y.ANODA, et al.,"Experiment Data of ROSA-III Test RUN 703 (Split Break Simulation Test with ECCS Actuation)", JAERI-M 8967 (1980).

(23) Y.ANODA, et al.,"Experiment Data of ROSA-III Test RUN 704 (Standard Test with ECCS Actuation)", JAERI-M 8968 (1980).

(24) M.OKAZAKI, et al.,"Experimet Test Data of ROSA-III Integral Test RUN 705 (Isothermal Blowdown Test without ECCS Actuation)", JAERI-M 8723 (1980).

(25) M.SUZUKI, et al.,"Experiment Data of ROSA-III Integral Test, RUN 706", JAERI-M 8737 (1980).

(26) M.OKAZAKI, et al.,"Experiment Data of ROSA-III Integral Test RUN 708 (Standard Test without ECCS Actuation)", JAERI-M 8738 (1980).

(27) Y.KOIZUMI, et al.,"Experiment Data of ROSA-III Integral Test, RUN 710", JAERI-M 9249 (1981).

(28) Y.ANODA, et al.,"Experimet Data of ROSA-III Integral Test RUN912 (5% Split Break Test without HPCS Actuation)", JAERI-M 82-010.

(29) H.NAKAMURA et al.,"Experiment Data of ROSA-III Integral Test RUN 901 (200% Double-Ended Break with Full ECCS Actuation)", JAERI-M 84-007.

(30) H.NAKAMURA, et al.,"Experiment Data of ROSA-III Integral Test RUN 926 (200% Double-Ended Break with HPCS Failure)", JAERI-M 84-008.

(31) M.SUZUKI, et al.,"Experiment Data of 200% Recirculation Pump Discharge Line Break Integral Test RUN 961 with HPCS Failure at ROSA-III and Comparison with Results of Suction Line Break Tests", JAERI-M 84-045, (1984).

(32) M.SUZUKI, et al.,"Recirculation Pump Suction Line 2.8% Break Integral Test at ROSA-III with HPCS Failure, RUN 984", JAERI-M 84-100, (1984).

(33) M.SUZUKI, et al.,"Recirculation Pump Suction Line 200% Break Integral Test at ROSA-III with Two LPCI Failures, RUN 983", JAERI-M 84-135, (1984).

(34) M.KAWAJI, et al.,"A Main Steam Line Break Experiment at ROSA-III RUN 952 (Standard Run with Full ECCS)", JAERI-M 84-229, (1984).

(35) M.KAWAJI, et al.,"A Main Steam Line Break Experiment at ROSA-III RUN 953 (100% Break with an HPCS Failure)", JAERI-M 85-029, (1985).

(36) M.SUZUKI, et al.,"BWR Recirculation Loop Discharge Line Break LOCA Tests with Break Areas of 50 and 100% Assuming HPCS Failure at ROSA-III Facility", JAERI-M 85-037, (1985).

(37) T.YONOMOTO, et al.,"ROSA-III 50% Break Integral Test RUN 916 (Break Area Parameter Test)", JAERI-M 85-109, (1985).

(38) H.NAKAMURA, et al.,"Recirculation Pump Suction Line 5% Split Break Test of ROSA-III (RUNs 922 and 932 with HPCS Failure)", JAERI-M 85-128, (1985).

(39) T.YONOMOTO, et al.,"ROSA-III 50% Break Integral Test RUN 928 (Break Configuration Sensitivity Test)", JAERI-M 85-151 (1985).

(40) K.TASAKA, et al.,"Comparison of ROSA-III and FIST BWR Loss of Coolant Accident Simulation Tests", JAERI-M 85-158 (1985).

(41) M.SUZUKI, et al.,"BWR Main Steam Line Break LOCA Tests RUNs 951, 954 and 956 at ROSA-III (Break Area Effects with HPCS Failure)", JAERI-M 85-202 (1985).

(42) S.ITOYA and N.ABE, "Analysis of TBL Main Steam Line Break Test by SAFER03 and TRAC-BD1", NUREG/CP-0072, Proceedings of the 13th WRSR Information Meeting, (Oct. 1985).

(43) H.NAKAMURA, et al.,"Recirculation Pump Suction Line 1% Split Break LOCA Test of ROSA-III (RUNs 921 and 931 with HPCS Failure)", JAERI-M 85-209 (1986).

(44) M.SUZUKI, et al.,"BWR 200% Recirculation Pump Suction Line Break LOCA Tests, RUNs 942 and 943 at ROSA-III without HPCS (Effects of Initial Fluid Conditions on LOCA)", JAERI-M 86-038 (1986).

(45) M.SUZUKI, et al.,"BWR 2% Main Recirculation Line Break LOCA Tests RUNs 915 and 920, without HPCS in ROSA-III Program (Effects of Pressure Control System)", JAERI-M 87-043, (1987).

(46) M.SUZUKI, et al.,"BWR LOCA Integral Test Simulating a 100% Main Steam Line Break outside Reactor Containment Vessel in ROSA-III Program, RUN 955 (Analogy of Steam and Recirculation Line Small Break LOCAs)", JAERI-M 87-044 (1987).

(47) T.YONOMOTO, et al.,"ROSA-III 100% Break Integral Test RUN 914 (Break Area Parameter Test)", JAERI-M 87-072 (1987).

(48) M.SUZUKI, et al.,"BWR 1% Main Recirculation Line Break LOCA Tests, RUNs 917 and 918, without HPCS at ROSA-III Program (Effects of ADS Delay in Small Break LOCA)", JAERI-M 88-141, (1988).

(49) M.SUZUKI, et al.,"Heat Loss and Fluid Leakage Tests of the ROSA-III Facility", JAERI-M 9834 (1981).

(50) M.SUZUKI, et al.,"Characteristics of the ROSA-III Test Facility (Characteristics Test of the Jet Pumps in Normal and Reverse Flow)", JAERI-M 8670, (1980) (in Japanese).

(51) M.SUZUKI, et al.,"Evaluation of a Jet Pump Model for RELAP5 Code", JAERI-M 84-245, (1985) (in Japanese).

(52) M.SOBAJIMA, et al.,"Instrumentation and Data Processing Method of the ROSA-III Test", JAERI-M 8499 (1979) (in Japanese).

(53) N.ABE, et al.,"Electric Power Tansient Curve for ROSA-III Tests", JAERI-M 8728 (1980).

(54) M.IRIKO, et al.,"Updated Core Power Curves for ROSA-III Facility", JAERI-M 84-029, (1984) (in Japanese).

(55) M.SUZUKI, et al.,"Break Location Effects on PWR Small Break LOCA Phenomena (Inadequate Core Cooling in Lower Plenum Break Test at LSTF)", JAERI-M 88-271 (1988).

Table 2.1 Primary chracteristics of BWR/6 and ROSA-III

Items	Unit	BWR*	ROSA-III	BWR / ROSA-III
Number of Recirc. Loops	-	2	2	1
Number of Jet Pumps	-	24	4	6
Number of Separators	-	212	1	212
Number of Fuel Assemblies	-	848	4	212
Active Fuel Length	m	3.76	1.88	2
Total Fluid Volume	m^3	621	1.42	437
Maximum Core Power	MW	3800	< 4.40	> 864
Steam Dome Pressure	MPa	7.23	7.23	1
Total core Flow Rate	kg/s	15400	< 36.4	> 424
Recirc. Flow Rate/Loop	kg/s	2240	< 5.26	> 424
Total Steam Flow Rate	kg/s	2060	< 4.86	> 424
Feedwater Temperature	K	489	489	1

* BWR/6 (251-848)

Table 3.1 ROSA-III instrumentation list

ITEM	SENSOR	NUMBER	NOTE
Pressure	Pressure Transducer	20	
Differential Pressure	DP Cell	60	PV and Loop 44 Level Measurement 5 Flow Meter 11
Fluid Temperature	CA Thermocouple	129	Primary Loop 23 DTT 4 Tie Rod 28 Upper Plenum 10 Lower Plenum 10 Tie Plate 40 Bypass 14
Fuel Rod Temperature	CA Thermocouple	213	
Slab Surface Temperature	CA Thermocouple	70	Core Barrel 24 Pressure Vessel 3 Channel Box 35 Shroud Support 8
Slab Inner Temperature	CA Thermocouple	9	JP Diffuser 4 PV Wall 5
Volumetric Flow Rate	Turbine Flow Meter Venturi Flow Meter Orifice Flow Meter	3 4 6	ECCS Loop 3 Primary Loop 10
Mass Flow Rate	Turbine Flow Meter Orifice Flow Meter	4 3	Recirculation Loop 4 Main Steam Line 3
Liquid Level	Conductivity Probe Capacitance Probe	138 2	
Density	Gamma Densitometer	10	2 Beam GD 2 3 Beam GD 2
Momentum Flux	Drag Disk	4	JP Spool Piece 2 Break Spool Piece 4 Break Orifice 1
Signal	ON/OFF Switch	14	
Pump Speed	Revolution Counter	2	
Electric Core Power	VA Meter	2	
TOTAL		693	

Table 4.1 Test conditions of RUN 992

Parameter	Unit	Measured Value	Parameter	Unit	Measured Value
Break Conditions			Steam Flow Rate	kg/s	2.07
Location		MSL inside RCV	Feedwater Flow Rate	"	2.05
Orifice Diameter	mm	10.1	Feedwater Temperature	K	489
1/424 Scaled Area	%	10.6			
			Transient Conditions		
Initial Conditions			Pressure Control System		$P \leq 6.67$ MPa
Steam Dome Pressure	MPa	7.36	MSIV Closure Trip		($P \leq 5.8$ MPa or L1 Level*2) +3s
Lower Plenum Temperature	K	552.6			
Lower Plenum Subcooling	K	10.6	SRV Operation		not used
Core Inlet Flow Rate	kg/s	15.7			
Total Core Power	MW	3.966	ECC Conditions		
Max. Linear Heat Rate			HPCS Actuation		Failure
Channel A (LPF=1.1)	kW/m	16.66	LPCS Actuation		Failure
(" =1.0)	"	15.15	LPCI Actuation Time	s	720
(" =0.875)	"	13.25	Initiation Pressure	MPa	1.7
Channels (" =1.1)	"	11.90	Trip Logic	s	L1 + 40
B,C,D (" =1.0)	"	10.82	Water Temperature	K	313
(" =0.875)	"	9.47	ADS Actuation Time	s	594
Upper Plenum Quality	%	13.0	Trip Logic		L1 + 120
Water Level	m	4.82*1	Orifice Diameter	mm	19.0

*1 Corrected value is 4.89 m, *2 L1 level : 3.90 m from PV bottom

Table 4.2 Normarized new power curve simulating BWR average power rod heat transfer rate into coolant

NO	TIME S	NORMALIZED POWER (P/P₀)	NO	TIME S	NORMALIZED POWER (P/P₀)
1	0.0	1.0000	36	20.0	0.1104
2	0.5	0.9267	37	21.0	0.1016
3	1.0	0.8344	38	22.0	0.0929
4	1.5	0.7694	39	23.0	0.0857
5	2.0	0.7044	40	24.0	0.0784
6	2.5	0.6718	41	25.0	0.0731
7	3.0	0.6392	42	26.0	0.0677
8	3.5	0.6017	43	27.0	0.0638
9	4.0	0.5642	44	28.0	0.0599
10	4.5	0.5374	45	29.0	0.0572
11	5.0	0.5106	46	30.0	0.0545
12	5.5	0.4874	47	32.0	0.0535
13	6.0	0.4642	48	34.0	0.0526
14	6.5	0.4428	49	36.0	0.0513
15	7.0	0.4214	50	38.0	0.0498
16	7.5	0.4035	51	40.0	0.0482
17	8.0	0.3856	52	42.0	0.0473
18	8.5	0.3624	53	44.0	0.0465
19	9.0	0.3392	54	46.0	0.0457
20	9.5	0.3214	55	48.0	0.0449
21	10.0	0.3035	56	50.0	0.0440
22	10.5	0.2813	57	55.0	0.0419
23	11.0	0.2590	58	60.0	0.0398
24	11.5	0.2368	59	65.0	0.0376
25	12.0	0.2145	60	70.0	0.0355
26	12.5	0.2055	61	80.0	0.0338
27	13.0	0.1965	62	90.0	0.0321
28	13.5	0.1875	63	100.0	0.0304
29	14.0	0.1785	64	200.0	0.0290
30	14.5	0.1689	65	300.0	0.0273
31	15.0	0.1592	66	400.0	0.0255
32	16.0	0.1400	67	500.0	0.0245
33	17.0	0.1320	68	1000.0	0.0208
34	18.0	0.1240	69	2000.0	0.0170
35	19.0	0.1172	70	3000.0	0.0152

Table 4.3 Characteristics of steam discharge line valves

Valve		Close to Open	Open to Close
AV165	(Transient Line)	0.1 s	1.5 s
AV168	(Steady Line)	-	0.1 s
AV169	(ADS)	0.3 s	2.0 s

Table 4.4 Control sequence for steam line valves in RUN 992

Valves	Simulation	Before Break	After Break
CV-130	PCS	open	Control
AV-168	MSIV	open	Close by trip logic
AV-165	Break	Close	Open by break signal
AV-169	ADS	Close	Open by L1 + 120s
CV-1		Open	Close
CV-2		Open	Close

Table 5.1 Major events and test procedures of RUN 992

Time (s)	Events
-120	• Initiation of data recording
-18	• Initiation of data plotting
0.0	• Initiation of break. (QOBV & AV-165 Open)
	• Initiation of recirc. pump trip (MRP-1,2)
	• Initiation of valve closure (CV-1,2)
1.5	• Feedwater line closure (- 4s)
7.0	• Initiation of core power decrease
12	• Pressure control system (PCS) actuation
18	• Completion of PCS
21	• Downcomer water flashing
29	• Lower plenum flashing
81	• P = 5.8 MPa (for MSIV closure)
425	• Core dryout at top of av. power bundle C
455	• Core dryout at top of high power bundle A
476	• L1 level trip
594	• ADS actuation
620	• Second core dryout at top of hi. power bundle
720	• LPCI actuation
744	• PCT recorded at A-11 rod, Position 3 (649 K)
760	• Completion of core quench
1182	• Completion of data plotting
1372	• Completion of data recording

Table 5.2 Steam flow rates in MSL and total discharged steam mass for RUN 992

Time T(s)	Steam Flow Rate (kg/s)				Discharged Mass M_D (kg)*2
	W_{steady}	W_{break}	W_{ADS}	W_{total}*1	
0	2.32*3	1.18	0.0	3.50	0.0
10	1.89*4	0.96*4	"	2.85	32.
18	0.0	0.75	"	0.75	46.
50	"	0.66	"	0.66	69.
100	"	0.58	"	0.58	100.
150	"	0.51	"	0.51	127.
200	"	0.46	"	0.46	151.
250	"	0.43	"	0.43	174.
300	"	0.40	"	0.40	194.
400	"	0.36	"	0.36	232.
500	"	0.33	"	0.33	267.
594	"	0.30	0.58	0.88	296.
650	"	0.24*5	0.45*5	0.69	340.
720	"	0.20	0.37	0.57	384.
800	"	0.14	0.27	0.41	424.
850	"	0.11	0.21	0.32	442.
900	"	0.10	0.19	0.29	457.
950	"	0.09	0.17	0.26	471.
1000	"	0.08	0.15	0.23	483.
1080	"	0.07	0.13	0.20	500.

*1 Measured by orifice flow meter (FM 711 and FM 713).

*2 Time integrated total steam flow rate after the break.

*3 As steady steam line is fully opened from 29.3% to 32.9% scaled MSL flow area, initial steam flow of 2.07 kg/s increaced to 2.32 kg/s immediately after break.

*4 Total steam flow at 10 s rate is distributed by a flow ratio at T=0 s.

*5 Total steam flows after 600 s are distributed into two parts (break flow and ADS flow) by their ratio at T=594 s.

Table 5.3 Mass balance for primary fluid system in RUN 992

Time T(s)	Pressure P(MPa)	Feedwater Mass M_F(kg)	Disch. Steam Mass M_D(kg)	Inj. Water Mass M_E(kg)	Remaining Fluid Mass M(kg)	Rem. Mass Ratio M/M_o *1
0	7.36	0	0	0	651*1	1.000
18	6.58	6	46	0	611	0.939
50	6.19	6	69	0	588	0.903
100	5.50	6	100	0	557	0.856
150	5.00	6	127	0	530	0.814
200	4.62	6	151	0	506	0.777
250	4.27	6	174	0	483	0.742
300	3.99	6	194	0	463	0.711
400	3.51	6	232	0	425	0.653
500	3.11	6	267	0	390	0.599
594	2.79	6	296	0	361	0.555
650	2.20	6	340	0	317	0.487
720	1.70	9*2	384	0	276	0.424
800	1.14	12*2	424	156	395	0.607
900	0.79	21*2	457	409	624	0.959
1000	0.64	21	483	684	873	1.341
1080	0.57	21	500	912	1084	1.665

*1 Initial fluid mass in RUN 992 is modified from RUN 952 condition (M_o=708 kg) due to lower DC level.

*2 50 percent of feedwater remaining in the line is assumed to flow into PV due to flashing below 2.1 MPa.

Table 5.4 Water level and void fraction in downcomer for RUN 992

Time T (s)	Pressure P (MPa)	Fluid Density		Collapsed Level*1		Void Fraction α*2	Mixture Level L_m(m)*3
		ρ' (kg/m^3)	ρ'' (kg/m^3)	U.DC L_u(m)	L.DC L_l(m)		
0	7.36	(754)	(39)	4.89*4	3.90	0.0	4.89
18	6.58	(754)	(34)	4.82	3.86	0.0	4.82
50	6.19	755	32	4.59	3.55	0.123	4.68
100	5.50	768	28	4.57	3.44	0.161	4.69
150	5.00	778	25	4.50	3.40	0.174	4.62
200	4.62	786	23	4.40	3.39	0.177	4.50
250	4.27	793	22	4.32	3.39	0.177	4.41
300	3.99	799	20	4.25	3.39	0.177	4.32
400	3.51	810	18	4.12	3.39	0.176	4.17
500	3.11	820	15	<3.9	3.34	0.176	3.84
594	2.79	828	14	<3.9	3.18	0.176	3.65
650	2.20	844	11	4.11	2.89	0.345	4.22
720	1.70	860	9	4.09	2.86	0.355	4.19
800	1.14	881	6	4.19	2.64	0.428	4.40
900	0.79	897	4	4.51	3.04	0.292	4.76
1000	0.64	907	3	4.93	3.43	0.159	5.12
1080	0.57	911	3	5.40	3.83	0.024	5.44

*1 Level is calculated from DP data as $L = DP/(\rho' g)$.

*2 Void fraction is calculated in the lower downcomer by correcting steam mass as shown below, $DP = \rho''\alpha gH + \rho'(1-\alpha)\, gH$, $H = 2.96$ m.

*3 Level is estimated from collapsed level by assuming an uniform void distribution at each time for the whole downcomer.

*4 Frictional effect on level data is corrected at T = 0 s.

Table 5.5 Estimation of downcomer mass inventory for RUN 992

Time T(s)	Void F. α	Mix. Level L_m(m)	Remaining Fluid Mass (kg)			Ratio M_{DC}/M_{DCO}
			L.DC*1	U.DC*2	Total(M_{DC})*3	
0	0.0	4.89	86.3	142.3	235.1	1.000
18	0.0	4.82	86.3	128.5	221.1	0.940
50	0.123	4.68	75.7	91.2	174.9	0.744
100	0.161	4.69	73.7	90.2	171.1	0.728
150	0.174	4.62	73.5	79.1	159.4	0.678
200	0.177	4.50	74.0	59.6	140.5	0.598
250	0.177	4.41	74.7	45.1	126.8	0.539
300	0.177	4.32	75.2	30.3	112.3	0.478
400	0.176	4.17	76.4	14.4	97.2	0.413
500	0.176	3.84	73.4	0.0	79.1	0.336
594	0.176	3.65	61.5	0.0	67.0	0.285
650	0.345	4.22	63.2	14.2	81.6	0.347
720	0.355	4.19	63.5	12.9	79.8	0.339
800	0.428	4.40	57.6	33.5	93.3	0.397
900	0.292	4.76	72.7	99.3	173.1	0.736
1000	0.159	5.12	87.3	202.6	290.4	1.235
1080	0.024	5.44	101.7	327.6	429.3	1.826

*1 Water Mass is calculated as $M = \rho'(1-\alpha)V_1$ for $L_m \geq 3.90$ m and $M = \rho'(1-\alpha)V_1 - \rho' A_1(3.90-L_m)$, for $3.50 \leq L_m < 3.90$ m where $V_1 = 0.1144$ m^3 and $A_1 = 0.0801$ m^2.

*2 Water Mass is similarly calculated depending on the mixture level height and corresponding downcomer flow area. $V_u = 0.3560$ m^3.

*3 Steam mass in downcomer ($V = 0.470 m^3$) is added and $M_{DCO} = 235.1$ kg.

Table 5.6 Estimation of fluid mass in jetpumps and recirculation loops for RUN 992

Time T(s)	Jet Pumps*1			Rec. Loops*2			Total Mass M_L*3	Mass Ratio M_L/M_{LO}
	-PD41 (kPa)	α_1 (-)	M_1 (kg)	PD37 (kPa)	α_2 (-)	M_2 (kg)		
0	-	0.0	48.0	-	0.0	81.7	129.7	1.000
18	-	0.0	48.0	-	0.0	81.7	129.7	1.000
50	15.0	0.055	45.4	40.4	0.061	76.8	122.5	0.945
100	13.3	0.181	40.1	35.5	0.194	67.0	108.0	0.833
150	13.3	0.191	40.1	35.7	0.199	67.5	108.4	0.836
200	13.3	0.199	40.1	35.8	0.205	67.7	108.6	0.837
250	13.3	0.206	40.1	36.4	0.198	68.9	109.8	0.846
300	13.3	0.212	40.1	36.9	0.192	69.9	110.7	0.853
400	13.5	0.210	40.8	37.1	0.199	70.3	111.7	0.861
500	13.1	0.243	39.5	37.3	0.203	70.8	110.9	0.855
594	12.9	0.262	38.9	35.7	0.246	67.6	107.1	0.826
650	8.6	0.521	25.8	27.1	0.441	51.1	77.8	0.600
720	6.1	0.669	18.1	27.5	0.442	52.0	70.9	0.547
800	9.2	0.506	27.7	15.1	0.703	28.3	56.7	0.437
900	12.0	0.364	36.3	16.8	0.673	31.8	68.5	0.528
1000	19.1	0.0	57.8	22.9	0.558	43.4	101.4	0.782
1080	19.6	0.0	58.0	28.2	0.457	53.6	111.7	0.862

*1 Total fluid volume (V_1) is 0.0637 m^3. Void fraction (α) is calculated from (-PD41) by assuming no frictional loss and using a following relation, $-PD41 = gH_1 \{\rho''\alpha_1 + \rho'(1-\alpha_1)\}$, where H_1 = 2.14 m. Water mass is calculated as $M_1 = \rho'(1-\alpha_1) V_1$.

*2 Total fluid volume (V_2) is 0.1083 m^3. Void fraction is calculated in the MRP discharge line (PD37) as a representative. H_2 is 5.80 m. Water mass is calculated as, $M_2 = \rho' (1-\alpha_2) V_2$.

*3 Steam mass in the mixture is included and M_{LO}= 129.7 kg.

Table 5.7 Fluid mass distribution in total system for RUN 992

Time T(s)	Total Mass M(kg)	JPs and Loops		Downcomer		In-Shroud & SD		
		Mass M_L(kg)	$\frac{M_L}{M}$	Mass M_{DC}(kg)	$\frac{M_{DC}}{M}$	Mass*1 M_C(kg)	$\frac{M_C}{M}$	Ratio (M_C/M_{CO})*
0	651	130	0.200	235	0.361	286	0.439	1.000
18	611	130	0.213	221	0.362	260	0.425	0.909
50	588	123	0.207	175	0.298	290	0.493	1.014
100	577	108	0.187	171	0.296	298	0.517	1.042
150	530	108	0.204	159	0.300	263	0.496	0.920
200	506	109	0.215	141	0.279	256	0.506	0.895
250	483	110	0.228	127	0.263	246	0.509	0.860
300	463	111	0.240	112	0.242	240	0.518	0.839
400	425	112	0.264	97	0.228	216	0.508	0.755
500	390	111	0.285	79	0.203	200	0.512	0.699
594	361	107	0.296	67	0.186	187	0.518	0.654
650	317	78	0.246	82	0.259	157	0.495	0.549
720	276	71	0.257	80	0.290	125	0.453	0.437
800	395	57	0.144	93	0.235	245	0.621	0.857
900	624	69	0.111	173	0.277	382	0.612	1.336
1000	873	101	0.116	290	0.332	482	0.552	1.685
1080	1084	112	0.103	429	0.396	543	0.501	1.899

*1 Fluid mass including steam mass inside core-shroud and steam dome is calculated by a following relation, as $M_C = M - M_L - M_{DC}$.

*2 M_{CO} = 286 kg.

Table 5.8 Transient mass and pressure for RUN 992

Time	Pressure		Total Mass*1		Shroud Mass*2	
T(s)	P(MPa)	P/P_0	M(kg)	M/M_0	M_C(kg)	M_C/M_0
0	7.36	1.000	651	1.000	286	0.439
18	6.58	0.894	611	0.939	260	0.399
50	6.19	0.841	588	0.903	290	0.445
100	5.50	0.747	557	0.856	298	0.458
150	5.00	0.679	530	0.814	263	0.404
200	4.62	0.628	506	0.777	256	0.393
250	4.27	0.580	483	0.742	246	0.378
300	3.99	0.542	463	0.711	240	0.369
400	3.51	0.477	425	0.653	216	0.332
500	3.11	0.423	390	0.599	200	0.307
594	2.79	0.379	361	0.555	187	0.287
650	2.20	0.299	317	0.487	157	0.241
720	1.70	0.231	276	0.424	125	0.192
800	1.14	0.155	395	0.607	245	0.376
900	0.79	0.107	624	0.959	382	0.587
1000	0.64	0.087	873	1.341	482	0.740
1080	0.57	0.077	1084	1.665	543	0.834

*1 Includes steam mass.

*2 Fluid mass inside core-shroud and steam dome above top of separator.

Table 5.9 Pressure balance inside core-shroud for RUN 992

Time T(s)	PD21 (kPa)	PD22 (kPa)	PD25 (kPa)	PD21+PD22 (kPa)	PD25-PD21-PD22 (kPa)
0	37.9	45.4	85.0	83.3	1.7
18	24.6	3.2	30.7	27.8	2.9
50	25.0	6.1	32.3	31.1	1.2
100	24.6	2.8	28.0	27.4	0.6
150	24.0	2.2	28.0	26.2	1.8
200	24.0	1.3	26.9	25.3	1.6
250	23.9	1.1	27.1	25.0	2.1
300	23.8	1.1	25.7	24.9	0.8
350	23.0	1.1	25.7	24.1	1.6
400	22.1	1.0	24.6	23.1	1.5
450	20.9	1.0	23.3	21.9	1.4
500	19.8	0.8	22.1	20.6	1.5
550	19.1	0.6	20.7	19.7	1.0
594	18.1	0.7	20.9	18.8	2.1
650	16.1	1.1	18.6	17.2	1.4
720	13.6	0.6	15.3	14.2	1.1
800	23.1	-0.1	25.0	23.0	2.0
900	33.9	-0.2	34.7	33.7	1.0
1000	36.5	5.4	44.9	41.9	3.0
1080	38.2	10.9	50.4	49.1	1.3

Elevation change for the DP measurements are PD21 : 4.06m, PD22 : 1.89 m and PD25 : 5.95 m.

Table 5.10 Pressure balance in PV for RUN 992

Time T(s)	PD25 (kPa)	DP through JP and Downcomer (kPa)					Difference*1 (kPa)
		-PD41	PD26	-PD39	PD56	Total	
0	85.0	15.0	77.2	-20.4	14.3	86.1	-1.1
18	30.7	15.0	0.0	-2.9	14.5	26.6	4.1
50	32.3	13.3	1.2	-0.2	12.5	26.8	5.5
100	28.0	13.3	-0.3	-0.2	12.1	24.9	3.1
150	28.0	13.3	-0.3	-0.2	11.5	24.3	3.7
200	26.9	13.3	-0.8	-0.2	11.0	23.3	3.6
250	27.1	13.3	-0.8	-0.1	10.4	22.8	4.3
300	25.7	13.3	-0.8	-0.1	9.9	22.3	3.4
350	25.7	13.3	-0.8	-0.1	9.7	22.1	3.6
400	24.6	13.5	-1.0	-0.1	9.0	21.4	3.2
450	23.3	13.5	-1.0	-0.1	8.0	20.4	2.9
500	22.1	13.1	-1.0	0.0	7.2	19.3	2.8
550	20.7	13.0	-1.1	0.0	6.5	18.4	2.3
594	20.9	12.9	-1.5	0.0	5.8	17.2	3.7
650	18.6	8.6	-0.9	0.2	7.4	15.3	3.3
720	15.3	6.1	-1.2	0.2	7.3	12.4	2.9
800	25.0	9.2	3.8	2.3	8.5	23.8	1.2
900	34.7	12.0	4.6	3.3	13.0	32.9	1.8
1000	44.9	19.1	4.5	1.7	17.8	43.1	1.8
1080	50.4	19.6	4.6	0.5	24.0	48.7	1.7

*1 Difference is PD25 - (-PD41 + PD26 - PD39 + PD56).

Elevation change for each DP data is,

PD25 : 5.94 m, PD41 : -2.14 m, PD26 : 0.57 m

PD39 : 0.0 m, PD56: 3.23 m.

Table 5.11 PCT list for RUN 992

** Order of PCT (RUN 992) **

No. 1	A-11 rod	Pos. 3	PCT =	648.7 (K)	Time =	744.0 (s)
No. 2	A-22 rod	Pos. 3	PCT =	636.7 (K)	Time =	742.8 (s)
No. 3	A-88 rod	Pos. 3	PCT =	634.3 (K)	Time =	744.0 (s)
No. 4	A-87 rod	Pos. 3	PCT =	632.4 (K)	Time =	740.4 (s)
No. 5	A-11 rod	Pos. 2	PCT =	631.9 (K)	Time =	750.0 (s)
No. 6	A-12 rod	Pos. 3	PCT =	630.7 (K)	Time =	742.8 (s)
No. 7	A-13 rod	Pos. 3	PCT =	628.3 (K)	Time =	740.4 (s)
No. 8	A-77 rod	Pos. 3	PCT =	620.9 (K)	Time =	742.8 (s)
No. 9	A-22 rod	Pos. 2	PCT =	619.9 (K)	Time =	746.4 (s)
No.10	A-12 rod	Pos. 2	PCT =	612.7 (K)	Time =	745.2 (s)

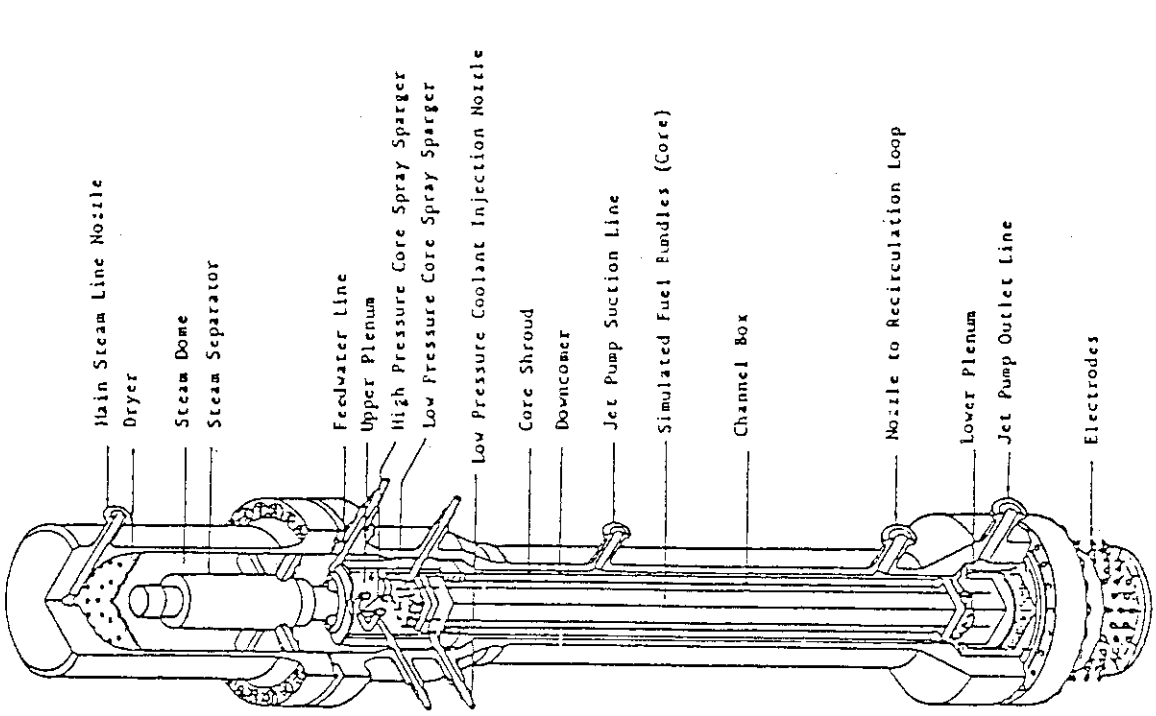

Fig. 2.2 Internal structure of pressure vessel of ROSA-III

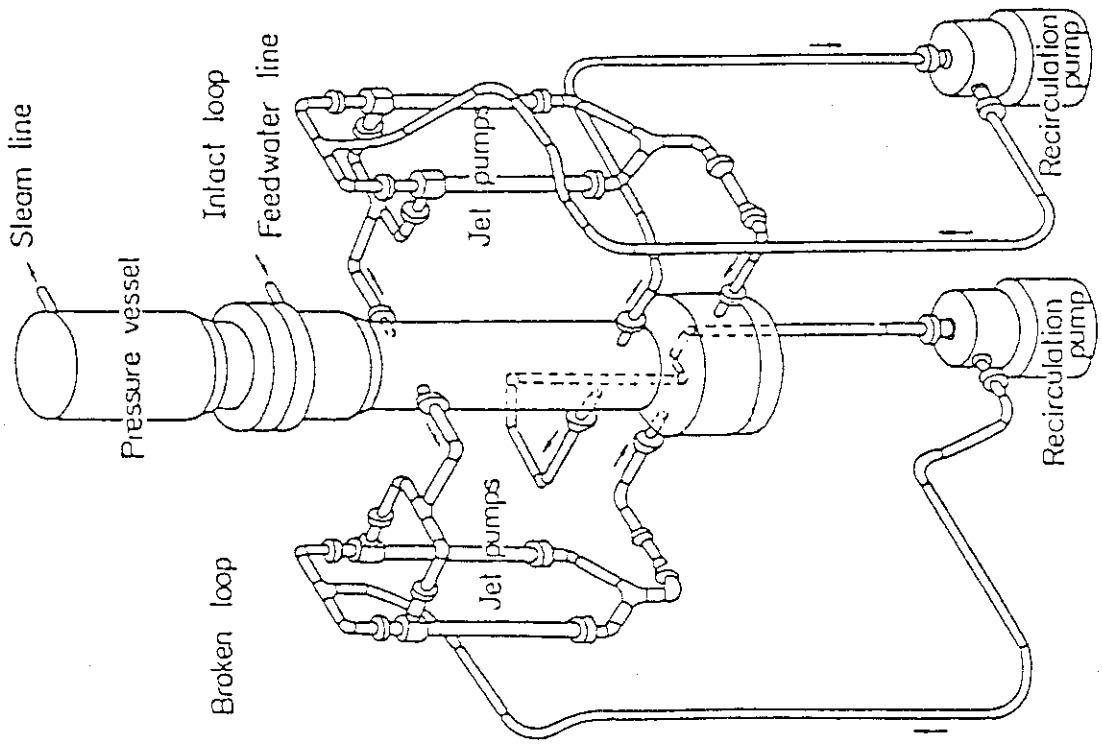

Fig. 2.1 Schematic diagram of ROSA-III test facility

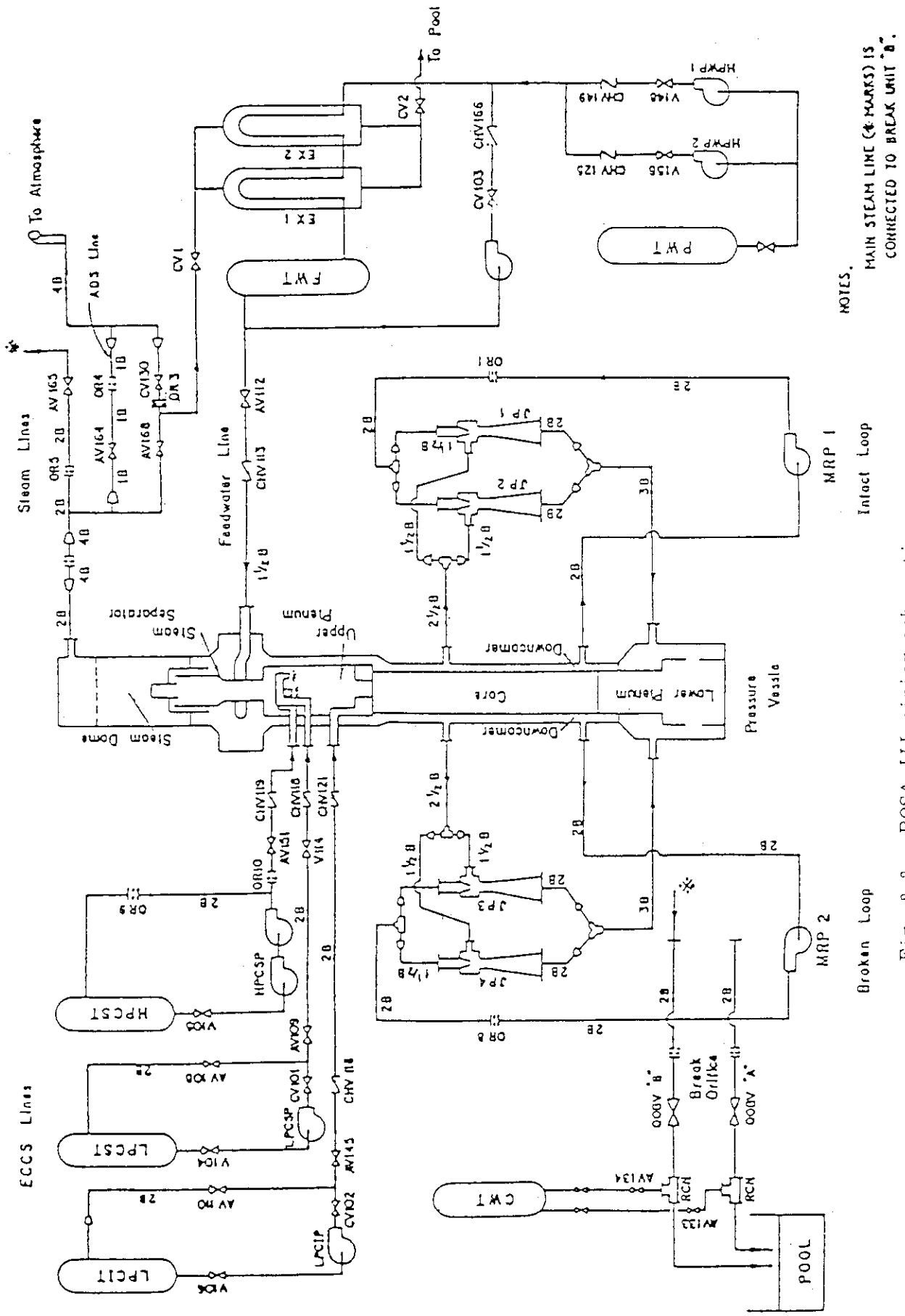

Fig. 2.3 ROSA-III piping schematic

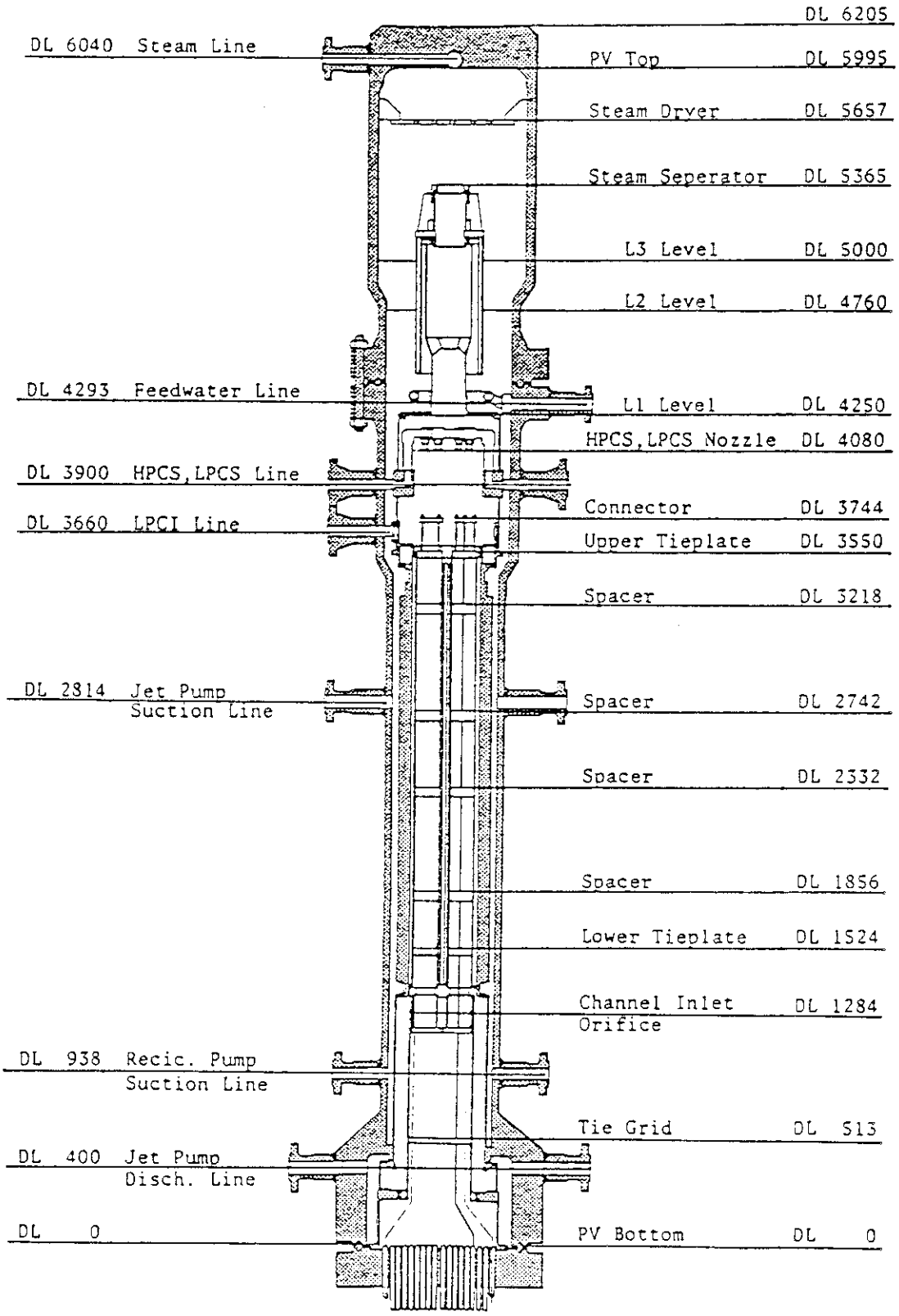

Fig. 2.4 Pressure vessel internals arrangement

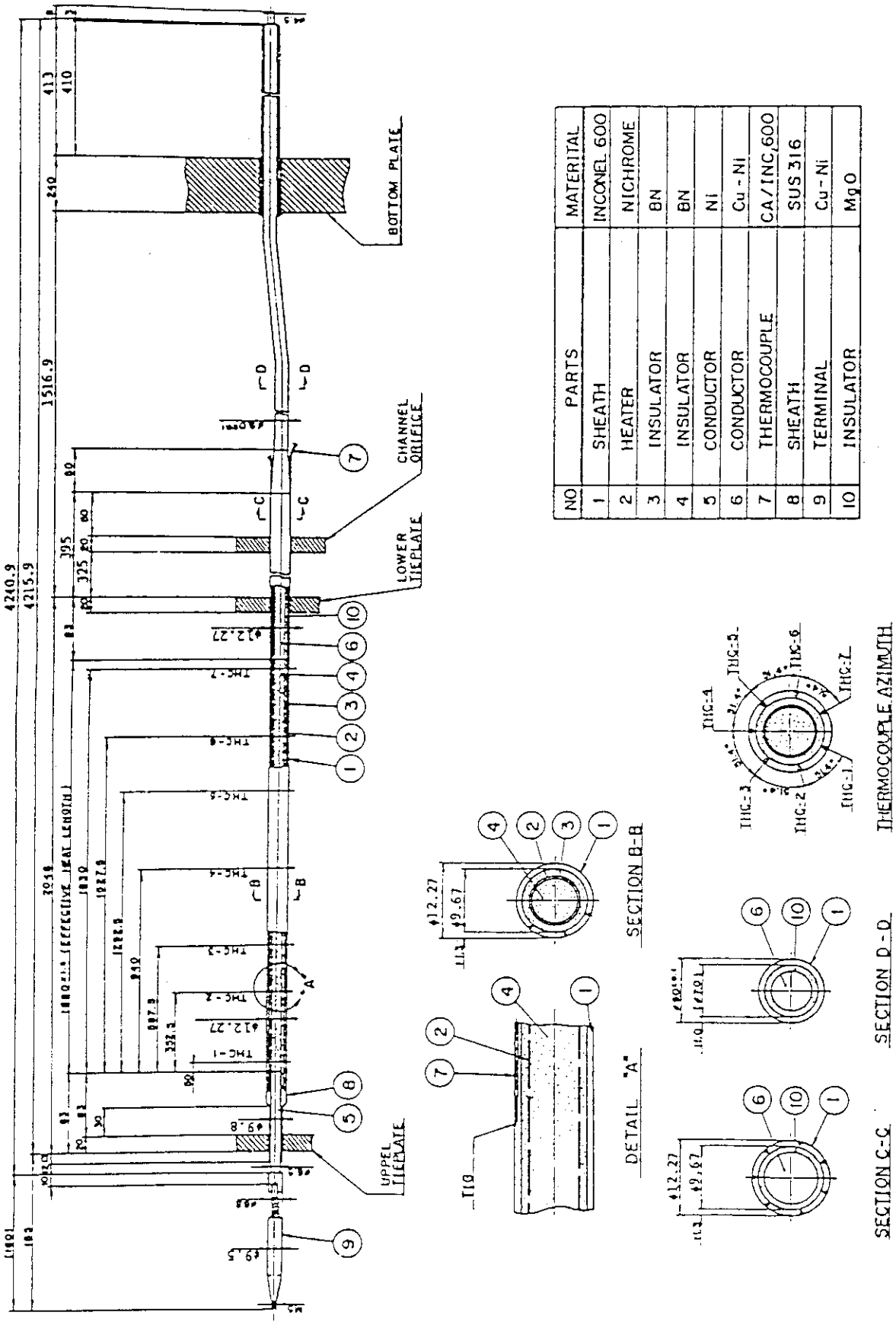

NO	PARTS	MATERITAL
1	SHEATH	INCONEL 600
2	HEATER	NICHROME
3	INSULATOR	BN
4	INSULATOR	BN
5	CONDUCTOR	Ni
6	CONDUCTOR	Cu - Ni
7	THERMOCOUPLE	CA/INC,600
8	SHEATH	SUS 316
9	TERMINAL	Cu - Ni
10	INSULATOR	MgO

Fig. 2.5 Simulated fuel rod of ROSA-III

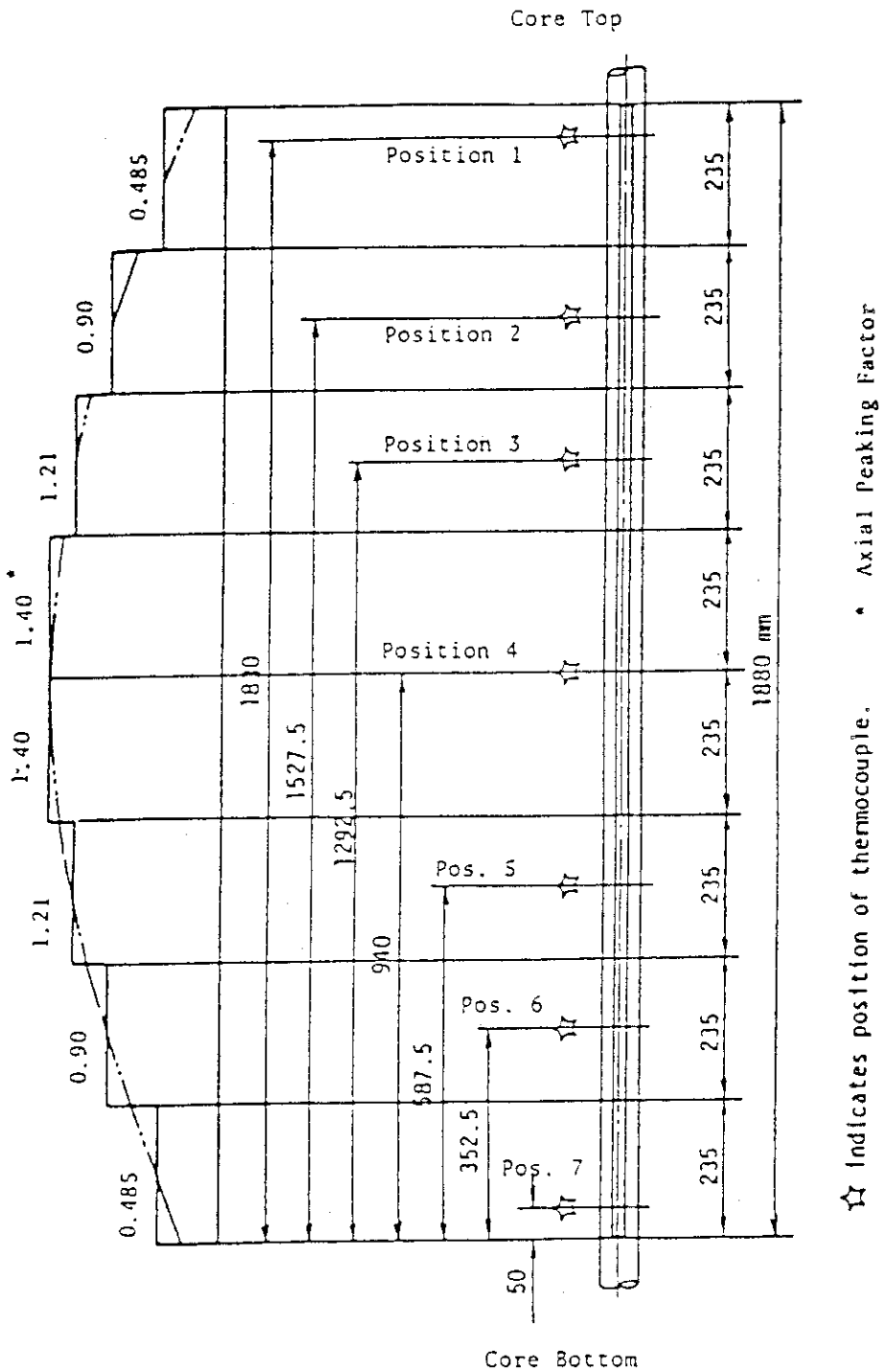

Fig. 2.6 Axial power distribution of heater rod

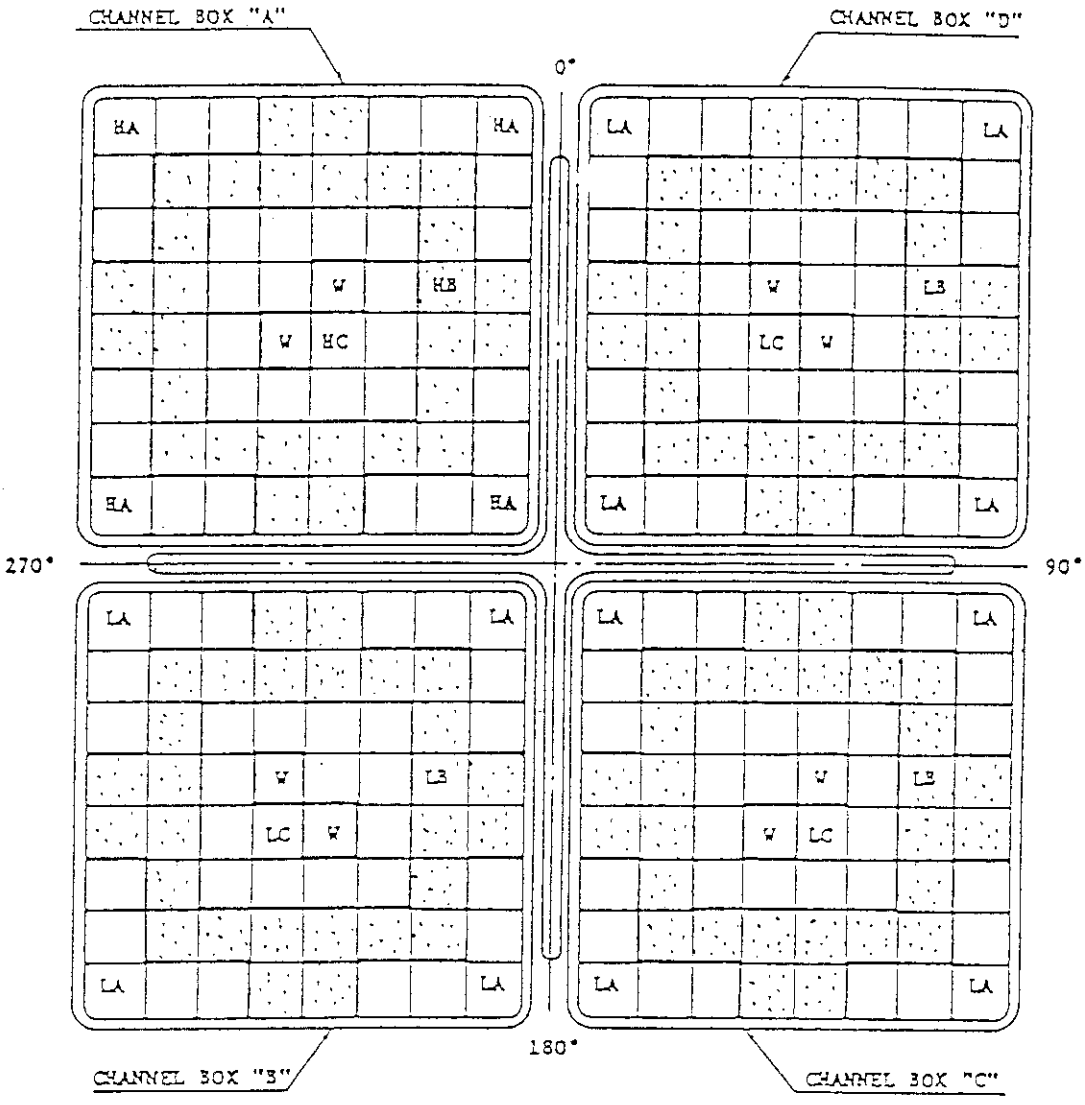

Region	HA	HB	HC	LA	LB	LC	W
Lenear Heac Rate (kW/m)	18.5	16.81	14.41	13.21	12.01	10.29	0.0
Local peaking factor	1.1	1.0	0.875	1.1	1.0	0.875	0.0
No. of Rods	20	28	14	60	84	42	8

* note : Radial peaking factor is 1.4

Fig. 2.7 Radial and local power distribution in core

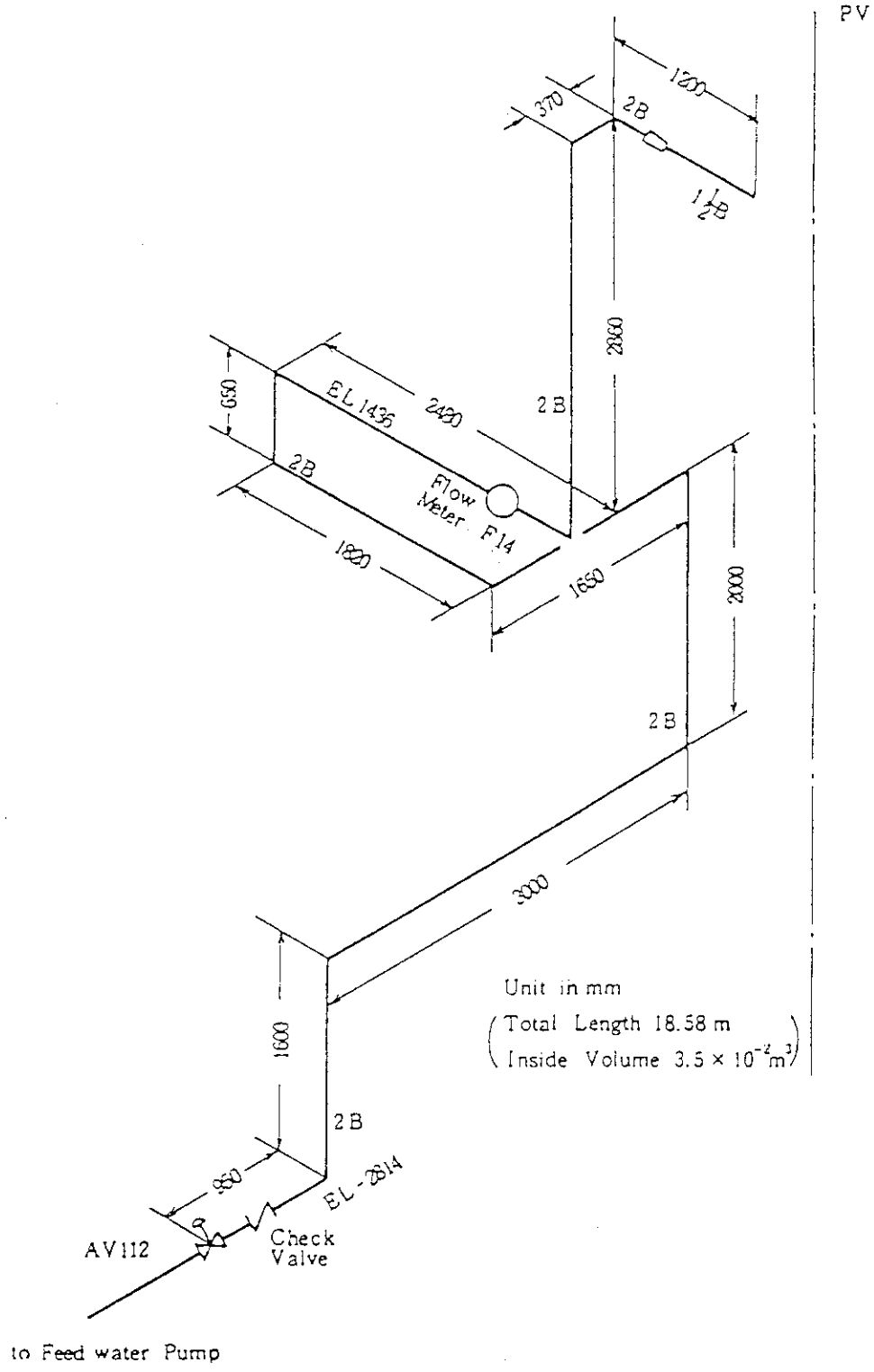

Fig. 2.8 Feedwater line between PV and AV-112

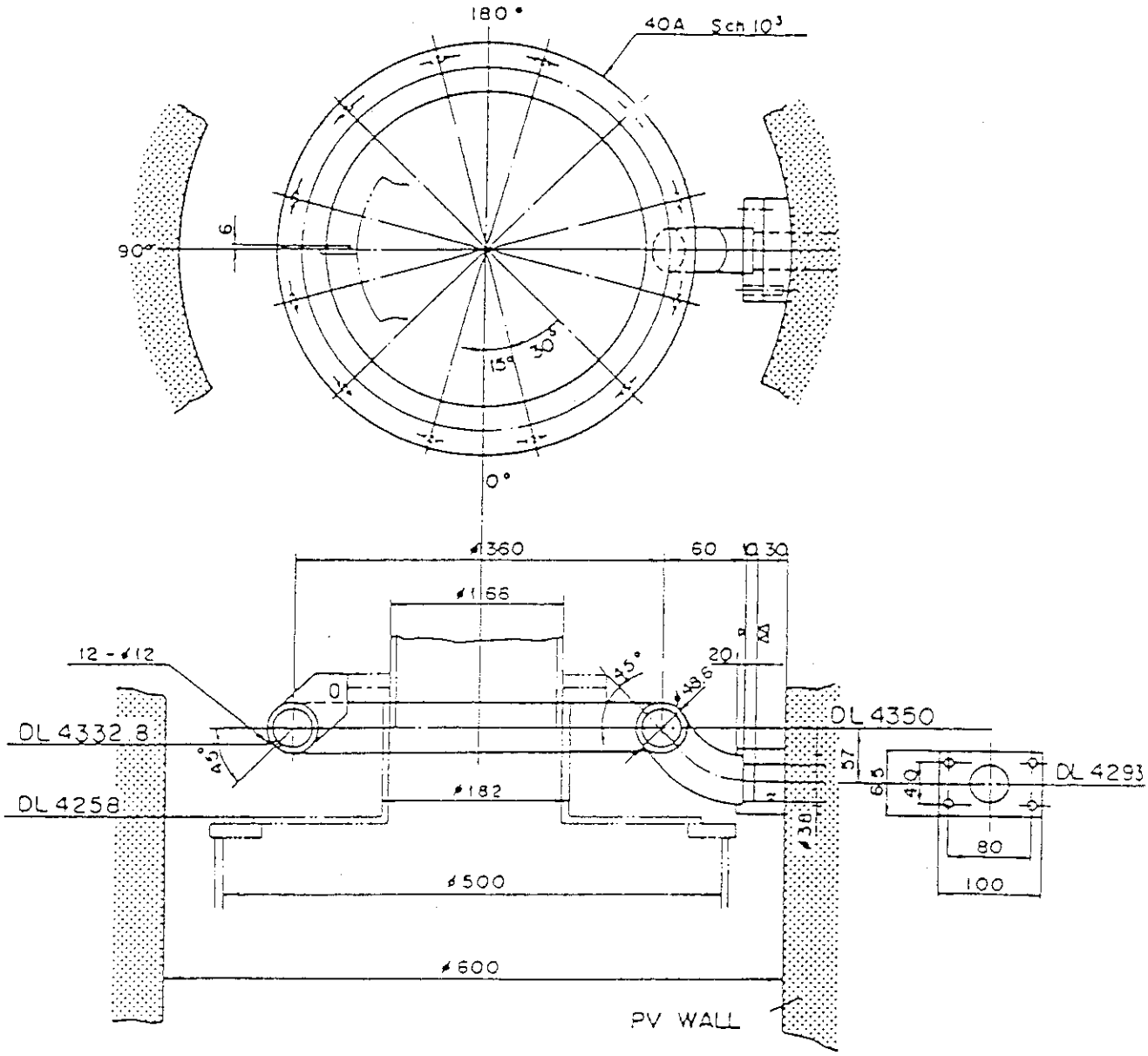

Fig. 2.9 Feedwater sparger configuration

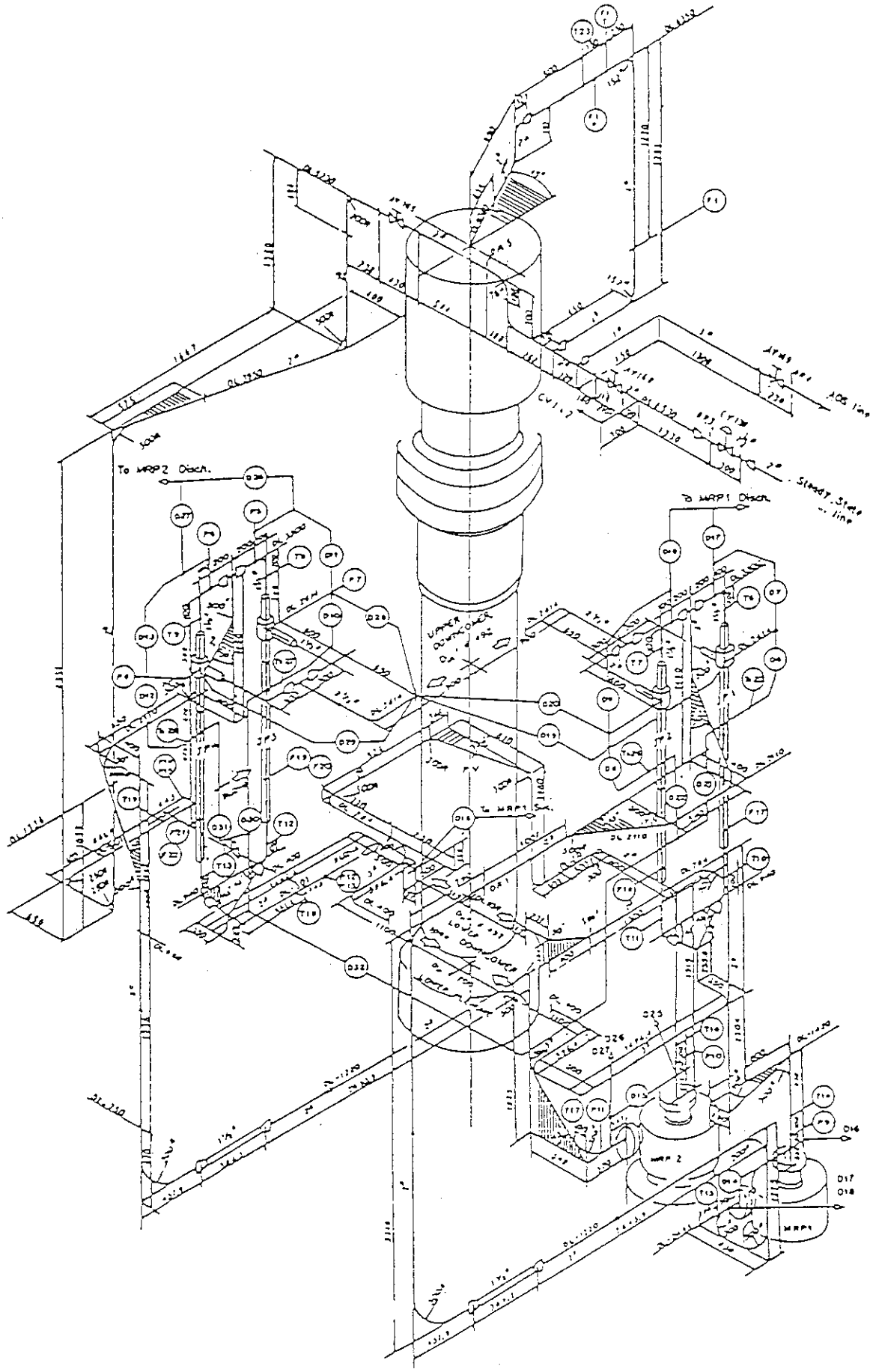

Fig. 2.10 Details of ROSA-III system piping

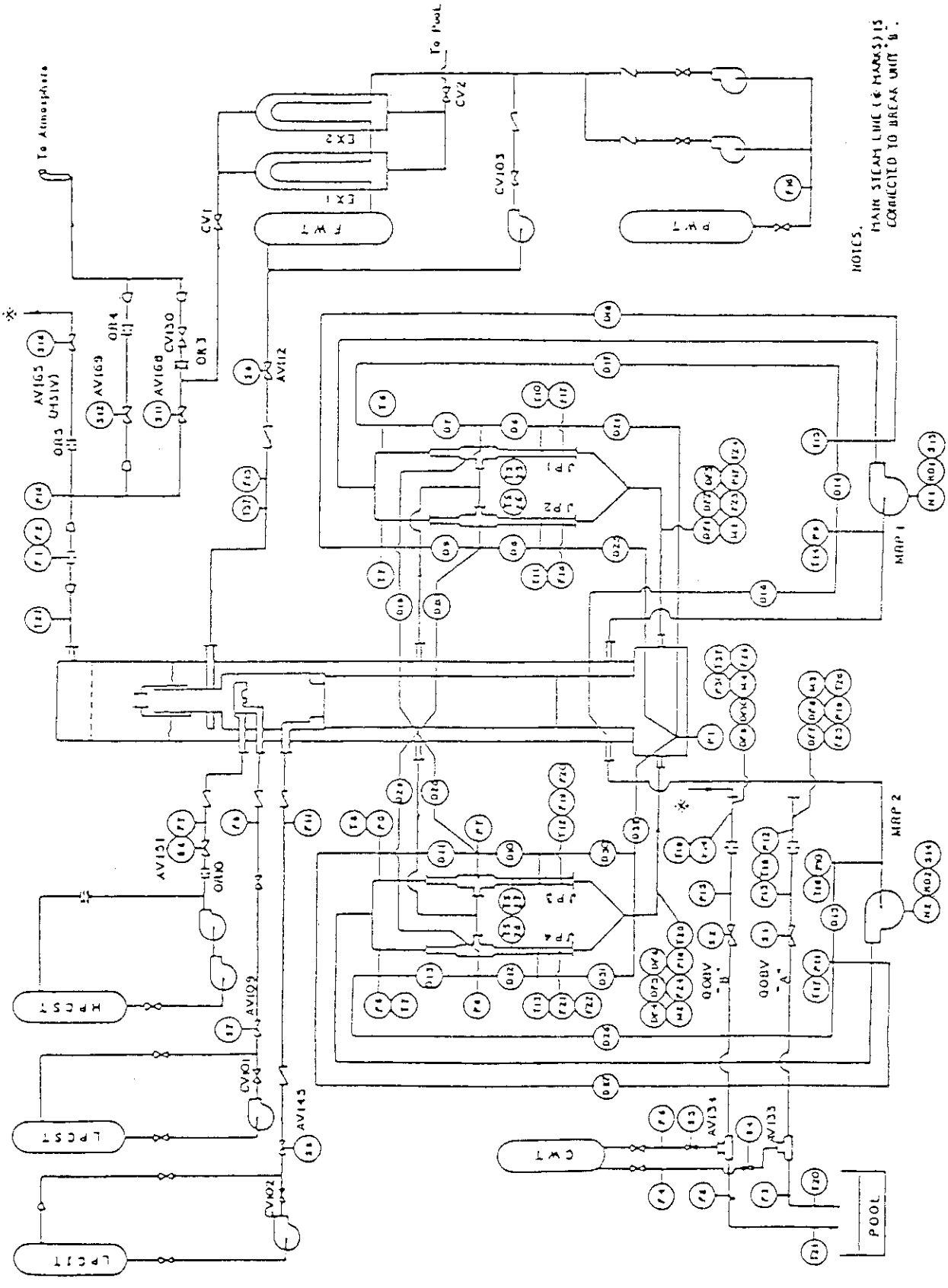

Fig. 3.1 Instrumentation location of ROSA-III test facility

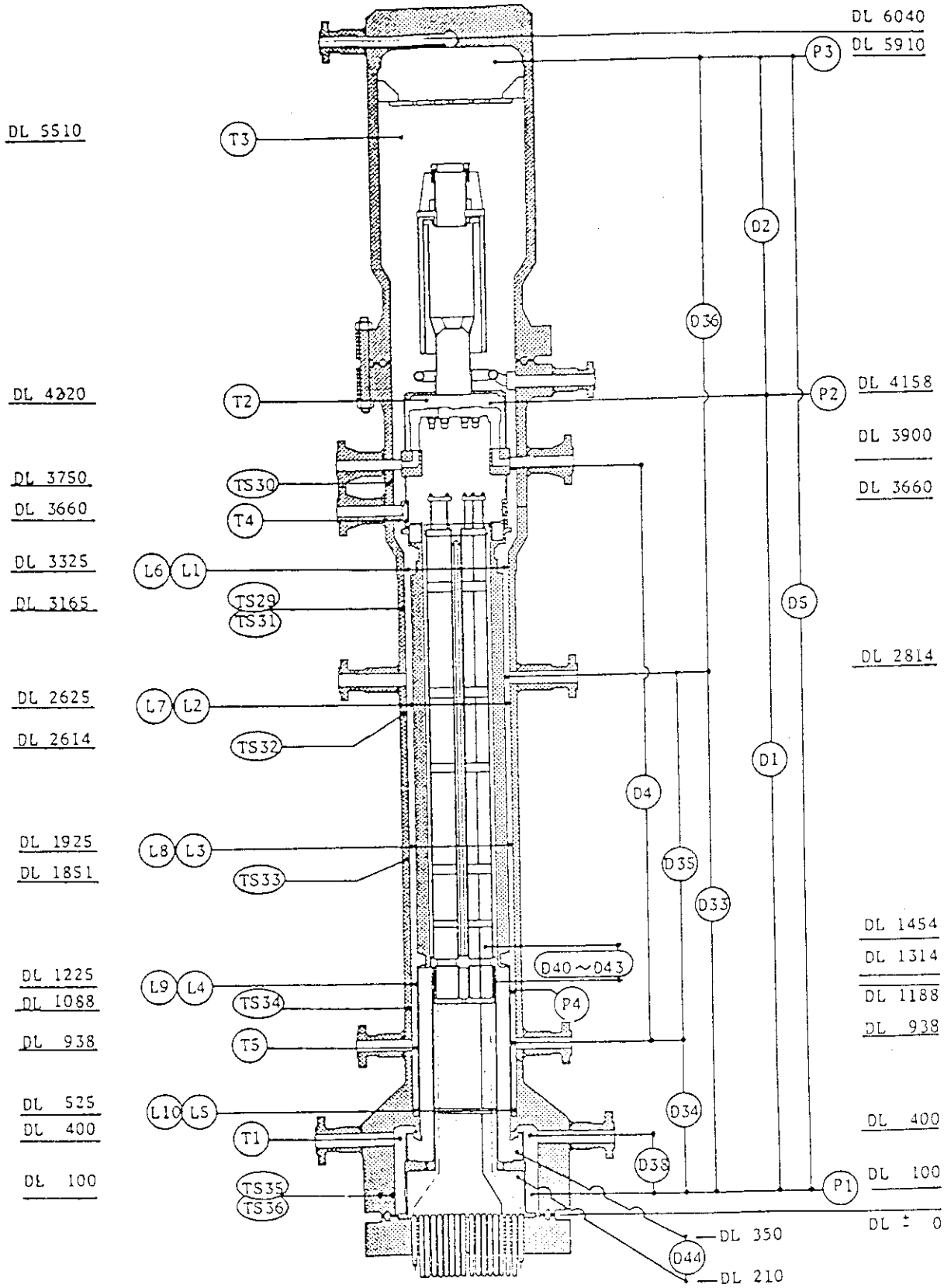

Fig. 3.2 Instrumentation location in pressure vessel

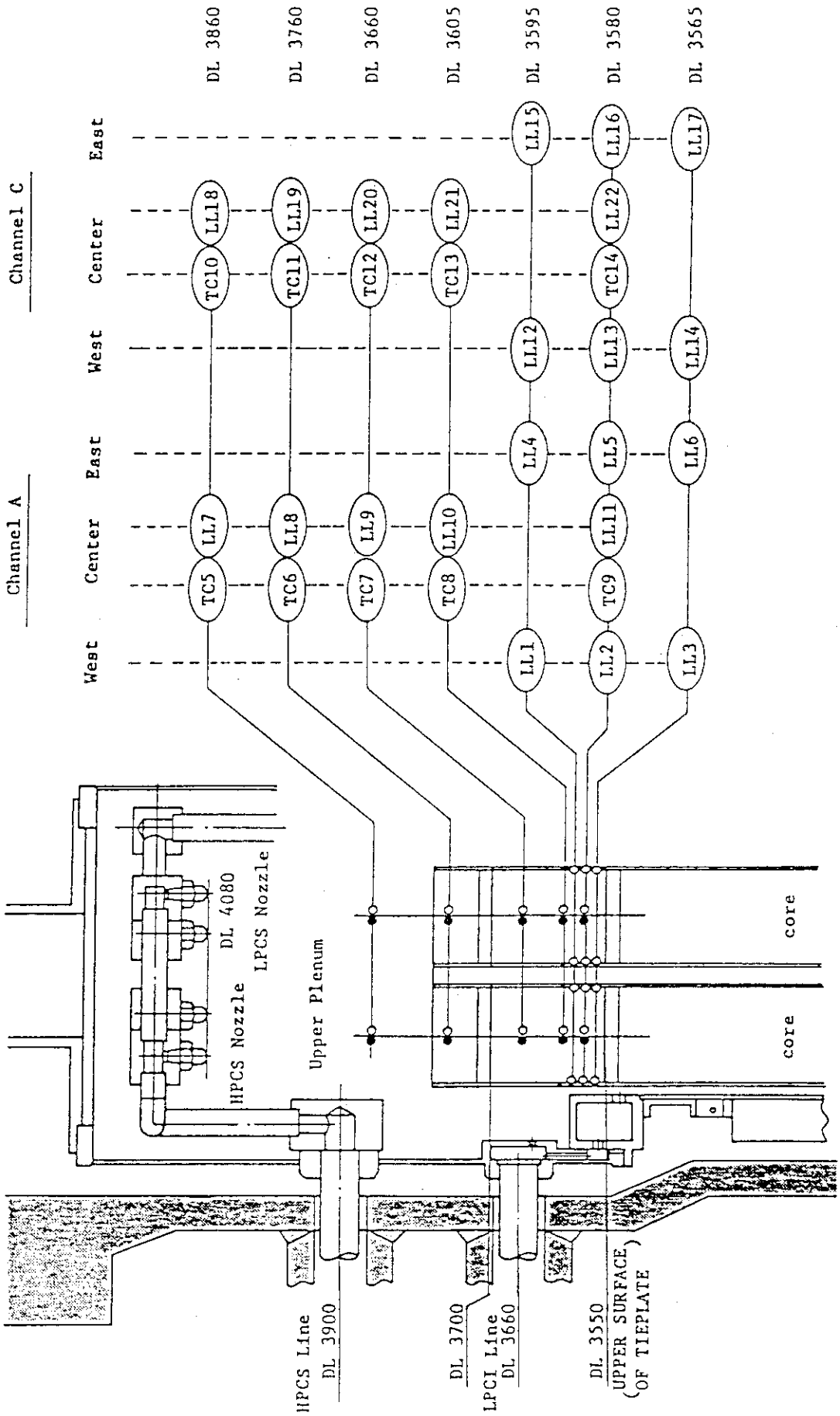

Fig. 3.3 Upper plenum instrumentations

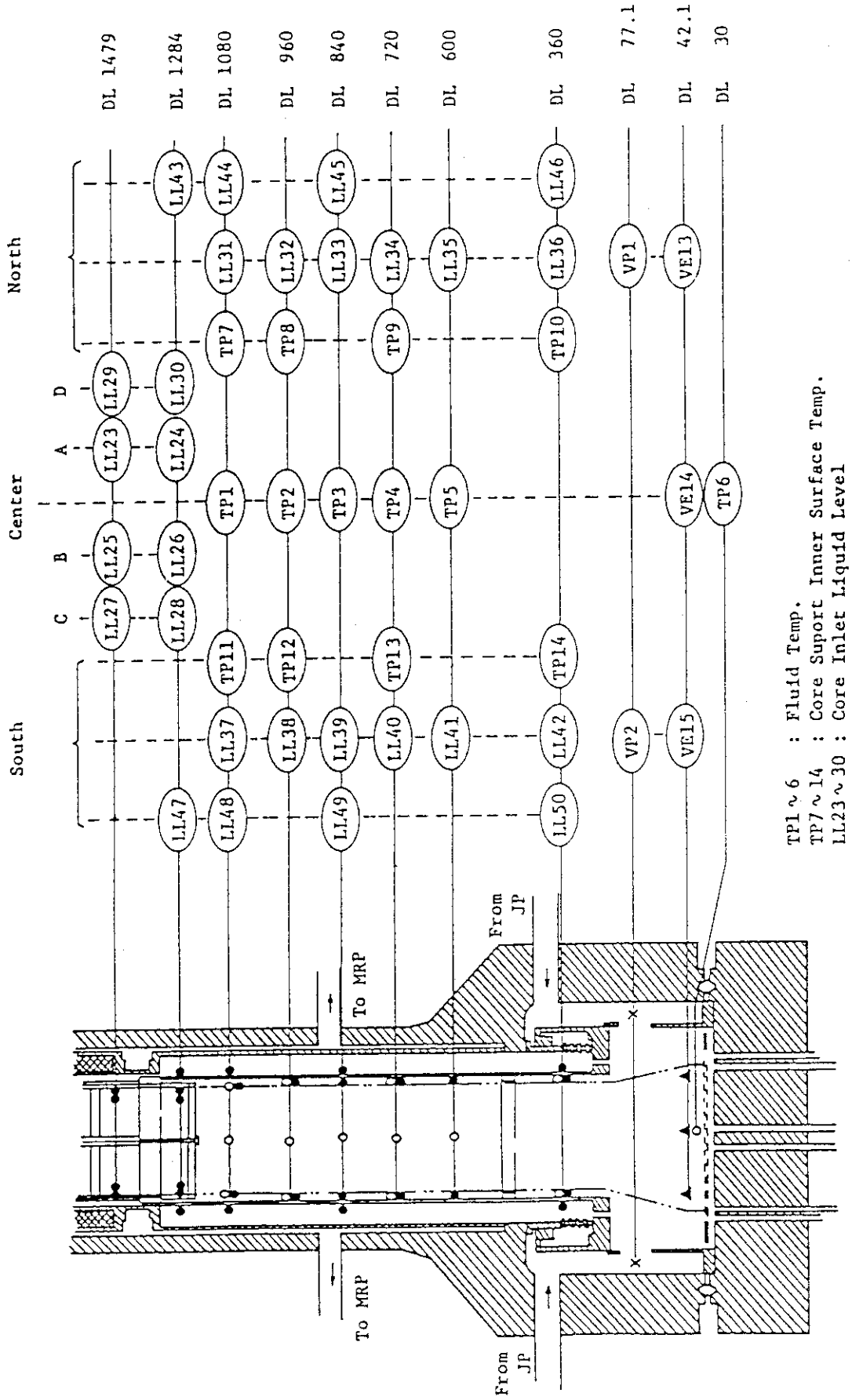

Fig. 3.4 Lower plenum instrumentations

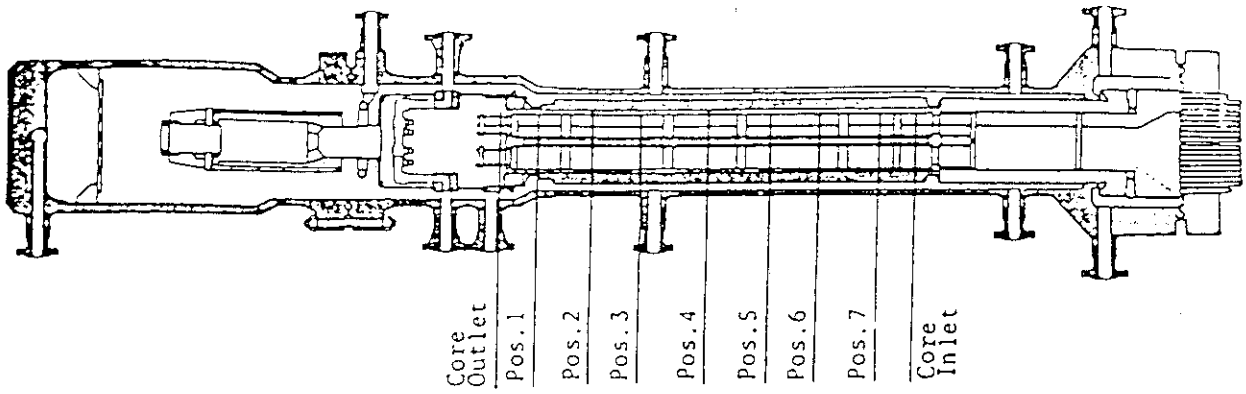

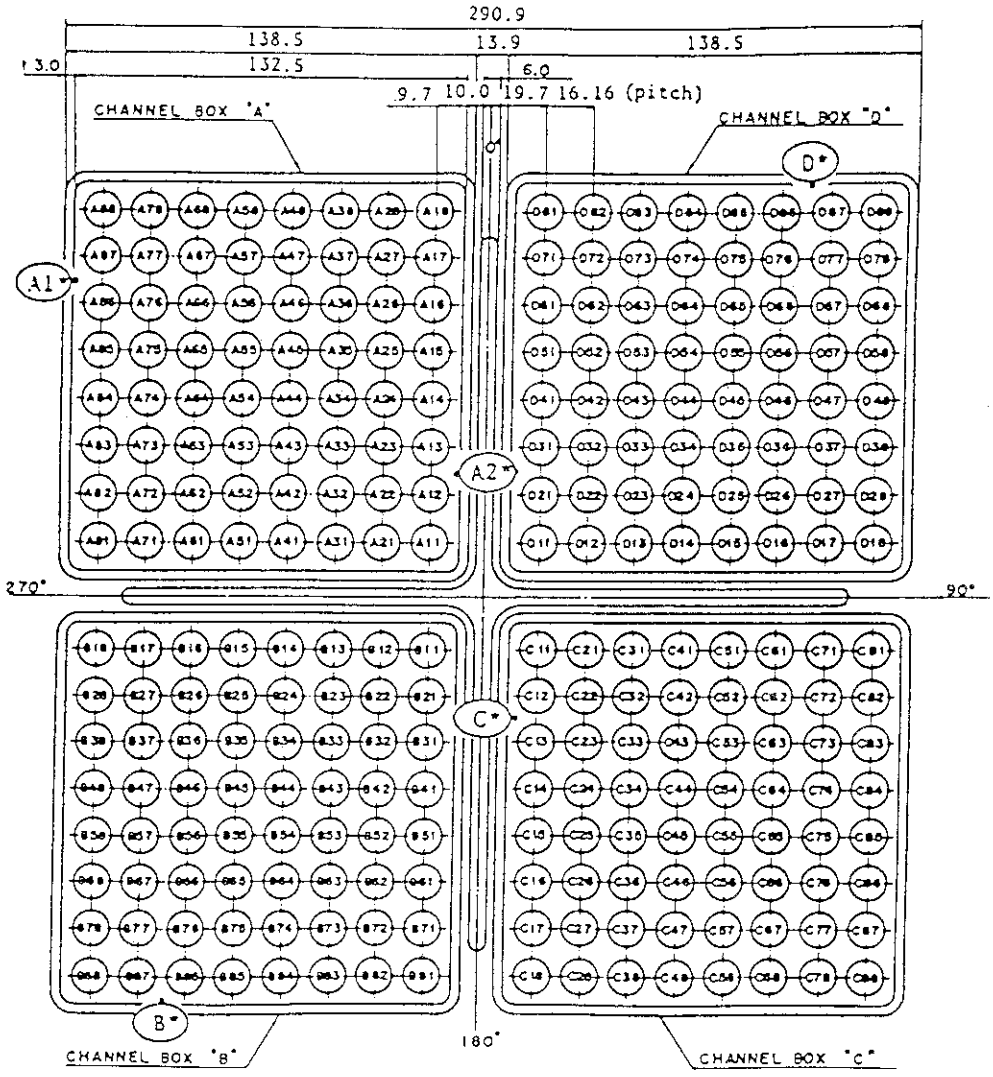

Heater rod O.D. is 12.27mm

A54,B54,C54 and D54 are water rod simulators with void probes, O.D.= 15.01mm

A45,B45,C45 and D45 are water rod simulators with thermocouples, O.D.= 15.01mm

Fig. 3.5 Core instrumentation (cf. Table A.3)

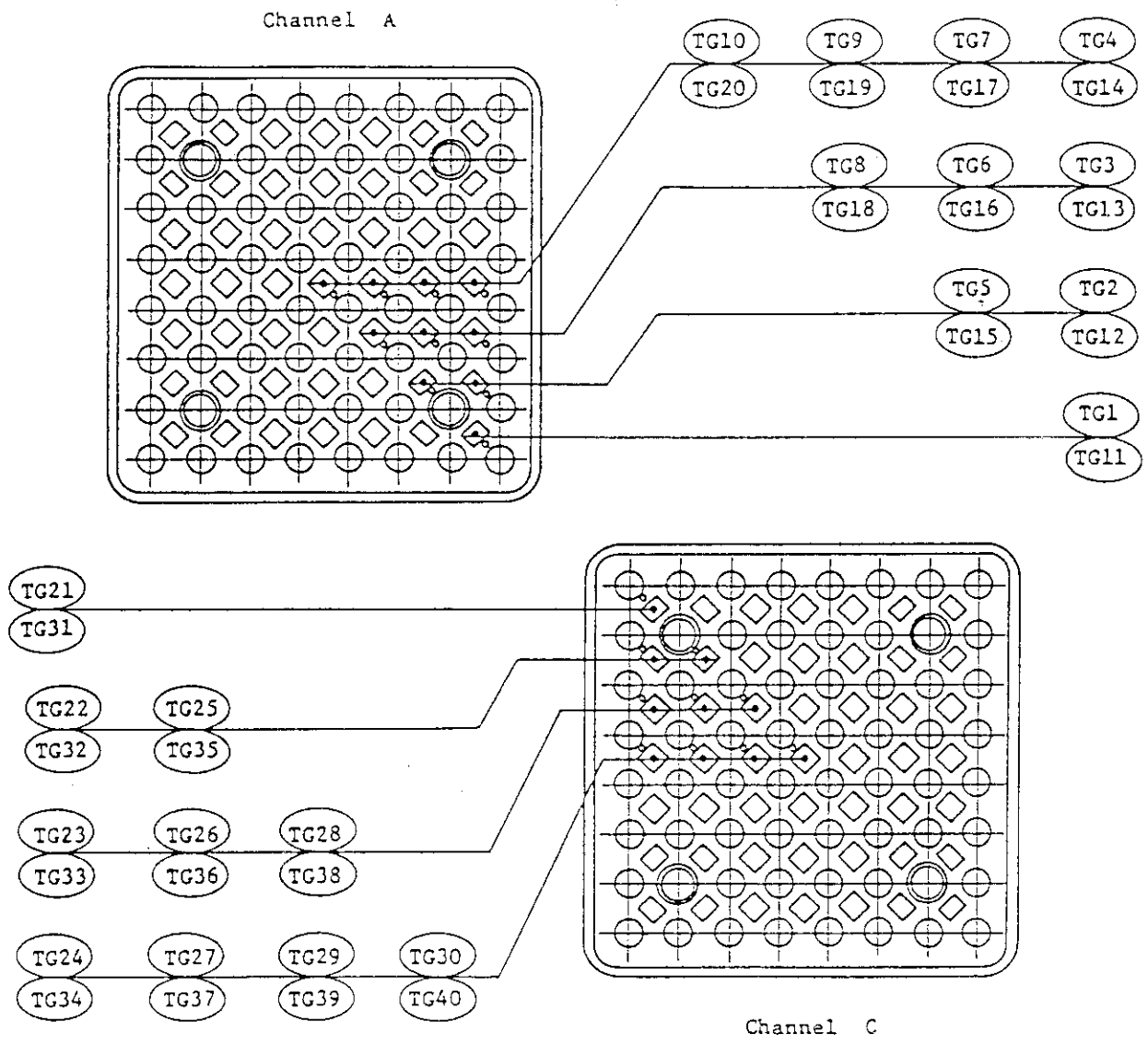

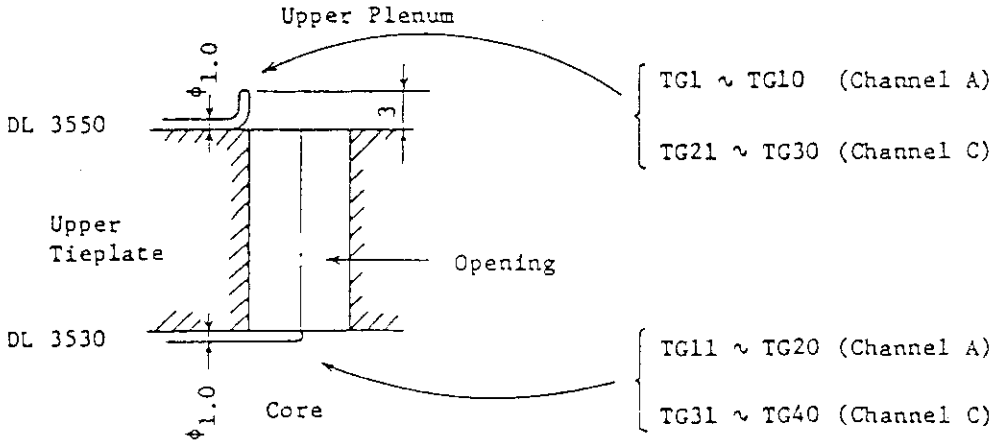

Fig. 3.6 Upper tieplate instrumentations

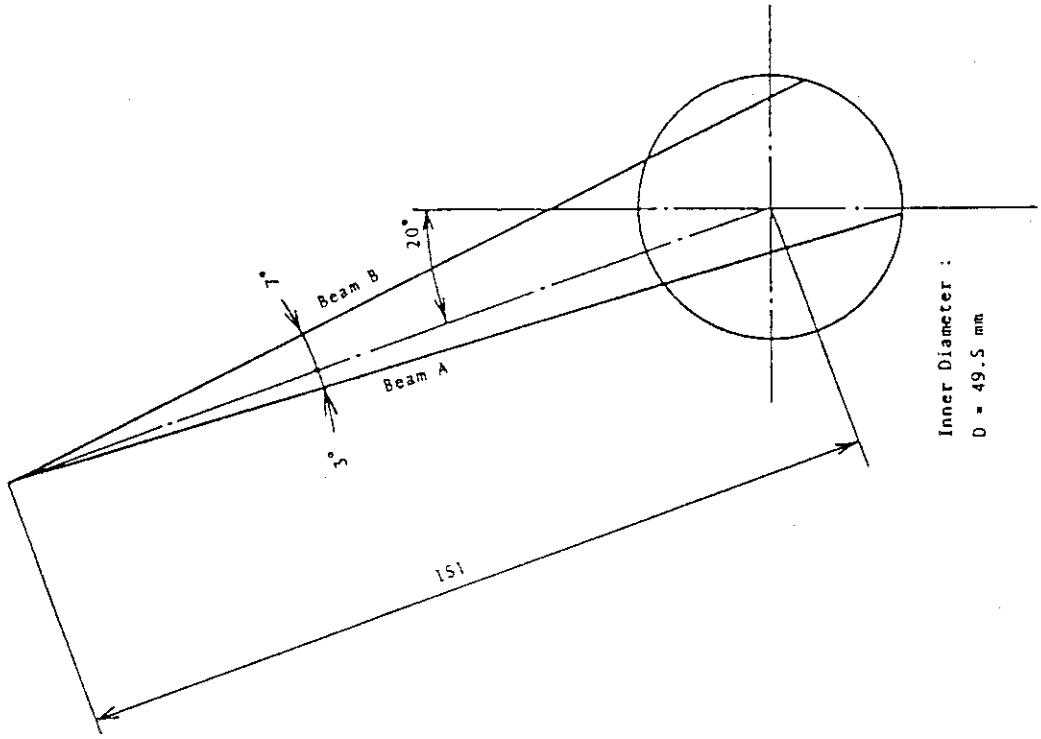

Fig. 3.8 Beam configuration of two-beam gamma densitometer

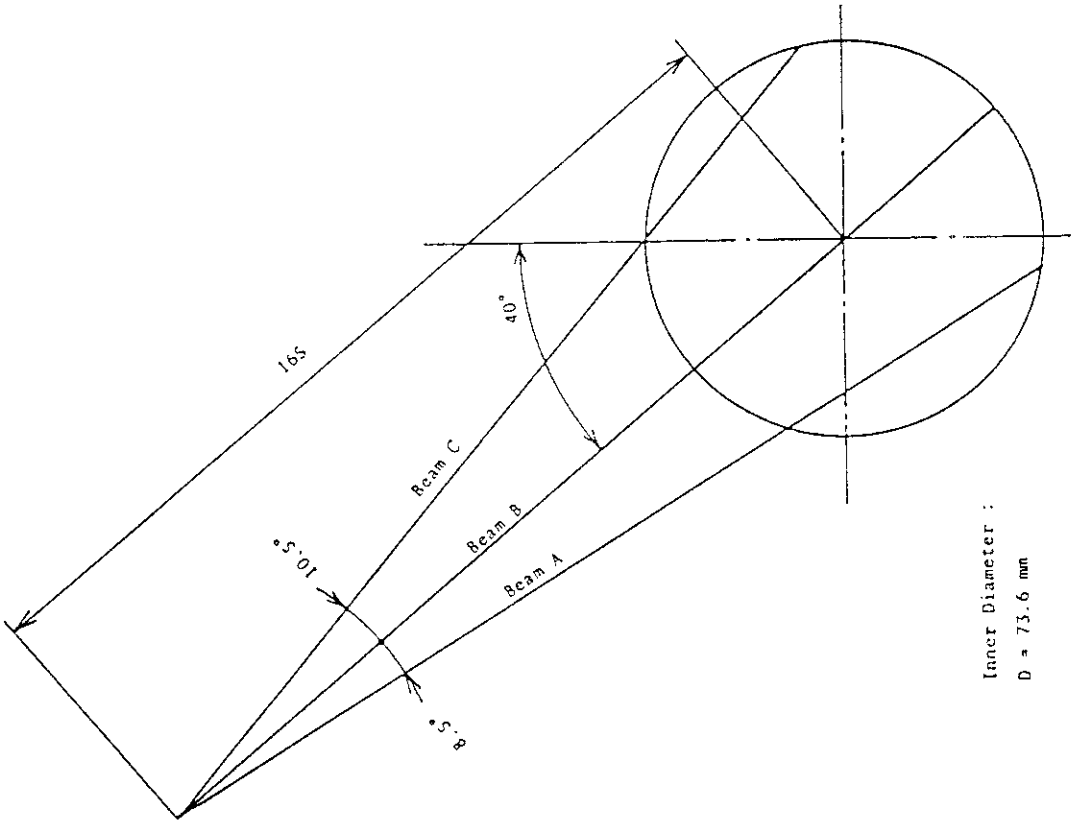

Fig. 3.7 Beam configuration of three-beam gamma densitometer

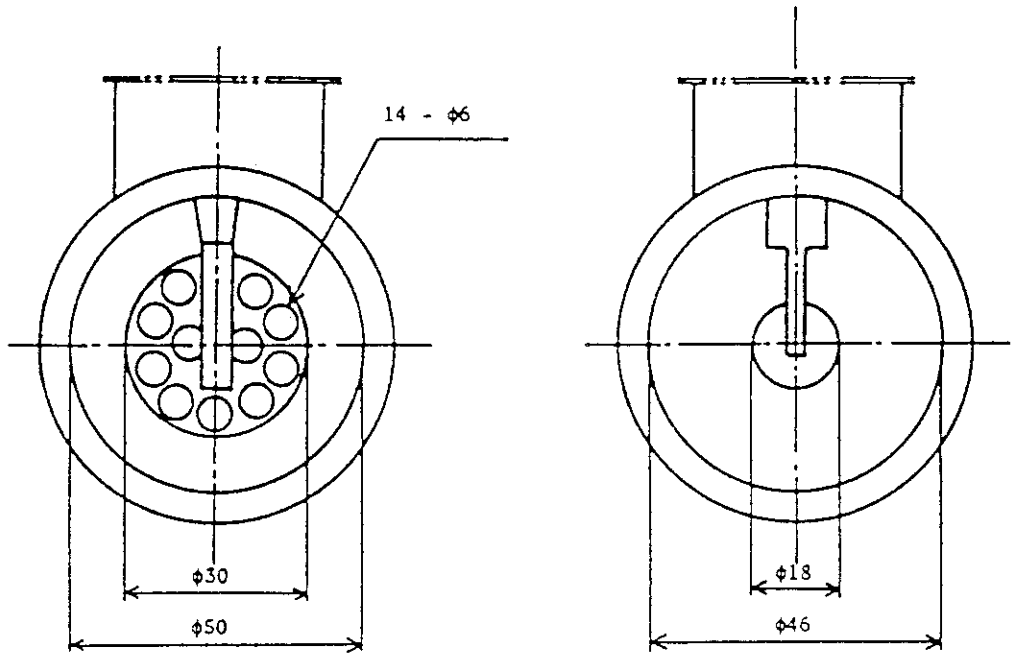

(a) High Range Drag Disc

(b) Low Range Drag Disc

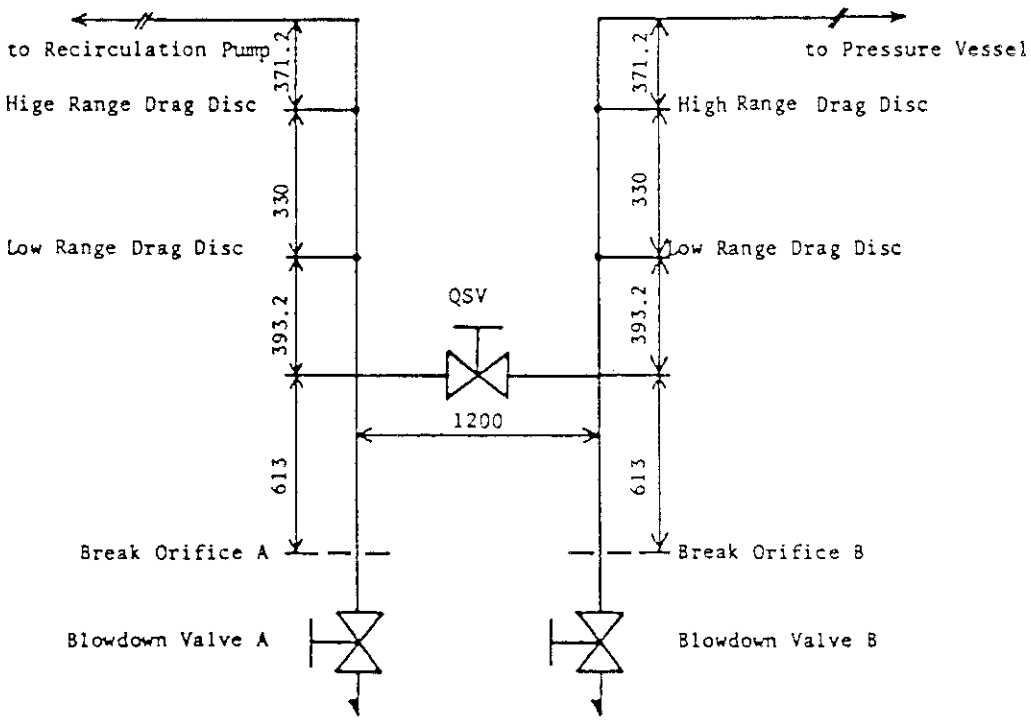

(c) Location of Drag Discs

Fig. 3.9 Arrangement and location of drag disks

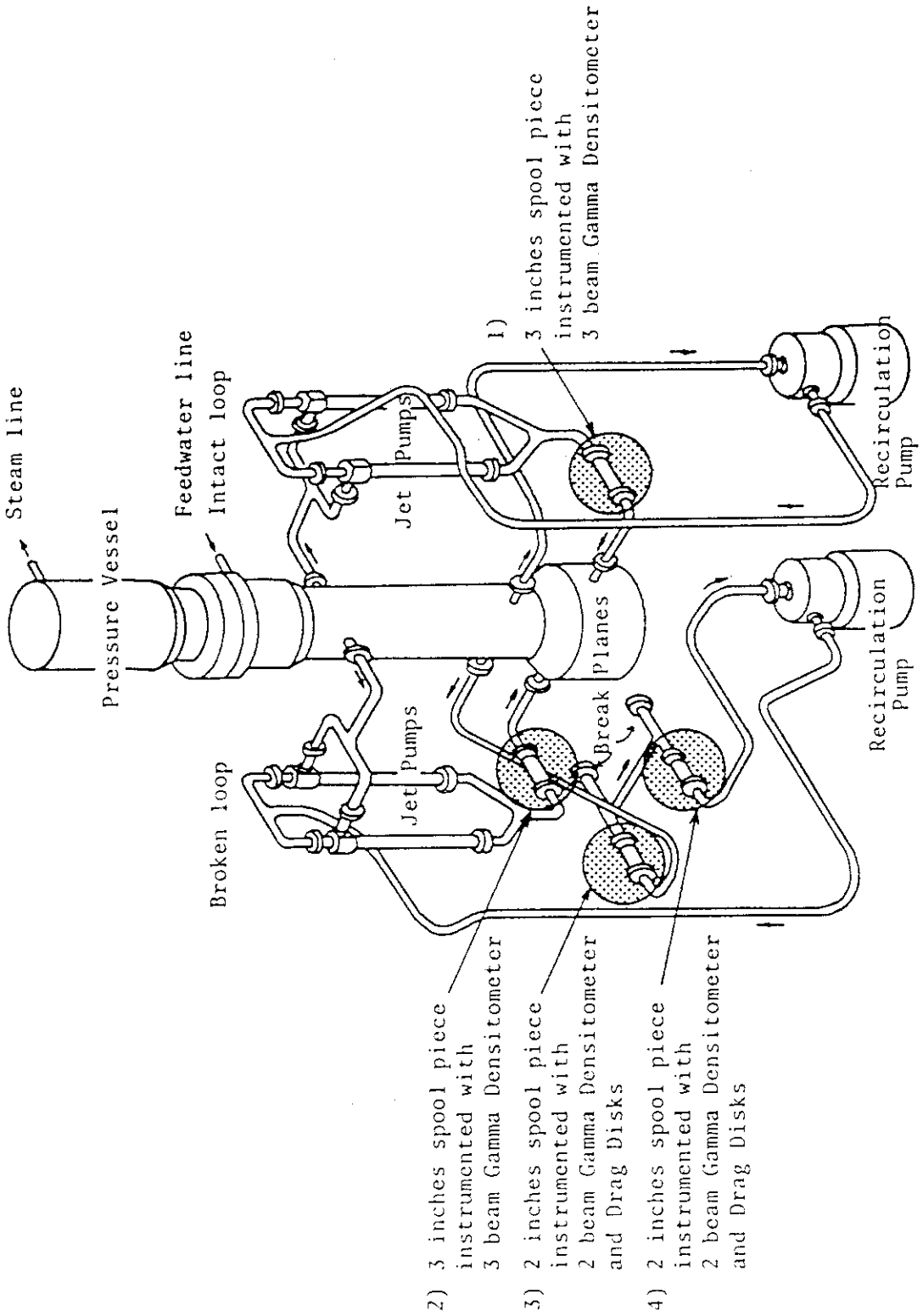

Fig. 3.10 Location of two-phase flow measurement spool pieces

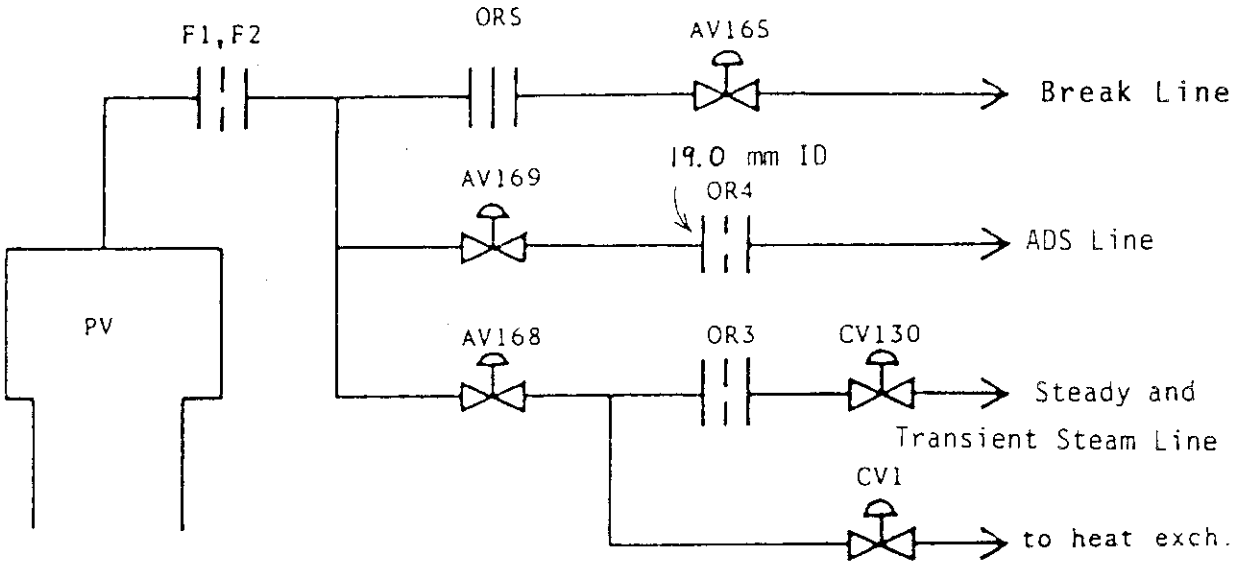

Fig. 4.1 Main steam line schematic

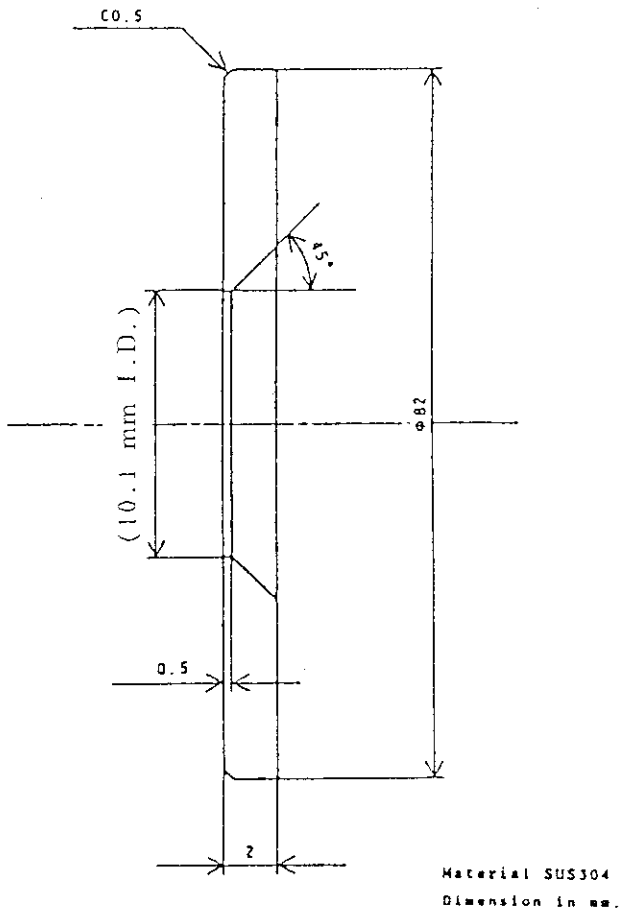

Fig. 4.2 Break orifice details

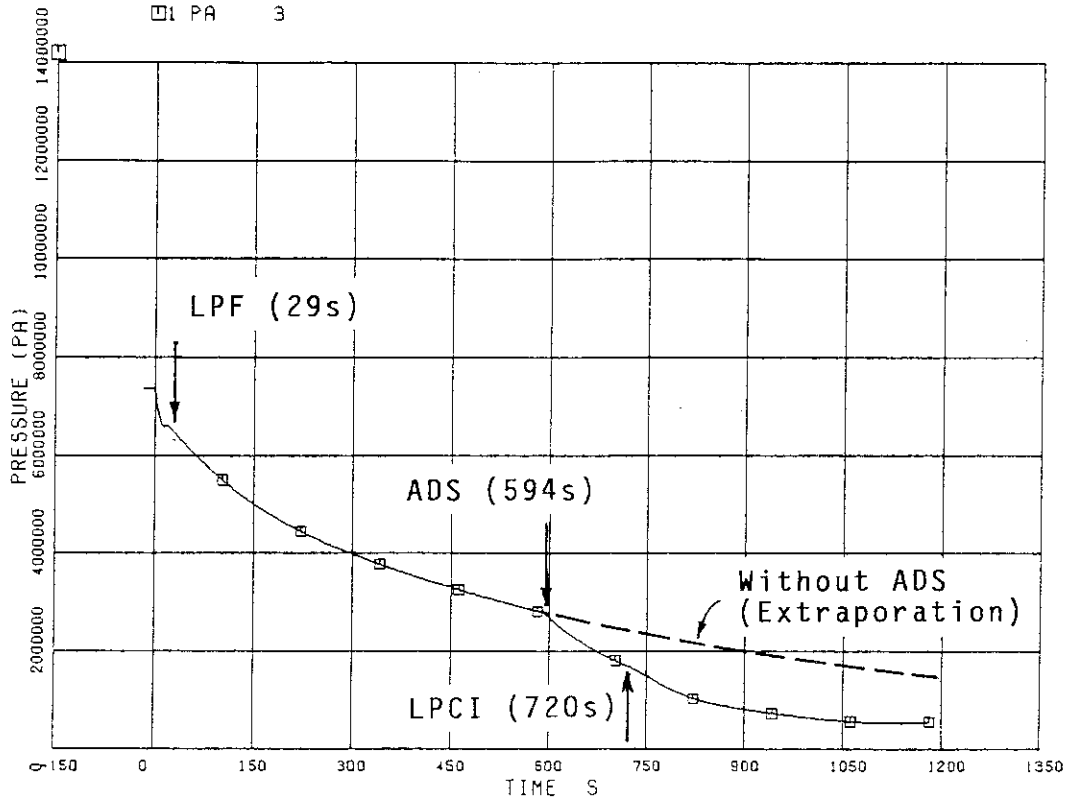

Fig. 5.1 Steam dome pressure and major events in RUN 992

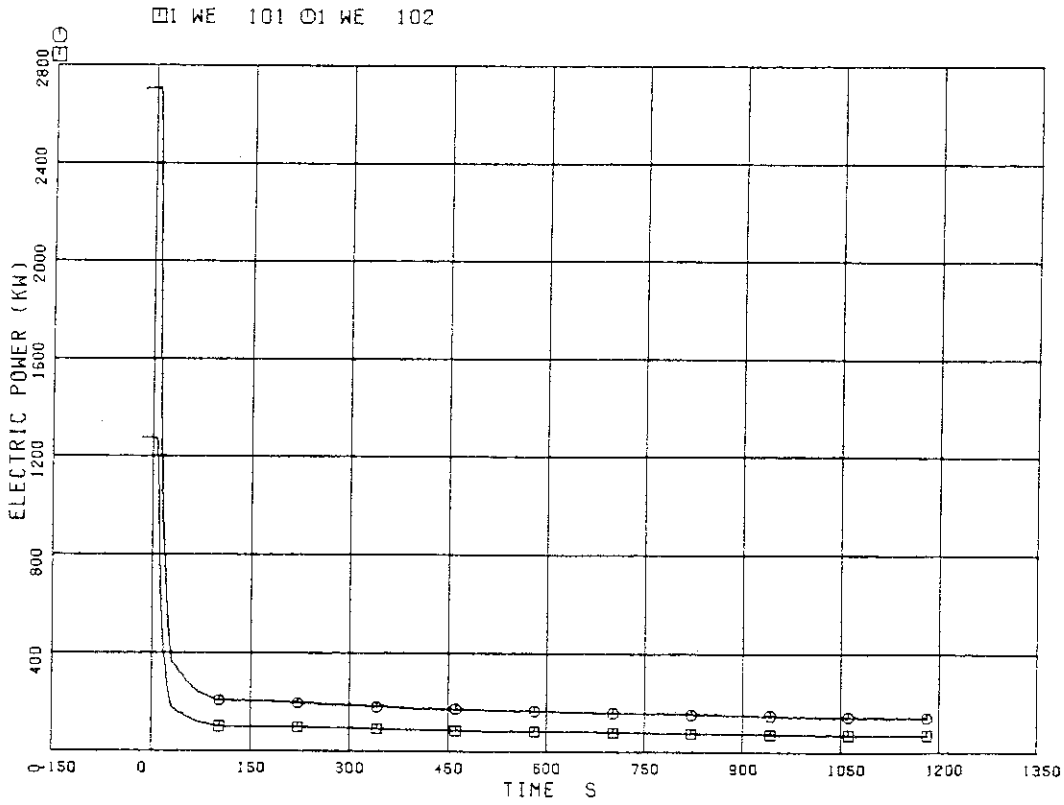

Fig. 5.2 Electric core powers for a high-power bundle (WE 101) and three avarage-power bundles (WE 102) in RUN 992

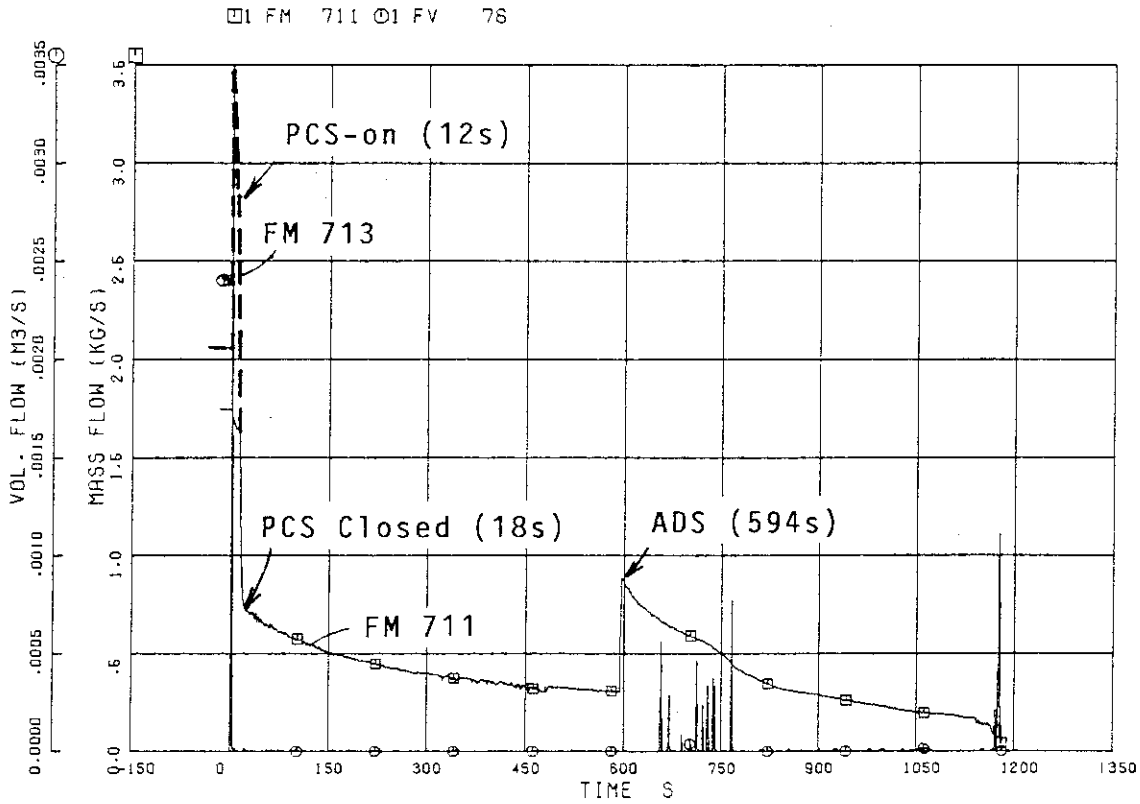

Fig. 5.3 Steam mass flow measured by orifice flow meter in MSL and feedwater volumetric flow rate

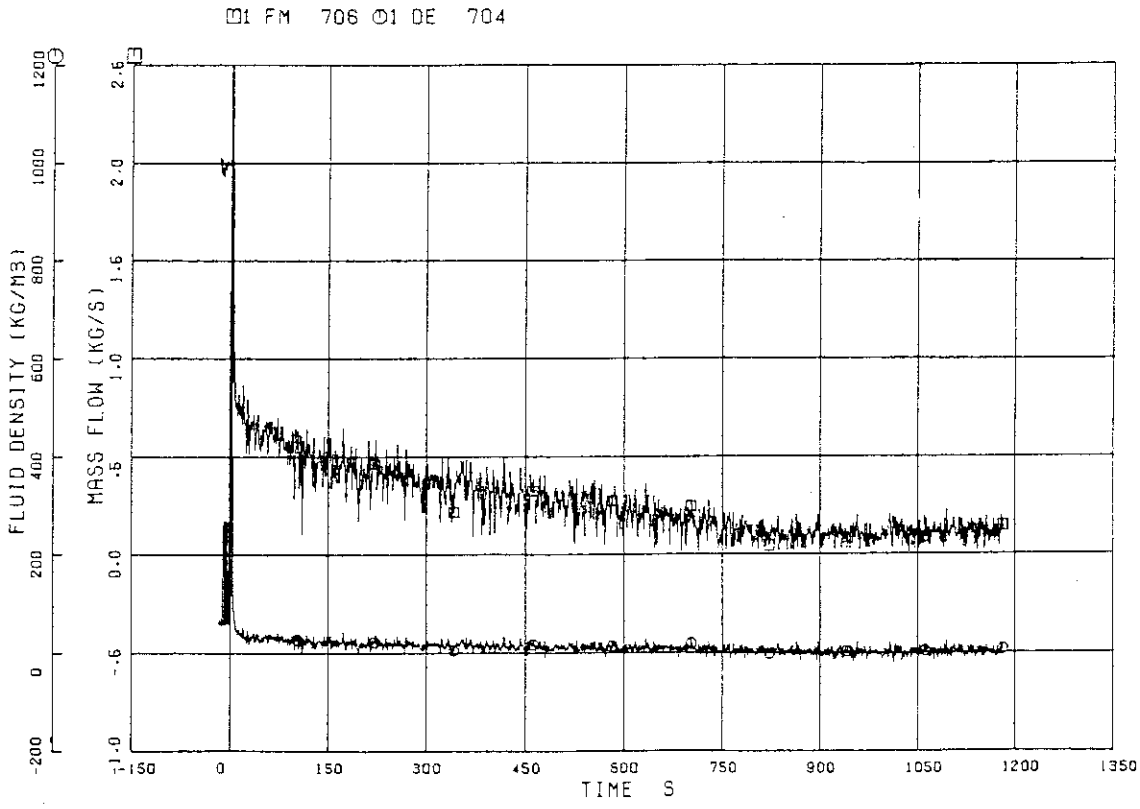

Fig. 5.4 Steam mass flow measured by drag-disk flow meter and average fluid density at break B

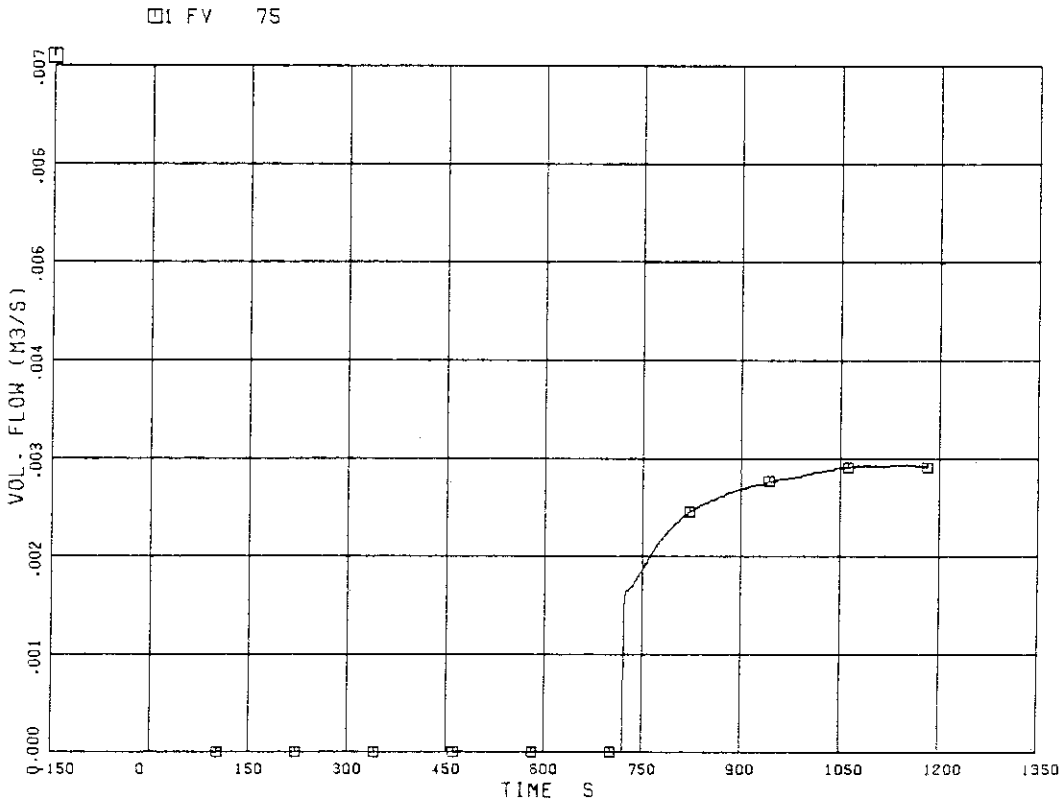

Fig. 5.5 Injection flow rate of LPCI

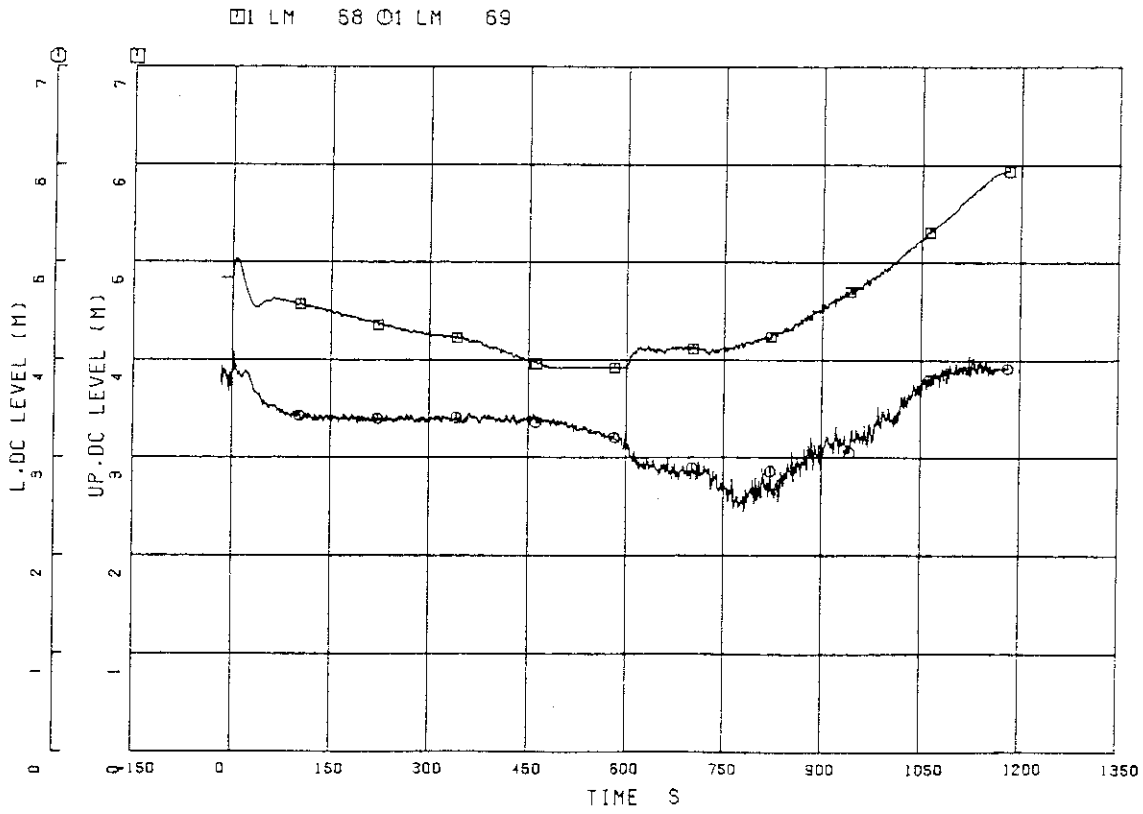

Fig. 5.6 Collapsed water levels in upper downcomer (LM 68) and lower downcomer (LM 69)

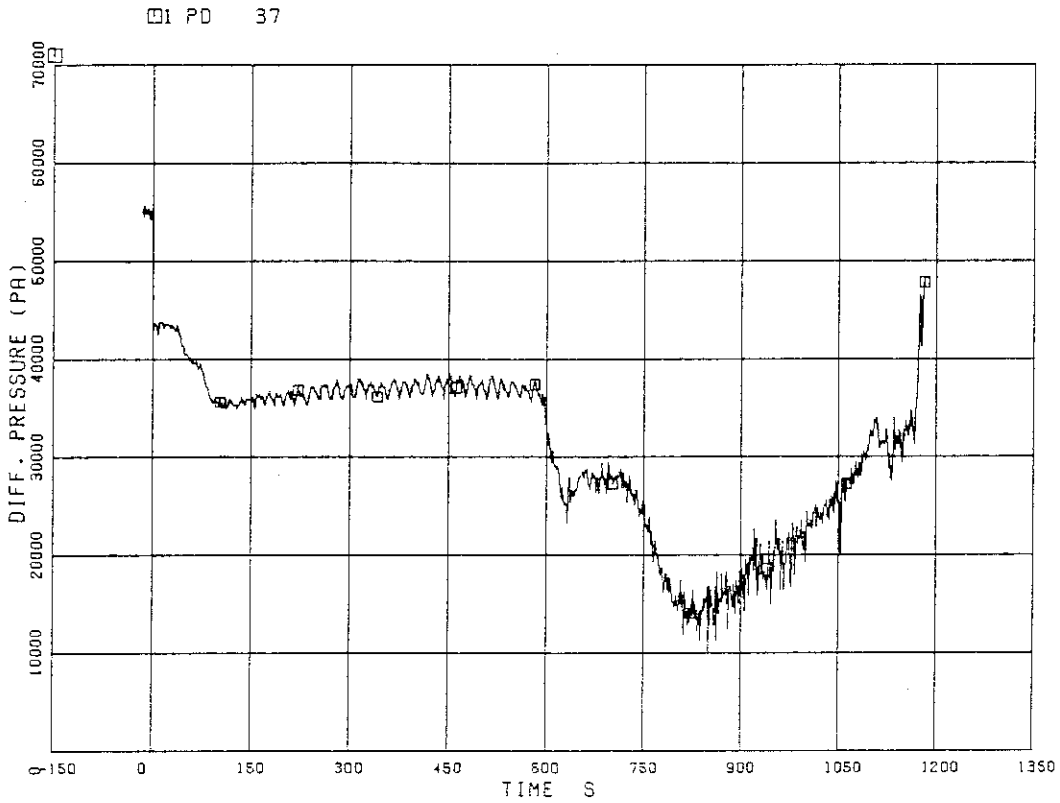

Fig. 5.7 Differential pressure between MRP1 delivery and JP-1 drive

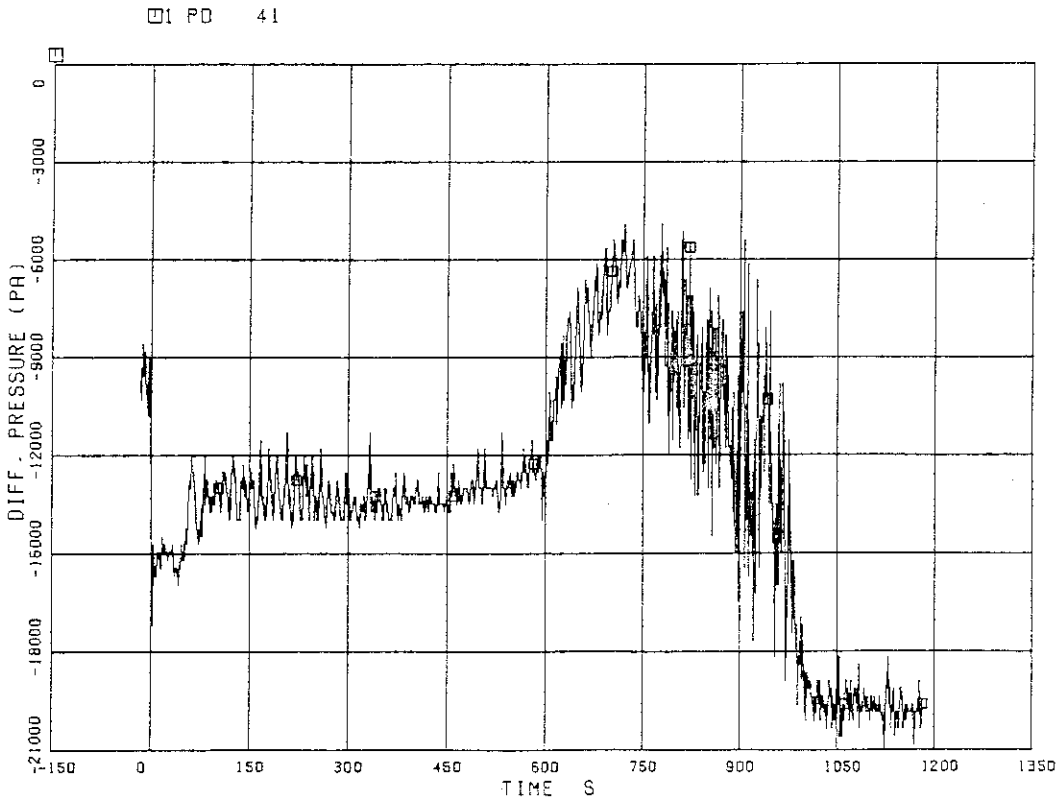

Fig. 5.8 Differential pressure between JP-1 discharge and LP

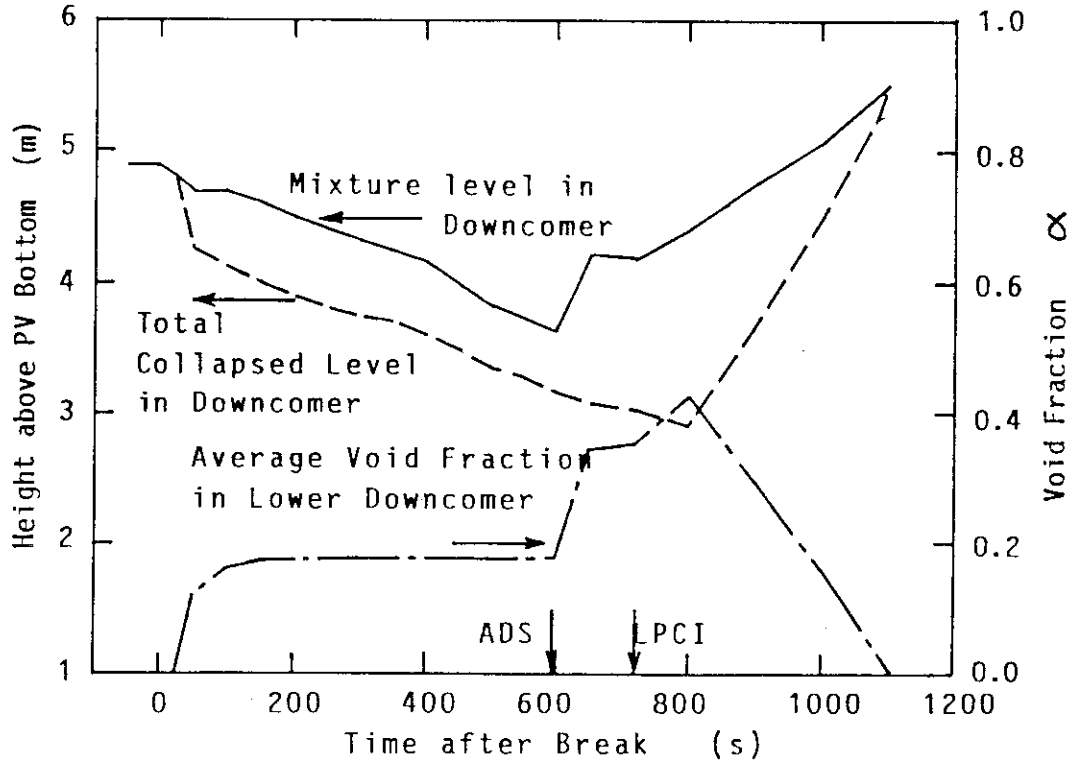

Fig. 5.9 Average void fraction in lower downcomer calculated from collapsed water level (LM 69)

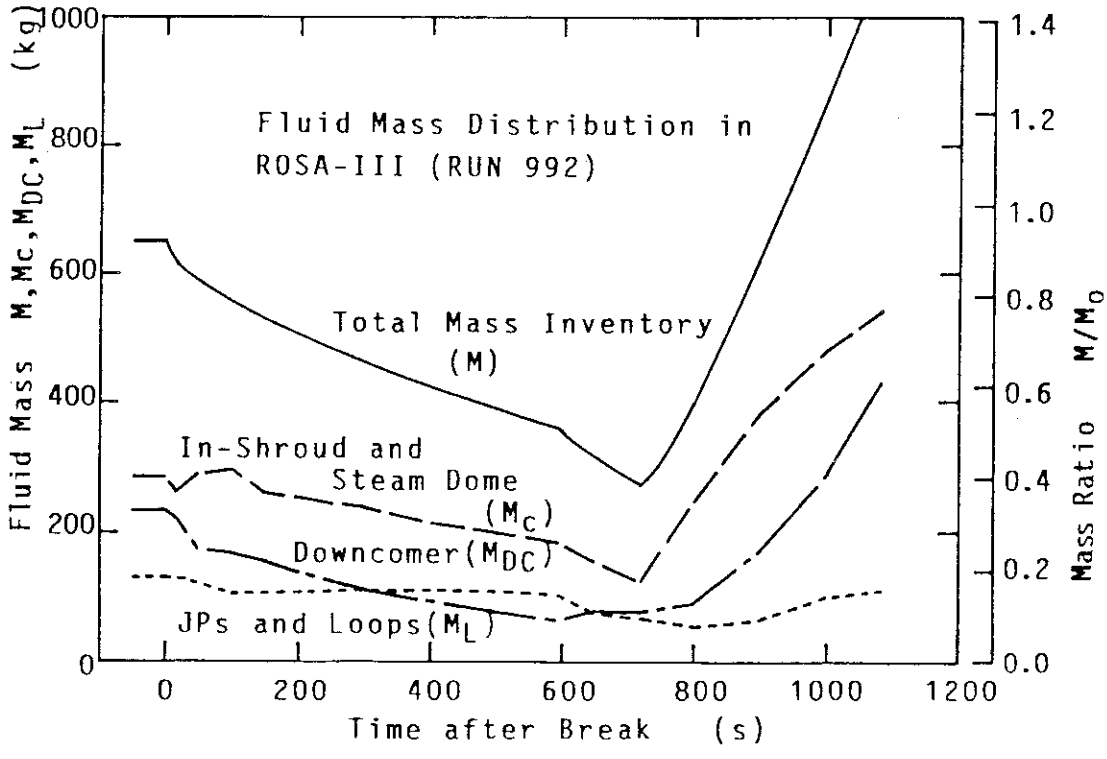

Fig. 5.10 Fluid mass distribution in downcomer, recirculation loops with jetpumps, and inside core-shroud and steam dome for RUN 992

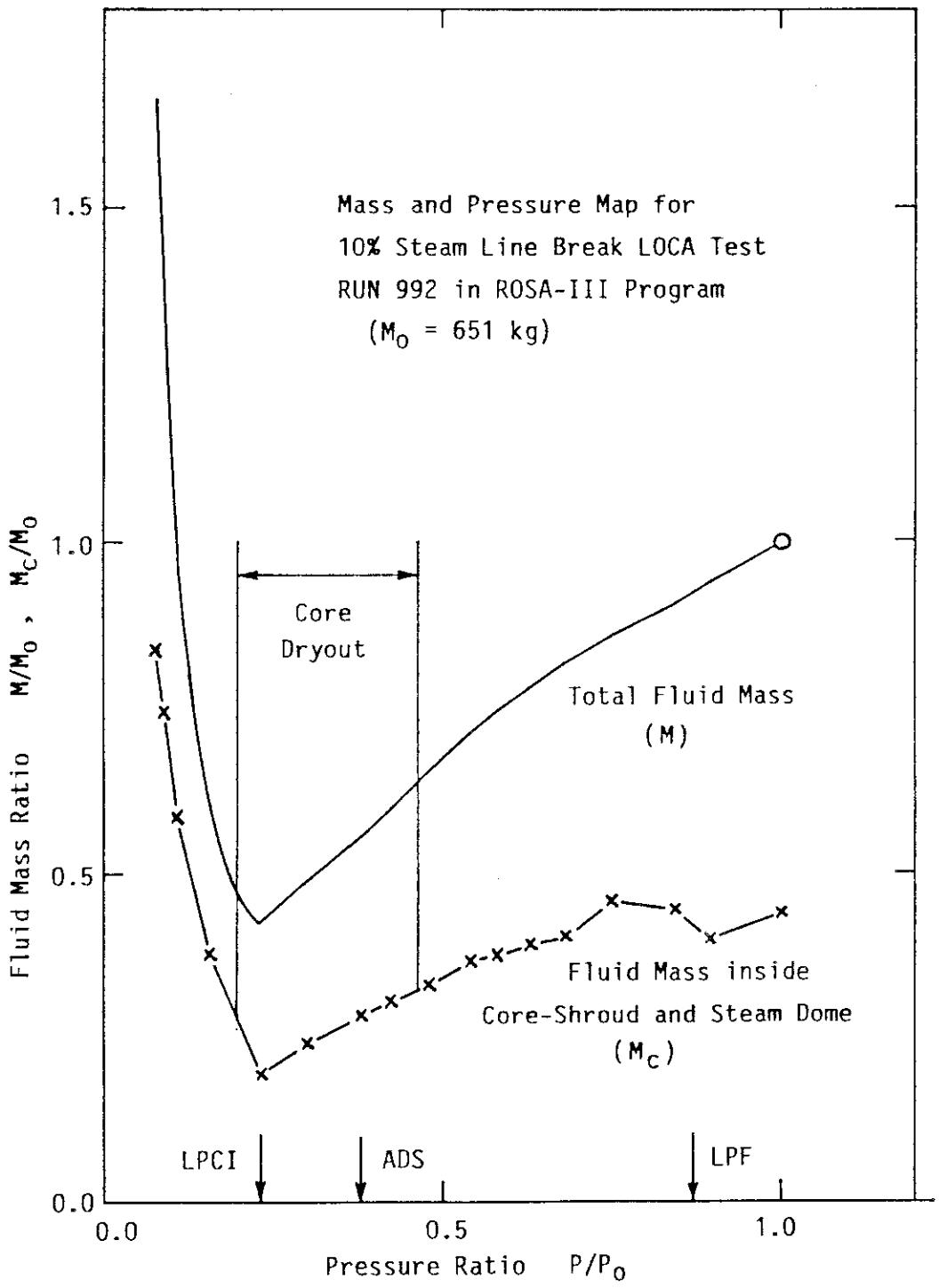

Fig. 5.11 Transient mass and pressure map for RUN 992

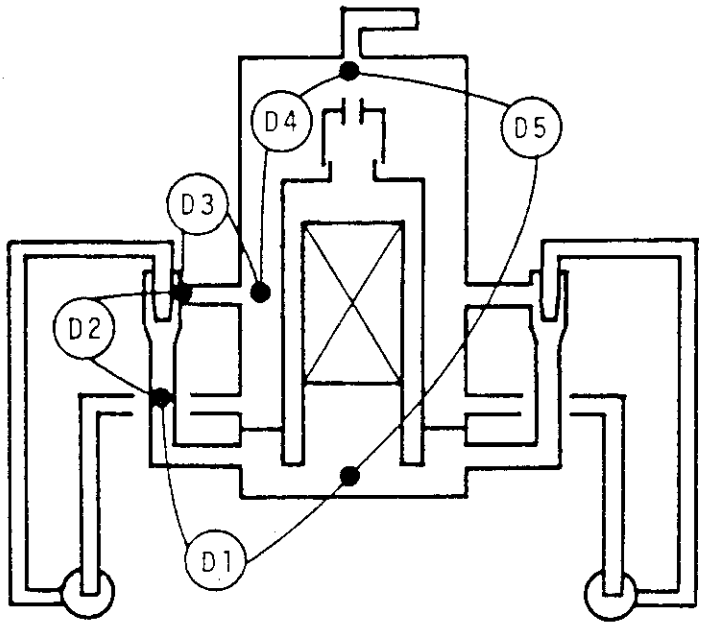

D5 = -D1+D2-D3+D4

Measurement Location of Differential Pressures

(PD 25)D5 : DP between top and bottom of PV
(Ch.25, EL 0.10 - 6.04m)

(PD 41)D1 : DP between JP1 discharge and lower plenum
(Ch.41, EL 2.244 - 0.10m)

(PD 26)D2 : DP between JP1 discharge and suction
(Ch.26, EL 2.244 - 2.814m)

(PD 39)D3 : DP between DC middle and JP1 suction
(Ch.19, EL 2.814m)

(PD 56)D4 : DP between Dc middle and steam dome
(Ch.56, EL 2.814 - 6.04m)

Fig. 5.12 Location of differential pressure measurements around PV

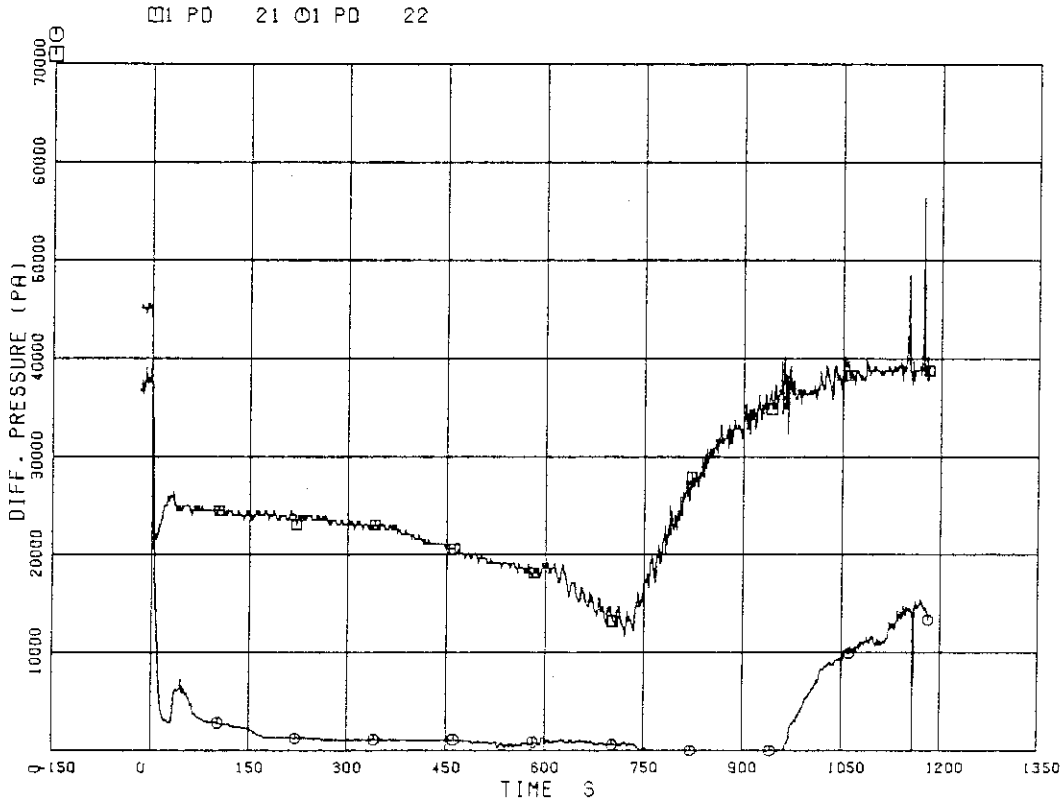

Fig. 5.13 Differential pressures between lower plenum (LP) and upper plenum (UP), and between UP and steam dome

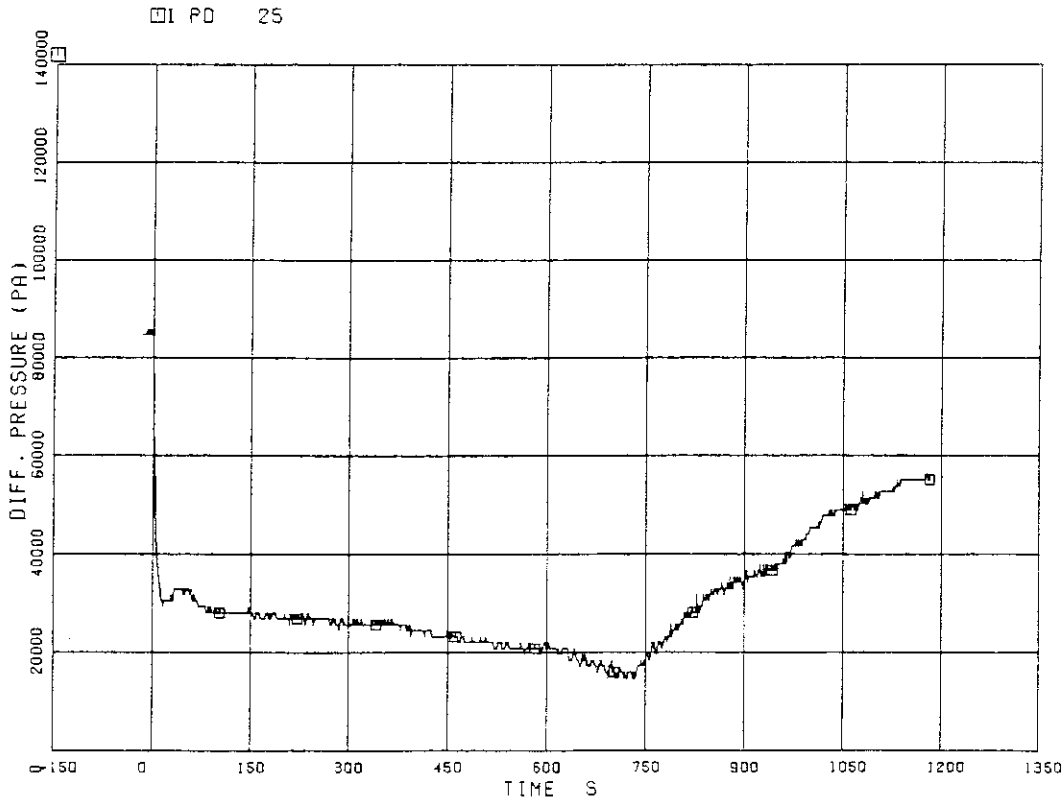

Fig. 5.14 Differential pressure between bottom and top of PV

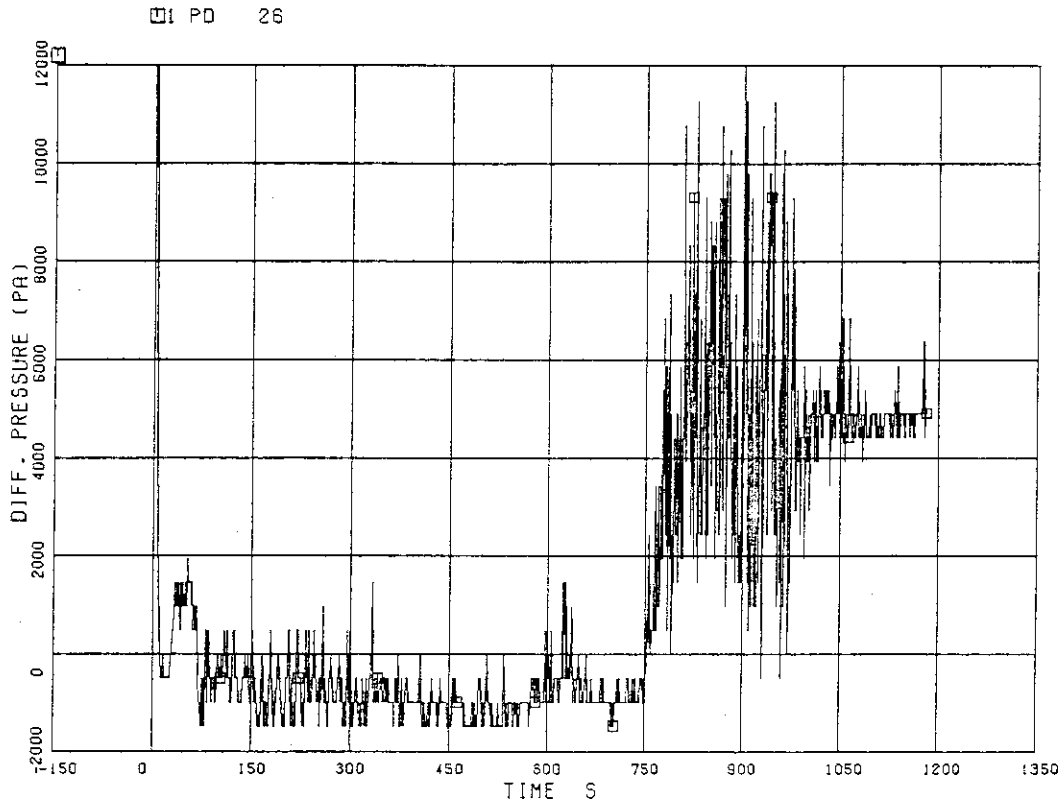

Fig. 5.15 Differential pressure between JP1 discharge and suction

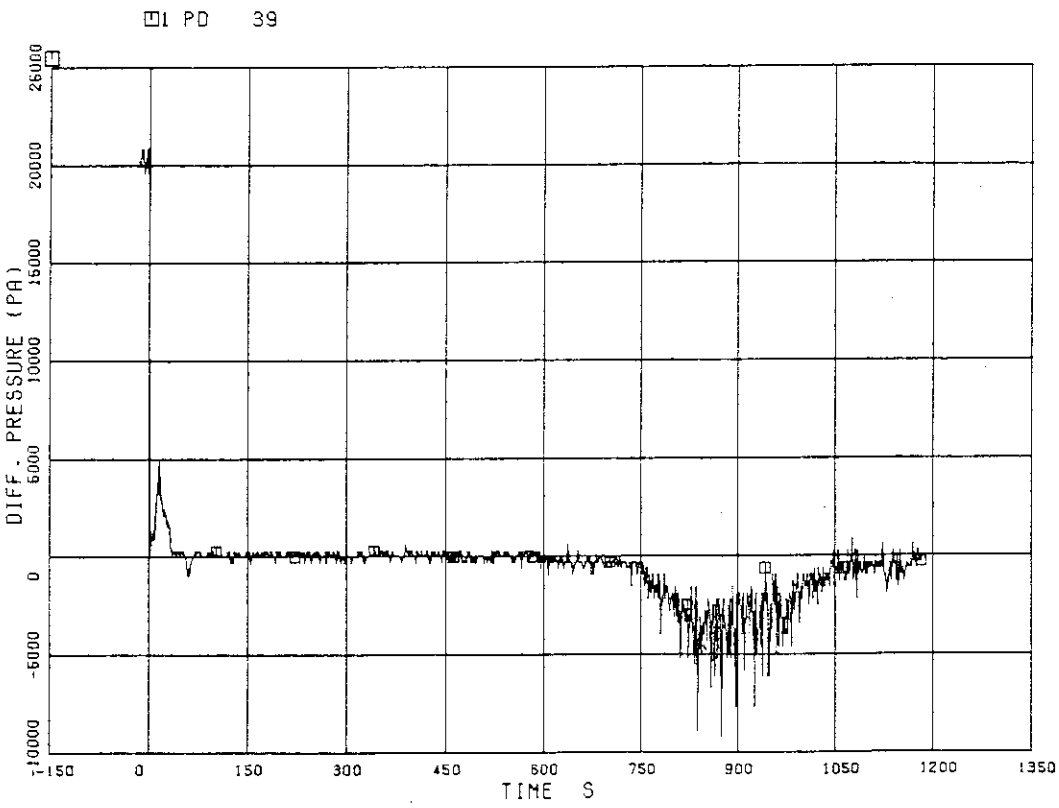

Fig. 5.16 Differential pressure between DC middle and JP-1 suction

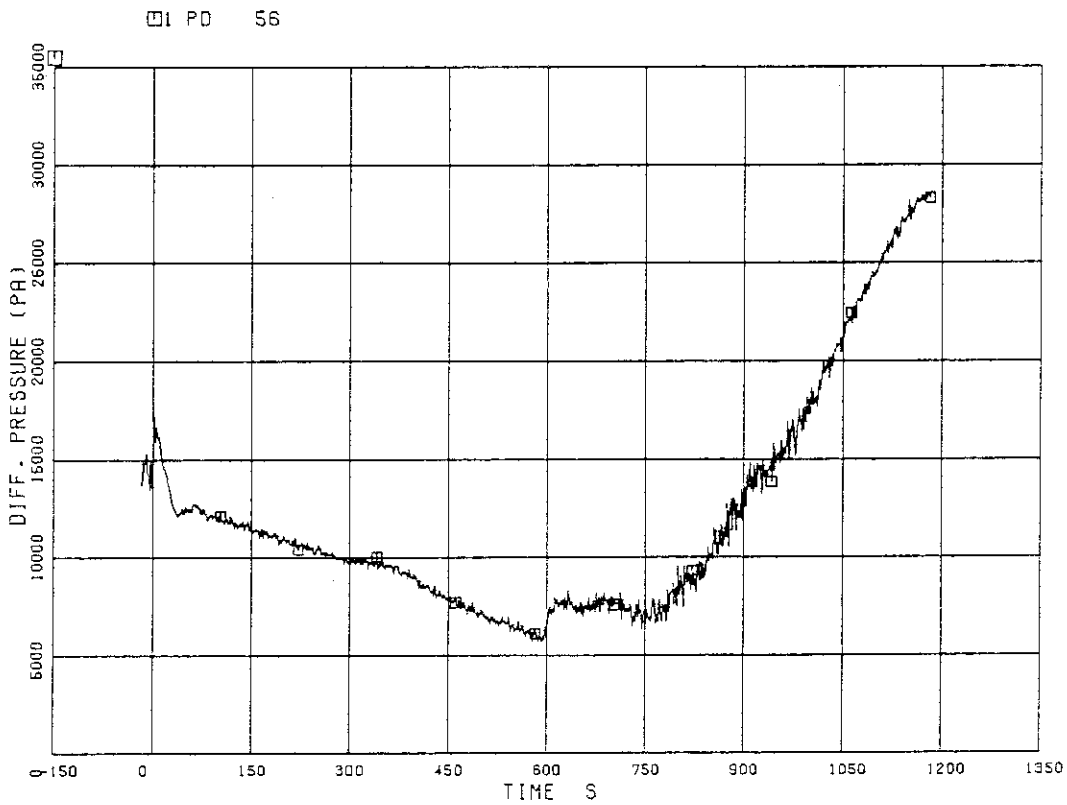

Fig. 5.17 Differential pressure between DC middle and steam dome

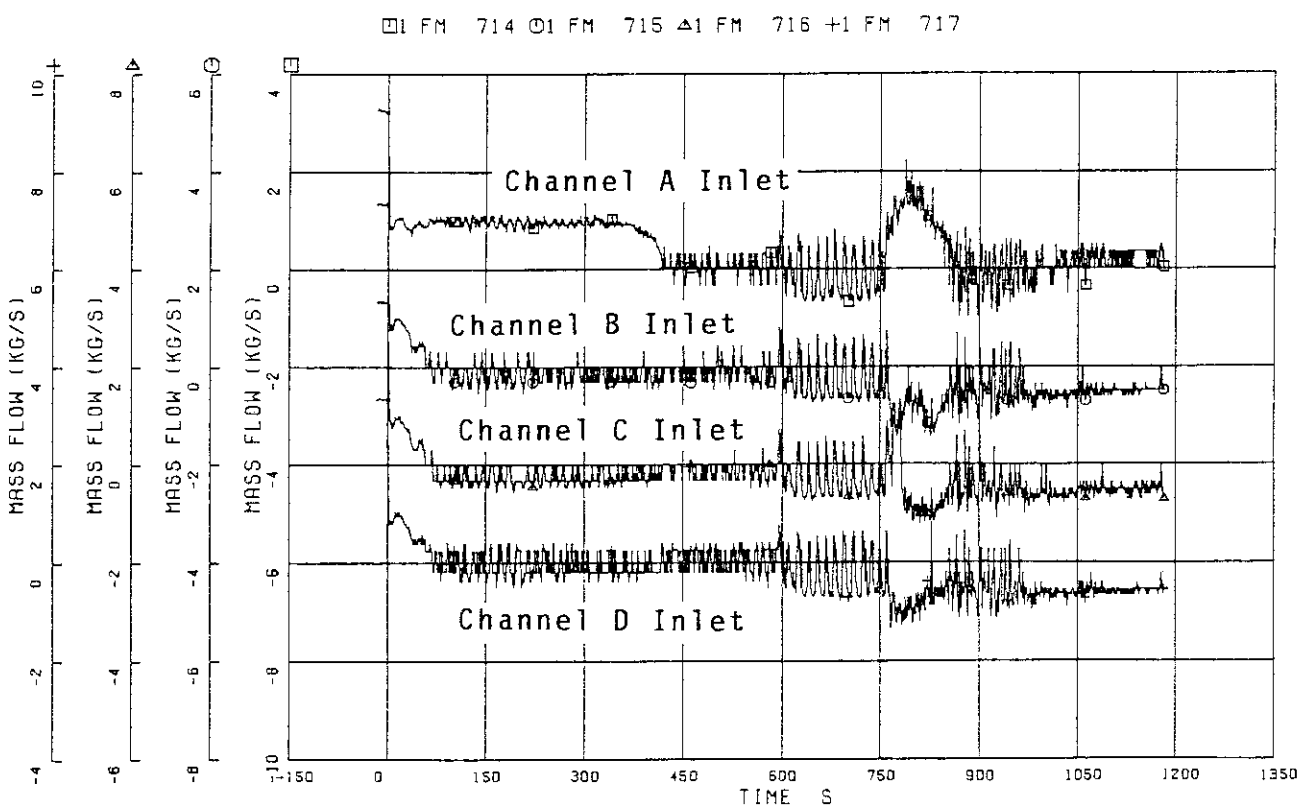

Fig. 5.18 Core inlet flow rates for four channels calculated from corresponding differential pressure data at channel inlet

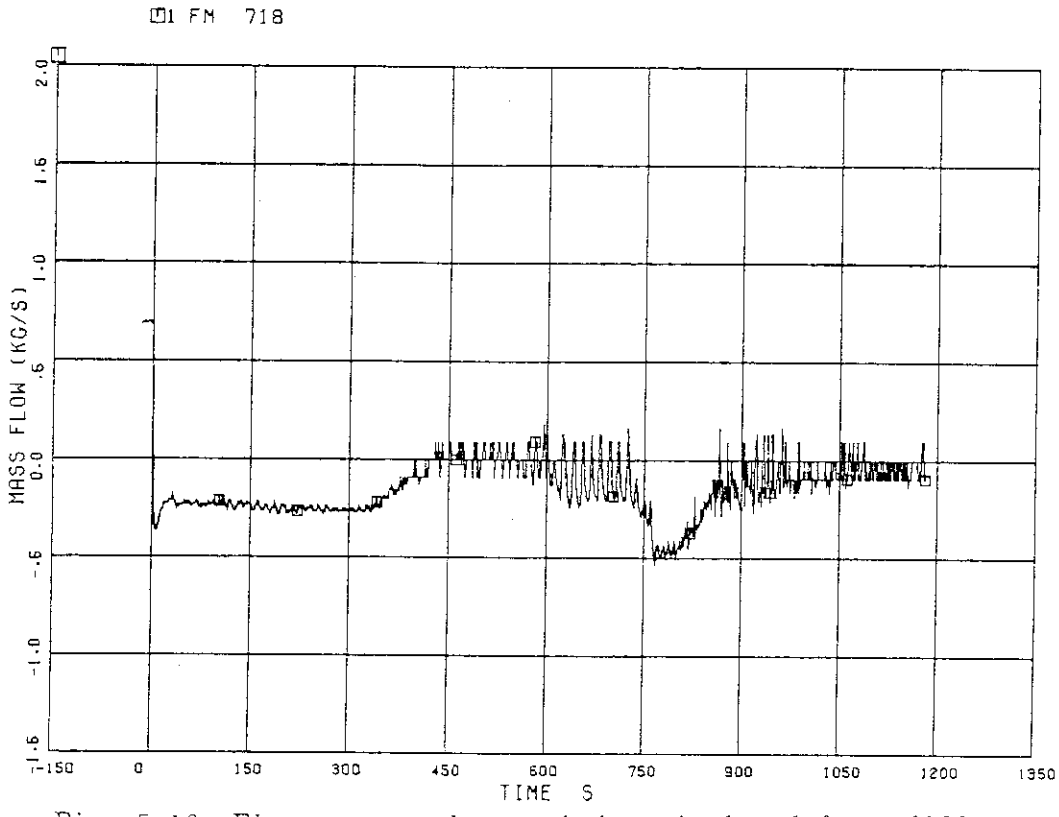

Fig. 5.19 Flow rate at bypass hole calculated from differential pressure data

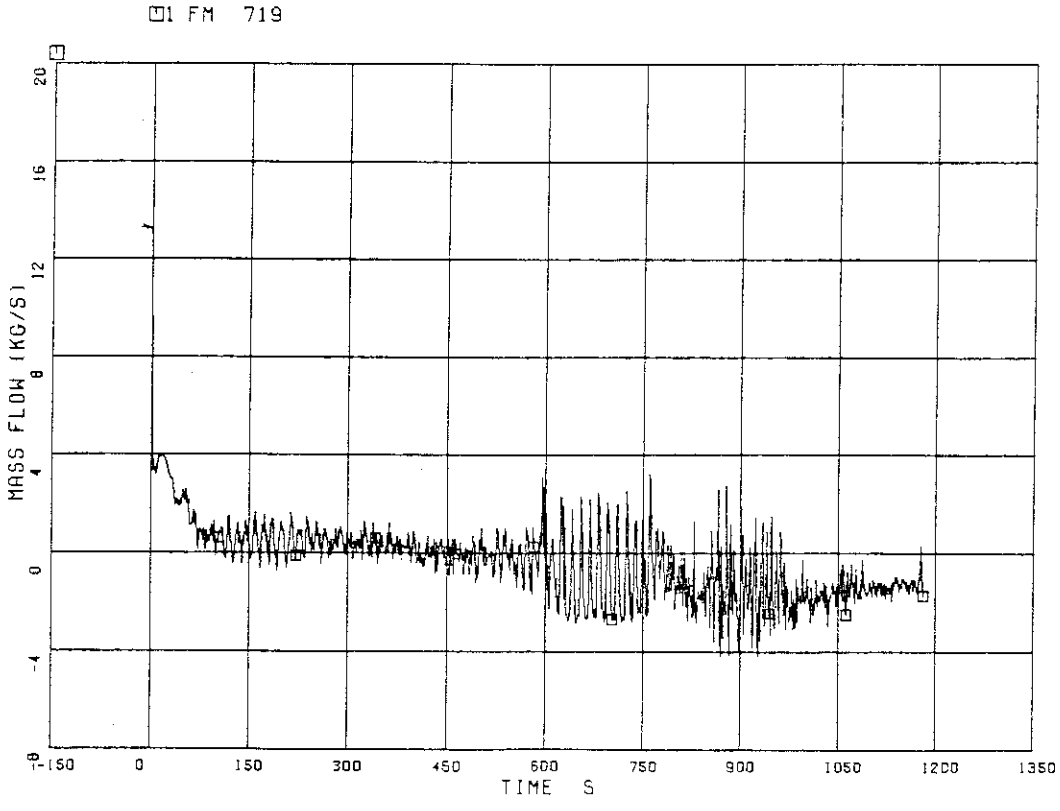

Fig. 5.20 Total core flow rate (sum of flow rates at core inlet orifices and bypass holes)

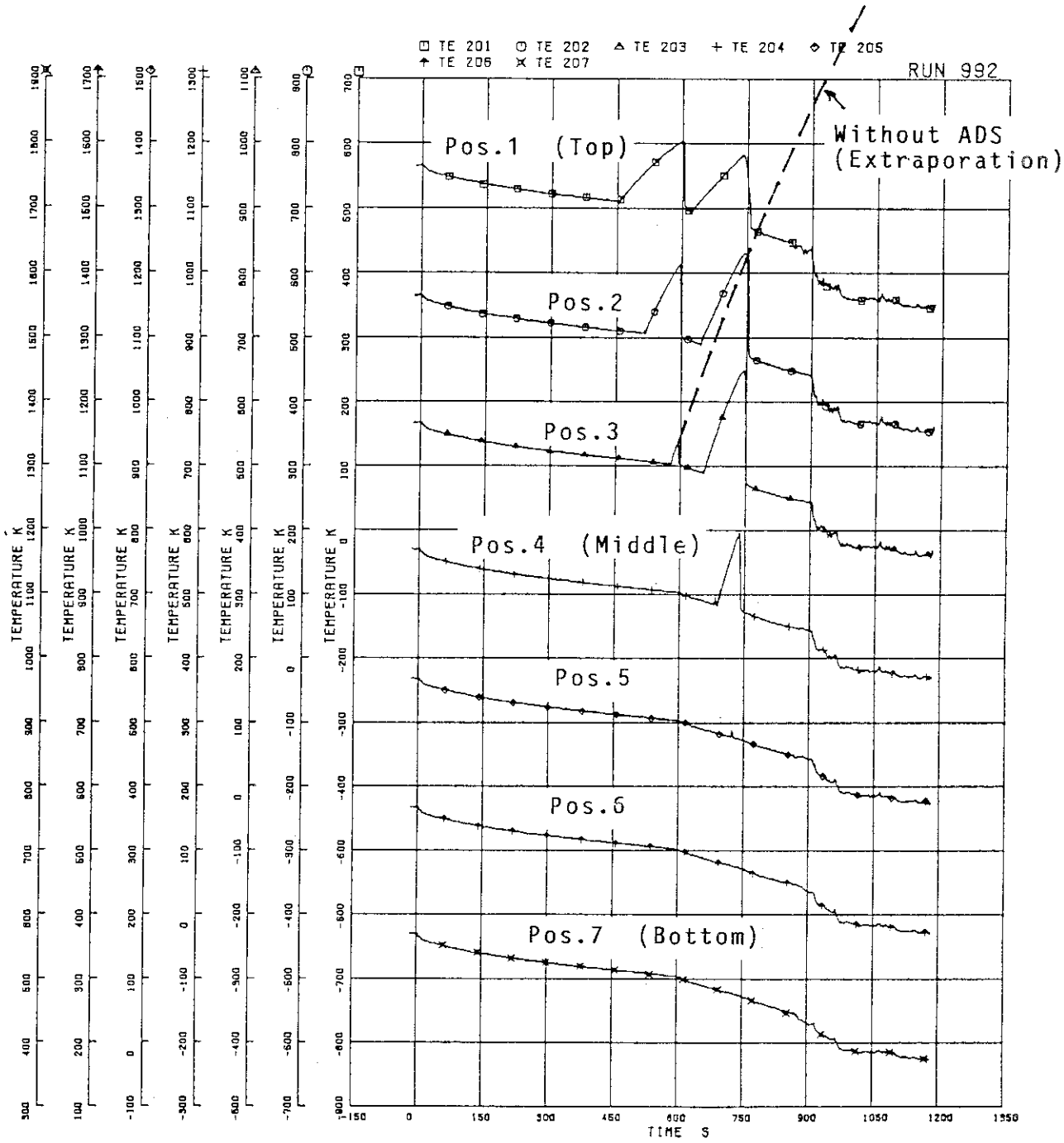

Fig. 5.21 Seven surface temperatures of All rod

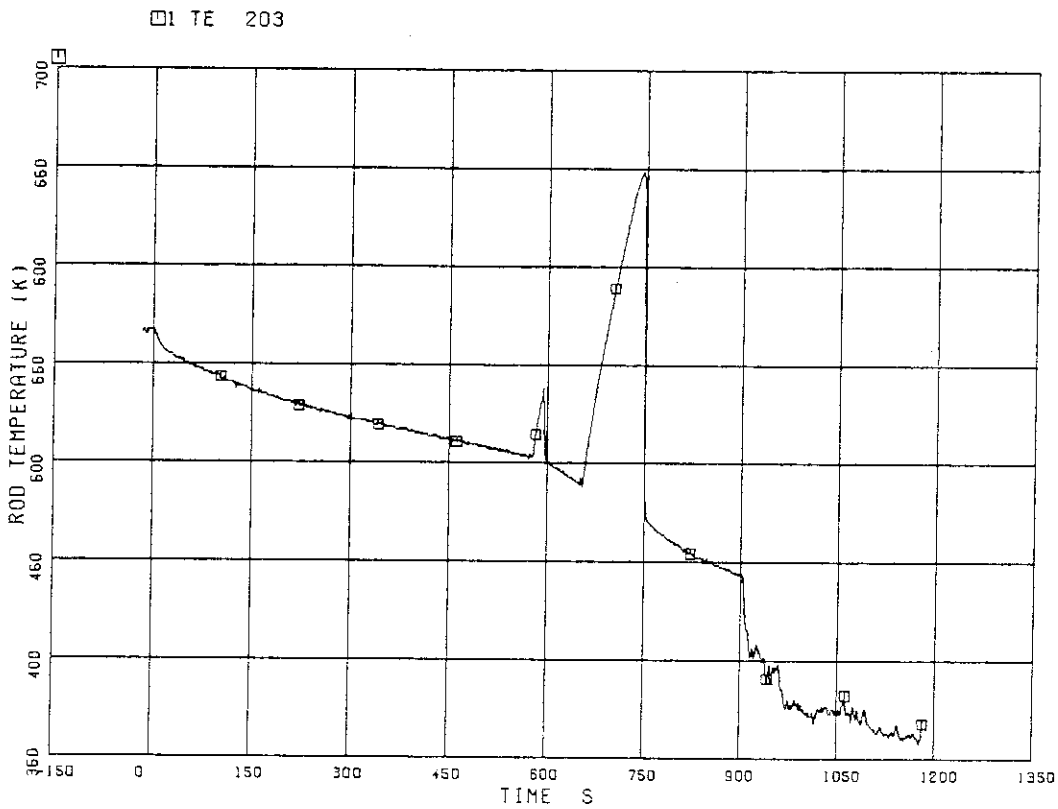

Fig. 5.22 Heater rod surface temperature recorded PCT of 649 K at A11 rod Position 3

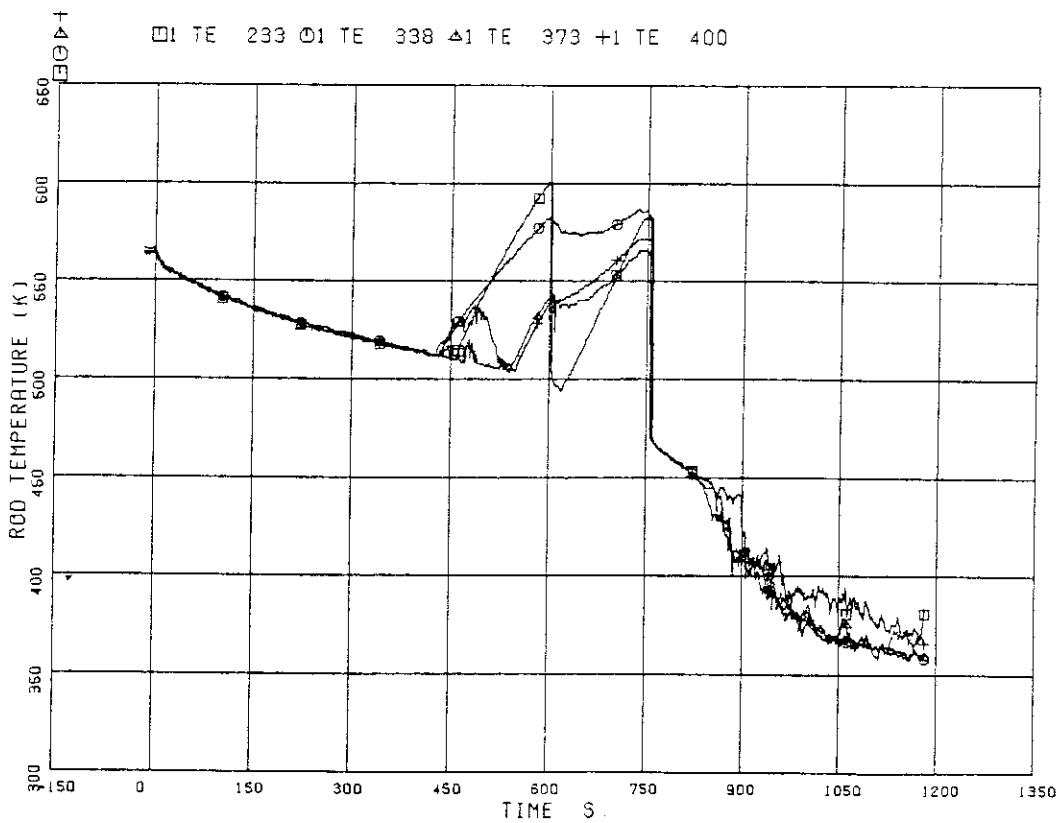

Fig. 5.23 Surface temperatures of heater rods in four bundles (A22, B22, C22 and D22 at Position 1)

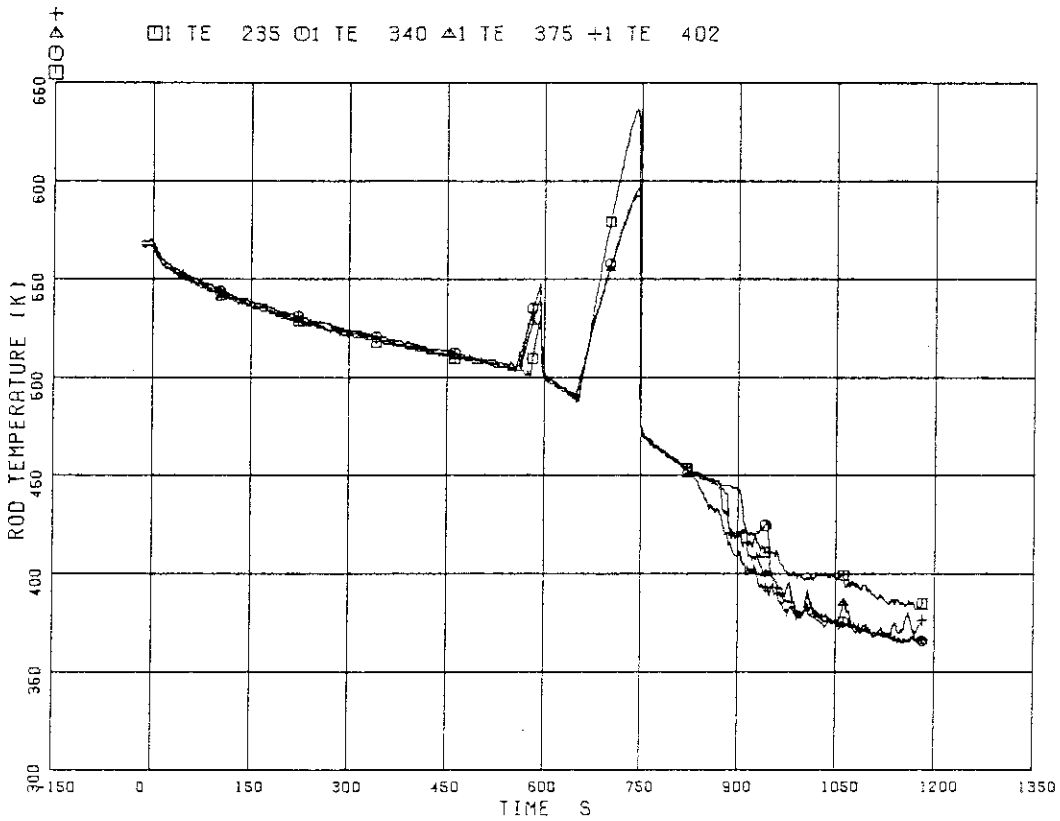

Fig. 5.24 Surface temperatures of heater rods in four bundles (A22, B22, C22 and D22 at Position 3)

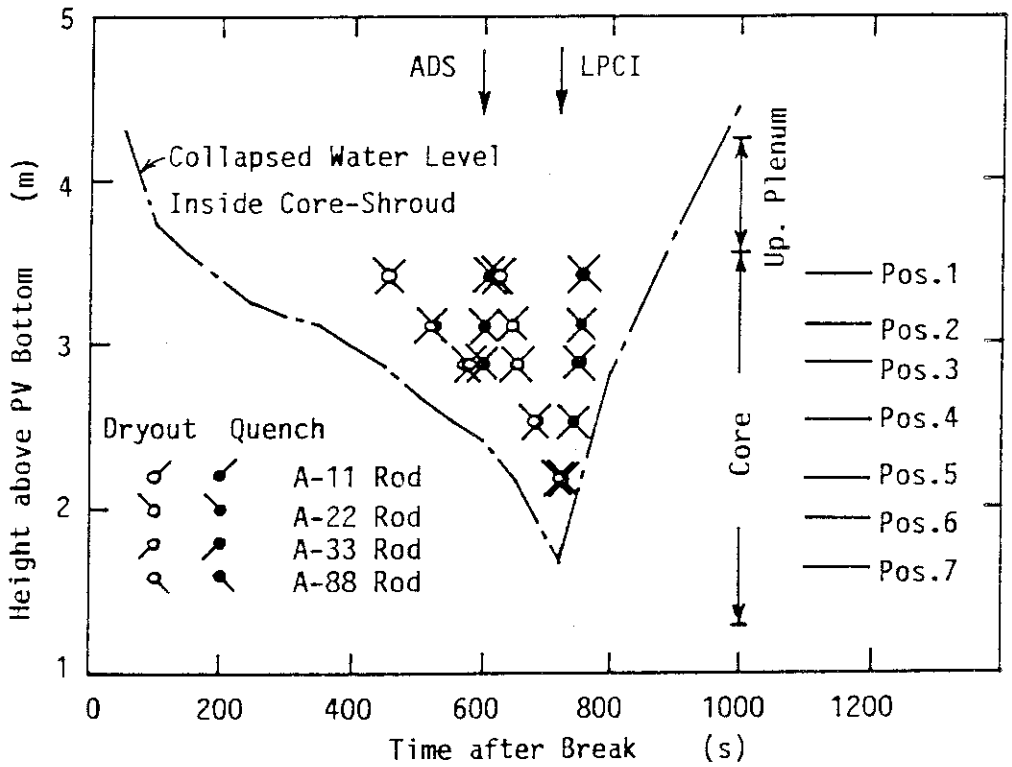

Fig. 5.25 Dryout and quench fronts of heater rods in high-power bundle related with PV collapsed level

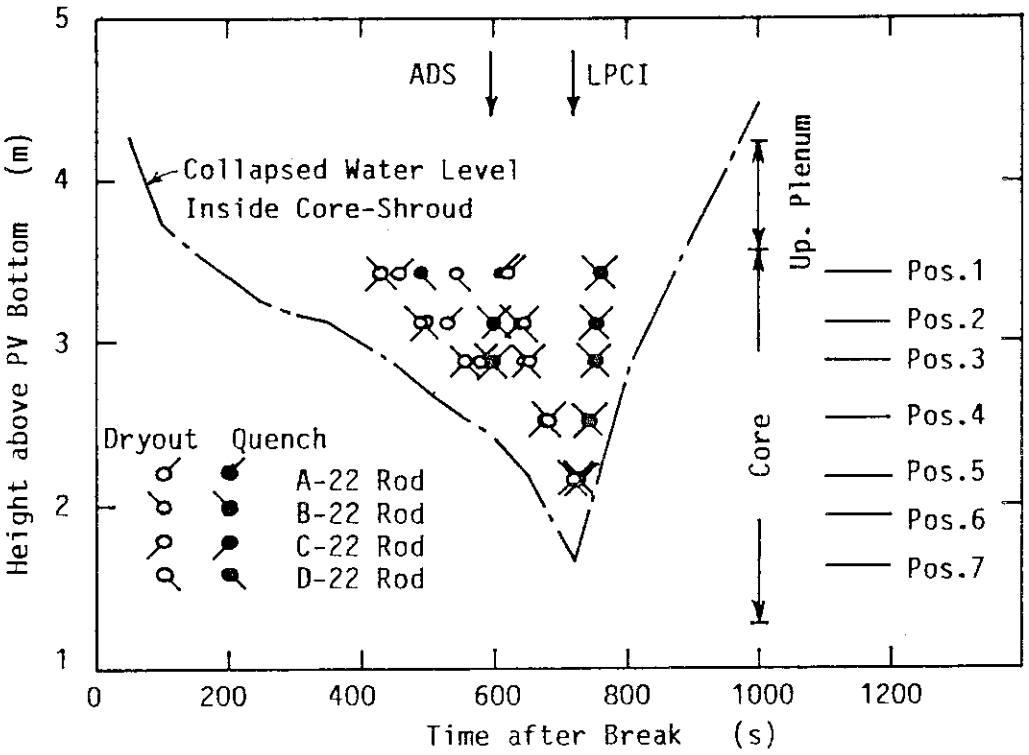

Fig. 5.26 Dryout and quench fronts of heater rods in four bundles related with PV collapsed level

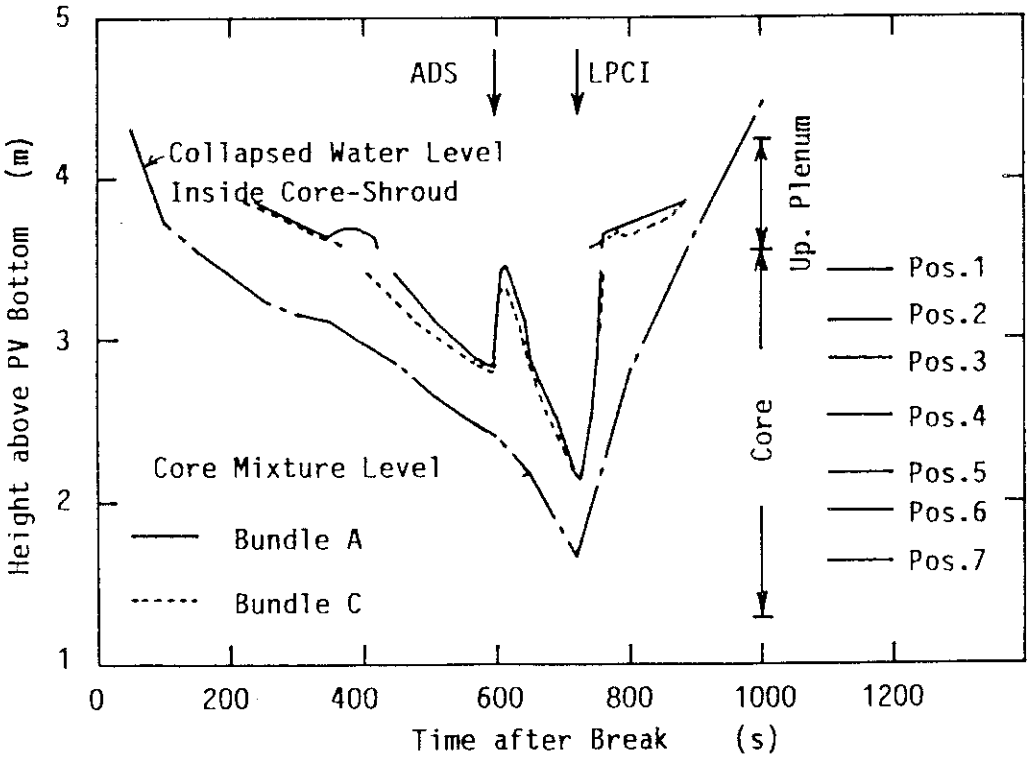

Fig. 5.27 Mixture level transients inside core shroud related with PV collapsed water level

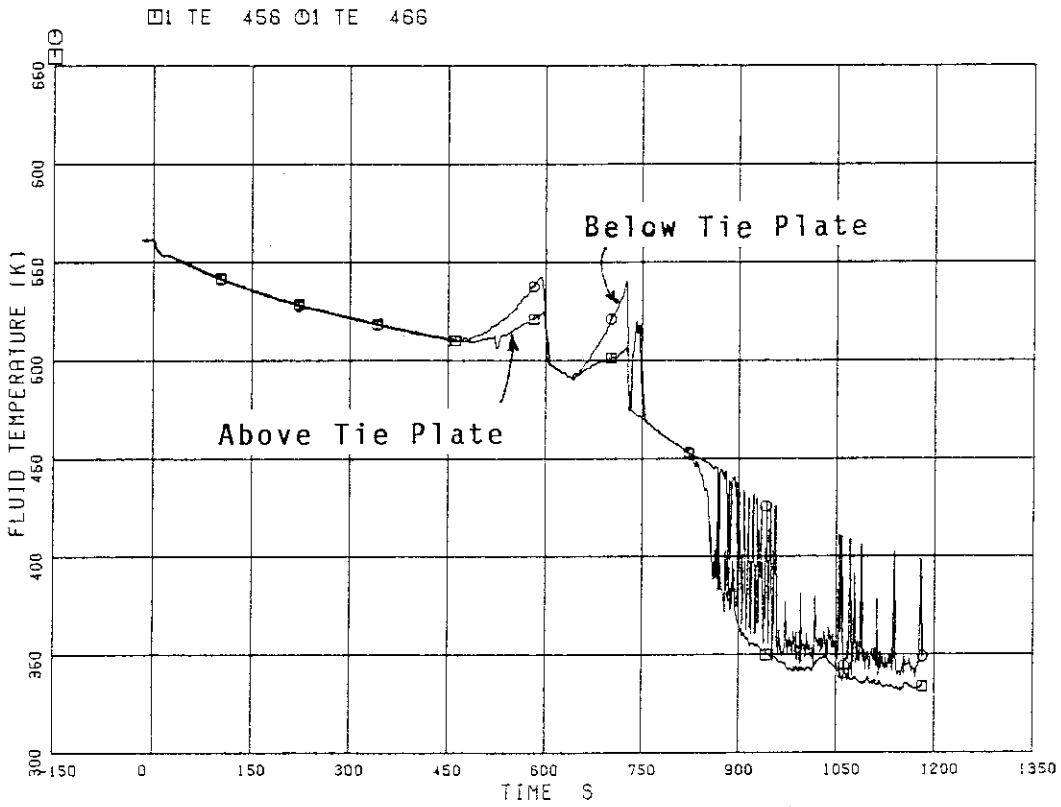

Fig. 5.28 Fluid temperatures at UTP in channel A, opening 1

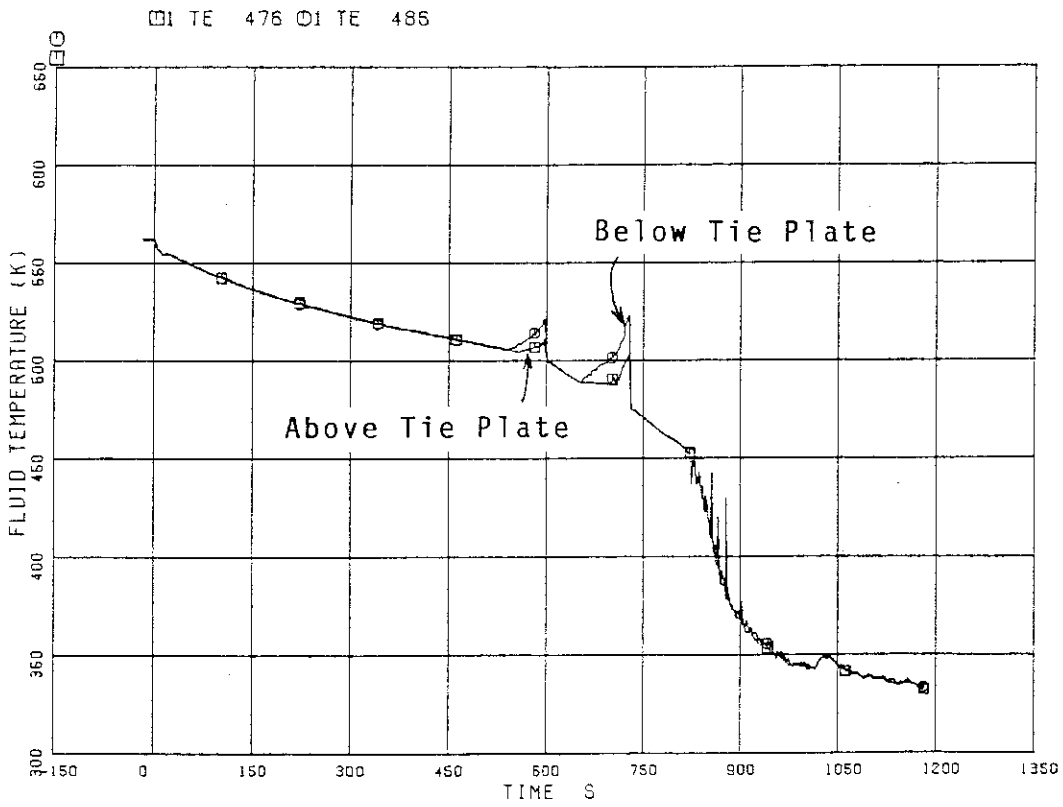

Fig. 5.29 Fluid temperatures at UTP in channel C, opening 1

Appendix I List of Measurements and Calculated Data in RUN 992

All of the measurements (Channels 1 through 698) in RUN 992 are listed in Table A.1. The blank data mainly mean that the recorded data were not shown in this report because those data were similar and could be represented by the other data shown in this report. Shown in Table A.2 is a list of calculated data by using the experimental results. The core instrumentations including the heater rod surface temperatures and fluid mixture level are listed in Table A.3. In this test, metal temperatures were measured at inner surface, inside and outer surface of metal structures in order to investigate stored heat release both into the primary fluid system and the outer atmosphere. Their measuring locations are listed in Table A.4.

Table A.1 Measurement list for RUN 992

Table A.2 Calculated data in RUN 992

Table A.3 Core instrumentation list

Table A.4 Metal temperature measurement list for PV wall, jetpump and recirculation line pipe wall

Table A.1 Measurement list for RUN 992

1Ch.- 50Ch.

Ch.	Item	Symbol	ID.		Location	Fig.No.	Range			Unit	Accuracy
1	Press.	P- 1	PA	1	Lower Plenum	Fig.A. 1	0.100	-	10.0	MPa	1.08%FS
2	Press.	P- 2	PA	2	Upper Plenum	Fig.A. 1	0.100	-	10.0	MPa	1.08%FS
3	Press.	P- 3	PA	3	Steam Dome	Fig.A. 1	0.100	-	10.0	MPa	1.08%FS
4	Press.	P- 4	PA	4	Downcomer Bottom	Fig.A. 1	0.100	-	10.0	MPa	1.08%FS
5	Press.	P- 5	PA	5	JP-3 Drive		0.100	-	10.0	MPa	1.08%FS
6	Press.	P- 6	PA	6	JP-4 Drive		0.100	-	10.0	MPa	1.08%FS
7	Press.	P- 7	PA	7	JP-3 Suction		0.100	-	10.0	MPa	1.08%FS
8	Press.	P- 8	PA	8	JP-4 Suction		0.100	-	10.0	MPa	1.08%FS
9	Press.	P- 9	PA	9	MRP-1 Suction		0.100	-	10.0	MPa	1.08%FS
10	Press.	P-10	PA	10	MRP-2 Suction		0.100	-	10.0	MPa	1.08%FS
11	Press.	P-11	PA	11	MRP-2 Delivery		0.100	-	10.0	MPa	1.08%FS
12	Press.	N-17	PA	12	Steam Line		0.100	-	10.0	MPa	1.08%FS
13	Press.	P-13	PA	13	Break A Downstream	Not Measured	0.100	-	10.0	MPa	1.08%FS
14	Press.	P-14	PA	14	Break B Upstream		0.100	-	10.0	MPa	1.08%FS
15	Press.	P-15	PA	15	Break B Downstream		0.100	-	10.0	MPa	1.08%FS
16	Press.	P-16	PA	16	Steam Line		0.100	-	10.0	MPa	1.08%FS
17	Press.	P-17	PA	17	JP-1,2 Outlet Spool		0.100	-	10.0	MPa	1.08%FS
18	Press.	P-18	PA	18	JP-3,4 Outlet Spool		0.100	-	10.0	MPa	1.08%FS
19	Press.	P-19	PA	19	Break A Spool Piece		0.100	-	10.0	MPa	1.08%FS
20	Press.	P-30	PA	20	Break B Spool Piece		0.100	-	10.0	MPa	1.08%FS
21	Diff.P.	D- 1	PD	21	Lower Pl.-Upper Pl.	Fig.A. 2	-50.0	-	350.	kPa	0.63%FS
22	Diff.P.	D- 2	PD	22	Upper Pl.-Steam Dome	Fig.A. 3	-10.0	-	90.0	kPa	0.63%FS
23	Diff.P.	D- 3	PD	23	Lower Plenum Head	Not Measured					
24	Diff.P.	D- 4	PD	24	Downcomer Head	Fig.A. 4	0.0	-	100.	kPa	0.63%FS
25	Diff.P.	D- 5	PD	25	PV Bottom-Top	Fig.A. 5	-100.	-	900.	kPa	0.63%FS
26	Diff.P.	D- 6	PD	26	JP-1 Disch.-Suction	Fig.A. 6	-100.	-	300.	kPa	0.63%FS
27	Diff.P.	D- 7	PD	27	JP-1 Drive -Suction	Fig.A. 7	0.0	-	2.50	MPa	0.63%FS
28	Diff.P.	D- 8	PD	28	JP-2 Disch.-Suction	Fig.A. 6	-100.	-	300.	kPa	0.63%FS
29	Diff.P.	D- 9	PD	29	JP-2 Drive -Suction	Fig.A. 7	0.0	-	2.50	MPa	0.63%FS
30	Diff.P.	D-10	PD	30	JP-3 Disch.-Suction	Fig.A. 8	-100.	-	300.	kPa	0.63%FS
31	Diff.P.	D-11	PD	31	JP-3 Drive -Suction	Fig.A. 9	-4.00	-	2.00	MPa	0.63%FS
32	Diff.P.	D-12	PD	32	JP-4 Disch.-Suction	Fig.A. 8	-100.	-	300.	kPa	0.63%FS
33	Diff.P.	D-13	PD	33	JP-4 Drive -Suction	Fig.A. 9	-4.00	-	2.00	MPa	0.63%FS
34	Diff.P.	D-14	PD	34	MRP-1 Deliv.-Suction	Fig.A.10	-0.100	-	2.50	MPa	0.63%FS
35	Diff.P.	D-15	PD	35	MRP-2 Deliv.-Suction	Fig.A.10	-0.100	-	2.50	MPa	0.63%FS
36	Diff.P.	D-16	PD	36	DC Bottom- MRP-1 Suc.	Fig.A.11	-50.0	-	50.0	kPa	0.63%FS
37	Diff.P.	D-17	PD	37	MRP1 Deliv.-JP1 Drive	Fig.A.12	0.0	-	250.	kPa	0.63%FS
38	Diff.P.	D-18	PD	38	MRP1 Deliv.-JP2 Drive	Fig.A.12	0.0	-	250.	kPa	0.63%FS
39	Diff.P.	D-19	PD	39	DC Middle-JP1 Suction	Fig.A.13	0.0	-	250.	kPa	0.63%FS
40	Diff.P.	D-20	PD	40	DC Middle-JP2 Suction	Fig.A.13	0.0	-	250.	kPa	0.63%FS
41	Diff.P.	D-21	PD	41	JP1 Disch.-Lower Pl.	Fig.A.14	-100.	-	100.	kPa	0.63%FS
42	Diff.P.	D-22	PD	42	JP2 Disch.-Lower Pl.	Fig.A.14	-100.	-	100.	kPa	0.63%FS
43	Diff.P.	D-23	PD	43	DC Bottom- Break B	Fig.A.15	-60.0	-	540.	kPa	0.63%FS
44	Diff.P.	D-24	PD	44	Break B- Break A	Not Measured	0.0	-	100.	kPa	0.63%FS
45	Diff.P.	D-25	PD	45	Break A- MRP2 Suction	Not Measured	-500.	-	100.	kPa	0.63%FS
46	Diff.P.	D-26	PD	46	MRP2 Deliv.-JP3 Drive	Fig.A.16	-500.	-	500.	kPa	0.63%FS
47	Diff.P.	D-27	PD	47	MRP2 Deliv.-JP4 Drive	Fig.A.16	-500.	-	500.	kPa	0.63%FS
48	Diff.P.	D-28	PD	48	DC Middle-JP3 Suction	Fig.A.17	-250.	-	250.	kPa	0.63%FS
49	Diff.P.	D-29	PD	49	DC Middle-JP4 Suction	Fig.A.17	-250.	-	250.	kPa	0.63%FS
50	Diff.P.	D-30	PD	50	JP3 Disch.-Confluence	Fig.A.18	-100.	-	100.	kPa	0.63%FS

Table A.1 Measurement list for RUN 992 (Cont'd)

51Ch.- 100Ch.

Ch.	Item	Symbol	ID.		Location	Fig.No.	Range			Unit	Accuracy
51	Diff.P.	D-31	PD	51	JP4 Disch.-Confluence	Fig.A.18	-100.	-	100.	kPa	0.63%FS
52	Diff.P.	D-32	PD	52	Confluence -Lower Pl.	Fig.A.19	-50.0	-	50.0	kPa	0.63%FS
53	Diff.P.	D-33	PD	53	Lower Pl.-DC Middle	Fig.A.20	-250.	-	250.	kPa	0.63%FS
54	Diff.P.	D-34	PD	54	Lower Pl.-DC Bottom	Fig.A.21	-250.	-	250.	kPa	0.63%FS
55	Diff.P.	D-35	PD	55	DC Bottom-DC Middle	Fig.A.22	-50.0	-	50.0	kPa	0.63%FS
56	Diff.P.	D-36	PD	56	DC Middle-Steam Dome	Fig.A.23	-50.0	-	50.0	kPa	0.63%FS
57	Diff.P.	D-37	PD	57	Lower Pl.Mid-Upper PL	Not Measured					
58	Diff.P.	D-38	PD	58	Lower Pl.Bottom-Mid.	Fig.A.24	0.0	-	50.0	kPa	0.63%FS
59	Diff.P.	D-39	PD	59	Upper Pl.-DC High		-20.0	-	100.	kPa	0.63%FS
60	Diff.P.	D-40	PD	60	Channel Orifice A	Fig.A.25	-50.0	-	50.0	kPa	0.63%FS
61	Diff.P.	D-41	PD	61	Channel Orifice B	Fig.A.26	-50.0	-	50.0	kPa	0.63%FS
62	Diff.P.	D-42	PD	62	Channel Orifice C	Fig.A.27	-25.0	-	75.0	kPa	0.63%FS
63	Diff.P.	D-43	PD	63	Channel Orifice D	Fig.A.28	-50.0	-	50.0	kPa	0.63%FS
64	Diff.P.	D-44	PD	64	Bypass Hole	Fig.A.29	-100.	-	100.	KPA	0.63%FS
65	Level	WL- 1	LM	65	HPCS Tank	Not Used	0.0	-	2.30	m	1.00%FS
66	Level	WL- 2	LM	66	LPCS Tank	Not Used	0.0	-	2.30	m	1.00%FS
67	Level	WL- 3	LM	67	LPCI Tank	Fig.A.30	0.0	-	4.25	m	1.00%FS
68	Level	WL- 4	LM	68	Upper Downcomer	Fig.A.31	3.90	-	6.04	m	1.00%FS
69	Level	WL- 5	LM	69	Lower Downcomer	Fig.A.31	0.938	-	3.90	m	1.00%FS
70	Mass.F.	F- 1	FM	70	Steam Line (Low Range)	Fig.A.32	0.0	-	1.13	kg/s	0.92%FS
71	Mass.F.	F- 2	FM	71	Steam Line(High Range)	Fig.A.32	0.0	-	3.00	kg/s	0.92%FS
72	Mass.F.	F- 3	FM	72	Steam Line (Mid Range)	Fig.A.32	0.0	-	1.94	kg/s	1.40%FS
73	Vol.F.	F- 7	FV	73	HPCS (Upper Plenum)	Not Used	0.0	-	0.250E-02	m3/s	0.79%FS
74	Vol.F.	F- 9	FV	74	LPCS (Upper Plenum)	Not Used	0.0	-	0.250E-02	m3/s	0.79%FS
75	Vol.F.	F-11	FV	75	LPCI (Core Bypass)	Fig.A.33	0.0	-	0.830E-02	m3/s	0.79%FS
76	Vol.F.	F-15	FV	76	Feedwater	Fig.A.34	0.0	-	0.100E-01	m3/s	0.79%FS
77	Vol.F.	F-16	FV	77	PWT Flow		0.0	-	0.420E-02	m3/s	0.79%FS
78	Vol.F.	F-17	FV	78	JP1 Discharge	Fig.A.35	0.0	-	0.170E-01	m3/s	0.88%FS
79	Vol.F.	F-18	FV	79	JP2 Discharge	Fig.A.35	0.0	-	0.170E-01	m3/s	0.88%FS
80	Vol.F.	F-19	FV	80	JP3 Disch. Positive	Fig.A.36	0.0	-	0.170E-01	m3/s	0.92%FS
81	Vol.F.	F-20	FV	81	JP3 Disch. Negative	Fig.A.37	0.0	-	0.500E-02	m3/s	0.92%FS
82	Vol.F.	F-21	FV	82	JP4 Disch. Positive	Fig.A.36	0.0	-	0.170E-01	m3/s	0.92%FS
83	Vol.F.	F-22	FV	83	JP4 Disch. Negative	Fig.A.37	0.0	-	0.500E-02	m3/s	0.92%FS
84	Mass.F.	F-23	FM	84	JP1,2 Outlet Spool	Not Measured	0.0	-	30.0	kg/s	1.40%FS
85	Mass.F.	F-24	FM	85	JP3,4 Outlet Spool	Not Measured	0.0	-	30.0	kg/s	1.40%FS
86	Mass.F.	F-25	FM	86	Break A Spool Piece	Not Measured	0.0	-	30.0	kg/s	1.40%FS
87	Mass.F.	F-26	FM	87	Break B Spool Piece	Not Measured	0.0	-	30.0	kg/s	1.40%FS
88	Vol.F.	F-27	FV	88	MRP-1	Fig.A.38	0.0	-	0.120E-01	m3/s	0.88%FS
89	Vol.F.	F-28	FV	89	MRP-2	Fig.A.38	0.0	-	0.120E-01	m3/s	0.63%FS
90	Diff.P.	D-F1	PD	90	F1 Orifice		0.0	-	4.90	kPa	0.63%FS
91	Diff.P.	D-F2	PD	91	F2 Orifice		0.0	-	34.9	kPa	0.63%FS
92	Diff.P.	D-F3	PD	92	F3 Orifice		0.0	-	14.6	kPa	0.63%FS
93	Diff.P.	D-F17	PD	93	F17 Venturi		0.0	-	98.1	kPa	0.63%FS
94	Diff.P.	D-F18	PD	94	F18 Venturi		0.0	-	98.1	kPa	0.63%FS
95	Diff.P.	D-F19	PD	95	F19 Orifice		0.0	-	147.	kPa	0.63%FS
96	Diff.P.	D-F20	PD	96	F20 Orifice		0.0	-	13.2	kPa	0.63%FS
97	Diff.P.	D-F21	PD	97	F21 Orifice		0.0	-	147.	kPa	0.63%FS
98	Diff.P.	D-F22	PD	98	F22 Orifice		0.0	-	13.2	kPa	0.63%FS
99	Diff.P.	D-F27	PD	99	F27 Venturi		0.0	-	200.	kPa	0.63%FS
100	Diff.P.	D-F28	PD	100	F28 Venturi		0.0	-	200.	kPa	0.63%FS

Table A.1 Measurement list for RUN 992 (Cont'd)

101Ch.- 150Ch.

Ch.	Item	Symbol	ID.	Location	Fig.No.	Range	Unit	Accuracy
101	Power	W- 1	WE 101	2100 kW Power Supplier	Fig.A.39	0.0 - 0.210E+04	kW	1.00%FS
102	Power	W- 2	WE 102	3150 kW Power Supplier	Fig.A.39	0.0 - 0.315E+04	kW	1.00%FS
103								
104	Rev.	N- 1	SR 104	MRP-1 Revolution	Failure	0.0 - 0.500E+04	RPM	1.08%FS
105	Rev.	N- 2	SR 105	MRP-2 Revolution	Fig.A.40	0.0 - 0.500E+04	RPM	1.08%FS
106	Signal	S- 1	EV 106	Break Signal A	Not Used			
107	Signal	S- 2	EV 107	Break Signal B	Fig.A.41			
108	Signal	S- 3	EV 108	QSV Signal	Not Used			
109	Signal	S- 6	EV 109	HPCS Valve	Not Used			
110	Signal	S- 7	EV 110	LPCS Valve	Not Used			
111	Signal	S- 8	EV 111	LPCI Valve	Fig.A.42			
112	Signal	S- 9	EV 112	Feedwater Control	Fig.A.41			
113	Signal	S-10	EV 113	MSIV Signal	Fig.A.41			
114	Signal	S-11	EV 114	Steam Line Valve	Not Used			
115	Signal	S-12	EV 115	ADS Valve	Fig.A.42			
116	Signal	S-13	EV 116	MRP-1 Power OFF	Fig.A.43			
117	Signal	S-14	EV 117	MRP-2 Power OFF	Fig.A.43			
118	Signal	RD- 1	EV 118	MRP-1 Rev. Direction	Failure			
119	Signal	RD- 2	EV 119	MRP-2 Rev. Direction	Failure			
120	Density	DF- 1	DE 120	JP1,2 Outlet Beam A	Not Measured	0.0 - 0.100E+04	kg/m3	1.00%FS
121	Density	DF- 2	DE 121	JP1,2 Outlet Beam B	Not Measured	0.0 - 0.100E+04	kg/m3	1.00%FS
122	Density	DF- 3	DE 122	JP1,2 Outlet Beam C	Not Measured	0.0 - 0.100E+04	kg/m3	1.00%FS
123	Density	DF- 4	DE 123	JP3,4 Outlet Beam A	Not Measured	0.0 - 0.100E+04	kg/m3	1.00%FS
124	Density	DF- 5	DE 124	JP3,4 Outlet Beam B	Not Measured	0.0 - 0.100E+04	kg/m3	1.00%FS
125	Density	DF- 6	DE 125	JP3,4 Outlet Beam C	Not Measured	0.0 - 0.100E+04	kg/m3	1.00%FS
126	Density	DF- 7	DE 126	Break A Beam A	Not Used	0.0 - 0.100E+04	kg/m3	1.00%FS
127	Density	DF- 8	DE 127	Break A Beam B	Not Used	0.0 - 0.100E+04	kg/m3	1.00%FS
128	Density	DF- 9	DE 128	Break B Beam A	Fig.A.44	0.0 - 0.100E+04	kg/m3	1.00%FS
129	Density	DF-10	DE 129	Break B Beam B	Fig.A.45	0.0 - 0.100E+04	kg/m3	1.00%FS
130	Mo.Flux	M- 1	MF 130	JP1,2 Outlet Spool	Fig.A.46	0.0 - 0.220E+05	kg/ms2	1.00%FS
131	Mo.Flux	M- 2	MF 131	JP3,4 Outlet Spool	Fig.A.47	0.0 - 0.220E+05	kg/ms2	1.00%FS
132	Mo.Flux	M- 3	MF 132	Break A (Low Range)	Not Used	0.0 - 0.220E+05	kg/ms2	1.00%FS
133	Mo.Flux	M- 4	MF 133	Break B (Low Range)	Fig.A.48	0.0 - 0.220E+05	kg/ms2	1.00%FS
134	Mo.Flux	M- 5	MF 134	Break A (High Range)	Not Used	0.0 - 0.220E+06	kg/ms2	1.00%FS
135	Mo.Flux	M- 6	MF 135	Break B (High Range)	Failure	0.0 - 0.220E+06	kg/ms2	1.00%FS
136	Mo.Flux	M- 7	MF 136	Break Orifice		0.0 - 0.220E+05	kg/ms2	1.00%FS
137								
138	Fluid T.	T- 1	TE 138	Lower Plenum	Fig.A.49	273. - 673.	K	0.64%FS
139	Fluid T.	T- 2	TE 139	Upper Plenum	Fig.A.49	273. - 673.	K	0.64%FS
140	Fluid T.	T- 3	TE 140	Steam Dome	Fig.A.50	273. - 673.	K	0.64%FS
141	Fluid T.	T- 4	TE 141	Upper Downcomer	Fig.A.51	273. - 673.	K	0.64%FS
142	Fluid T.	T- 5	TE 142	Lower Downcomer	Fig.A.51	273. - 673.	K	0.64%FS
143	Fluid T.	T- 6	TE 143	JP-1 Drive	Fig.A.52	273. - 673.	K	0.64%FS
144	Fluid T.	T- 7	TE 144	JP-2 Drive	Fig.A.52	273. - 673.	K	0.64%FS
145	Fluid T.	T- 8	TE 145	JP-3 Drive	Fig.A.53	273. - 673.	K	0.64%FS
146	Fluid T.	T- 9	TE 146	JP-4 Drive	Fig.A.53	273. - 673.	K	0.64%FS
147	Fluid T.	T-10	TE 147	JP-1 Discharge	Fig.A.54	273. - 673.	K	0.64%FS
148	Fluid T.	T-11	TE 148	JP-2 Discharge	Fig.A.54	273. - 673.	K	0.64%FS
149	Fluid T.	T-12	TE 149	JP-3 Discharge	Fig.A.55	273. - 673.	K	0.64%FS
150	Fluid T.	T-13	TE 150	JP-4 Discharge	Fig.A.55	273. - 673.	K	0.64%FS

Table A.1 Measurement list for RUN 992 (Cont'd)

151Ch.- 200Ch.

Ch.	Item	Symbol	ID.		Location	Fig.No.	Range			Unit	Accuracy
151	Fluid T.	T-14	TE	151	MRP-1 Suction	Fig.A.52	273.	-	673.	K	0.64%FS
152	Fluid T.	T-15	TE	152	MRP-1 Delivery	Fig.A.52	273.	-	673.	K	0.64%FS
153	Fluid T.	T-16	TE	153	MRP-2 Suction	Fig.A.53	273.	-	673.	K	0.64%FS
154	Fluid T.	T-17	TE	154	MRP-2 Delivery	Fig.A.53	273.	-	673.	K	0.64%FS
155	Fluid T.	T-18	TE	155	Break A Upstream	Not Used	273.	-	673.	K	0.64%FS
156	Fluid T.	T-19	TE	156	Break B Upstream	Fig.A.56	273.	-	673.	K	0.64%FS
157	Fluid T.	T-20	TE	157	RCN A Condenced Water	Not Used	273.	-	698.	K	0.64%FS
158	Fluid T.	T-21	TE	158	RCN B Condenced Water		273.	-	698.	K	0.64%FS
159	Fluid T.	T-22	TE	159	Discharged Steam	Fig.A.50	273.	-	673.	K	0.64%FS
160	Fluid T.	T-24	TE	160	JP-1,2 Outlet Spool	Fig.A.54	273.	-	763.	K	0.64%FS
161	Fluid T.	T-25	TE	161	JP-3,4 Outlet Spool	Fig.A.55	273.	-	763.	K	0.64%FS
162	Fluid T.	T-26	TE	162	Break A Spool Piece	Not Used	273.	-	763.	K	0.64%FS
163	Fluid T.	T-27	TE	163	Break B Spool Piece	Fig.A.57	273.	-	763.	K	0.64%FS
164	Fluid T.	T-28	TE	164	Feedwater	Fig.A.58	273.	-	673.	K	0.64%FS
165	Fluid T.	T-29	TE	165	Break B Upstream	Fig.A.56	273.	-	673.	K	0.64%FS
166	Fluid T.	T-30	TE	166	Break B Downstream	Fig.A.56	273.	-	673.	K	0.64%FS
167	Fluid T.	T-31	TE	167	Break A Down DD(Low)	Not Measured	273.	-	673.	K	0.64%FS
168	Fluid T.	T-32	TE	168	Break B Down DD(Low)	Not Measured	273.	-	673.	K	0.64%FS
169	Fluid T.	T-33	TE	169	Break A Up. DD(High)	Not Used	273.	-	673.	K	0.64%FS
170	Fluid T.	T-34	TE	170	Break B Up. DD(High)	Fig.A.57	273.	-	673.	K	0.64%FS
171	Fluid T.	T-F17	TE	171	JP1 Fluid D. Correc.		273.	-	673.	K	0.64%FS
172	Fluid T.	T-F18	TE	172	JP2 Fluid D. Correc.		273.	-	673.	K	0.64%FS
173	Fluid T.	T-F19	TE	173	JP3 Fluid D. Correc.		273.	-	673.	K	0.64%FS
174	Fluid T.	T-F21	TE	174	JP4 Fluid D. Correc.		273.	-	673.	K	0.64%FS
175	Slab T.	TS-35	TE	175	Feedwater Temperat.	Fig.A.58	273.	-	673.	K	0.64%FS
176	Slab T.		TE	176	Steam Line (F110-3)	Fig.A.57	273.	-	673.	K	0.64%FS
177	Slab T.	TS-13	TE	177	Filler Block C Pos.1	Not Measured	273.	-	673.	K	0.64%FS
178	Slab T.	TS-14	TE	178	Filler Block C Pos.2	Not Measured	273.	-	673.	K	0.64%FS
179	Slab T.	TS-15	TE	179	Filler Block C Pos.3	Fig.A.59	273.	-	673.	K	0.64%FS
180	Slab T.	TS-16	TE	180	Filler Block C Pos.4	Not Measured	273.	-	673.	K	0.64%FS
181	Slab T.	TS-17	TE	181	Filler Block C Pos.5	Not Measured	273.	-	673.	K	0.64%FS
182	Slab T.	TS-18	TE	182	Filler Block C Pos.6	Fig.A.59	273.	-	673.	K	0.64%FS
183	Slab T.	TS-19	TE	183	Filler Block A Pos.1	Not Measured	273.	-	673.	K	0.64%FS
184	Slab T.	TS-20	TE	184	Filler Block A Pos.2	Not Measured	273.	-	673.	K	0.64%FS
185	Slab T.	TS-21	TE	185	Filler Block A Pos.3	Not Measured	273.	-	673.	K	0.64%FS
186	Slab T.	TS-22	TE	186	Filler Block A Pos.4	Not Measured	273.	-	673.	K	0.64%FS
187	Slab T.	TS-23	TE	187	Filler Block A Pos.5	Not Measured	273.	-	673.	K	0.64%FS
188	Slab T.	TS-24	TE	188	Filler Block A Pos.6	Not Measured	273.	-	673.	K	0.64%FS
189	Slab T.	TS-25	TE	189	JP-1 Diffuser Wall	Not Measured	273.	-	673.	K	0.64%FS
190	Slab T.	TS-26	TE	190	JP-2 Diffuser Wall	Not Measured	273.	-	673.	K	0.64%FS
191	Slab T.	TS-27	TE	191	JP-3 Diffuser Wall	Not Measured	273.	-	673.	K	0.64%FS
192	Slab T.	TS-28	TE	192	JP-4 Diffuser Wall	Not Measured	273.	-	673.	K	0.64%FS
193	Slab T.	TS-29	TE	193	PV Wall Inside 1-1	Fig.A.60	273.	-	673.	K	0.64%FS
194	Slab T.	TS-30	TE	194	PV Inner Surface 1-2	Not Measured	273.	-	673.	K	0.64%FS
195	Slab T.	TS-31	TE	195	PV Inner Surface 1-3	Fig.A.60	273.	-	673.	K	0.64%FS
196	Slab T.	TS-32	TE	196	PV Wall Inside 2	Fig.A.61	273.	-	673.	K	0.64%FS
197	Slab T.	TS-33	TE	197	PV Wall Inside 3	Fig.A.62	273.	-	673.	K	0.64%FS
198	Slab T.	TS-34	TE	198	PV Wall Inside 4	Fig.A.62	273.	-	673.	K	0.64%FS
199	Slab T.	TS-35	TE	199	L.P. Inner Surface	Not Measured	273.	-	673.	K	0.64%FS
200	Slab T.	TS-36	TE	200	L.P. Wall Inside	Fig.A.63	273.	-	673.	K	0.64%FS

Table A.1 Measurement list for RUN 992 (Cont'd)

201Ch.- 250Ch.

Ch.	Item	Symbol	ID.	Location	Fig.No.	Range	Unit	Accuracy
201	Temp.	TF- 1	TE 201	A11 Fuel Rod Pos.1	Fig.A.65, 85	273. - 0.147E+04	K	0.64%FS
202	Temp.	TF- 2	TE 202	A11 Fuel Rod Pos.2	Fig.A.65, 86	273. - 0.147E+04	K	0.64%FS
203	Temp.	TF- 3	TE 203	A11 Fuel Rod Pos.3	Fig.A.65, 87	273. - 0.147E+04	K	0.64%FS
204	Temp.	TF- 4	TE 204	A11 Fuel Rod Pos.4	Fig.A.65, 88	273. - 0.147E+04	K	0.64%FS
205	Temp.	TF- 5	TE 205	A11 Fuel Rod Pos.5	Fig.A.65, 89	273. - 0.147E+04	K	0.64%FS
206	Temp.	TF- 6	TE 206	A11 Fuel Rod Pos.6	Fig.A.65, 90	273. - 0.147E+04	K	0.64%FS
207	Temp.	TF- 7	TE 207	A11 Fuel Rod Pos.7	Fig.A.65, 91	273. - 0.147E+04	K	0.64%FS
208	Temp.	TF- 8	TE 208	A12 Fuel Rod Pos.1	Fig.A.66, 85	273. - 0.147E+04	K	0.64%FS
209	Temp.	TF- 9	TE 209	A12 Fuel Rod Pos.2	Fig.A.66, 86	273. - 0.147E+04	K	0.64%FS
210	Temp.	TF- 10	TE 210	A12 Fuel Rod Pos.3	Fig.A.66, 87	273. - 0.147E+04	K	0.64%FS
211	Temp.	TF- 11	TE 211	A12 Fuel Rod Pos.4	Fig.A.66, 88	273. - 0.147E+04	K	0.64%FS
212	Temp.	TF- 12	TE 212	A12 Fuel Rod Pos.5	Fig.A.66, 89	273. - 0.147E+04	K	0.64%FS
213	Temp.	TF- 13	TE 213	A12 Fuel Rod Pos.6	Fig.A.66, 90	273. - 0.147E+04	K	0.64%FS
214	Temp.	TF- 14	TE 214	A12 Fuel Rod Pos.7	Fig.A.66, 91	273. - 0.147E+04	K	0.64%FS
215	Temp.	TF- 15	TE 215	A13 Fuel Rod Pos.1	Fig.A.67, 85	273. - 0.147E+04	K	0.64%FS
216	Temp.	TF- 16	TE 216	A13 Fuel Rod Pos.2	Fig.A.67, 86	273. - 0.147E+04	K	0.64%FS
217	Temp.	TF- 17	TE 217	A13 Fuel Rod Pos.3	Fig.A.67, 87	273. - 0.147E+04	K	0.64%FS
218	Temp.	TF- 18	TE 218	A13 Fuel Rod Pos.4	Fig.A.67, 88	273. - 0.147E+04	K	0.64%FS
219	Temp.	TF- 19	TE 219	A13 Fuel Rod Pos.5	Fig.A.67, 89	273. - 0.147E+04	K	0.64%FS
220	Temp.	TF- 20	TE 220	A13 Fuel Rod Pos.6	Fig.A.67, 90	273. - 0.147E+04	K	0.64%FS
221	Temp.	TF- 21	TE 221	A13 Fuel Rod Pos.7	Fig.A.67, 91	273. - 0.147E+04	K	0.64%FS
222	Temp.	TF- 22	TE 222	A14 Fuel Rod Pos.1	Not Measured	273. - 0.147E+04	K	0.64%FS
223	Temp.	TF- 23	TE 223	A14 Fuel Rod Pos.2	Not Measured	273. - 0.147E+04	K	0.64%FS
224	Temp.	TF- 24	TE 224	A14 Fuel Rod Pos.3	Not Measured	273. - 0.147E+04	K	0.64%FS
225	Temp.	TF- 25	TE 225	A14 Fuel Rod Pos.4	Not Measured	273. - 0.147E+04	K	0.64%FS
226	Temp.	TF- 26	TE 226	A14 Fuel Rod Pos.5	Not Measured	273. - 0.147E+04	K	0.64%FS
227	Temp.	TF- 27	TE 227	A14 Fuel Rod Pos.6	Not Measured	273. - 0.147E+04	K	0.64%FS
228	Temp.	TF- 28	TE 228	A14 Fuel Rod Pos.7	Not Measured	273. - 0.147E+04	K	0.64%FS
229	Temp.	TF- 29	TE 229	A15 Fuel Rod Pos.1	Not Measured	273. - 0.147E+04	K	0.64%FS
230	Temp.	TF- 30	TE 230	A15 Fuel Rod Pos.4	Not Measured	273. - 0.147E+04	K	0.64%FS
231	Temp.	TF- 31	TE 231	A17 Fuel Rod Pos.1	Not Measured	273. - 0.147E+04	K	0.64%FS
232	Temp.	TF- 32	TE 232	A17 Fuel Rod Pos.4	Fig.A.82	273. - 0.147E+04	K	0.64%FS
233	Temp.	TF- 33	TE 233	A22 Fuel Rod Pos.1	Fig.A.68, 92	273. - 0.147E+04	K	0.64%FS
234	Temp.	TF- 34	TE 234	A22 Fuel Rod Pos.2	Fig.A.68, 93	273. - 0.147E+04	K	0.64%FS
235	Temp.	TF- 35	TE 235	A22 Fuel Rod Pos.3	Fig.A.68, 94	273. - 0.147E+04	K	0.64%FS
236	Temp.	TF- 36	TE 236	A22 Fuel Rod Pos.4	Fig.A.68, 95	273. - 0.125E+04	K	0.64%FS
237	Temp.	TF- 37	TE 237	A22 Fuel Rod Pos.5	Fig.A.68, 96	273. - 0.125E+04	K	0.64%FS
238	Temp.	TF- 38	TE 238	A22 Fuel Rod Pos.6	Fig.A.68, 97	273. - 0.125E+04	K	0.64%FS
239	Temp.	TF- 39	TE 239	A22 Fuel Rod Pos.7	Fig.A.68, 98	273. - 0.125E+04	K	0.64%FS
240	Temp.	TS- 41	TE 240	PV Out.Surf.(TS30)	Fig.A.60	273. - 0.125E+04	K	0.64%FS
241	Temp.	TS- 42	TE 241	PV Out.Surf.(TS32)	Fig.A.61	273. - 0.125E+04	K	0.64%FS
242	Temp.	TS- 43	TE 242	PV Out.Surf.(TS34)	Fig.A.62	273. - 0.125E+04	K	0.64%FS
243	Temp.	TS- 44	TE 243	PV Out.Surf.(TS36)	Fig.A.63	273. - 0.125E+04	K	0.64%FS
244	Temp.	TS- 45	TE 244	PV Bottom Out.Suf.	Fig.A.63	273. - 0.125E+04	K	0.64%FS
245	Temp.	TS- 46	TE 245	JP Out.Surf.(TS28)	Fig.A.64	273. - 0.125E+04	K	0.64%FS
246	Temp.	TS- 47	TE 246	Pipe Out.Suf.(T17)	Fig.A.64	273. - 0.125E+04	K	0.64%FS
247	Temp.	TS- 48	TE 247	Pipe Out.Suf.(T24)	Fig.A.64	273. - 0.125E+04	K	0.64%FS
248	Temp.	TF- 48	TE 248	A26 Fuel Rod Pos.2	Not Measured	273. - 0.125E+04	K	0.64%FS
249	Temp.	TF- 49	TE 249	A28 Fuel Rod Pos.1	Not Measured	273. - 0.125E+04	K	0.64%FS
250	Temp.	TF- 50	TE 250	A28 Fuel Rod Pos.4	Fig.A.83	273. - 0.125E+04	K	0.64%FS

Table A.1 Measurement list for RUN 992 (Cont'd)

251Ch.- 300Ch.

Ch.	Item	Symbol	ID.	Location	Fig.No.	Range	Unit	Accuracy
251	Temp.	TF- 51	TE 251	A31 Fuel Rod Pos.1	Not Measured	273. - 0.125E+04	K	0.64%FS
252	Temp.	TF- 52	TE 252	A31 Fuel Rod Pos.4	Fig.A.82	273. - 0.125E+04	K	0.64%FS
253	Temp.	TF- 53	TE 253	A33 Fuel Rod Pos.1	Fig.A.69	273. - 0.125E+04	K	0.64%FS
254	Temp.	TF- 54	TE 254	A33 Fuel Rod Pos.2	Fig.A.69	273. - 0.125E+04	K	0.64%FS
255	Temp.	TF- 55	TE 255	A33 Fuel Rod Pos.3	Fig.A.69	273. - 0.125E+04	K	0.64%FS
256	Temp.	TF- 56	TE 256	A33 Fuel Rod Pos.4	Fig.A.69	273. - 0.125E+04	K	0.64%FS
257	Temp.	TF- 57	TE 257	A33 Fuel Rod Pos.5	Fig.A.69	273. - 0.125E+04	K	0.64%FS
258	Temp.	TF- 58	TE 258	A33 Fuel Rod Pos.6	Fig.A.69	273. - 0.125E+04	K	0.64%FS
259	Temp.	TF- 59	TE 259	A33 Fuel Rod Pos.7	Fig.A.69	273. - 0.125E+04	K	0.64%FS
260	Temp.	TF- 60	TE 260	A34 Fuel Rod Pos.1	Not Measured	273. - 0.125E+04	K	0.64%FS
261	Temp.	TF- 61	TE 261	A34 Fuel Rod Pos.2	Not Measured	273. - 0.125E+04	K	0.64%FS
262	Temp.	TF- 62	TE 262	A34 Fuel Rod Pos.3	Not Measured	273. - 0.125E+04	K	0.64%FS
263	Temp.	TF- 63	TE 263	A34 Fuel Rod Pos.4	Not Measured	273. - 0.125E+04	K	0.64%FS
264	Temp.	TF- 64	TE 264	A34 Fuel Rod Pos.5	Not Measured	273. - 0.125E+04	K	0.64%FS
265	Temp.	TF- 65	TE 265	A34 Fuel Rod Pos.6	Not Measured	273. - 0.125E+04	K	0.64%FS
266	Temp.	TF- 66	TE 266	A34 Fuel Rod Pos.7	Not Measured	273. - 0.125E+04	K	0.64%FS
267	Temp.	TF- 67	TE 267	A37 Fuel Rod Pos.1	Not Measured	273. - 0.125E+04	K	0.64%FS
268	Temp.	TF- 68	TE 268	A37 Fuel Rod Pos.4	Not Measured	273. - 0.125E+04	K	0.64%FS
269	Temp.	TF- 69	TE 269	A42 Fuel Rod Pos.1	Not Measured	273. - 0.125E+04	K	0.64%FS
270	Temp.	TF- 70	TE 270	A42 Fuel Rod Pos.4	Not Measured	273. - 0.125E+04	K	0.64%FS
271	Temp.	TF- 71	TE 271	A44 Fuel Rod Pos.1	Not Measured	273. - 0.125E+04	K	0.64%FS
272	Temp.	TF- 72	TE 272	A44 Fuel Rod Pos.2	Not Measured	273. - 0.125E+04	K	0.64%FS
273	Temp.	TF- 73	TE 273	A44 Fuel Rod Pos.3	Not Measured	273. - 0.125E+04	K	0.64%FS
274	Temp.	TF- 74	TE 274	A44 Fuel Rod Pos.4	Not Measured	273. - 0.125E+04	K	0.64%FS
275	Temp.	TF- 75	TE 275	A44 Fuel Rod Pos.5	Not Measured	273. - 0.125E+04	K	0.64%FS
276	Temp.	TF- 76	TE 276	A44 Fuel Rod Pos.6	Not Measured	273. - 0.125E+04	K	0.64%FS
277	Temp.	TF- 77	TE 277	A44 Fuel Rod Pos.7	Not Measured	273. - 0.125E+04	K	0.64%FS
278	Temp.	TF- 78	TE 278	A48 Fuel Rod Pos.1	Not Measured	273. - 0.125E+04	K	0.64%FS
279	Temp.	TF- 79	TE 279	A48 Fuel Rod Pos.4	Not Measured	273. - 0.125E+04	K	0.64%FS
280	Temp.	TF- 80	TE 280	A51 Fuel Rod Pos.1	Not Measured	273. - 0.125E+04	K	0.64%FS
281	Temp.	TF- 81	TE 281	A51 Fuel Rod Pos.4	Not Measured	273. - 0.125E+04	K	0.64%FS
282	Temp.	TF- 82	TE 282	A53 Fuel Rod Pos.1	Not Measured	273. - 0.125E+04	K	0.64%FS
283	Temp.	TF- 83	TE 283	A53 Fuel Rod Pos.4	Not Measured	273. - 0.125E+04	K	0.64%FS
284	Temp.	TF- 84	TE 284	A57 Fuel Rod Pos.1	Not Measured	273. - 0.125E+04	K	0.64%FS
285	Temp.	TF- 85	TE 285	A57 Fuel Rod Pos.4	Fig.A.83	273. - 0.125E+04	K	0.64%FS
286	Temp.	TF- 86	TE 286	A62 Fuel Rod Pos.1	Not Measured	273. - 0.125E+04	K	0.64%FS
287	Temp.	TF- 87	TE 287	A62 Fuel Rod Pos.4	Not Measured	273. - 0.125E+04	K	0.64%FS
288	Temp.	TF- 88	TE 288	A66 Fuel Rod Pos.1	Not Measured	273. - 0.125E+04	K	0.64%FS
289	Temp.	TF- 89	TE 289	A66 Fuel Rod Pos.4	Not Measured	273. - 0.125E+04	K	0.64%FS
290	Temp.	TF- 90	TE 290	A68 Fuel Rod Pos.1	Not Measured	273. - 0.125E+04	K	0.64%FS
291	Temp.	TF- 91	TE 291	A68 Fuel Rod Pos.4	Fig.A.82	273. - 0.125E+04	K	0.64%FS
292	Temp.	TF- 92	TE 292	A71 Fuel Rod Pos.1	Not Measured	273. - 0.125E+04	K	0.64%FS
293	Temp.	TF- 93	TE 293	A71 Fuel Rod Pos.4	Fig.A.82	273. - 0.125E+04	K	0.64%FS
294	Temp.	TF- 94	TE 294	A73 Fuel Rod Pos.1	Not Measured	273. - 0.125E+04	K	0.64%FS
295	Temp.	TF- 95	TE 295	A73 Fuel Rod Pos.4	Fig.A.83	273. - 0.125E+04	K	0.64%FS
296	Temp.	TF- 96	TE 296	A75 Fuel Rod Pos.1	Not Measured	273. - 0.125E+04	K	0.64%FS
297	Temp.	TF- 97	TE 297	A75 Fuel Rod Pos.4	Not Measured	273. - 0.125E+04	K	0.64%FS
298	Temp.	TF- 98	TE 298	A77 Fuel Rod Pos.1	Fig.A.70, 99	273. - 0.125E+04	K	0.64%FS
299	Temp.	TF- 99	TE 299	A77 Fuel Rod Pos.2	Fig.A.70,100	273. - 0.125E+04	K	0.64%FS
300	Temp.	TF-100	TE 300	A77 Fuel Rod Pos.3	Fig.A.70,101	273. - 0.125E+04	K	0.64%FS

Table A.1 Measurement list for RUN 992 (Cont'd)

301Ch.- 350Ch.

Ch.	Item	Symbol	ID.	Location	Fig.No.	Range	Unit	Accuracy
301	Temp.	TF-101	TE 301	A77 Fuel Rod Pos.4	Fig.A.70,102	273. - 0.125E+04	K	0.64%FS
302	Temp.	TF-102	TE 302	A77 Fuel Rod Pos.5	Fig.A.70,103	273. - 0.125E+04	K	0.64%FS
303	Temp.	TF-103	TE 303	A77 Fuel Rod Pos.6	Fig.A.70,104	273. - 0.125E+04	K	0.64%FS
304	Temp.	TF-104	TE 304	A77 Fuel Rod Pos.7	Failure	273. - 0.125E+04	K	0.64%FS
305	Temp.	TF-105	TE 305	A82 Fuel Rod Pos.1	Not Measured	273. - 0.125E+04	K	0.64%FS
306	Temp.	TF-106	TE 306	A82 Fuel Rod Pos.4	Not Measured	273. - 0.125E+04	K	0.64%FS
307	Temp.	TF-107	TE 307	A84 Fuel Rod Pos.1	Fig.A.82	273. - 0.125E+04	K	0.64%FS
308	Temp.	TF-108	TE 308	A84 Fuel Rod Pos.4	Fig.A.83	273. - 0.125E+04	K	0.64%FS
309	Temp.	TF-109	TE 309	A85 Fuel Rod Pos.1	Not Measured	273. - 0.125E+04	K	0.64%FS
310	Temp.	TF-110	TE 310	A85 Fuel Rod Pos.2	Not Measured	273. - 0.125E+04	K	0.64%FS
311	Temp.	TF-111	TE 311	A85 Fuel Rod Pos.3	Not Measured	273. - 0.125E+04	K	0.64%FS
312	Temp.	TF-112	TE 312	A85 Fuel Rod Pos.4	Not Measured	273. - 0.125E+04	K	0.64%FS
313	Temp.	TF-113	TE 313	A85 Fuel Rod Pos.5	Not Measured	273. - 0.125E+04	K	0.64%FS
314	Temp.	TF-114	TE 314	A85 Fuel Rod Pos.6	Not Measured	273. - 0.125E+04	K	0.64%FS
315	Temp.	TF-115	TE 315	A85 Fuel Rod Pos.7	Not Measured	273. - 0.125E+04	K	0.64%FS
316	Temp.	TF-116	TE 316	A87 Fuel Rod Pos.1	Fig.A.71, 85	273. - 0.125E+04	K	0.64%FS
317	Temp.	TF-117	TE 317	A87 Fuel Rod Pos.2	Fig.A.71, 86	273. - 0.125E+04	K	0.64%FS
318	Temp.	TF-118	TE 318	A87 Fuel Rod Pos.3	Fig.A.71, 87	273. - 0.125E+04	K	0.64%FS
319	Temp.	TF-119	TE 319	A87 Fuel Rod Pos.4	Fig.A.71, 88	273. - 0.125E+04	K	0.64%FS
320	Temp.	TF-120	TE 320	A87 Fuel Rod Pos.5	Fig.A.71, 89	273. - 0.125E+04	K	0.64%FS
321	Temp.	TF-121	TE 321	A87 Fuel Rod Pos.6	Fig.A.71, 90	273. - 0.125E+04	K	0.64%FS
322	Temp.	TF-122	TE 322	A87 Fuel Rod Pos.7	Fig.A.71, 91	273. - 0.125E+04	K	0.64%FS
323	Temp.	TF-123	TE 323	A88 Fuel Rod Pos.1	Fig.A.72, 85	273. - 0.125E+04	K	0.64%FS
324	Temp.	TF-124	TE 324	A88 Fuel Rod Pos.2	Fig.A.72, 86	273. - 0.125E+04	K	0.64%FS
325	Temp.	TF-125	TE 325	A88 Fuel Rod Pos.3	Fig.A.72, 87	273. - 0.125E+04	K	0.64%FS
326	Temp.	TF-126	TE 326	A88 Fuel Rod Pos.4	Fig.A.72, 88	273. - 0.125E+04	K	0.64%FS
327	Temp.	TF-127	TE 327	A88 Fuel Rod Pos.5	Fig.A.72, 89	273. - 0.125E+04	K	0.64%FS
328	Temp.	TF-128	TE 328	A88 Fuel Rod Pos.6	Fig.A.72, 90	273. - 0.125E+04	K	0.64%FS
329	Temp.	TF-129	TE 329	A88 Fuel Rod Pos.7	Fig.A.72, 91	273. - 0.125E+04	K	0.64%FS
330	Temp.	TF-130	TE 330	B11 Fuel Rod Pos.1		273. - 0.125E+04	K	0.64%FS
331	Temp.	TF-131	TE 331	B11 Fuel Rod Pos.2		273. - 0.125E+04	K	0.64%FS
332	Temp.	TF-132	TE 332	B11 Fuel Rod Pos.3		273. - 0.125E+04	K	0.64%FS
333	Temp.	TF-133	TE 333	B11 Fuel Rod Pos.4		273. - 0.125E+04	K	0.64%FS
334	Temp.	TF-134	TE 334	B11 Fuel Rod Pos.5		273. - 0.125E+04	K	0.64%FS
335	Temp.	TF-135	TE 335	B11 Fuel Rod Pos.6		273. - 0.125E+04	K	0.64%FS
336	Temp.	TF-136	TE 336	B11 Fuel Rod Pos.7	Not Measured	273. - 0.125E+04	K	0.64%FS
337	Temp.	TF-137	TE 337	B13 Fuel Rod Pos.4	Fig.A.84	273. - 0.125E+04	K	0.64%FS
338	Temp.	TF-138	TE 338	B22 Fuel Rod Pos.1	Fig.A.73, 92	273. - 0.125E+04	K	0.64%FS
339	Temp.	TF-139	TE 339	B22 Fuel Rod Pos.2	Fig.A.73, 93	273. - 0.125E+04	K	0.64%FS
340	Temp.	TF-140	TE 340	B22 Fuel Rod Pos.3	Fig.A.73, 94	273. - 0.125E+04	K	0.64%FS
341	Temp.	TF-141	TE 341	B22 Fuel Rod Pos.4	Fig.A.73 95	273. - 0.125E+04	K	0.64%FS
342	Temp.	TF-142	TE 342	B22 Fuel Rod Pos.5	Fig.A.73, 96	273. - 0.125E+04	K	0.64%FS
343	Temp.	TF-143	TE 343	B22 Fuel Rod Pos.6	Fig.A.73, 97	273. - 0.125E+04	K	0.64%FS
344	Temp.	TF-144	TE 344	B22 Fuel Rod Pos.7	Fig.A.73, 98	273. - 0.125E+04	K	0.64%FS
345	Temp.	TF-145	TE 345	B31 Fuel Rod Pos.4	Not Measured	273. - 0.125E+04	K	0.64%FS
346	Temp.	TF-146	TE 346	B33 Fuel Rod Pos.4	Not Measured	273. - 0.125E+04	K	0.64%FS
347	Temp.	TF-147	TE 347	B51 Fuel Rod Pos.4	Not Measured	273. - 0.125E+04	K	0.64%FS
348	Temp.	TF-148	TE 348	B53 Fuel Rod Pos.4	Not Measured	273. - 0.125E+04	K	0.64%FS
349	Temp.	TF-149	TE 349	B66 Fuel Rod Pos.4	Not Measured	273. - 0.125E+04	K	0.64%FS
350	Temp.	TF-150	TE 350	B77 Fuel Rod Pos.1	Fig.A. 99	273. - 0.125E+04	K	0.64%FS

Table A.1 Measurement list for RUN 992 (Cont'd)

351Ch.- 400Ch.

Ch.	Item	Symbol	ID.		Location	Fig.No.	Range			Unit	Accuracy
351	Temp.	TF-151	TE	351	B77 Fuel Rod Pos.2	Fig.A.100	273.	-	0.125E+04	K	0.64%FS
352	Temp.	TF-152	TE	352	B77 Fuel Rod Pos.3	Fig.A.101	273.	-	0.125E+04	K	0.64%FS
353	Temp.	TF-153	TE	353	B77 Fuel Rod Pos.4	Fig.A.102	273.	-	0.125E+04	K	0.64%FS
354	Temp.	TF-154	TE	354	B77 Fuel Rod Pos.5	Fig.A.103	273.	-	0.125E+04	K	0.64%FS
355	Temp.	TF-155	TE	355	B77 Fuel Rod Pos.6	Fig.A.104	273.	-	0.125E+04	K	0.64%FS
356	Temp.	TF-156	TE	356	B77 Fuel Rod Pos.7	Fig.A.105	273.	-	0.125E+04	K	0.64%FS
357	Temp.	TF-157	TE	357	B86 Fuel Rod Pos.4	Not Measured	273.	-	0.125E+04	K	0.64%FS
358	Temp.	TF-158	TE	358	C11 Fuel Rod Pos.1	Fig.A.74	273.	-	0.125E+04	K	0.64%FS
359	Temp.	TF-159	TE	359	C11 Fuel Rod Pos.2	Fig.A.74	273.	-	0.125E+04	K	0.64%FS
360	Temp.	TF-160	TE	360	C11 Fuel Rod Pos.3	Fig.A.74	273.	-	0.125E+04	K	0.64%FS
361	Temp.	TF-161	TE	361	C11 Fuel Rod Pos.4	Fig.A.74	273.	-	0.125E+04	K	0.64%FS
362	Temp.	TF-162	TE	362	C11 Fuel Rod Pos.5	Fig.A.74	273.	-	0.125E+04	K	0.64%FS
363	Temp.	TF-163	TE	363	C11 Fuel Rod Pos.6	Fig.A.74	273.	-	0.125E+04	K	0.64%FS
364	Temp.	TF-164	TE	364	C11 Fuel Rod Pos.7	Fig.A.74	273.	-	0.125E+04	K	0.64%FS
365	Temp.	TF-165	TE	365	C13 Fuel Rod Pos.1		273.	-	0.125E+04	K	0.64%FS
366	Temp.	TF-166	TE	366	C13 Fuel Rod Pos.2		273.	-	0.125E+04	K	0.64%FS
367	Temp.	TF-167	TE	367	C13 Fuel Rod Pos.3		273.	-	0.125E+04	K	0.64%FS
368	Temp.	TF-168	TE	368	C13 Fuel Rod Pos.4		273.	-	0.125E+04	K	0.64%FS
369	Temp.	TF-169	TE	369	C13 Fuel Rod Pos.5		273.	-	0.125E+04	K	0.64%FS
370	Temp.	TF-170	TE	370	C13 Fuel Rod Pos.6		273.	-	0.125E+04	K	0.64%FS
371	Temp.	TF-171	TE	371	C13 Fuel Rod Pos.7		273.	-	0.125E+04	K	0.64%FS
372	Temp.	TF-172	TE	372	C15 Fuel Rod Pos.4	Not Measured	273.	-	0.125E+04	K	0.64%FS
373	Temp.	TF-173	TE	373	C22 Fuel Rod Pos.1	Fig.A.75, 92	273.	-	0.125E+04	K	0.64%FS
374	Temp.	TF-174	TE	374	C22 Fuel Rod Pos.2	Fig.A.75, 93	273.	-	0.125E+04	K	0.64%FS
375	Temp.	TF-175	TE	375	C22 Fuel Rod Pos.3	Fig.A.75, 94	273.	-	0.125E+04	K	0.64%FS
376	Temp.	TF-176	TE	376	C22 Fuel Rod Pos.4	Fig.A.75, 95	273.	-	0.125E+04	K	0.64%FS
377	Temp.	TF-177	TE	377	C22 Fuel Rod Pos.5	Fig.A.75, 96	273.	-	0.125E+04	K	0.64%FS
378	Temp.	TF-178	TE	378	C22 Fuel Rod Pos.6	Fig.A.75, 97	273.	-	0.125E+04	K	0.64%FS
379	Temp.	TF-179	TE	379	C22 Fuel Rod Pos.7	Fig.A.75, 98	273.	-	0.125E+04	K	0.64%FS
380	Temp.	TF-180	TE	380	C31 Fuel Rod Pos.4	Not Measured	273.	-	0.125E+04	K	0.64%FS
381	Temp.	TF-181	TE	381	C33 Fuel Rod Pos.1	Fig.A.76	273.	-	0.125E+04	K	0.64%FS
382	Temp.	TF-182	TE	382	C33 Fuel Rod Pos.2	Fig.A.76	273.	-	0.125E+04	K	0.64%FS
383	Temp.	TF-183	TE	383	C33 Fuel Rod Pos.3	Fig.A.76	273.	-	0.125E+04	K	0.64%FS
384	Temp.	TF-184	TE	384	C33 Fuel Rod Pos.4	Fig.A.76	273.	-	0.125E+04	K	0.64%FS
385	Temp.	TF-185	TE	385	C33 Fuel Rod Pos.5	Fig.A.76	273.	-	0.125E+04	K	0.64%FS
386	Temp.	TF-186	TE	386	C33 Fuel Rod Pos.6	Fig.A.76	273.	-	0.125E+04	K	0.64%FS
387	Temp.	TF-187	TE	387	C33 Fuel Rod Pos.7	Fig.A.76	273.	-	0.125E+04	K	0.64%FS
388	Temp.	TF-188	TE	388	C35 Fuel Rod Pos.4	Not Measured	273.	-	0.125E+04	K	0.64%FS
389	Temp.	TF-189	TE	389	C66 Fuel Rod Pos.4	Not Measured	273.	-	0.125E+04	K	0.64%FS
390	Temp.	TF-190	TE	390	C68 Fuel Rod Pos.4	Not Measured	273.	-	0.125E+04	K	0.64%FS
391	Temp.	TF-191	TE	391	C77 Fuel Rod Pos.1	Fig.A.77, 99	273.	-	0.125E+04	K	0.64%FS
392	Temp.	TF-192	TE	392	C77 Fuel Rod Pos.2	Fig.A.77,100	273.	-	0.125E+04	K	0.64%FS
393	Temp.	TF-193	TE	393	C77 Fuel Rod Pos.3	Fig.A.77,101	273.	-	0.125E+04	K	0.64%FS
394	Temp.	TF-194	TE	394	C77 Fuel Rod Pos.4	Fig.A.77,102	273.	-	0.125E+04	K	0.64%FS
395	Temp.	TF-195	TE	395	C77 Fuel Rod Pos.5	Fig.A.77,103	273.	-	0.125E+04	K	0.64%FS
396	Temp.	TF-196	TE	396	C77 Fuel Rod Pos.6	Fig.A.77,104	273.	-	0.125E+04	K	0.64%FS
397	Temp.	TF-197	TE	397	C77 Fuel Rod Pos.7	Fig.A.77,105	273.	-	0.125E+04	K	0.64%FS
398	Temp.	TF-198	TE	398	D11 Fuel Rod Pos.4	Fig.A.84	273.	-	0.125E+04	K	0.64%FS
399	Temp.	TF-199	TE	399	D13 Fuel Rod Pos.4	Fig.A.84	273.	-	0.125E+04	K	0.64%FS
400	Temp.	TF-200	TE	400	D22 Fuel Rod Pos.1	Fig.A.78, 92	273.	-	0.125E+04	K	0.64%FS

Table A.1 Measurement list for RUN 992 (Cont'd)

401Ch.- 450Ch.

Ch.	Item	Symbol	ID.	Location	Fig.No.	Range	Unit	Accuracy
401	Temp.	TF-201	TE 401	D22 Fuel Rod Pos.2	Fig.A.78, 93	273. - 0.125E+04	K	0.64%FS
402	Temp.	TF-202	TE 402	D22 Fuel Rod Pos.3	Fig.A.78, 94	273. - 0.125E+04	K	0.64%FS
403	Temp.	TF-203	TE 403	D22 Fuel Rod Pos.4	Fig.A.78, 95	273. - 0.125E+04	K	0.64%FS
404	Temp.	TF-204	TE 404	D22 Fuel Rod Pos.5	Fig.A.78, 96	273. - 0.125E+04	K	0.64%FS
405	Temp.	TF-205	TE 405	D22 Fuel Rod Pos.6	Fig.A.78, 97	273. - 0.125E+04	K	0.64%FS
406	Temp.	TF-206	TE 406	D22 Fuel Rod Pos.7	Fig.A.78, 98	273. - 0.125E+04	K	0.64%FS
407	Temp.	TF-207	TE 407	D31 Fuel Rod Pos.4	Not Measured	273. - 0.125E+04	K	0.64%FS
408	Temp.	TF-208	TE 408	D33 Fuel Rod Pos.4	Not Measured	273. - 0.125E+04	K	0.64%FS
409	Temp.	TF-209	TE 409	D51 Fuel Rod Pos.4	Not Measured	273. - 0.125E+04	K	0.64%FS
410	Temp.	TF-210	TE 410	D53 Fuel Rod Pos.4	Not Measured	273. - 0.125E+04	K	0.64%FS
411	Temp.	TF-211	TE 411	D66 Fuel Rod Pos.4	Not Measured	273. - 0.125E+04	K	0.64%FS
412	Temp.	TF-212	TE 412	D77 Fuel Rod Pos.4		273. - 0.125E+04	K	0.64%FS
413	Temp.	TF-213	TE 413	D86 Fuel Rod Pos.4	Fig.A.84	273. - 0.125E+04	K	0.64%FS
414	Fluid T.	TW- 1	TE 414	A45 Tie Rod Pos.1	Fig.A.79	273. - 0.125E+04	K	0.64%FS
415	Fluid T.	TW- 2	TE 415	A45 Tie Rod Pos.2	Fig.A.79	273. - 0.125E+04	K	0.64%FS
416	Fluid T.	TW- 3	TE 416	A45 Tie Rod Pos.3	Fig.A.79	273. - 0.125E+04	K	0.64%FS
417	Fluid T.	TW- 4	TE 417	A45 Tie Rod Pos.4	Fig.A.79	273. - 0.125E+04	K	0.64%FS
418	Fluid T.	TW- 5	TE 418	A45 Tie Rod Pos.5	Fig.A.79	273. - 0.125E+04	K	0.64%FS
419	Fluid T.	TW- 6	TE 419	A45 Tie Rod Pos.6	Fig.A.79	273. - 0.125E+04	K	0.64%FS
420	Fluid T.	TW- 7	TE 420	A45 Tie Rod Pos.7	Fig.A.79	273. - 0.125E+04	K	0.64%FS
421	Fluid T.	TW- 8	TE 421	B45 Tie Rod Pos.1	Not Measured	273. - 0.125E+04	K	0.64%FS
422	Fluid T.	TW- 9	TE 422	B45 Tie Rod Pos.2	Not Measured	273. - 0.125E+04	K	0.64%FS
423	Fluid T.	TW-10	TE 423	B45 Tie Rod Pos.3	Not Measured	273. - 0.125E+04	K	0.64%FS
424	Fluid T.	TW-11	TE 424	B45 Tie Rod Pos.4	Not Measured	273. - 0.125E+04	K	0.64%FS
425	Fluid T.	TW-12	TE 425	B45 Tie Rod Pos.5	Not Measured	273. - 0.125E+04	K	0.64%FS
426	Fluid T.	TW-13	TE 426	B45 Tie Rod Pos.6	Not Measured	273. - 0.125E+04	K	0.64%FS
427	Fluid T.	TW-14	TE 427	B45 Tie Rod Pos.7	Not Measured	273. - 0.125E+04	K	0.64%FS
428	Fluid T.	TW-15	TE 428	C45 Tie Rod Pos.1	Fig.A.80	273. - 0.125E+04	K	0.64%FS
429	Fluid T.	TW-16	TE 429	C45 Tie Rod Pos.2	Fig.A.80	273. - 0.125E+04	K	0.64%FS
430	Fluid T.	TW-17	TE 430	C45 Tie Rod Pos.3	Fig.A.80	273. - 0.125E+04	K	0.64%FS
431	Fluid T.	TW-18	TE 431	C45 Tie Rod Pos.4	Fig.A.80	273. - 0.125E+04	K	0.64%FS
432	Fluid T.	TW-19	TE 432	C45 Tie Rod Pos.5	Fig.A.80	273. - 0.125E+04	K	0.64%FS
433	Fluid T.	TW-20	TE 433	C45 Tie Rod Pos.6	Fig.A.80	273. - 0.125E+04	K	0.64%FS
434	Fluid T.	TW-21	TE 434	C45 Tie Rod Pos.7	Fig.A.80	273. - 0.125E+04	K	0.64%FS
435	Fluid T.	TW-22	TE 435	D45 Tie Rod Pos.1	Not Measured	273. - 0.125E+04	K	0.64%FS
436	Fluid T.	TW-23	TE 436	D45 Tie Rod Pos.2	Not Measured	273. - 0.125E+04	K	0.64%FS
437	Fluid T.	TW-24	TE 437	D45 Tie Rod Pos.3	Not Measured	273. - 0.125E+04	K	0.64%FS
438	Fluid T.	TW-25	TE 438	D45 Tie Rod Pos.4	Not Measured	273. - 0.125E+04	K	0.64%FS
439	Fluid T.	TW-26	TE 439	D45 Tie Rod Pos.5	Not Measured	273. - 0.125E+04	K	0.64%FS
440	Fluid T.	TW-27	TE 440	D45 Tie Rod Pos.6	Not Measured	273. - 0.125E+04	K	0.64%FS
441	Fluid T.	TW-28	TE 441	D45 Tie Rod Pos.7	Not Measured	273. - 0.125E+04	K	0.64%FS
442	Fluid T.	TC- 1	TE 442	Channel Box A Inlet	Fig.A.106	273. - 0.125E+04	K	0.64%FS
443	Fluid T.	TC- 2	TE 443	Channel Box B Inlet	Fig.A.106	273. - 0.125E+04	K	0.64%FS
444	Fluid T.	TC- 3	TE 444	Channel Box C Inlet	Fig.A.106	273. - 0.125E+04	K	0.64%FS
445	Fluid T.	TC- 4	TE 445	Channel Box D Inlet	Fig.A.106	273. - 0.125E+04	K	0.64%FS
446	Fluid T.	TC- 5	TE 446	Channel Box Outlet A-1	Fig.A.107	273. - 0.125E+04	K	0.64%FS
447	Fluid T.	TC- 6	TE 447	Channel Box Outlet A-2	Fig.A.107	273. - 0.125E+04	K	0.64%FS
448	Fluid T.	TC- 7	TE 448	Channel Box Outlet A-3	Fig.A.107	273. - 0.125E+04	K	0.64%FS
449	Fluid T.	TC- 8	TE 449	Channel Box Outlet A-4	Fig.A.107	273. - 0.125E+04	K	0.64%FS
450	Fluid T.	TC- 9	TE 450	Channel Box Outlet A-6	Fig.A.107	273. - 0.125E+04	K	0.64%FS

Table A.1 Measurement list for RUN 992 (Cont'd)

451Ch.- 500Ch.

Ch.	Item	Symbol	ID.	Location	Fig.No.	Range	Unit	Accuracy
451	Fluid T.	TC-10	TE 451	Channel Box Outlet C-1	Fig.A.108	273. - 0.125E+04	K	0.64%FS
452	Fluid T.	TC-11	TE 452	Channel Box Outlet C-2	Fig.A.108	273. - 0.125E+04	K	0.64%FS
453	Fluid T.	TC-12	TE 453	Channel Box Outlet C-3	Fig.A.108	273. - 0.125E+04	K	0.64%FS
454	Fluid T.	TC-13	TE 454	Channel Box Outlet C-4	Fig.A.108	273. - 0.125E+04	K	0.64%FS
455	Fluid T.	TC-14	TE 455	Channel Box Outlet C-6	Fig.A.108	273. - 0.125E+04	K	0.64%FS
456	Fluid T.	TG- 1	TE 456	Upper Tieplate A Up.1	Fig.A.109,111	273. - 0.125E+04	K	0.64%FS
457	Fluid T.	TG- 2	TE 457	Upper Tieplate A Up.2	Not Measured	273. - 0.125E+04	K	0.64%FS
458	Fluid T.	TG- 3	TE 458	Upper Tieplate A Up.3	Not Measured	273. - 0.125E+04	K	0.64%FS
459	Fluid T.	TG- 4	TE 459	Upper Tieplate A Up.4	Fig.A.109,112	273. - 0.125E+04	K	0.64%FS
460	Fluid T.	TG- 5	TE 460	Upper Tieplate A Up.5	Not Measured	273. - 0.125E+04	K	0.64%FS
461	Fluid T.	TG- 6	TE 461	Upper Tieplate A Up.6	Not Measured	273. - 0.125E+04	K	0.64%FS
462	Fluid T.	TG- 7	TE 462	Upper Tieplate A Up.7	Not Measured	273. - 0.125E+04	K	0.64%FS
463	Fluid T.	TG- 8	TE 463	Upper Tieplate A Up.8	Not Measured	273. - 0.125E+04	K	0.64%FS
464	Fluid T.	TG- 9	TE 464	Upper Tieplate A Up.9	Not Measured	273. - 0.125E+04	K	0.64%FS
465	Fluid T.	TG-10	TE 465	Upper Tieplate A Up.10	Fig.A.109,113	273. - 0.125E+04	K	0.64%FS
466	Fluid T.	TG-11	TE 466	Upper Tieplate A Lo.1	Fig.A.110,111	273. - 0.125E+04	K	0.64%FS
467	Fluid T.	TG-12	TE 467	Upper Tieplate A Lo.2	Not Measured	273. - 0.125E+04	K	0.64%FS
468	Fluid T.	TG-13	TE 468	Upper Tieplate A Lo.3	Not Measured	273. - 0.125E+04	K	0.64%FS
469	Fluid T.	TG-14	TE 469	Upper Tieplate A Lo.4	Fig.A.110,112	273. - 0.125E+04	K	0.64%FS
470	Fluid T.	TG-15	TE 470	Upper Tieplate A Lo.5	Not Measured	273. - 0.125E+04	K	0.64%FS
471	Fluid T.	TG-16	TE 471	Upper Tieplate A Lo.6	Not Measured	273. - 0.125E+04	K	0.64%FS
472	Fluid T.	TG-17	TE 472	Upper Tieplate A Lo.7	Not Measured	273. - 0.125E+04	K	0.64%FS
473	Fluid T.	TG-18	TE 473	Upper Tieplate A Lo.8	Not Measured	273. - 0.125E+04	K	0.64%FS
474	Fluid T.	TG-19	TE 474	Upper Tieplate A Lo.9	Not Measured	273. - 0.125E+04	K	0.64%FS
475	Fluid T.	TG-20	TE 475	Upper Tieplate A Lo.10	Fig.A.110,113	273. - 0.125E+04	K	0.64%FS
476	Fluid T.	TG-21	TE 476	Upper Tieplate C Up.1	Fig.A.114,116	273. - 0.125E+04	K	0.64%FS
477	Fluid T.	TG-22	TE 477	Upper Tieplate C Up.2	Not Measured	273. - 0.125E+04	K	0.64%FS
478	Fluid T.	TG-23	TE 478	Upper Tieplate C Up.3	Not Measured	273. - 0.125E+04	K	0.64%FS
479	Fluid T.	TG-24	TE 479	Upper Tieplate C Up.4	Fig.A.114,117	273. - 0.125E+04	K	0.64%FS
480	Fluid T.	TG-25	TE 480	Upper Tieplate C Up.5	Not Measured	273. - 0.125E+04	K	0.64%FS
481	Fluid T.	TG-26	TE 481	Upper Tieplate C Up.6	Not Measured	273. - 0.125E+04	K	0.64%FS
482	Fluid T.	TG-27	TE 482	Upper Tieplate C Up.7	Not Measured	273. - 0.125E+04	K	0.64%FS
483	Fluid T.	TG-28	TE 483	Upper Tieplate C Up.8	Not Measured	273. - 0.125E+04	K	0.64%FS
484	Fluid T.	TG-29	TE 484	Upper Tieplate C Up.9	Not Measured	273. - 0.125E+04	K	0.64%FS
485	Fluid T.	TG-30	TE 485	Upper Tieplate C Up.10	Fig.A.114,118	273. - 0.125E+04	K	0.64%FS
486	Fluid T.	TG-31	TE 486	Upper Tieplate C Lo.1	Fig.A.115,116	273. - 0.125E+04	K	0.64%FS
487	Fluid T.	TG-32	TE 487	Upper Tieplate C Lo.2	Not Measured	273. - 0.125E+04	K	0.64%FS
488	Fluid T.	TG-33	TE 488	Upper Tieplate C Lo.3	Not Measured	273. - 0.125E+04	K	0.64%FS
489	Fluid T.	TG-34	TE 489	Upper Tieplate C Lo.4	Fig.A.115,117	273. - 0.125E+04	K	0.64%FS
490	Fluid T.	TG-35	TE 490	Upper Tieplate C Lo.5	Not Measured	273. - 0.125E+04	K	0.64%FS
491	Fluid T.	TG-36	TE 491	Upper Tieplate C Lo.6	Not Measured	273. - 0.125E+04	K	0.64%FS
492	Fluid T.	TG-37	TE 492	Upper Tieplate C Lo.7	Not Measured	273. - 0.125E+04	K	0.64%FS
493	Fluid T.	TG-38	TE 493	Upper Tieplate C Lo.8	Not Measured	273. - 0.125E+04	K	0.64%FS
494	Fluid T.	TG-39	TE 494	Upper Tieplate C Lo.9	Not Measured	273. - 0.125E+04	K	0.64%FS
495	Fluid T.	TG-40	TE 495	Upper Tieplate C Lo.10	Fig.A.115,118	273. - 0.125E+04	K	0.64%FS
496	Slab T.	TB- 1	TE 496	C.B. A1 Inner ,Pos.1	Not Measured	273. - 0.125E+04	K	0.64%FS
497	Slab T.	TB- 2	TE 497	C.B. A1 Inner ,Pos.2	Not Measured	273. - 0.125E+04	K	0.64%FS
498	Slab T.	TB- 3	TE 498	C.B. A1 Inner ,Pos.3	Not Measured	273. - 0.125E+04	K	0.64%FS
499	Slab T.	TB- 4	TE 499	C.B. A1 Inner ,Pos.4	Not Measured	273. - 0.125E+04	K	0.64%FS
500	Slab T.	TB- 5	TE 500	C.B. A1 Inner ,Pos.5	Not Measured	273. - 0.125E+04	K	0.64%FS

Table A.1 Measurement list for RUN 992 (Cont'd)

501Ch.- 550Ch.

Ch.	Item	Symbol	ID.	Location	Fig.No.	Range	Unit	Accuracy
501	Slab T.	TB- 6	TE 501	C.B. A1 Inner ,Pos.6	Not Measured	273. - 0.125E+04	K	0.64%FS
502	Slab T.	TB- 7	TE 502	C.B. A1 Inner ,Pos.7	Not Measured	273. - 0.125E+04	K	0.64%FS
503	Slab T.	TB- 8	TE 503	C.B. A2 Inner ,Pos.1	Not Measured	273. - 0.125E+04	K	0.64%FS
504	Slab T.	TB- 9	TE 504	C.B. A2 Inner ,Pos.2	Not Measured	273. - 0.125E+04	K	0.64%FS
505	Slab T.	TB-10	TE 505	C.B. A2 Inner ,Pos.3	Not Measured	273. - 0.125E+04	K	0.64%FS
506	Slab T.	TB-11	TE 506	C.B. A2 Inner ,Pos.4	Not Measured	273. - 0.125E+04	K	0.64%FS
507	Slab T.	TB-12	TE 507	C.B. A2 Inner ,Pos.5	Not Measured	273. - 0.125E+04	K	0.64%FS
508	Slab T.	TB-13	TE 508	C.B. A2 Inner ,Pos.6	Not Measured	273. - 0.125E+04	K	0.64%FS
509	Slab T.	TB-14	TE 509	C.B. A2 Inner ,Pos.7	Not Measured	273. - 0.125E+04	K	0.64%FS
510	Slab T.	TB-15	TE 510	C.B. B Inner ,Pos.1	Not Measured	273. - 0.125E+04	K	0.64%FS
511	Slab T.	TB-16	TE 511	C.B. B Inner ,Pos.2	Not Measured	273. - 0.125E+04	K	0.64%FS
512	Slab T.	TB-17	TE 512	C.B. B Inner ,Pos.3	Not Measured	273. - 0.125E+04	K	0.64%FS
513	Slab T.	TB-18	TE 513	C.B. B Inner ,Pos.4	Not Measured	273. - 0.125E+04	K	0.64%FS
514	Slab T.	TB-19	TE 514	C.B. B Inner ,Pos.5	Not Measured	273. - 0.125E+04	K	0.64%FS
515	Slab T.	TB-20	TE 515	C.B. B Inner ,Pos.6	Not Measured	273. - 0.125E+04	K	0.64%FS
516	Slab T.	TB-21	TE 516	C.B. B Inner ,Pos.7	Not Measured	273. - 0.125E+04	K	0.64%FS
517	Slab T.	TB-22	TE 517	C.B. C Inner ,Pos.1	Not Measured	273. - 0.125E+04	K	0.64%FS
518	Slab T.	TB-23	TE 518	C.B. C Inner ,Pos.2	Not Measured	273. - 0.125E+04	K	0.64%FS
519	Slab T.	TB-24	TE 519	C.B. C Inner ,Pos.3	Not Measured	273. - 0.125E+04	K	0.64%FS
520	Slab T.	TB-25	TE 520	C.B. C Inner ,Pos.4	Not Measured	273. - 0.125E+04	K	0.64%FS
521	Slab T.	TB-26	TE 521	C.B. C Inner ,Pos.5	Not Measured	273. - 0.125E+04	K	0.64%FS
522	Slab T.	TB-27	TE 522	C.B. C Inner ,Pos.6	Not Measured	273. - 0.125E+04	K	0.64%FS
523	Slab T.	TB-28	TE 523	C.B. C Inner ,Pos.7	Not Measured	273. - 0.125E+04	K	0.64%FS
524	Slab T.	TB-29	TE 524	C.B. D Inner ,Pos.1	Not Measured	273. - 0.125E+04	K	0.64%FS
525	Slab T.	TB-30	TE 525	C.B. D Inner ,Pos.2	Not Measured	273. - 0.125E+04	K	0.64%FS
526	Slab T.	TB-31	TE 526	C.B. D Inner ,Pos.3	Not Measured	273. - 0.125E+04	K	0.64%FS
527	Slab T.	TB-32	TE 527	C.B. D Inner ,Pos.4	Not Measured	273. - 0.125E+04	K	0.64%FS
528	Slab T.	TB-33	TE 528	C.B. D Inner ,Pos.5	Not Measured	273. - 0.125E+04	K	0.64%FS
529	Slab T.	TB-34	TE 529	C.B. D Inner ,Pos.6	Not Measured	273. - 0.125E+04	K	0.64%FS
530	Slab T.	TB-35	TE 530	C.B. D Inner ,Pos.7	Not Measured	273. - 0.125E+04	K	0.64%FS
531	Fluid T.	TB-36	TE 531	C.B. A Outer ,Pos.1	Fig.A.81	273. - 0.125E+04	K	0.64%FS
532	Fluid T.	TB-37	TE 532	C.B. A Outer ,Pos.2	Fig.A.81	273. - 0.125E+04	K	0.64%FS
533	Fluid T.	TB-38	TE 533	C.B. A Outer ,Pos.3	Fig.A.81	273. - 0.125E+04	K	0.64%FS
534	Fluid T.	TB-39	TE 534	C.B. A Outer ,Pos.4	Fig.A.81	273. - 0.125E+04	K	0.64%FS
535	Fluid T.	TB-40	TE 535	C.B. A Outer ,Pos.5	Fig.A.81	273. - 0.125E+04	K	0.64%FS
536	Fluid T.	TB-41	TE 536	C.B. A Outer ,Pos.6	Fig.A.81	273. - 0.125E+04	K	0.64%FS
537	Fluid T.	TB-42	TE 537	C.B. A Outer ,Pos.7	Fig.A.81	273. - 0.125E+04	K	0.64%FS
538	Fluid T.	TB-43	TE 538	C.B. C Outer ,Pos.1	Not Measured	273. - 0.125E+04	K	0.64%FS
539	Fluid T.	TB-44	TE 539	C.B. C Outer ,Pos.2	Not Measured	273. - 0.125E+04	K	0.64%FS
540	Fluid T.	TB-45	TE 540	C.B. C Outer ,Pos.3	Not Measured	273. - 0.125E+04	K	0.64%FS
541	Fluid T.	TB-46	TE 541	C.B. C Outer ,Pos.4	Not Measured	273. - 0.125E+04	K	0.64%FS
542	Fluid T.	TB-47	TE 542	C.B. C Outer ,Pos.5	Not Measured	273. - 0.125E+04	K	0.64%FS
543	Fluid T.	TB-48	TE 543	C.B. C Outer ,Pos.6	Not Measured	273. - 0.125E+04	K	0.64%FS
544	Fluid T.	TB-49	TE 544	C.B. C Outer ,Pos.7	Not Measured	273. - 0.125E+04	K	0.64%FS
545	Fluid T.	TP- 1	TE 545	Lower Pl. Center 1	Fig.A.119	273. - 0.125E+04	K	0.64%FS
546	Fluid T.	TP- 2	TE 546	Lower Pl. Center 2	Fig.A.119	273. - 0.125E+04	K	0.64%FS
547	Fluid T.	TP- 3	TE 547	Lower Pl. Center 3	Fig.A.119	273. - 0.125E+04	K	0.64%FS
548	Fluid T.	TP- 4	TE 548	Lower Pl. Center 4	Fig.A.119	273. - 0.125E+04	K	0.64%FS
549	Fluid T.	TP- 5	TE 549	Lower Pl. Center 5	Fig.A.119	273. - 0.125E+04	K	0.64%FS
550	Fluid T.	TP- 6	TE 550	Lower Pl. Center 7	Fig.A.119	273. - 0.125E+04	K	0.64%FS

Table A.1 Measurement list for RUN 992 (Cont'd)

551Ch.- 600Ch.

Ch.	Item	Symbol	ID.		Location		Fig.No.	Range			Unit	Accuracy
551	Slab T.	TP- 7	TE	551	Lower Pl. North	1	Not Measured	273.	-	0.125E+04	K	0.64%FS
552	Slab T.	TP- 8	TE	552	Lower Pl. North	2	Not Measured	273.	-	673.	K	0.64%FS
553	Slab T.	TP- 9	TE	553	Lower Pl. North	4	Not Measured	273.	-	673.	K	0.64%FS
554	Slab T.	TP-10	TE	554	Lower Pl. North	6	Not Measured	273.	-	673.	K	0.64%FS
555	Slab T.	TP-11	TE	555	Lower Pl. South	1	Not Measured	273.	-	673.	K	0.64%FS
556	Slab T.	TP-12	TE	556	Lower Pl. South	2	Not Measured	273.	-	673.	K	0.64%FS
557	Slab T.	TP-13	TE	557	Lower Pl. South	4	Not Measured	273.	-	673.	K	0.64%FS
558	Slab T.	TP-14	TE	558	Lower Pl. South	6	Not Measured	273.	-	673.	K	0.64%FS
559	Level	LB- 1	LM	559	C.B.Liquid Level	A1-1	Not Measured					
560	Level	LB- 2	LM	560	C.B.Liquid Level	A1-2	Not Measured					
561	Level	LB- 3	LM	561	C.B.Liquid Level	A1-3	Not Measured					
562	Level	LB- 4	LM	562	C.B.Liquid Level	A1-4	Not Measured					
563	Level	LB- 5	LM	563	C.B.Liquid Level	A1-5	Not Measured					
564	Level	LB- 6	LM	564	C.B.Liquid Level	A1-6	Not Measured					
565	Level	LB- 7	LM	565	C.B.Liquid Level	A1-7	Not Measured					
566	Level	LB- 8	LM	566	C.B.Liquid Level	A2-1	Fig.A.120					
567	Level	LB- 9	LM	567	C.B.Liquid Level	A2-2	Fig.A.120					
568	Level	LB-10	LM	568	C.B.Liquid Level	A2-3	Fig.A.120					
569	Level	LB-11	LM	569	C.B.Liquid Level	A2-4	Fig.A.120					
570	Level	LB-12	LM	570	C.B.Liquid Level	A2-5	Fig.A.120					
571	Level	LB-13	LM	571	C.B.Liquid Level	A2-6	Fig.A.120					
572	Level	LB-14	LM	572	C.B.Liquid Level	A2-7	Fig.A.120					
573	Level	LB-15	LM	573	C.B.Liquid Level	B-1	Fig.A.120					
574	Level	LB-16	LM	574	C.B.Liquid Level	B-2	Fig.A.121					
575	Level	LB-17	LM	575	C.B.Liquid Level	B-3	Fig.A.121					
576	Level	LB-18	LM	576	C.B.Liquid Level	B-4	Fig.A.121					
577	Level	LB-19	LM	577	C.B.Liquid Level	B-5	Fig.A.121					
578	Level	LB-20	LM	578	C.B.Liquid Level	B-6	Fig.A.121					
579	Level	LB-21	LM	579	C.B.Liquid Level	B-7	Fig.A.121					
580	Level	LB-22	LM	580	C.B.Liquid Level	C-1	Fig.A.122					
581	Level	LB-23	LM	581	C.B.Liquid Level	C-2	Fig.A.122					
582	Level	LB-24	LM	582	C.B.Liquid Level	C-3	Fig.A.122					
583	Level	LB-25	LM	583	C.B.Liquid Level	C-4	Fig.A.122					
584	Level	LB-26	LM	584	C.B.Liquid Level	C-5	Fig.A.122					
585	Level	LB-27	LM	585	C.B.Liquid Level	C-6	Fig.A.122					
586	Level	LB-28	LM	586	C.B.Liquid Level	C-7	Fig.A.122					
587	Level	LB-29	LM	587	C.B.Liquid Level	D-1	Not Measured					
588	Level	LB-30	LM	588	C.B.Liquid Level	D-2	Not Measured					
589	Level	LB-31	LM	589	C.B.Liquid Level	D-3	Not Measured					
590	Level	LB-32	LM	590	C.B.Liquid Level	D-4	Not Measured					
591	Level	LB-33	LM	591	C.B.Liquid Level	D-5	Not Measured					
592	Level	LB-34	LM	592	C.B.Liquid Level	D-6	Not Measured					
593	Level	LB-35	LM	593	C.B.Liquid Level	D-7	Not Measured					
594	Level	LL- 1	LM	594	Ch.Box Outlet	A1-5	Not Measured					
595	Level	LL- 2	LM	595	Ch.Box Outlet	A1-6	Not Measured					
596	Level	LL- 3	LM	596	Ch.Box Outlet	A1-7	Not Measured					
597	Level	LL- 4	LM	597	Ch.Box Outlet	A2-5	Fig.A.123					
598	Level	LL- 5	LM	598	Ch.Box Outlet	A2-6	Fig.A.123					
599	Level	LL- 6	LM	599	Ch.Box Outlet	A2-7	Fig.A.123					
600	Level	LL- 7	LM	600	Ch.Box Outlet	A-1	Fig.A.124					

Table A.1 Measurement list for RUN 992 (Cont'd)

601Ch.- 650Ch.

Ch.	Item	Symbol	ID.		Location	Fig.No.	Range	Unit	Accuracy
601	Level	LL- 8	LM	601	Ch.Box Outlet A-2	Fig.A.124			
602	Level	LL- 9	LM	602	Ch.Box Outlet A-3	Fig.A.124			
603	Level	LL-10	LM	603	Ch.Box Outlet A-4	Fig.A.124			
604	Level	LL-11	LM	604	Ch.Box Outlet A-6	Failure			
605	Level	LL-12	LM	605	Ch.Box Outlet C1-5	Fig.A.125			
606	Level	LL-13	LM	606	Ch.Box Outlet C1-6	Fig.A.125			
607	Level	LL-14	LM	607	Ch.Box Outlet C1-7	Fig.A.125			
608	Level	LL-15	LM	608	Ch.Box Outlet C2-5	Not Measured			
609	Level	LL-16	LM	609	Ch.Box Outlet C2-6	Not Measured			
610	Level	LL-17	LM	610	Ch.Box Outlet C2-7	Not Measured			
611	Level	LL-18	LM	611	Ch.Box Outlet C-1	Fig.A.126			
612	Level	LL-19	LM	612	Ch.Box Outlet C-2	Fig.A.126			
613	Level	LL-20	LM	613	Ch.Box Outlet C-3	Fig.A.126			
614	Level	LL-21	LM	614	Ch.Box Outlet C-4	Fig.A.126			
615	Level	LL-22	LM	615	Ch.Box Outlet C-6	Fig.A.126			
616	Level	LL-23	LM	616	Ch.Box Inlet A-1	Fig.A.127			
617	Level	LL-24	LM	617	Ch.Box Inlet A-2	Fig.A.127			
618	Level	LL-25	LM	618	Ch.Box Inlet B-1	Not Measured			
619	Level	LL-26	LM	619	Ch.Box Inlet B-2	Not Measured			
620	Level	LL-27	LM	620	Ch.Box Inlet C-1	Fig.A.128			
621	Level	LL-28	LM	621	Ch.Box Inlet C-2	Fig.A.128			
622	Level	LL-29	LM	622	Ch.Box Inlet D-1	Not Measured			
623	Level	LL-30	LM	623	Ch.Box Inlet D-2	Not Measured			
624	Level	LL-31	LM	624	Lower Pl. North 1	Fig.A.129			
625	Level	LL-32	LM	625	Lower Pl. North 2	Fig.A.129			
626	Level	LL-33	LM	626	Lower Pl. North 3	Fig.A.129			
627	Level	LL-34	LM	627	Lower Pl. North 4	Failure			
628	Level	LL-35	LM	628	Lower Pl. North 5	Fig.A.129			
629	Level	LL-36	LM	629	Lower Pl. North 6	Failure			
630	Level	LL-37	LM	630	Lower Pl. South 1	Not Measured			
631	Level	LL-38	LM	631	Lower Pl. South 2	Not Measured			
632	Level	LL-39	LM	632	Lower Pl. South 3	Not Measured			
633	Level	LL-40	LM	633	Lower Pl. South 4	Not Measured			
634	Level	LL-41	LM	634	Lower Pl. South 5	Not Measured			
635	Level	LL-42	LM	635	Lower Pl. South 6	Not Measured			
636	Level	LL-43	LM	636	Guide Tube North 0	Fig.A.130			
637	Level	LL-44	LM	637	Guide Tube North 1	Fig.A.130			
638	Level	LL-45	LM	638	Guide Tube North 3	Fig.A.130			
639	Level	LL-46	LM	639	Guide Tube North 6	Fig.A.130			
640	Level	LL-47	LM	640	Guide Tube South 0	Not Measured			
641	Level	LL-48	LM	641	Guide Tube South 1	Not Measured			
642	Level	LL-49	LM	642	Guide Tube South 3	Not Measured			
643	Level	LL-50	LM	643	Guide Tube South 6	Not Measured			
644	Level	L- 1	LM	644	Downcomer D-Side 1	Fig.A.131			
645	Level	L- 2	LM	645	Downcomer D-Side 2	Fig.A.131			
646	Level	L- 3	LM	646	Downcomer D-Side 3	Fig.A.131			
647	Level	L- 4	LM	647	Downcomer D-Side 4	Fig.A.131			
648	Level	L- 5	LM	648	Downcomer D-Side 5	Failure			
649	Level	L- 6	LM	649	Downcomer B-Side 1	Not Measured			
650	Level	L- 7	LM	650	Downcomer B-Side 2	Not Measured			

Table A.1 Measurement list for RUN 992 (Cont'd)

651Ch.- 700Ch.

Ch.	Item	Symbol	ID.		Location	Fig.No.	Range			Unit	Accuracy
651	Level	L- 8	LM	651	Downcomer B-Side 3	Not Measured					
652	Level	L- 9	LM	652	Downcomer B-Side 4	Not Measured					
653	Level	L-10	LM	653	Downcomer B-Side 5	Not Measured					
654	Void	VF- 1	VD	654	A54 Tie Rod Pos.1	Not Measured	0.0	-	1.00		
655	Void	VF- 2	VD	655	A54 Tie Rod Pos.2	Not Measured	0.0	-	1.00		
656	Void	VF- 3	VD	656	A54 Tie Rod Pos.3	Not Measured	0.0	-	1.00		
657	Void	VF- 4	VD	657	A54 Tie Rod Pos.4	Not Measured	0.0	-	1.00		
658	Void	VF- 5	VD	658	A54 Tie Rod Pos.5	Not Measured	0.0	-	1.00		
659	Void	VF- 6	VD	659	A54 Tie Rod Pos.6	Not Measured	0.0	-	1.00		
660	Void	VF- 7	VD	660	A54 Tie Rod Pos.7	Not Measured	0.0	-	1.00		
661	Void	VF- 8	VD	661	B54 Tie Rod Pos.1	Not Measured	0.0	-	1.00		
662	Void	VF- 9	VD	662	B54 Tie Rod Pos.2	Not Measured	0.0	-	1.00		
663	Void	VF-10	VD	663	B54 Tie Rod Pos.3	Not Measured	0.0	-	1.00		
664	Void	VF-11	VD	664	B54 Tie Rod Pos.4	Not Measured	0.0	-	1.00		
665	Void	VF-12	VD	665	B54 Tie Rod Pos.5	Not Measured	0.0	-	1.00		
666	Void	VF-13	VD	666	B54 Tie Rod Pos.6	Not Measured	0.0	-	1.00		
667	Void	VF-14	VD	667	B54 Tie Rod Pos.7	Not Measured	0.0	-	1.00		
668	Void	VF-15	VD	668	C54 Tie Rod Pos.1	Not Measured	0.0	-	1.00		
669	Void	VF-16	VD	669	C54 Tie Rod Pos.2	Not Measured	0.0	-	1.00		
670	Void	VF-17	VD	670	C54 Tie Rod Pos.3	Not Measured	0.0	-	1.00		
671	Void	VF-18	VD	671	C54 Tie Rod Pos.4	Not Measured	0.0	-	1.00		
672	Void	VF-19	VD	672	C54 Tie Rod Pos.5	Not Measured	0.0	-	1.00		
673	Void	VF-20	VD	673	C54 Tie Rod Pos.6	Not Measured	0.0	-	1.00		
674	Void	VF-21	VD	674	C54 Tie Rod Pos.7	Not Measured	0.0	-	1.00		
675	Void	VF-22	VD	675	D54 Tie Rod Pos.7	Not Measured	0.0	-	1.00		
676	Void	VF-23	VD	676	D54 Tie Rod Pos.7	Not Measured	0.0	-	1.00		
677	Void	VF-24	VD	677	D54 Tie Rod Pos.7	Not Measured	0.0	-	1.00		
678	Void	VF-25	VD	678	D54 Tie Rod Pos.7	Not Measured	0.0	-	1.00		
679	Void	VF-26	VD	679	D54 Tie Rod Pos.7	Not Measured	0.0	-	1.00		
680	Void	VF-27	VD	680	D54 Tie Rod Pos.7	Not Measured	0.0	-	1.00		
681	Void	VF-28	VD	681	D54 Tie Rod Pos.7	Not Measured	0.0	-	1.00		
682	Void	VE- 1	VD	682	Channel A Outlet 1	Not Measured	0.0	-	1.00		
683	Void	VE- 2	VD	683	Channel A Outlet 2	Not Measured	0.0	-	1.00		
684	Void	VE- 3	VD	684	Channel A Outlet 3	Not Measured	0.0	-	1.00		
685	Void	VE- 4	VD	685	Channel B Outlet 1	Not Measured	0.0	-	1.00		
686	Void	VE- 5	VD	686	Channel B Outlet 2	Not Measured	0.0	-	1.00		
687	Void	VE- 6	VD	687	Channel B Outlet 3	Not Measured	0.0	-	1.00		
688	Void	VE- 7	VD	688	Channel C Outlet 1	Not Measured	0.0	-	1.00		
689	Void	VE- 8	VD	689	Channel C Outlet 2	Not Measured	0.0	-	1.00		
690	Void	VE- 9	VD	690	Channel C Outlet 3	Not Measured	0.0	-	1.00		
691	Void	VE-10	VD	691	Channel D Outlet 1	Not Measured	0.0	-	1.00		
692	Void	VE-11	VD	692	Channel D Outlet 2	Not Measured	0.0	-	1.00		
693	Void	VE-12	VD	693	Channel D Outlet 3	Not Measured	0.0	-	1.00		
694	Void	VE-13	VD	694	Lower Plenum Bottom 1	Not Measured	0.0	-	1.00		
695	Void	VE-14	VD	695	Lower Plenum Bottom 2	Not Measured	0.0	-	1.00		
696	Void	VE-15	VD	696	Lower Plenum Bottom 3	Not Measured	0.0	-	1.00		
697	Void	VP- 1	VD	697	Lower Plenum Inlet	Not Measured	0.0	-	1.00		
698	Void	VP- 2	VD	698	Lower Plenum Inlet	Not Measured	0.0	-	1.00		

Table A.2 Calculated Data in RUN 992

No.	Item	Symbol	Location	Fig. No.	Unit
1	Density	DE 701	JP1,2 Outlet, Average		kg/m^3
2	Density	DE 702	JP3,4 Outlet, Average		kg/m^3
3	Density	DE 703	MRP-Side Break, Average		kg/m^3
4	Density	DE 704	PV-Side Break, Average	A. 132	kg/m^3
5	Flow Rate	FM 705	MRP-Side Break, (Low)		kg/m^3
6	Flow Rate	FM 706	PV-Side Break, (Low)	A. 133	kg/s
7	Flow Rate	FM 707	MRP-Side Break, (High)		kg/s
8	Flow Rate	FM 708	PV-Side Break, (High)		kg/s
9	Flow Rate	FM 709	Total Break Flow (Low)		kg/s
10	FLow Rate	FM 710	Total Break Flow (High)		kg/s
11	Flow Rate	FM 711	Steam Flow (Low)	A. 134	kg/s
12	FLow Rate	FM 712	Steam Flow (High)	A. 134	kg/s
13	Flow Rate	FM 713	Steam Flow (Middle)	A. 134	kg/s
14	Flow Rate	FM 714	Channel A Inlet	A. 135	kg/s
15	Flow Rate	FM 715	Channel B Inlet	A. 136	kg/s
16	Flow Rate	FM 716	Channel C Inlet	A. 137	kg/s
17	Flow Rate	FM 717	Channel D Inlet	A. 138	kg/s
18	Flow Rate	FM 718	Bypass Hole Flow	A. 139	kg/s
19	Flow Rate	FM 719	Total Core Flow	A. 140	kg/s
20	FLow Rate	FM 720	JP1 Outlet (Pos. Flow)	A. 141	kg/s
21	Flow Rate	FM 721	JP2 Outlet (Pos. Flow)	A. 141	kg/s
22	Flow Rate	FM 722	JP3 Outlet (Pos. Flow)	A. 142	kg/s
23	Flow Rate	FM 723	JP3 Outlet (Neg. Flow)		kg/s
24	Flow Rate	FM 724	JP4 Outlet (Pos. Flow)	A. 142	kg/s
25	Flow Rate	FM 725	JP4 Outlet (Neg. Flow)		kg/s
26	Flow Rate	FM 726	Total JP Outlet Flow		kg/s
27	Water Level	LM 727	Collapsed DC Level	A. 143	m
28	Water Level	LM 728	Collapsed In-Shroud Level	A. 144	m
29	Fluid Mass	EV 729	Downcomer Mass	A. 145	kg
30	Fluid Mass	EV 730	In-Shroud Mass	A. 146	kg
31	Fluid Mass	EV 731	Total Mass in PV	A. 147	kg
32	Fluid Mass	EV 732	Mass Balance in PV		kg
33	Fluid Mass	EV 733	Discharged Mass		kg
34	Flow Rate	FM 734	Discharged Flow Rate		kg/s
35	Flow Rate	FM 735	Discharged Flow Rate		kg/s

Table A.3 Core Instrumentation list

Item	Pos. / DL / Rod NO.	Core Outlet	Pos.1	Pos.2	Pos.3	Pos.4	Pos.5	Pos.6	Pos.7	Core Inlet
		3660	3417	3114.5	2879.5	2527	2174.5	1939.5	1637	1454
Surface Temp.	A11		TF 1	TF 2	TF 3	TF 4	TF 5	TF 6	TF 7	
	A12		TF 8	TF 9	TF 10	TF 11	TF 12	TF 13	TF 14	
	A13		TF 15	TF 16	TF 17	TF 18	TF 19	TF 20	TF 21	
	A14		TF 22	TF 23	TF 24	TF 25	TF 26	TF 27	TF 28	
	A15		TF 29			TF 30				
	A17		TF 31			TF 32				
	A22		TF 33	TF 34	TF 35	TF 36	TF 37	TF 38	TF 39	
	A23		TF 40	TF 41	TF 42	TF 43	TF 44	TF 45	TF 46	
	A24		TF 47	TF 48	TF 49	TF 50	TF.51	TF 52	TF 53	
	A26		TF 54			TF 55				
	A28		TF 56			TF 57				
	A31		TF 58			TF 59				
	A33		TF 60	TF 61	TF 62	TF 63	TF 64	TF 65	TF 66	
	A34		TF 67	TF 68	TF 69	TF 70	TF 71	TF 72	TF 73	
	A35		TF 74			TF 75				
	A37		TF 76			TF 77				
	A42		TF 78			TF 79				
Fluid Temp.	A44	TC 1	TF180	TF181	TF182	TF183	TF184	TF185	TF186	TC 2
Surface Temp.	A45		TF 80			TF 81				
	A46		TF 82			TF 83				
	A48		TF 84			TF 85				
	A51		TF 86			TF 87				
	A53		TF 88			TF 89				
	A54		TF 90							
	A57		TF 91			TF 92				
	A62		TF 93			TF 94				
	A64		TF 95			TF 96				
	A66		TF 97			TF 98				
	A68		TF 99			TF100				
	A71		TF101			TF102				
	A73		TF103			TF104				
	A75		TF105			TF106				
	A77		TF107			TF108				

Table A.3 Core Instrumentation list (Cont'd)

Item	Pos. / DL / Rod NO.	Core Outlet	Pos.1	Pos.2	Pos.3	Pos.4	Pos.5	Pos.6	Pos.7	Core Inlet
		3660	3417	3114.5	2879.5	2527	2174.5	1939.5	1637	1454
Surface Temp.	A82		TF109			TF110				
	A84		TF111			TF112				
	A86		TF113			TF114				
	A88		TF115			TF116				
	B11					TF117				
	B13					TF118				
	B15		TF119	TF120	TF121	TF122	TF123	TF124	TF125	
	B31					TF126				
	B33					TF127				
	B35					TF128				
Fluid Temp.	B44	TC 3	TF187	TF188	TF189	TF190	TF191	TF192	TF193	TC 4
Surface Temp.	B51					TF129				
	B53					TF130				
	B85		TF131	TF132	TF133	TF134	TF135	TF136	TF137	
	C11					TF138				
	C13					TF139				
	C15					TF140				
	C31					TF141				
	C33		TF142	TF143	TF144	TF145	TF146	TF147	TF148	
	C35					TF149				
Fluid Temp.	C44	TC 5	TF194	TF195	TF196	TF197	TF198	TF199	TF200	TC 6
Surface Temp.	C51					TF150				
	C53					TF151				
	C77		TF152	TF153	TF154	TF155	TF156	TF157	TF158	
	D11					TF159				
	D13					TF160				
	D27		TF161	TF162	TF163	TF164	TF165	TF166	TF167	
	D31					TF168				
	D33					TF169				
	D35					TF170				
Fluid Temp.	D44	TC 7	TF201	TF202	TF203	TF204	TF205	TF206	TF207	TC 8
Surface Temp.	D51					TF171				
	D53					TF172				
	D88		TF173	TF174	TF175	TF176	TF177	TF178	TF179	

Table A.3 Core Instrumentation list (Cont'd)

Item	Pos. / DL / Rod NO.	Core Outlet	Pos.1	Pos.2	Pos.3	Pos.4	Pos.5	Pos.6	Pos.7	Core Inlet
		3660	3417	3114.5	2879.5	2527	2174.5	1939.5	1673	1454
Void	A55		VF 1	VF 2	VF 3	VF 4	VF 5	VF 6	VF 7	
	B55		VF 8	VF 9	VF 10	VF 11	VF 12	VF 13	VF 14	
	C55		VF 15	VF 16	VF 17	VF 18	VF 19	VF 20	VF 21	
	D55		VF 22	VF 23	VF 24	VF 25	VF 26	VF 27	VF 28	
Channel Box Surface Temp.	A1*		TB 1	TB 2	TB 3	TB 4	TB 5	TB 6	TB 7	
	A2*		TB 8	TB 9	TB 10	TB 11	TB 12	TB 13	TB 14	
	B*		TB 15	TB 16	TB 17	TB 18	TB 19	TB 20	TB 21	
	C*		TB 22	TB 23	TB 24	TB 25	TB 26	TB 27	TB 28	
	D*		TB 29	TB 30	TB 31	TB 32	TB 33	TB 34	TB 35	
Liquid Level in the Channel Box	A1*		LB 1	LB 2	LB 3	LB 4	LB 5	LB 6	LB 7	
	A2*		LB 8	LB 9	LB 10	LB 11	LB 12	LB 13	LB 14	
	B*		LB 15	LB 16	LB 17	LB 18	LB 19	LB 20	LB 21	
	C*		LB 22	LB 23	LB 24	LB 25	LB 26	LB 27	LB 28	
	D*		LB 29	LB 30	LB 31	LB 32	LB 33	LB 34	LB 35	

Table A.4 Metal temperature measurement list for PV wall, jetpump and recirculation line pipe wall

ID No.	TAG No.	Location (Elevation)	Type	Position in Metal	Contact Region	Distance from fluid contact Surface (mm)
TE 179	TS 15	Filler Block C, Pos.3 (EL2.61m)	Cylindrical	Out. Surf.	DC	0.5 (spot welded)
TE 182	TS 18	Filler Block C, Pos.6 (EL1.56m)	Cylindrical	Out. Surf.	DC	0.5 (spor welded)
TE 193	TS 29	PV Wall Inside (EL3.17m)	Cylindrical	Inside	DC	3.4 (Ag-welded)
TE 195	TS 31	PV Inner Surface (EL3.17m)	Cylindrical	In. Surf.	DC	0.0 (Spot-welded)
TE 196	TS 32	PV Wall Inside (EL2.61m)	Cylindrical	Inside	DC	4.3 (Ag-welded)
TE 197	TS 33	PV Wall Inside (EL1.85m)	Cylindrical	Inside	DC	3.8 (Ag-welded)
TE 198	TS 34	PV Wall Inside (EL1.09m)	Cylindrical	Inside	DC	3.1 (Ag-welded)
TE 200	TS 36	LP Side Wall Inside (EL0.10m)	Cylindrical	Inside	LP	78.9 (Ag-welded)
TE 240	TS 41	PV Wall Outer Surface (EL3.75m)	Cylindrical	Out. Surf.	Insulation	45 (Spot welded)
TE 241	TS 42	PV Wall Outer Surface (EL2.61m)	Cylindrical	Out. Surf.	Insulation	40.6 (Spot welded)
TE 242	TS 43	PV Wall Outer Surface (EL1.09m)	Cylindrical	Out. Surf.	Insulation	40.5 (Spot welded)
TE 243	TS 44	LP Wall Outer Surface (EL0.10m)	Cylindrical	Out. Surf.	Insulation	155 (Spot welded)
TE 244	TS 45	PV Bot. Flange Outer Surface	Plate	Out. Surf.	Air	180 (Spot welded)
TE 245	TS 46	JP Wall Outer Surface (EL2.24m)	Cylindrical	Out. Surf.	Insulation	15.3 (Ag-welded)
TE 246	TS 47	MRP2 Outlet Pipe Wall Out. Surface	Cylindrical	Out. Surf.	Insulation	5.5 (Ag-welded)
TE 247	TS 48	JP Outlet Pipe Wall Out. Surface	Cylindrical	Out. Surf.	Insulation	7.6 (Ag-welded)

Appendix II Data Processing and Experiment Data for RUN 992

In the Appendix II, the experiment data of RUN 992 are presented with their data processing methods. The data acquisition frequency was 5 Hz. The test data were processed and reduced to 1000 data points in each data channel for computer plotting. The test data of RUN 992 are shown in Figs.A.1 through A.147. In these figures, the measured quantity is identified by the channel number and the alphabetic characters (ref. Table A.1).

Figure A.1 shows the representative pressure data in the pressure vessel (PV). Figures A.2 through A.29 show differential pressure data between various positions in the pressure vessel and the recirculation loops. Figures A.30 and A.31 show the liquid levels in the ECCS tank and downcomer. Figures A.32 through A.38 show the flow rates for MSL steam flow, ECC water, feedwater, jet pumps discharge flows and main recirculation pump (MRP) discharge flows.

Figure A.39 shows the electric powers supplied to the heater rod bundle A and other three bundles (B,C and D) with the maximum capacities of 2100 and 3150 kW, respectively. The pump speed of the recirculation pump (MRP2) is shown in Fig.A.40. The trip signals such as the break initiation signal and the ECCS actuation signals are shown in Figs.A.41 through A.43.

Figs.A.44 and A.45 show the fluid densities measured by the gamma densitometer at the break B. The fluid density data are corrected at two known points, one is the initial condition and another is a steam-phase condition. Figures A.46 and A.47 show momentum fluxes measured by drag-disks at the outlet of jetpumps. The drag-disk data are corrected at two known points, one is the initial condition, in which the volumetric flow rate for the initial water flow is known, and another one is the final test condition, in which the recirculation flow was terminated by closing the QSV after the end of test period. Figure A.48 shows momentum flux at the break B, which was corrected similarly at the two points. One is the initial condition, in which no break flow exists. Another is a steam flow condition, which is determined by the orifice flow data and the

fluid density data for a single-phase steam flow just before the ADS actuation at 594 s.

Figures A.49 through A.58 show the fluid temperatures at various positions in the system. Vessel and pipe wall temperatures are measured and compared with each corresponding fluid temperature as shown in Figs.A.59 through A.64. As the data processing was inadequate for the metal temperatures of TE 240 through TE 247, correction should be necessary by using a following relation, as

$$T_C = 0.51545 \times T + 127.2 \qquad (A.1)$$

where T_C and T are correct temperature and data value included in the data file, respectively. In Figs.A.59 through A.64, this correction was completed for each metal temperature.

The heater rod cladding temperature and the surface temperatures of the water rods and the channel boxes are measured at positions 1 through 7 as given in Figs.A.65 through A.81. Figures A.82 through A.105 show the heater rod cladding temperatures in a different manner. Figures A.106 through A.119 show the fluid temperatures at the outlet of the channel boxes. The liquid level signals in the core, the upper and lower plena, the guide tube and the downcomer are shown in Figs.A.120 through A.131.

Quantities reduced from these test data are shown in Figs.A.132 through A.147. Figure A.132 shows the average fluid density calculated from the data shown in Figs.A.44 and A.45. The average density is calculated as an arithmetic mean of the densities in multi-directions with the weight of each cord length.

For the two-beam densitometer at the break spool piece,

$$\rho_{av} = 0.5863\rho_A + 0.4137\rho_B \qquad (A.2)$$

where,

ρ_{av}: average density obtained from the two-beam gamma densitometer,

ρ_A : density measured by beam A (bottom),

ρ_B : density measured by beam B (top).

Figure A.133 shows steam break flow rate calculated by using the momentum flux data (see Fig.A.48) of the low-range drag-disk flow meter and the average steam density (see Fig.A.132).

Figures A.134 through A.139 show the fluid flow rates at the main

steam line, channel inlet orifices and the bypass hole. The fluid flow rates are calculated from the test data which are the pressure drop across the orifices or venturi flow meters and the liquid density obtained from the temperature and the pressure condition. The equation used for the calculation is as follows :

$$G = C_D \cdot A \cdot \sqrt{2g \cdot \rho_l \cdot \Delta P} \qquad (A.3)$$

where,

G : flow rate,

ΔP : pressure drop across the orifice,

C_D : discharge coefficient,

= 0.6552 (the orifice to measure the steam discharge flow rate)

= 0.4761 (the channel inlet orifice)

= 0.8032 (the bypass hole)

A : flow area (m^2)

= 2.875×10^{-3} (the orifice to measure the steam discharge flow rate)

= 1.521×10^{-3} (the channel inlet orifice)

= 1.758×10^{-4} (the bypass hole)

g : gravitational acceleration (= 9.807 m/s^2),

ρ_l : density of the single-phase liquid (kg/m^3),

This calculation method is not applicable for two-phase flow condition after the LPF initiation at the channel inlet orifice and the bypass hole. Those calculated values show only a trend in the two-phase flow condition. Total channel inlet flow rate presents the sum of four channel inlet flow rates and a bypass hole flow rate as shown in Fig.A.140. Shown in Figs. A.141 and 142 are the calculated jetpump outlet flow rates, which are derived from the corresponding differential pressure data in a similar way.

Figures A.143 and A.144 show the collapsed water levels in the downcomer and inside the core-shroud, respectively. Each level is obtained from the corresponding differential pressure. The differential pressure includes an effect of flow resistance, which becomes negligible after slowdown of the recirculation pump speed, lower plenum flashing and ADS actuation.

Figure A.145 shows the fluid mass inventory in downcomer. The fluid mass inventory is determined from the density and configurational data outside the core shroud,

$$M = \rho_l \cdot Q \tag{A.4}$$

where,

M : fluid inventory,

ρ_l : liquid density estimated from the satulation temperature and/or pressure,

Q : liquid volume calculated from the liquid level.

The volume Q (m^3) inside the shroud is also given as a function of collapsed water level in downcomer (L),

$$\begin{aligned}
Q &= 0.0 && (\quad L \leqq 0.494) \\
Q &= 0.0225L - 0.0111 && (0.494 < L \leqq 1.384) \\
Q &= 0.0697L - 0.0769 && (1.384 < L \leqq 1.519) \\
Q &= 0.0225L - 0.0048 && (1.519 < L \leqq 3.355) \\
Q &= 0.0801L - 0.1980 && (3.355 < L \leqq 4.250) \\
Q &= 0.2443L - 0.8959 && (4.250 < L \leqq 4.413) \\
Q &= 0.2611L - 0.9700 && (4.413 < L \leqq 4.578) \\
Q &= 0.2504L - 0.9211 && (4.578 < L \leqq 4.654) \\
Q &= 0.2375L - 0.8610 && (4.654 < L \leqq 4.815) \\
Q &= 0.2866L - 1.0974 && (4.815 < L \leqq 4.915) \\
Q &= 0.3396L - 1.3580 && (4.915 < L \leqq 5.143) \\
Q &= 0.3607L - 1.4665 && (5.143 < L \leqq 5.365) \\
Q &= 0.3848L - 1.5960 && (5.365 < L \leqq 5.995) \\
Q &= 0.7111 && (5.995 < L \quad)
\end{aligned} \tag{A.5}$$

Figure A.146 shows the fluid mass inventory inside the core-shroud. The fluid mass inventory is determined from the density and configurational data inside the core-shroud,

$$M = \rho_l \cdot Q \tag{A.6}$$

where,

M : fluid inventory,

ρ_l : liquid density estimated from the saturation temperature and/or

pressure,

Q : liquid volume calculated from the liquid level.

The volume Q (m^3) inside the shroud is also given as a function of collapsed water level inside core-shroud (L),

$$
\begin{aligned}
Q &= 0.0 && (\quad L \leqq 0.0\quad) \\
Q &= 0.2350L && (\ 0.0 < L \leqq 0.497\ ) \\
Q &= 0.1245L + 0.0549 && (\ 0.497 < L \leqq 1.354\ ) \\
Q &= 0.0698L + 0.1290 && (\ 1.354 < L \leqq 3.589\ ) \\
Q &= 0.1648L - 0.2120 && (\ 3.589 < L \leqq 3.744\ ) \\
Q &= 0.1963L - 0.3299 && (\ 3.744 < L \leqq 4.243\ ) \\
Q &= 0.0196L + 0.4199 && (\ 4.243 < L \leqq 4.578\ ) \\
Q &= 0.0186L + 0.4244 && (\ 4.578 < L \leqq 4.654\ ) \\
Q &= 0.0410L + 0.3201 && (\ 4.654 < L \leqq 5.099\ ) \\
Q &= 0.0196L + 0.4292 && (\ 5.099 < L \leqq 5.365\ ) \\
Q &= 0.5344 && (\ 5.365 < L\quad)
\end{aligned}
\qquad (A.7)
$$

Figure A.147 shows a total fluid inventory in PV, which is a sum of fluid mass in the downcomer (see Fig.A.145) and inside the core-shroud (see Fig.A.146).

List of Figures

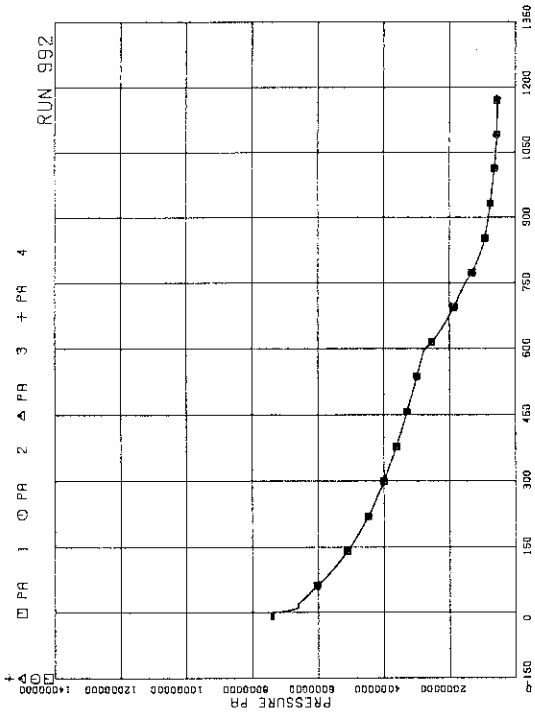

FIG.A. 1 PRESSURE IN PV (PRESSURE VESSEL)

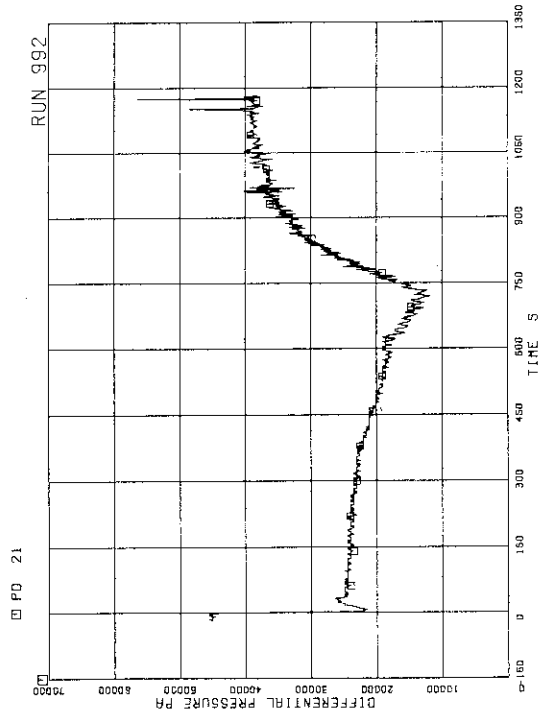

FIG.A. 2 DIFFERENTIAL PRESSURE BETWEEN LOWER PLENUM (LP) AND UPPER PLENUM (UP)

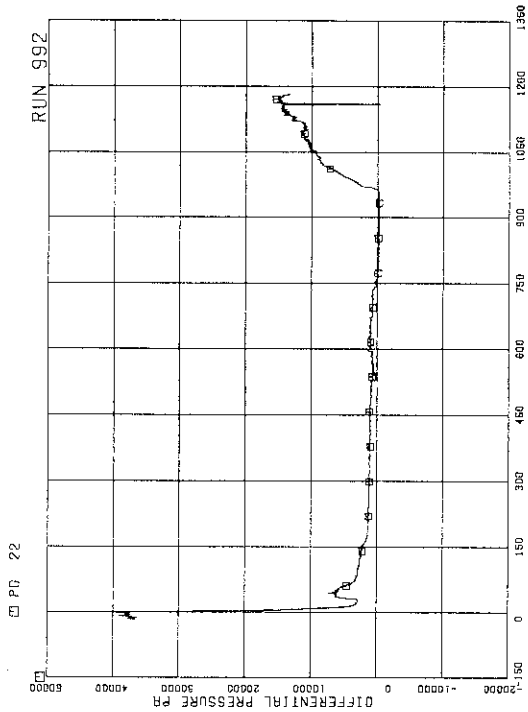

FIG.A. 3 DIFFERENTIAL PRESSURE BETWEEN UP AND STEAM DOME

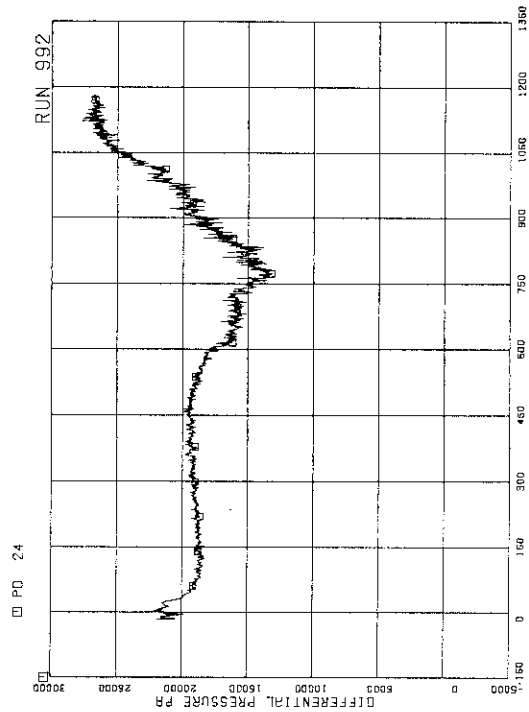

FIG.A. 4 DC (DOWNCOMER) HEAD

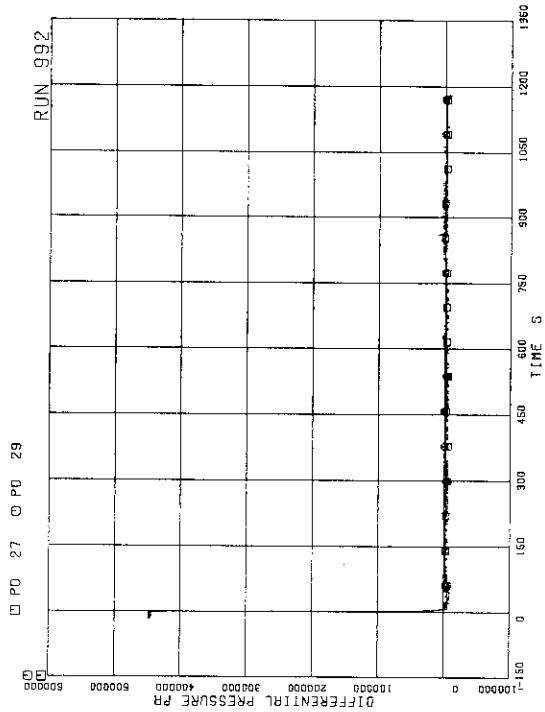

FIG.A. 7 DIFFERENTIAL PRESSURE BETWEEN JP-1,2 DRIVE AND SUCTION

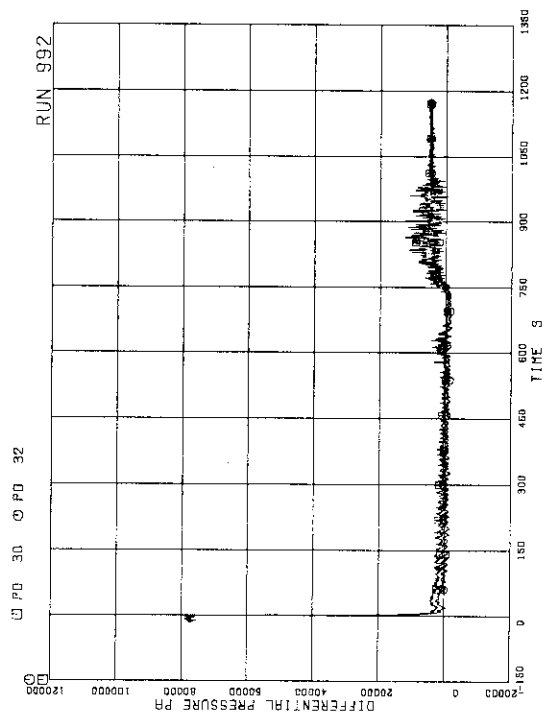

FIG.A. 8 DIFFERENTIAL PRESSURE BETWEEN JP-3,4 DISCHARGE AND SUCTION

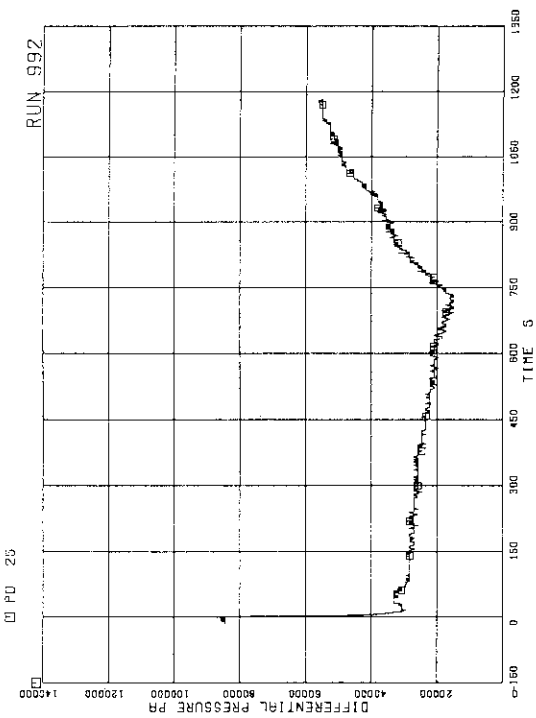

FIG.A. 5 DIFFERENTIAL PRESSURE BETWEEN PV BOTTOM AND TOP

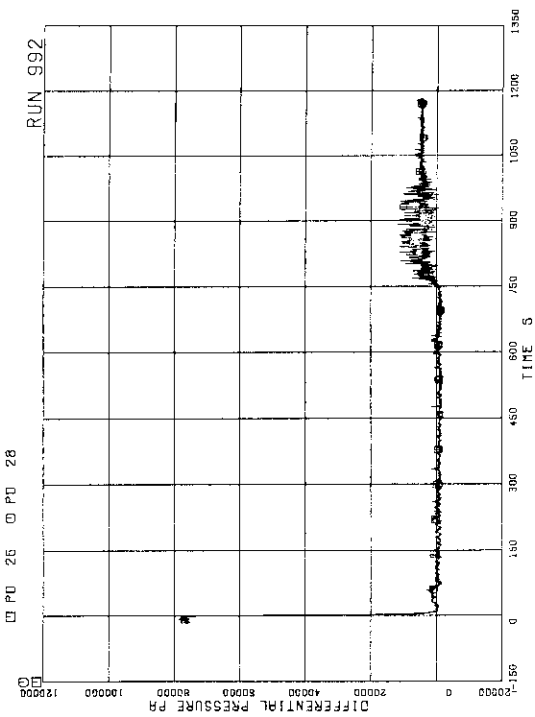

FIG.A. 6 DIFFERENTIAL PRESSURE BETWEEN JP-1,2 DISCHARGE AND SUCTION

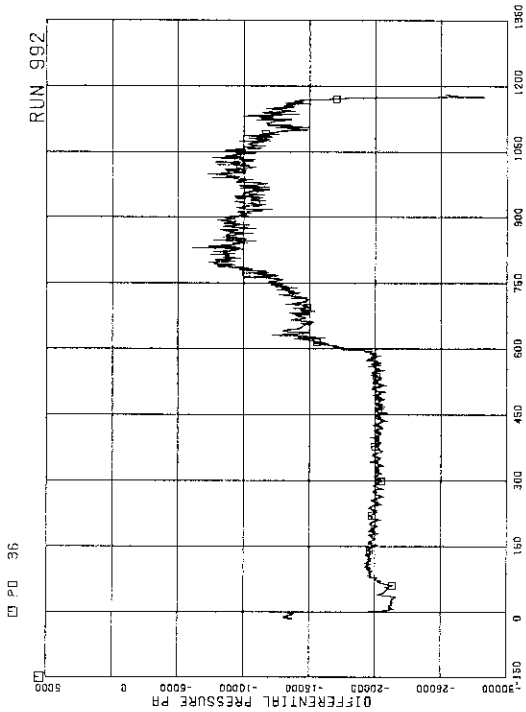

FIG.A. 11 DIFFERENTIAL PRESSURE BETWEEN DC BOTTOM AND MRP1 SUCTION

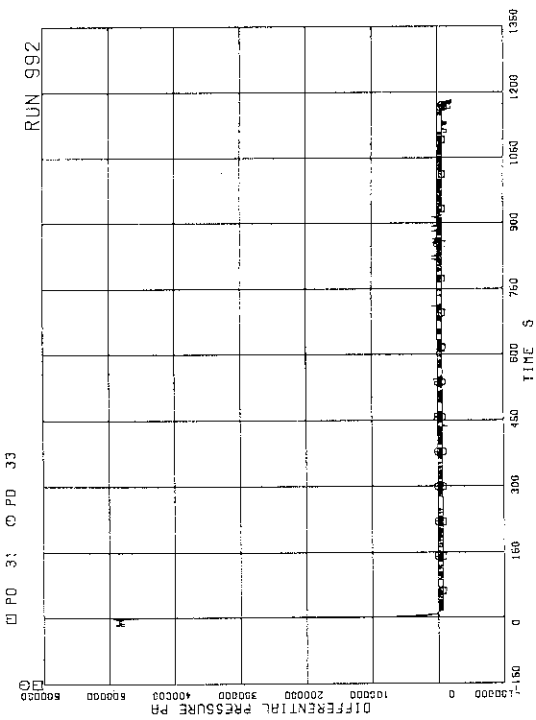

FIG.A. 9 DIFFERENTIAL PRESSURE BETWEEN JP-3,4 DRIVE AND SUCTION

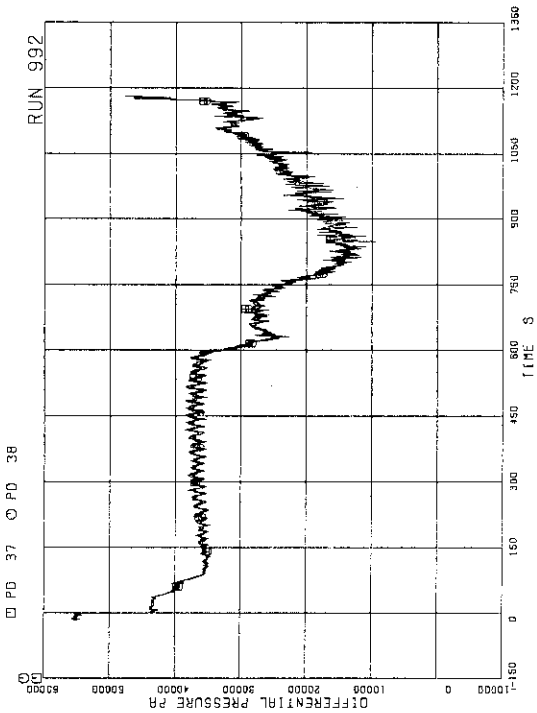

FIG.A. 12 DIFFERENTIAL PRESSURE BETWEEN MRP1 DELIVERY AND JP-1,2 DRIVE

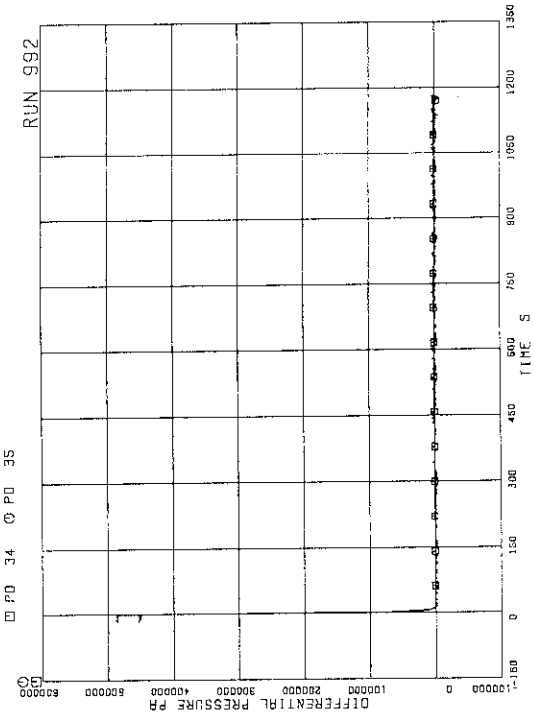

FIG.A. 10 DIFFERENTIAL PRESSURE BETWEEN MRP DELIVERY AND SUCTION

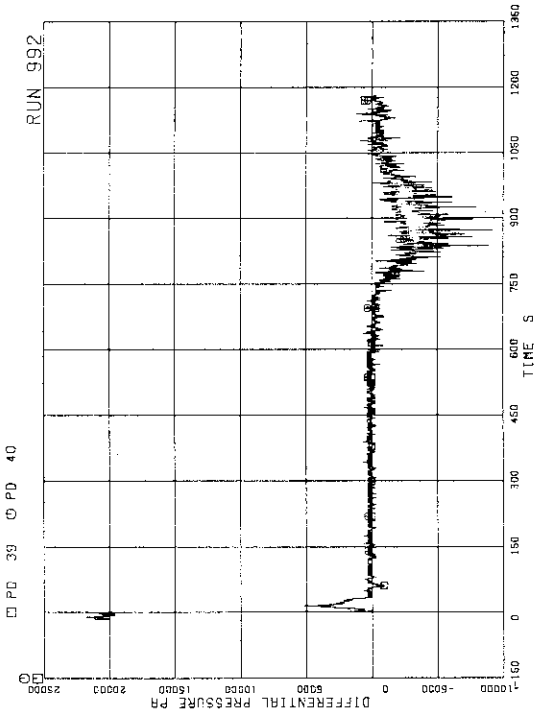

FIG.A. 13 DIFFERENTIAL PRESSURE BETWEEN DC MIDDLE AND JP-1,2 SUCTION

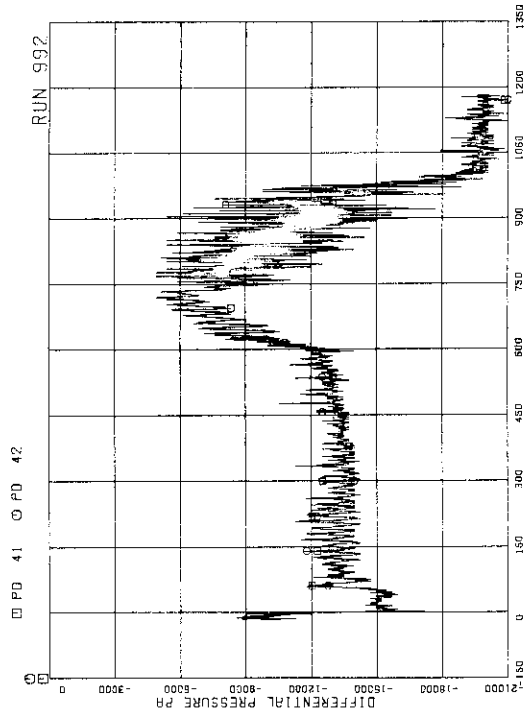

FIG.A. 14 DIFFERENTIAL PRESSURE BETWEEN JP-1,2 DISCHARGE AND LP

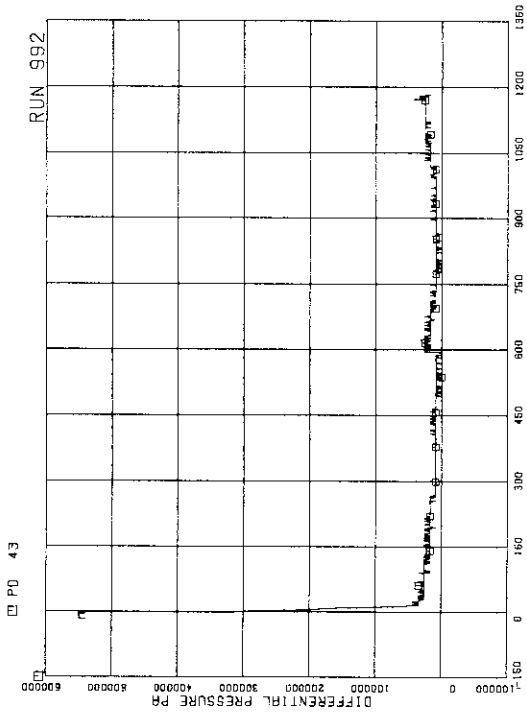

FIG.A. 15 DIFFERENTIAL PRESSURE BETWEEN DC BOTTOM AND BREAK B

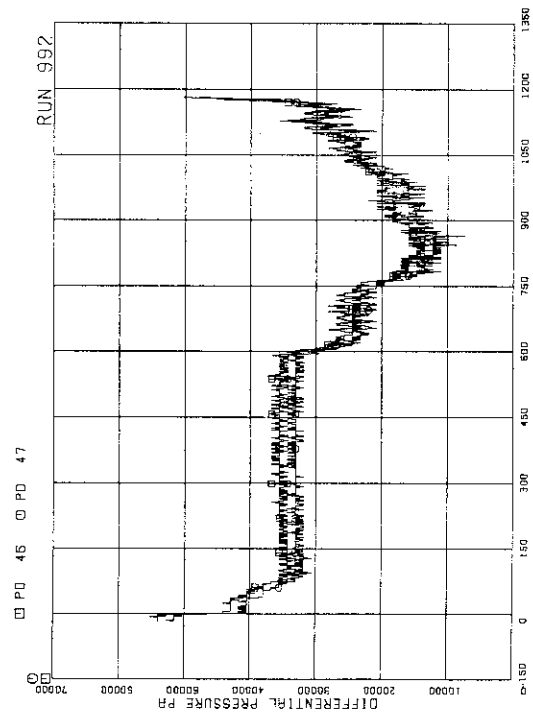

FIG.A. 16 DIFFERENTIAL PRESSURE BETWEEN MRP2 DELIVERY AND JP-3,4 DRIVE

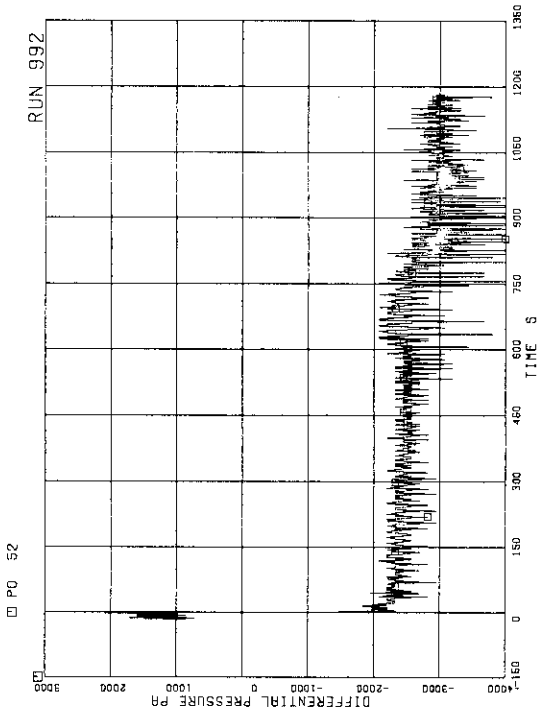

FIG.A. 19 DIFFERENTIAL PRESSURE BETWEEN CONFLUENCE IN BROKEN LOOP AND LP

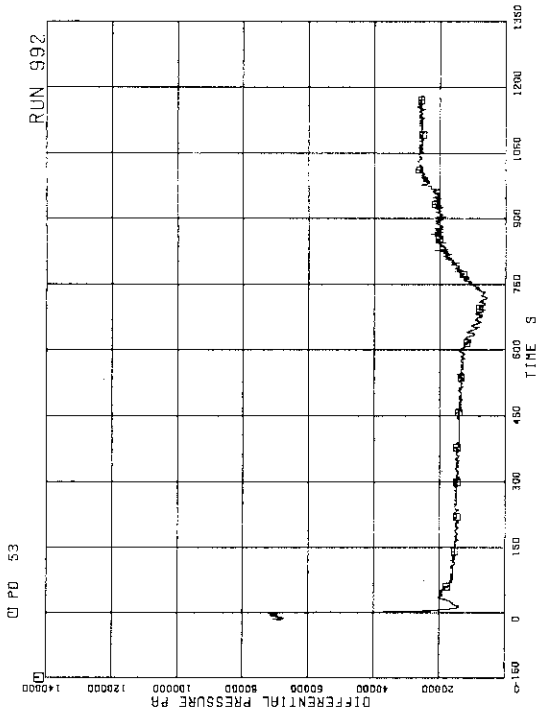

FIG.A. 20 DIFFERENTIAL PRESSURE BETWEEN LP AND DC MIDDLE

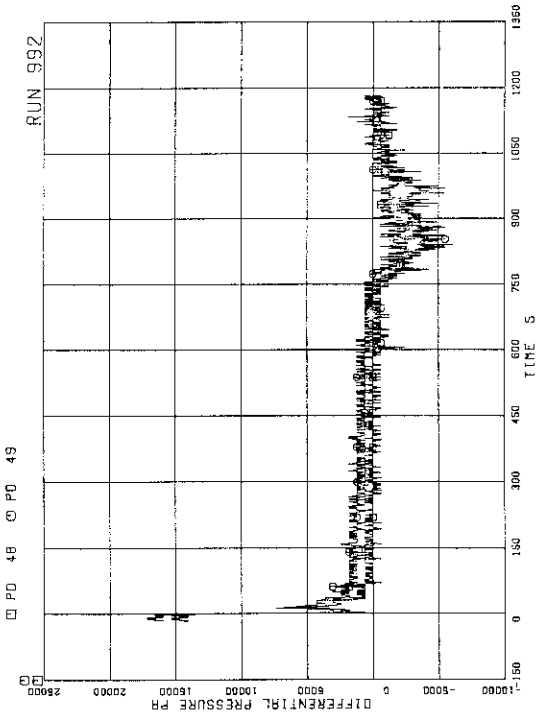

FIG.A. 17 DIFFERENTIAL PRESSURE BETWEEN DC MIDDLE AND JP-3,4 SUCTION

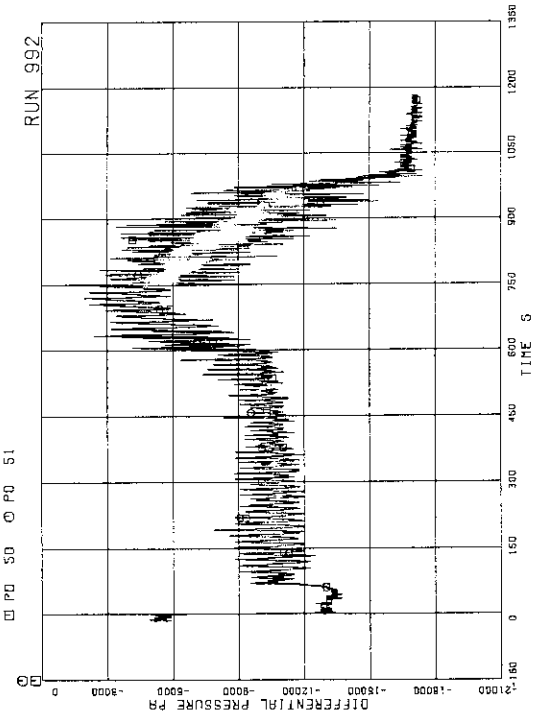

FIG.A. 18 DIFFERENTIAL PRESSURE BETWEEN JP-3,4 DISCHARGE AND CONFLUENCE

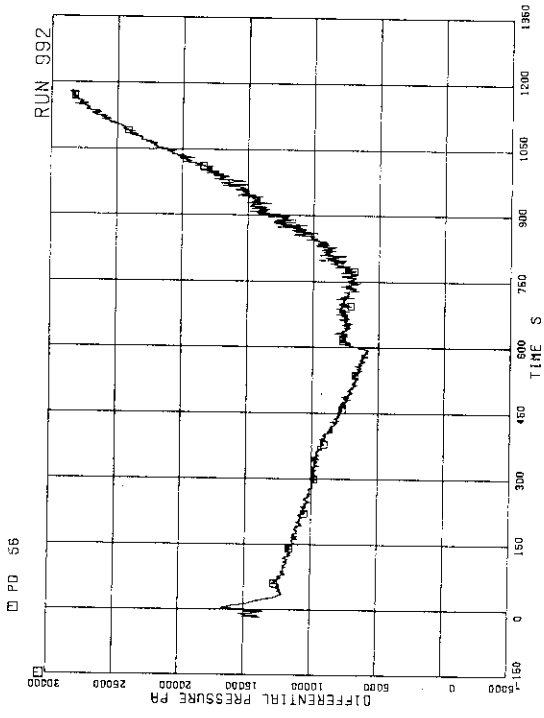

FIG.A. 23 DIFFERENTIAL PRESSURE BETWEEN DC MIDDLE AND STEAM DOME

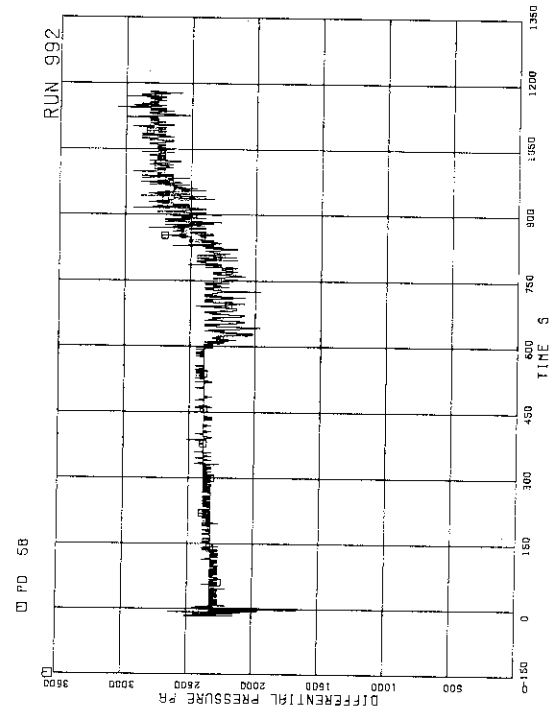

FIG.A. 24 DIFFERENTIAL PRESSURE BETWEEN LP BOTTOM AND LP MIDDLE

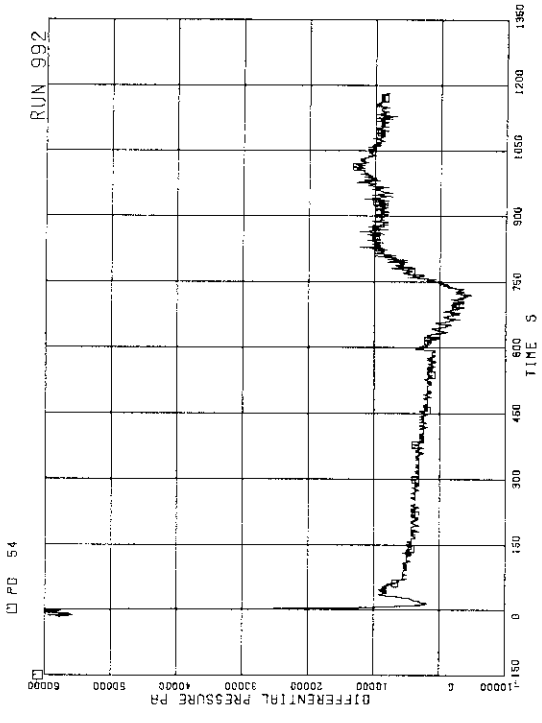

FIG.A. 21 DIFFERENTIAL PRESSURE BETWEEN DC AND LP BOTTOM

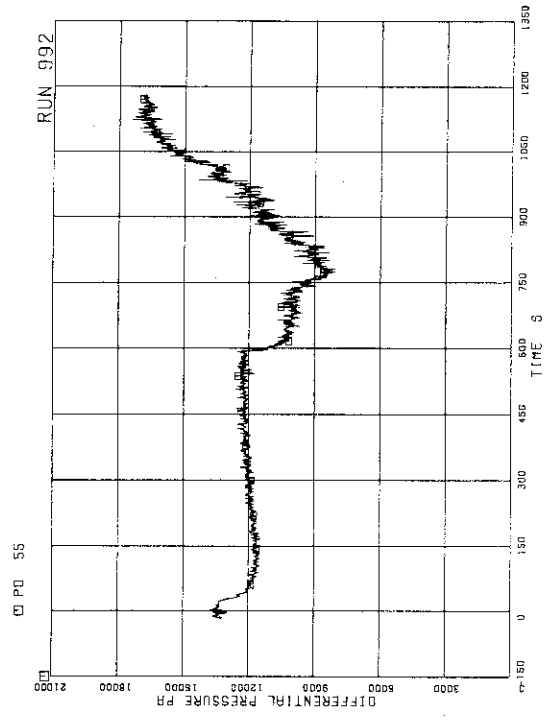

FIG.A. 22 DIFFERENTIAL PRESSURE BETWEEN DC BOTTOM AND DC MIDDLE

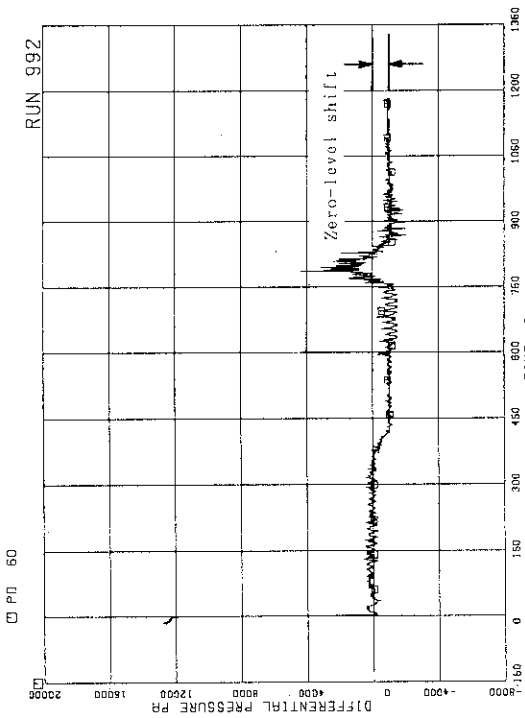

FIG.A. 25 DIFFERENTIAL PRESSURE ACROSS CHANNEL INLET ORIFICE A

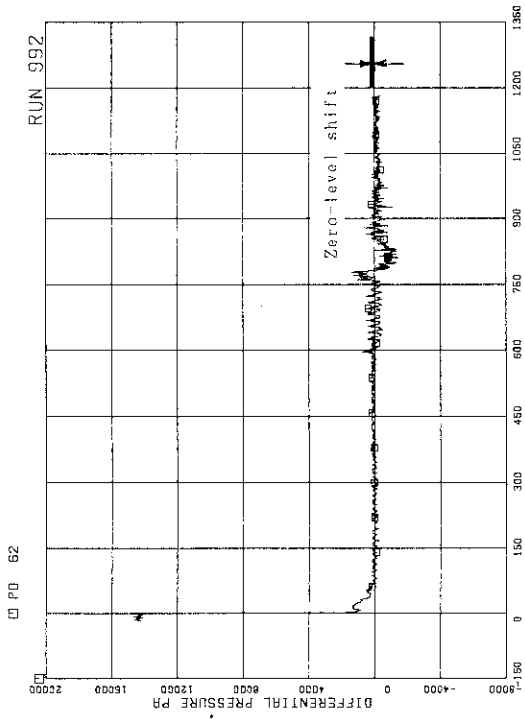

FIG.A. 27 DIFFERENTIAL PRESSURE ACROSS CHANNEL INLET ORIFICE C

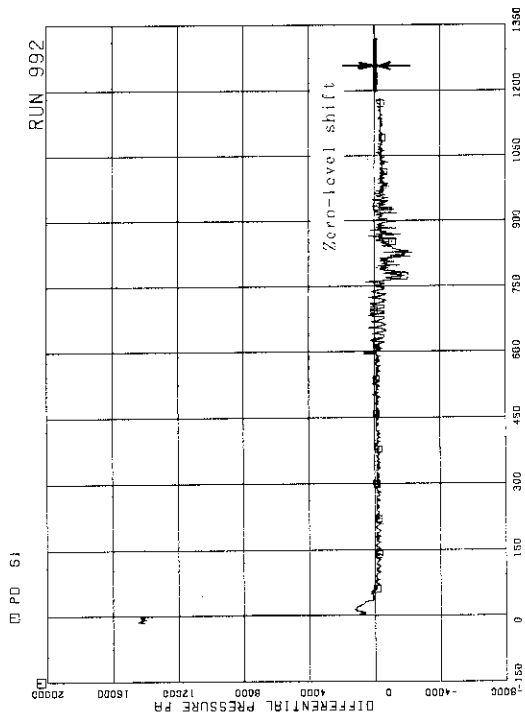

FIG.A. 26 DIFFERENTIAL PRESSURE ACROSS CHANNEL INLET ORIFICE B

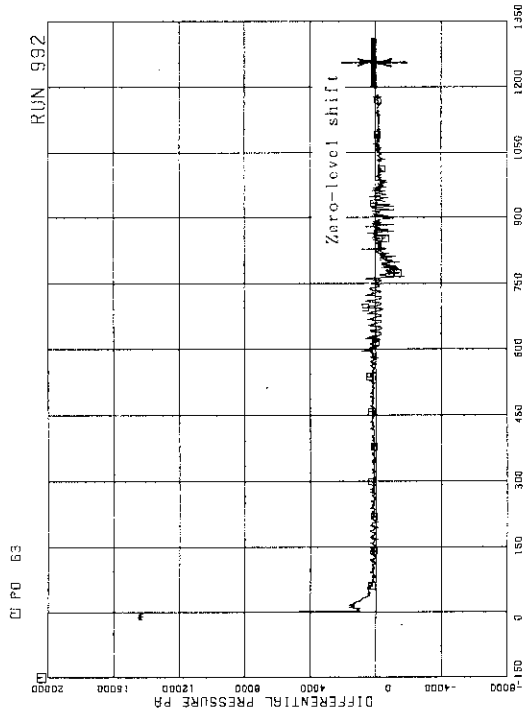

FIG.A. 28 DIFFERENTIAL PRESSURE ACROSS CHANNEL INLET ORIFICE D

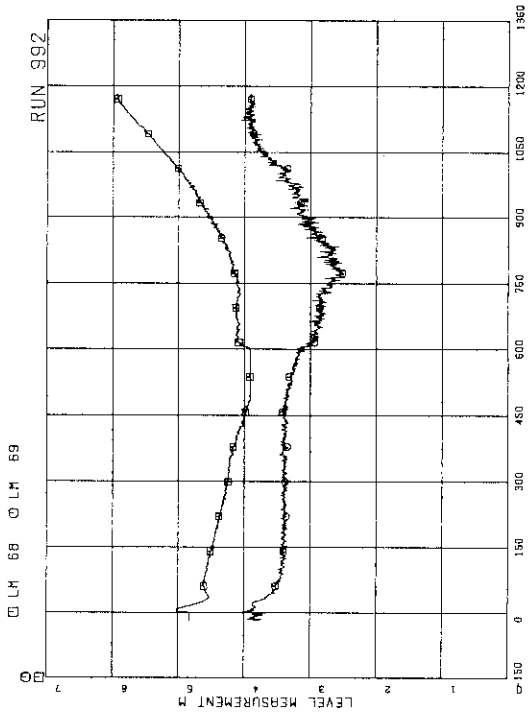

FIG.A. 31 LIQUID LEVEL IN DOWNCOMER

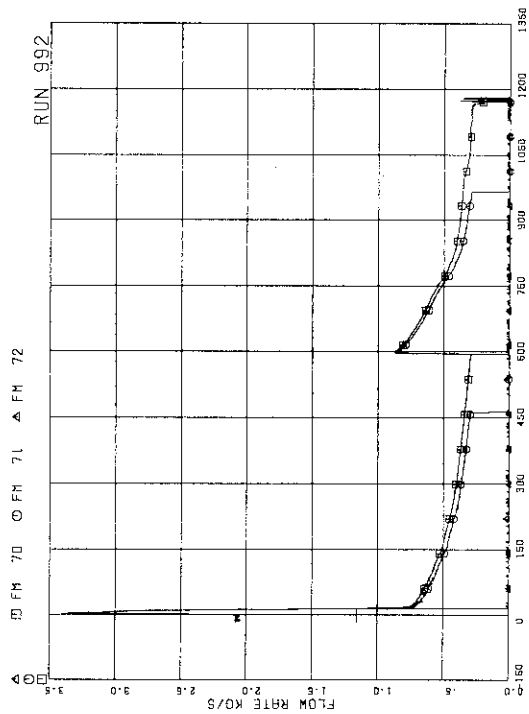

FIG.A. 32 MASS FLOW RATE IN MSL

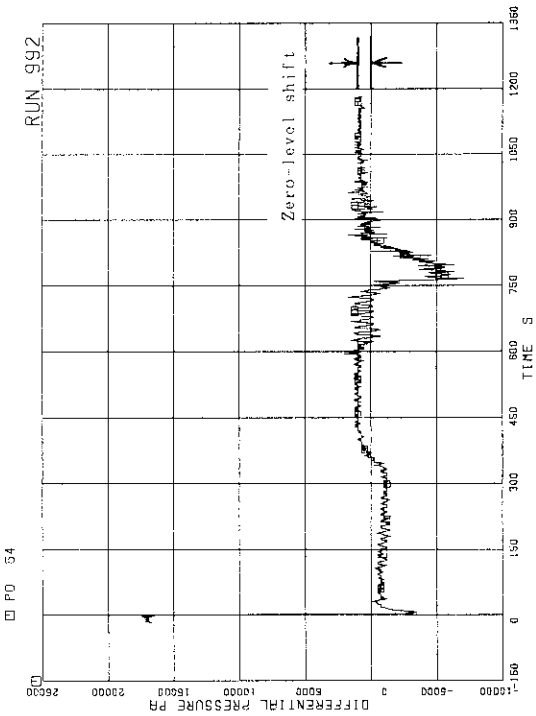

FIG.A. 29 DIFFERENTIAL PRESSURE ACROSS BYPASS HOLE

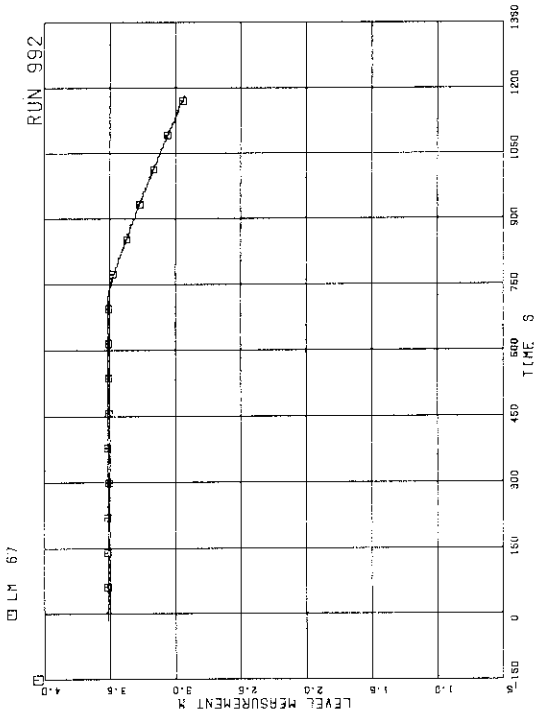

FIG.A. 30 LIQUID LEVEL IN ECCS TANK

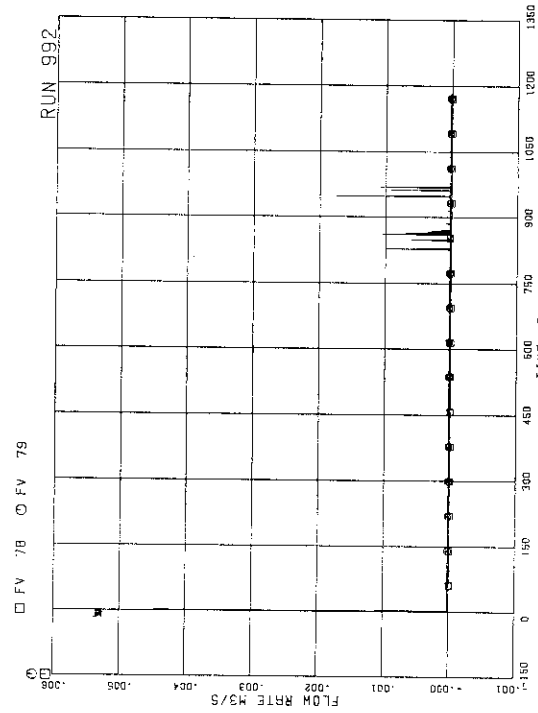

FIG.A. 35 JP-1,2 DISCHARGE FLOW RATE

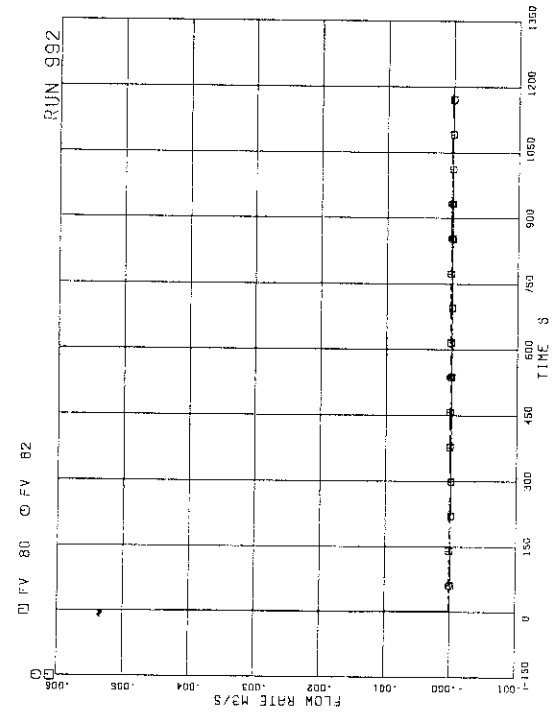

FIG.A. 36 JP-3,4 DISCHARGE FLOW RATE (NORMAL)

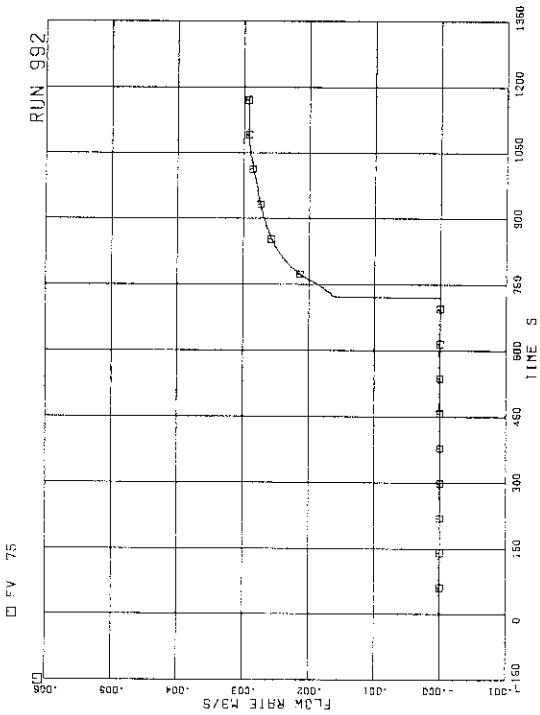

FIG.A. 33 ECC INJECTION FLOW RATE

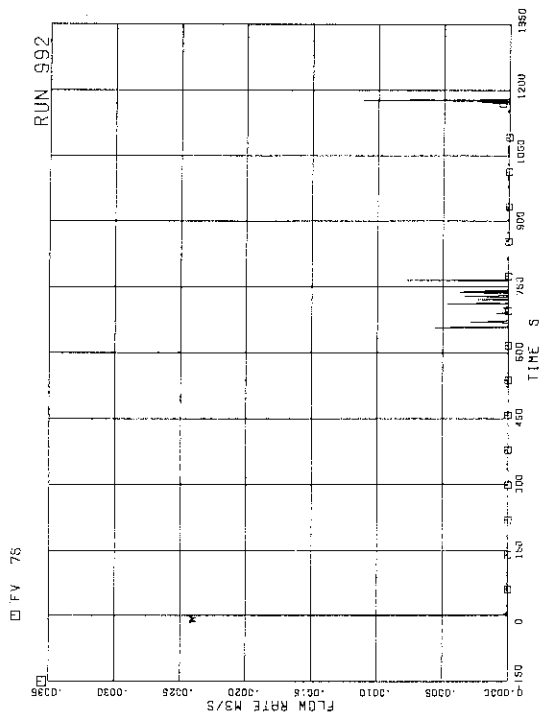

FIG.A. 34 FEEDWATER FLOW RATE

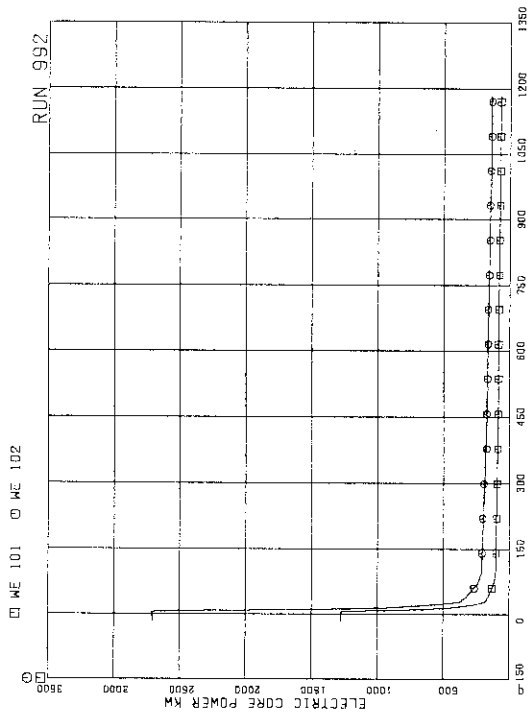

FIG.A. 39 ELECTRIC CORE POWER

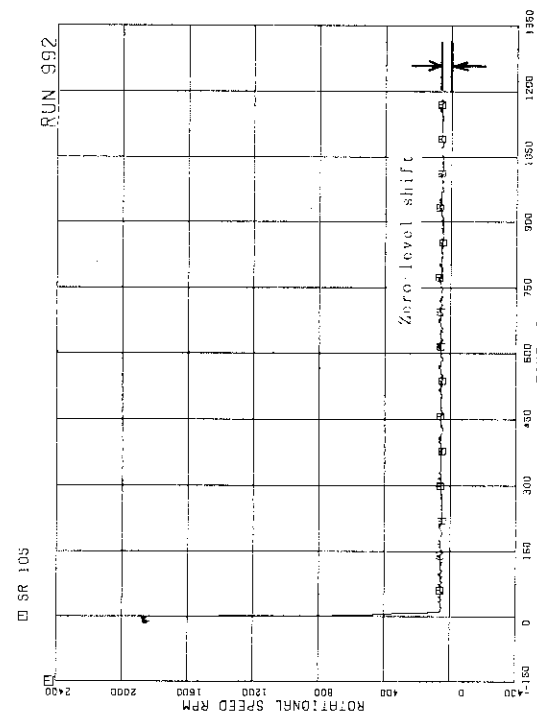

FIG.A. 40 MRP PUMP SPEED

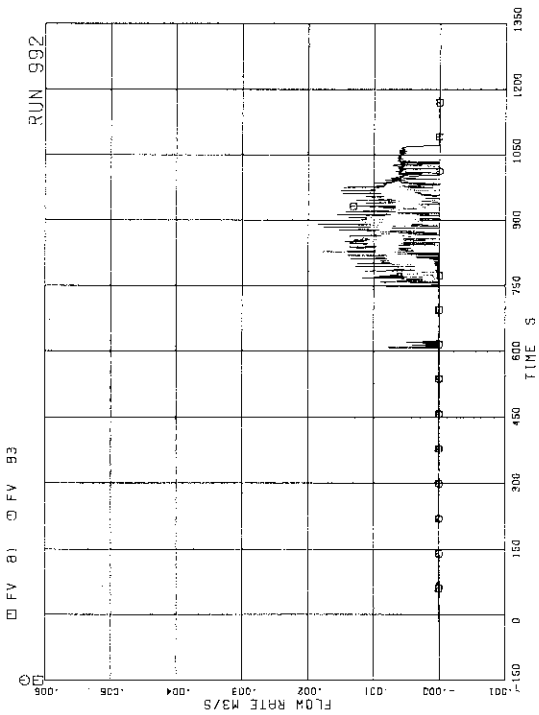

FIG.A. 37 JP-3,4 DISCHARGE FLOW RATE (REVERSE)

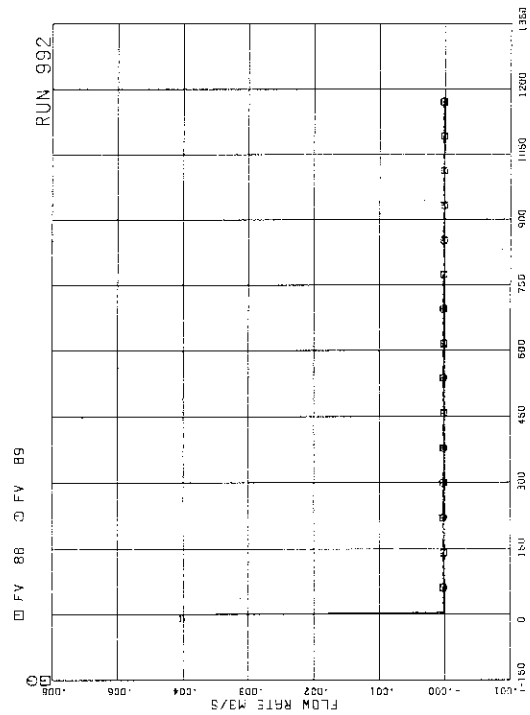

FIG.A. 38 MRP DISCHARGE FLOW RATE

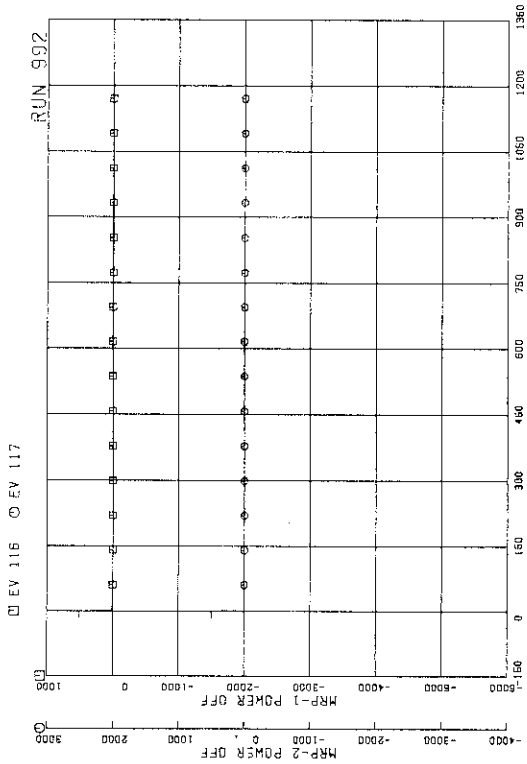

FIG.A. 43 MRP OPERATION SIGNAL

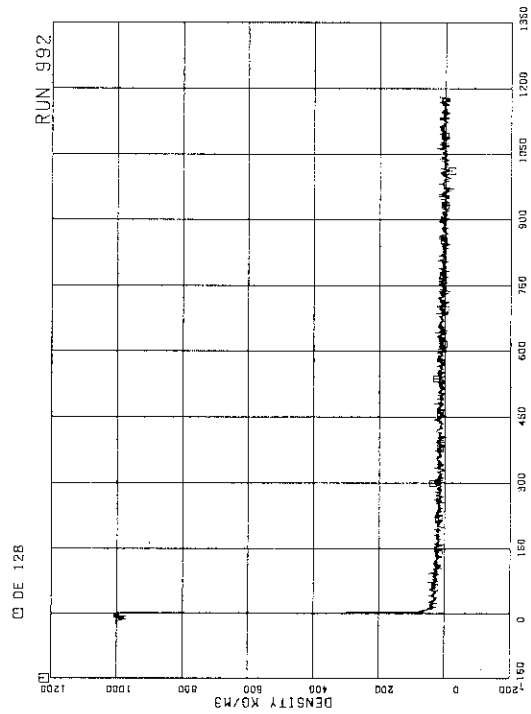

FIG.A. 44 FLUID DENSITY IN MSL DOWN THE BREAK ORIFICE,BEAM A

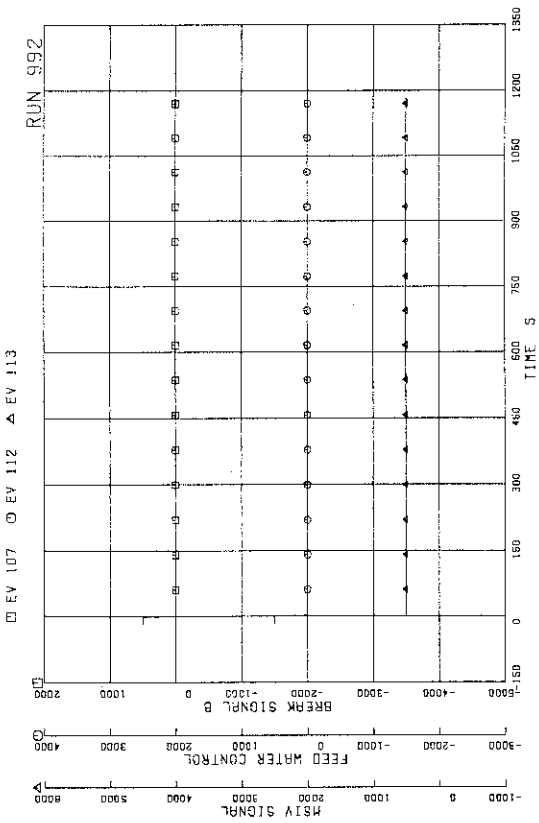

FIG.A. 41 VALVE OPERATION SIGNAL

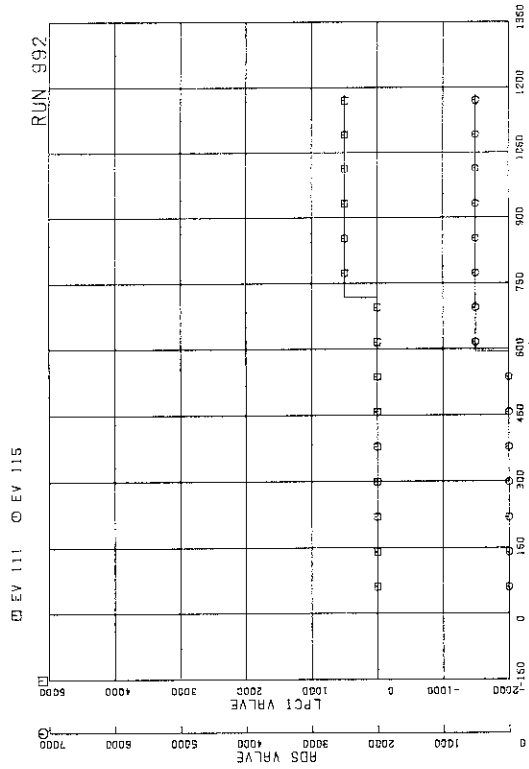

FIG.A. 42 ECCS OPERATION SIGNAL

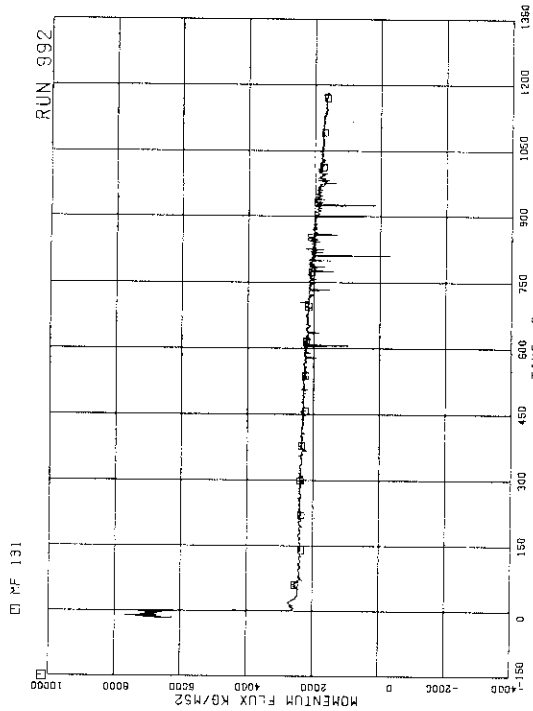

FIG.A. 47 MOMENTUM FLUX AT JP-3,4 OUTLET SPOOL

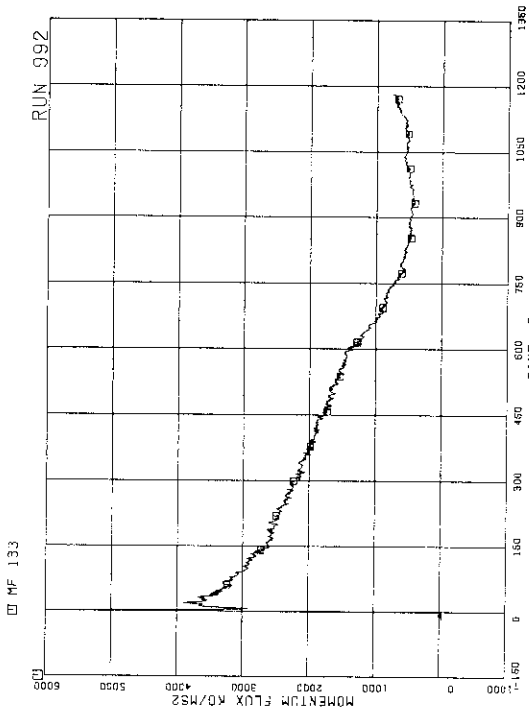

FIG.A. 48 MOMENTUM FLUX AT BREAK BELOW RANGE)

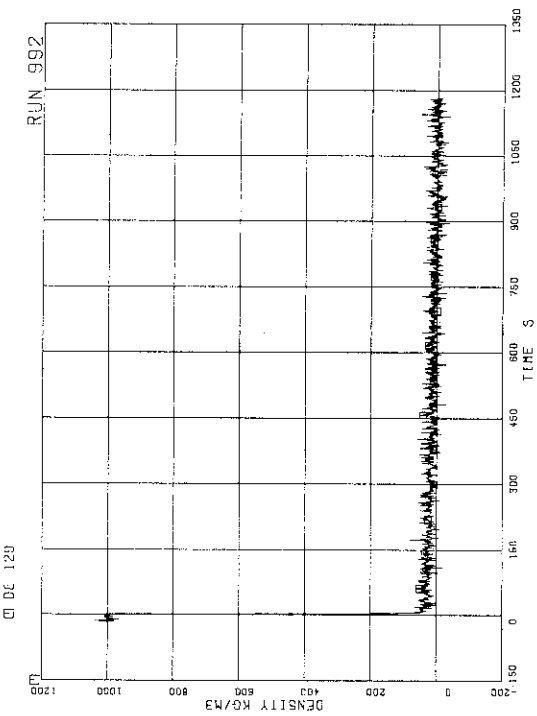

FIG.A. 45 FLUID DENSITY IN MSL DOWN THE BREAK ORIFICE,BEAM B

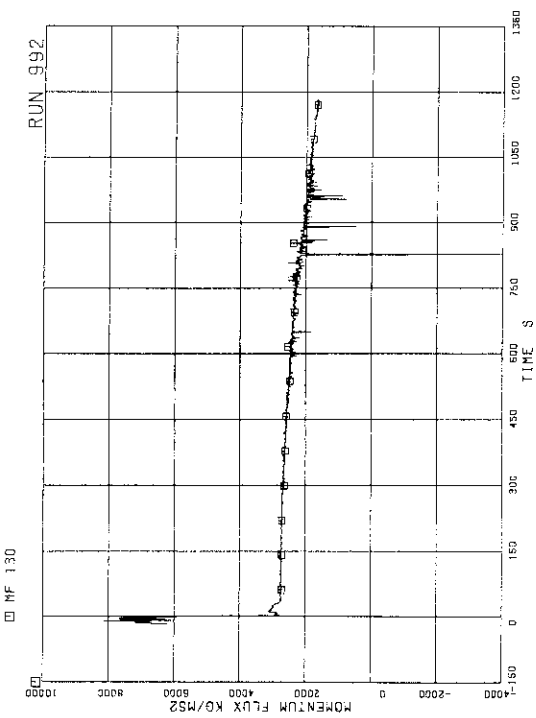

FIG.A. 46 MOMENTUM FLUX AT JP-1,2 OUTLET SPOOL

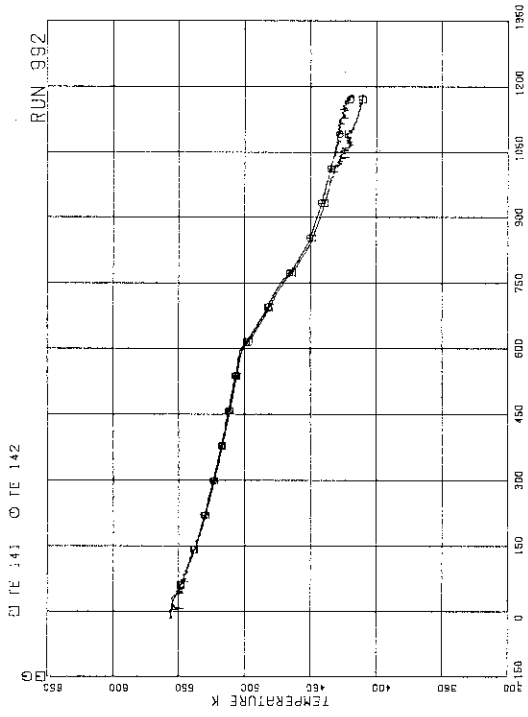

FIG.A. 49 FLUID TEMPERATURE IN LOWER PLENUM AND UPPER PLENUM

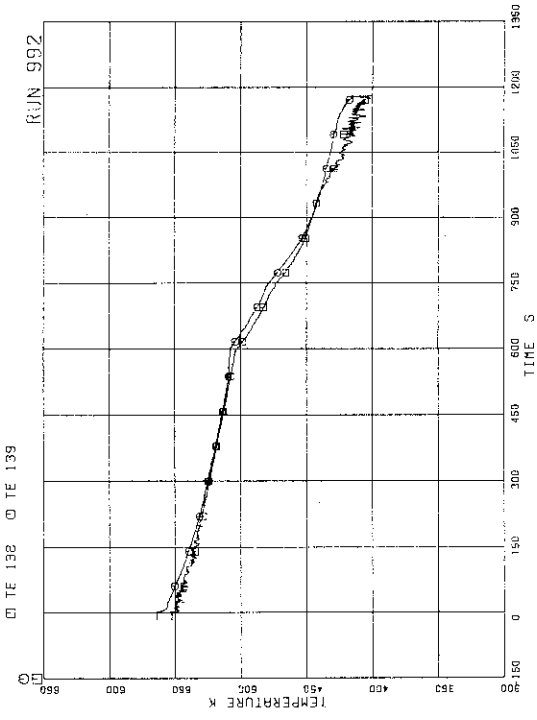

FIG.A. 51 FLUID TEMPERATURE IN DOWNCOMER

FIG.A. 50 FLUID TEMPERATURE IN STEAM DOME AND MSL

FIG.A. 52 FLUID TEMPERATURE IN INTACT RECIRCULATION LOOP

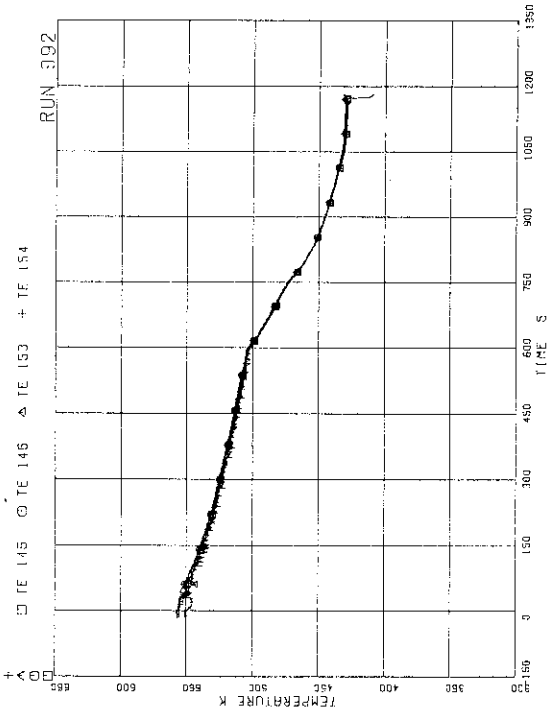

FIG.A. 53 FLUID TEMPERATURE IN BROKEN RECIRCULATION LOOP

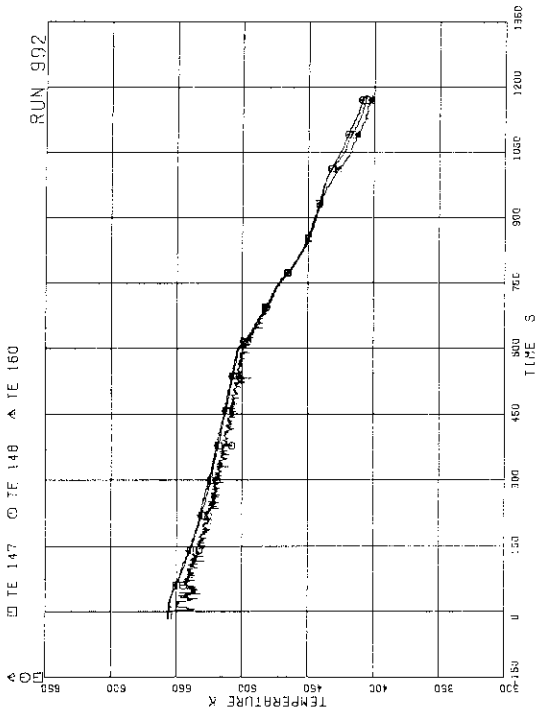

FIG.A. 54 FLUID TEMPERATURE AT JP-1,2 OUTLET

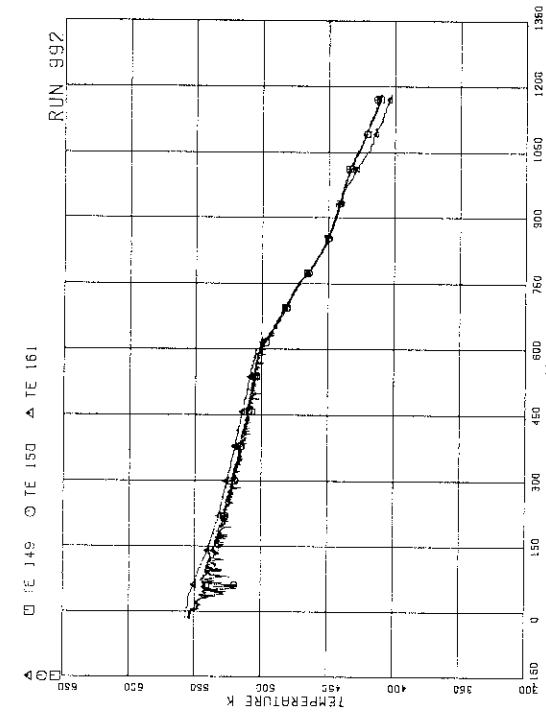

FIG.A. 55 FLUID TEMPERATURE AT JP-3,4 OUTLET

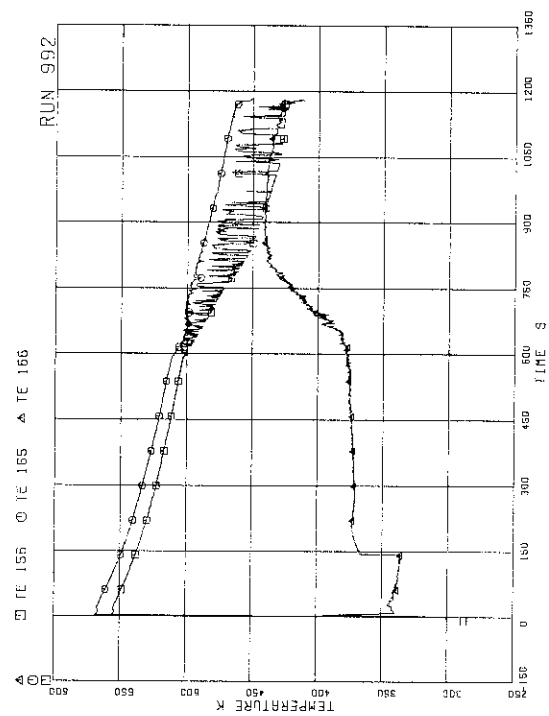

FIG.A. 56 FLUID TEMPERATURE NEAR BREAK B

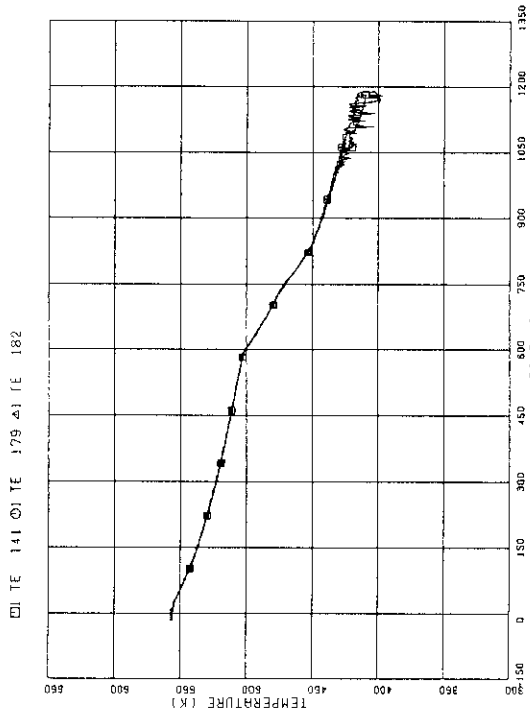

FIG.A. 59 METAL TEMP. AT FILLER BLOCK C POS.3,5

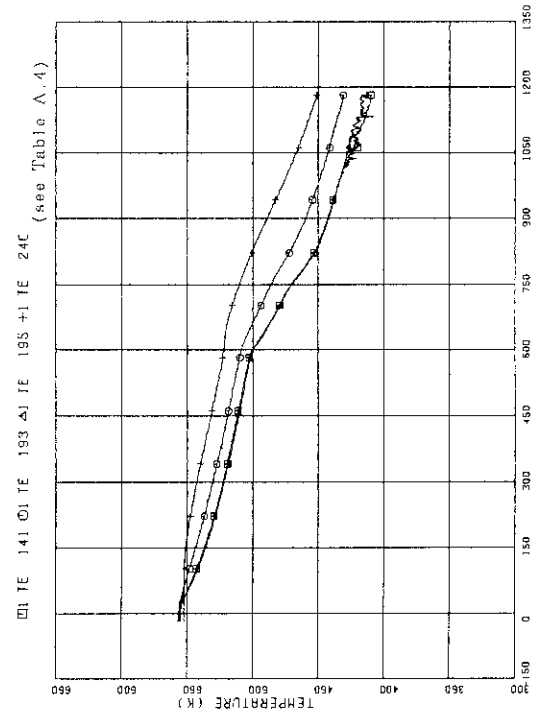

FIG.A. 60 METAL TEMP. AT MIDDLE OF PV-WALL (INSIDE TO OUTER SURFACE)

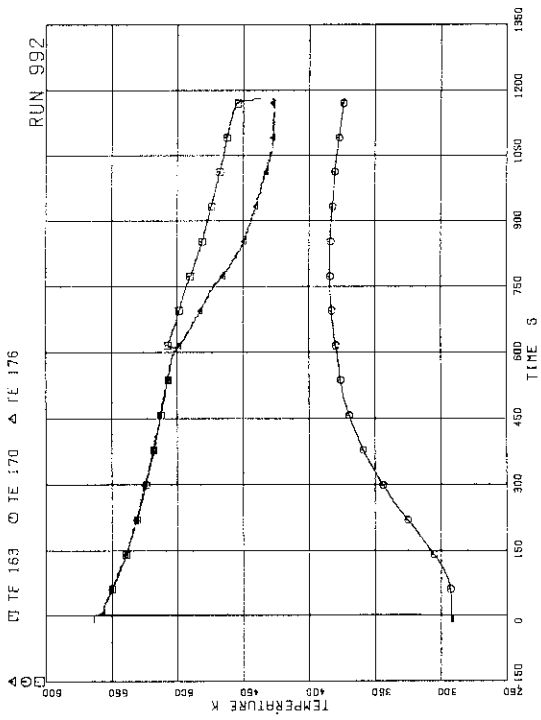

FIG.A. 57 FLUID TEMPERATURE IN MSL

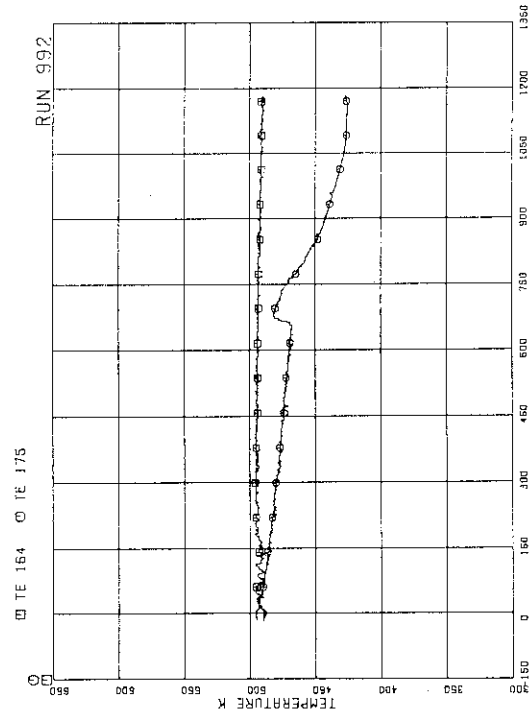

FIG.A. 58 FEEDWATER TEMPERATURE

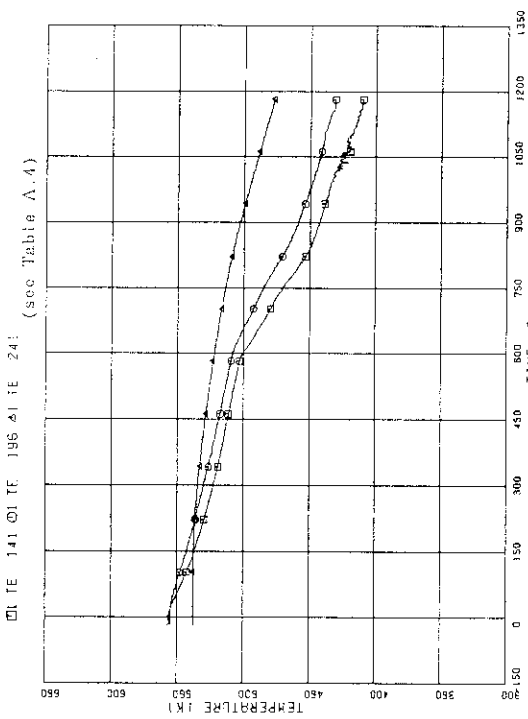

FIG.A. 61 METAL TEMP. AT LOWER DC PV-WALL (INSIDE TO OUTER SURFACE)

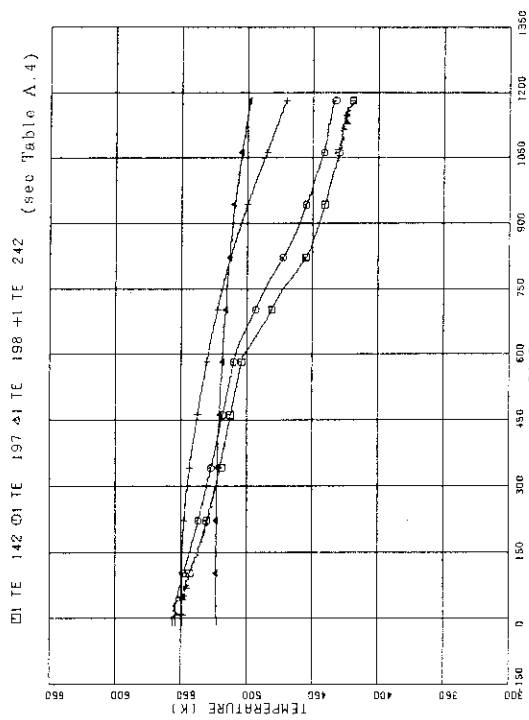

FIG.A. 62 METAL TEMP. AT DC BOTTOM PV-WALL (INSIDE TO OUTER SURFACE)

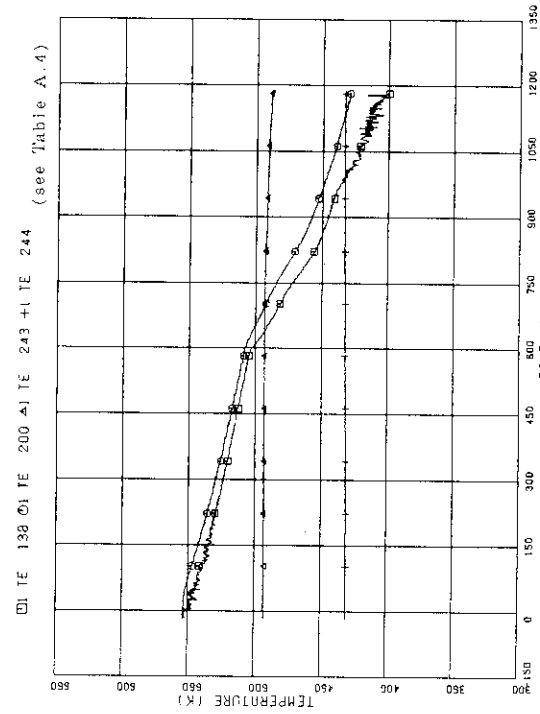

FIG.A. 63 METAL TEMP. AT L.PLENUM WALL (SIDE WALL AND BOTTOM FLANGE)

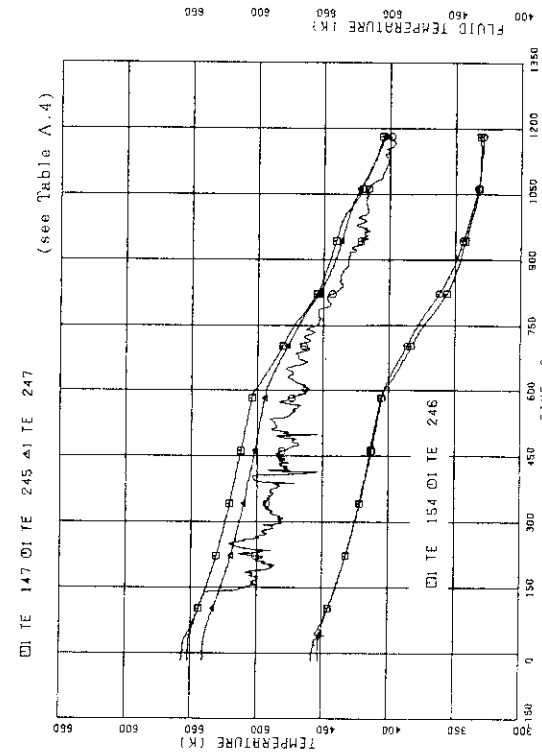

FIG.A. 64 METAL TEMP. AT PIPE OUTER SURFACE (OUTLET OF JP AND MRP)

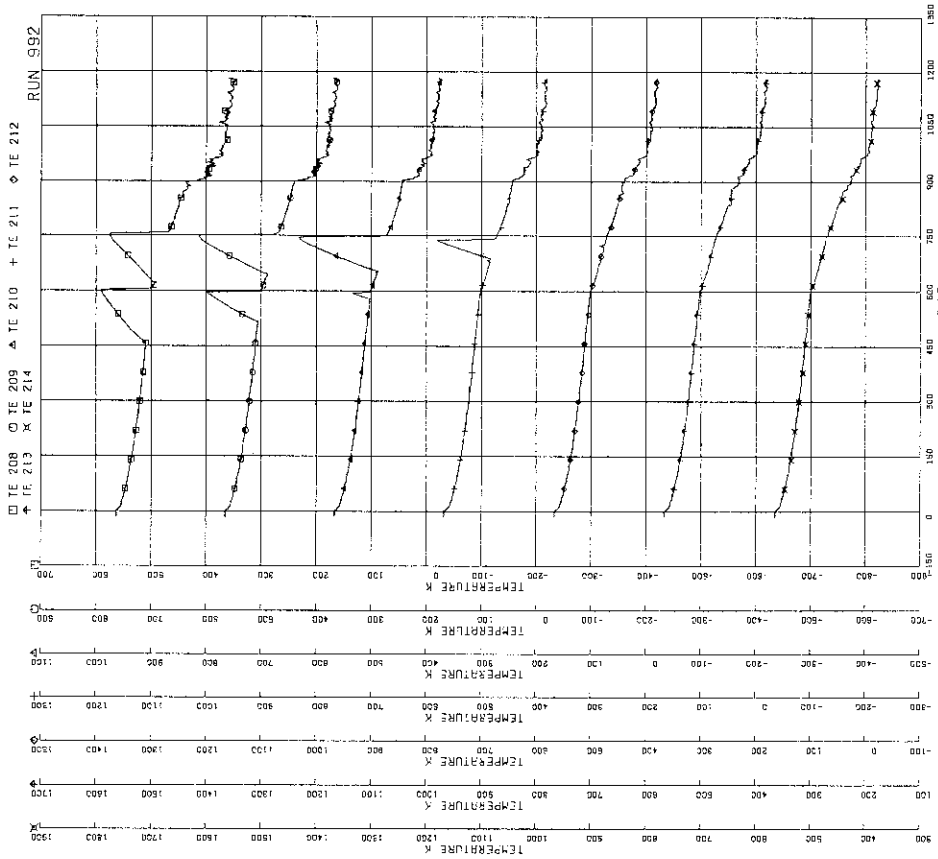

FIG.A. 66 SURFACE TEMPERATURE OF FUEL ROD A12

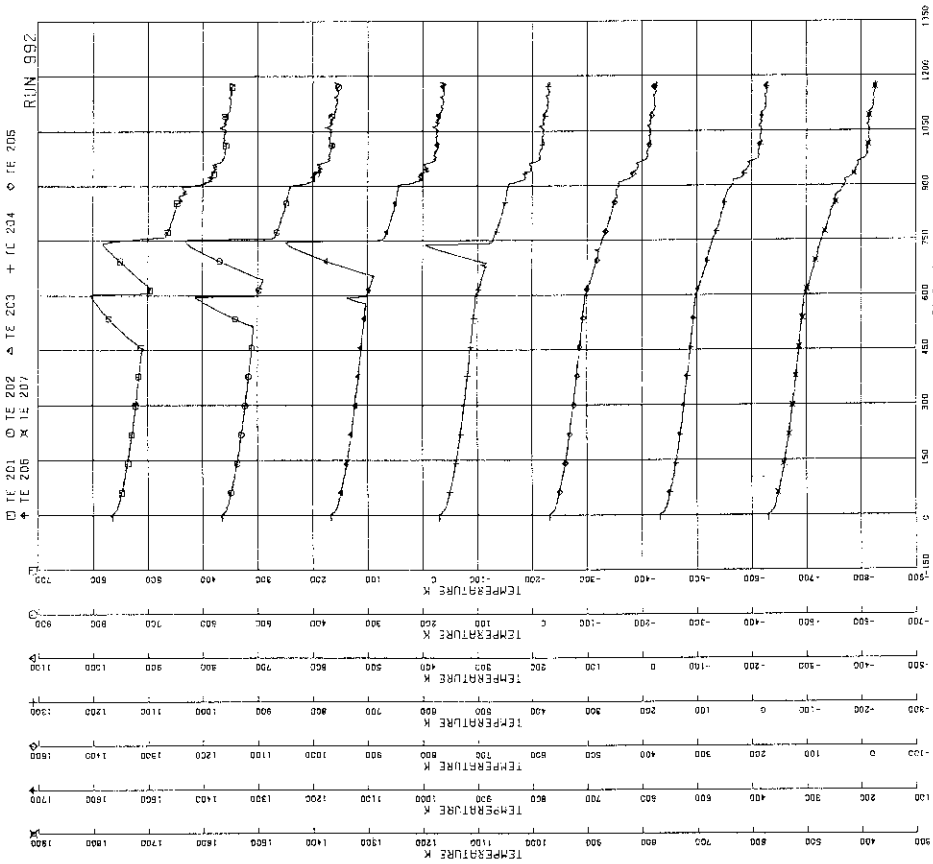

FIG.A. 65 SURFACE TEMPERATURE OF FUEL ROD A11

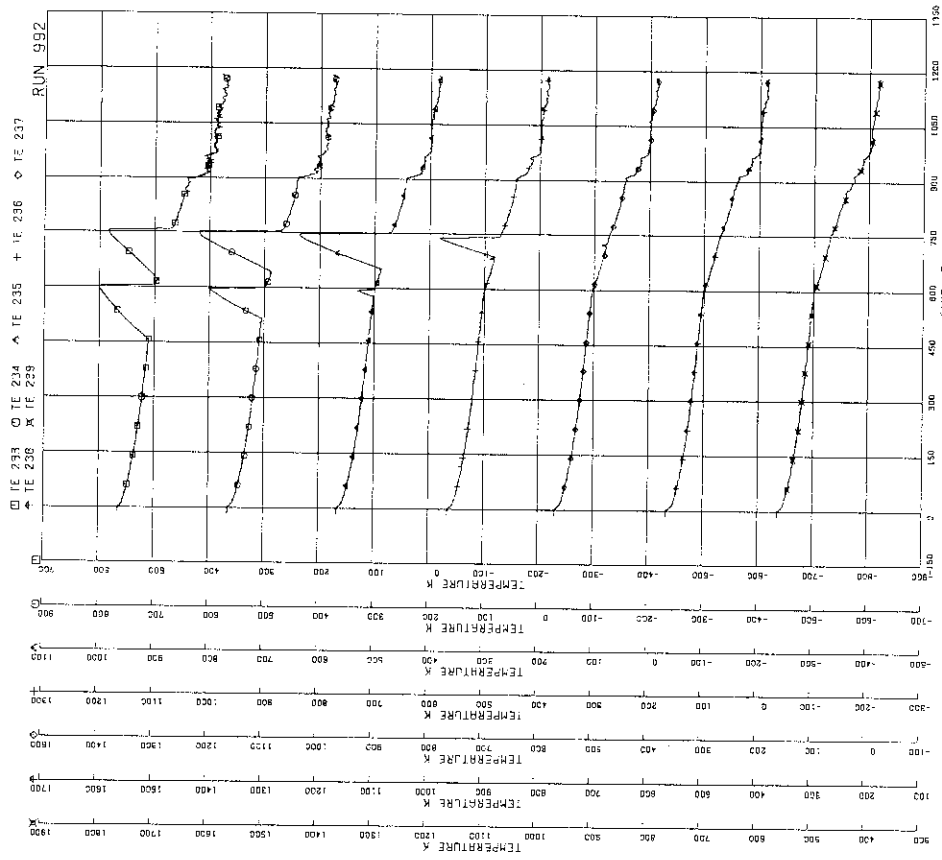

FIG.A. 68 SURFACE TEMPERATURE OF FUEL ROD A22

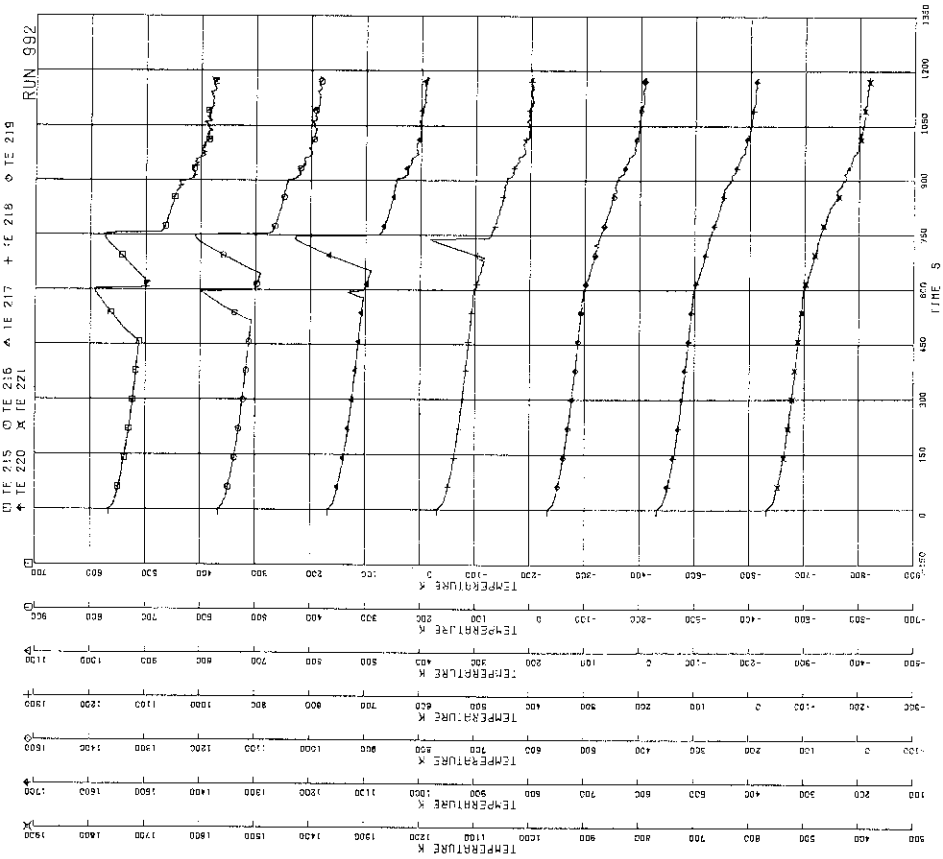

FIG.A. 67 SURFACE TEMPERATURE OF FUEL ROD A13

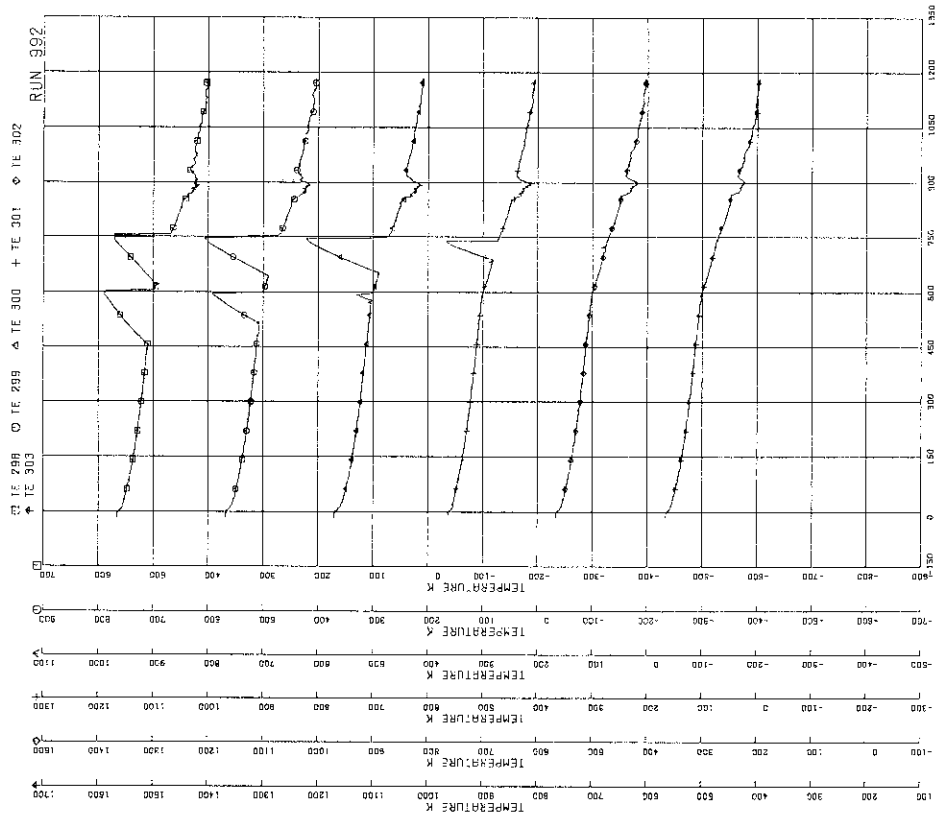

FIG.A. 70 SURFACE TEMPERATURE OF FUEL ROD A77

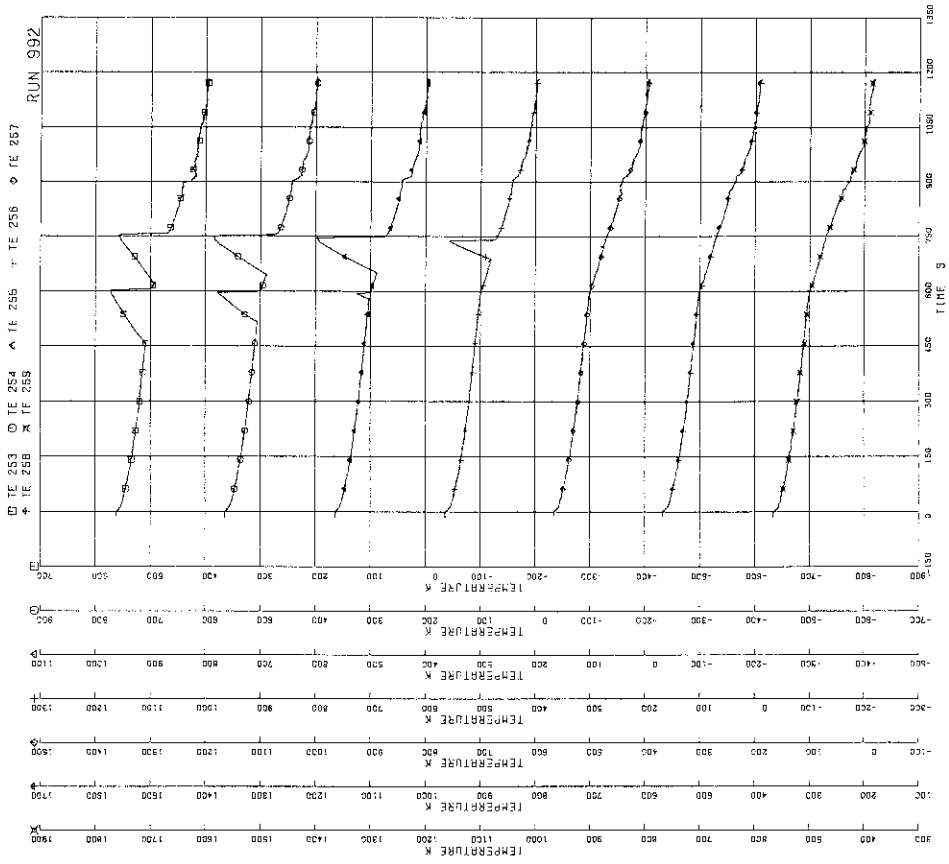

FIG.A. 69 SURFACE TEMPERATURE OF FUEL ROD A33

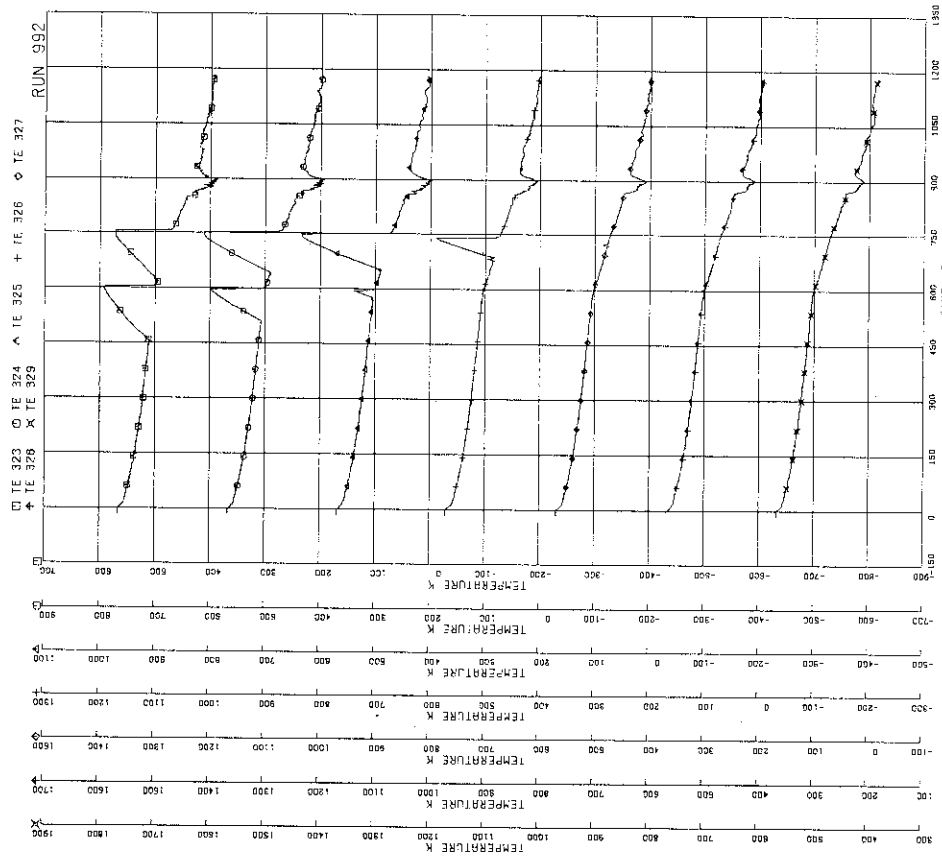

FIG.A. 72 SURFACE TEMPERATURE OF FUEL ROD A88

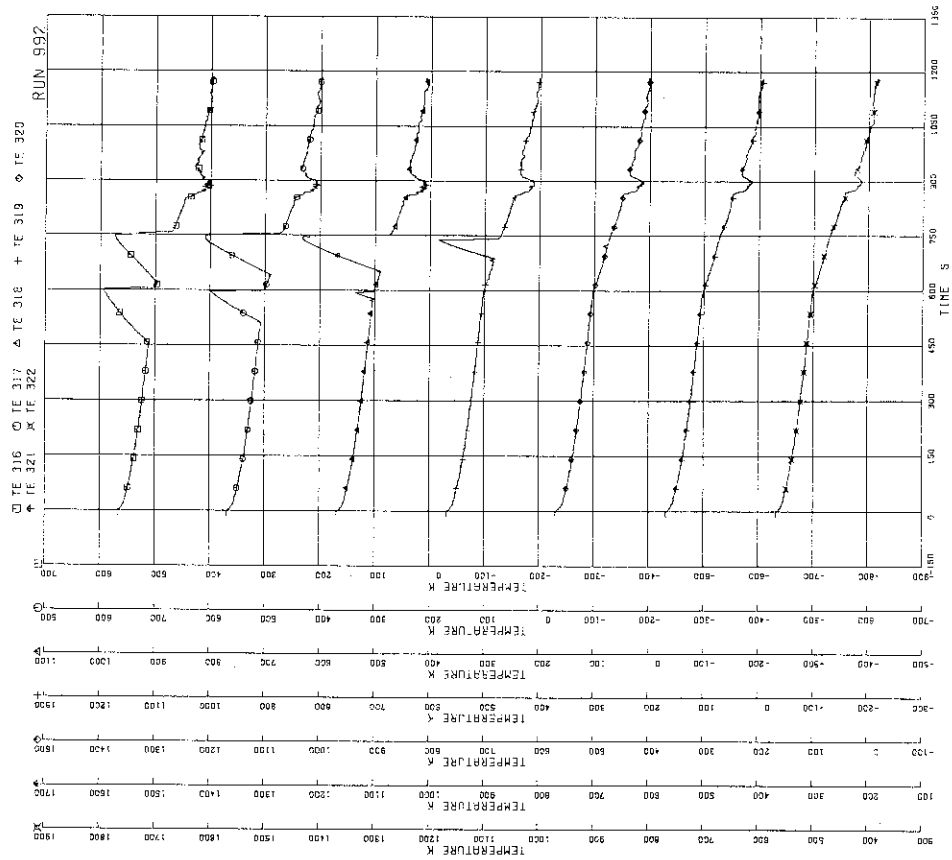

FIG.A. 71 SURFACE TEMPERATURE OF FUEL ROD A87

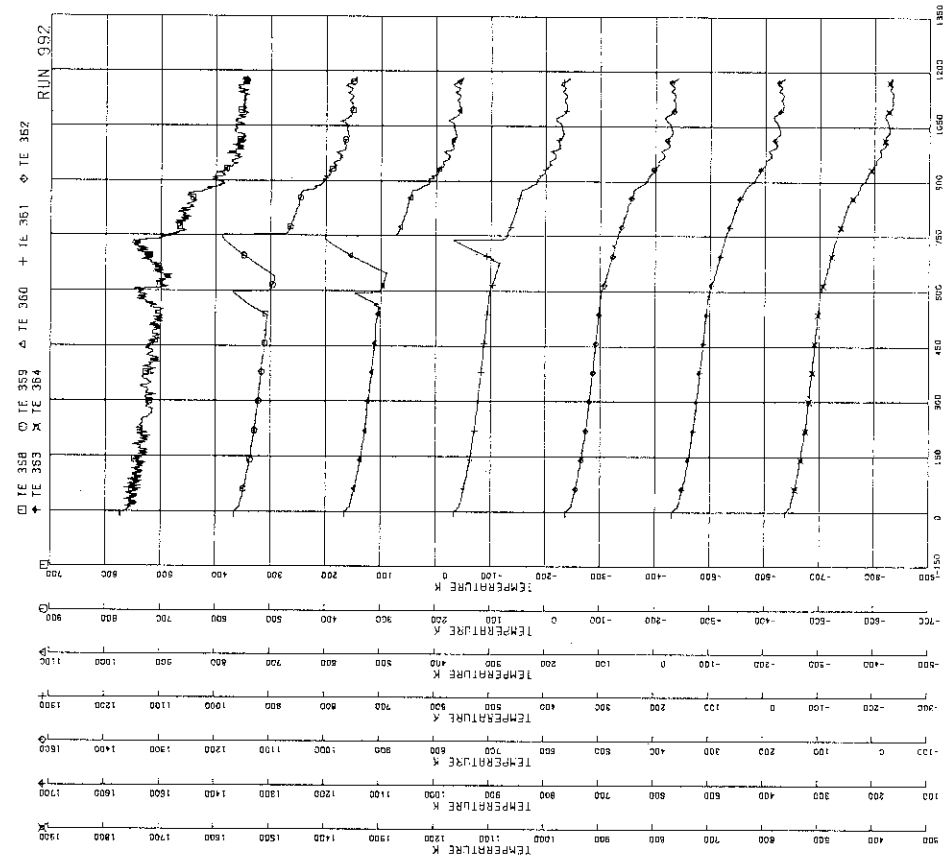

FIG.A. 74 SURFACE TEMPERATURE OF FUEL ROD C11

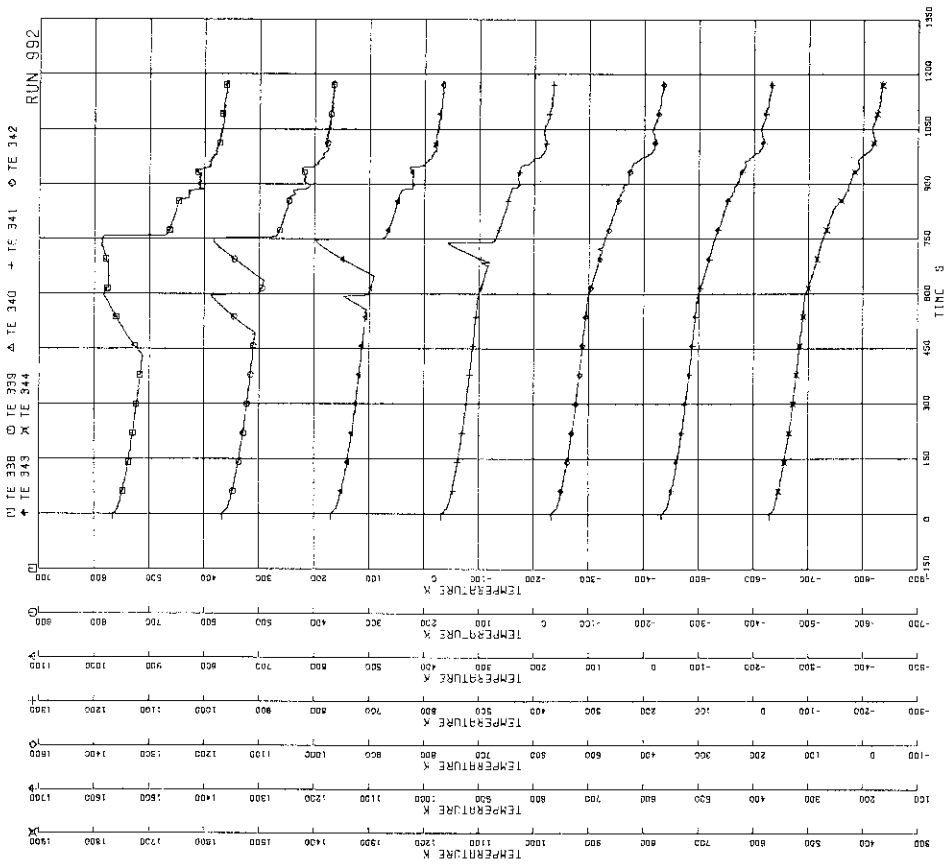

FIG.A. 73 SURFACE TEMPERATURE OF FUEL ROD B22

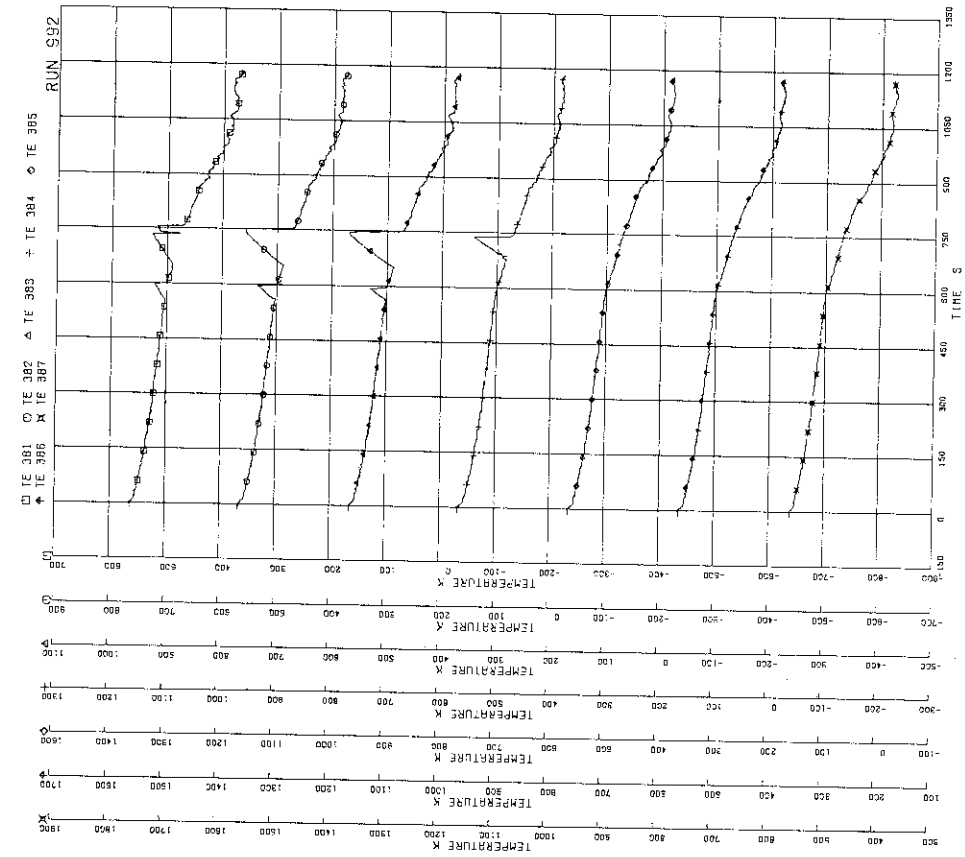

FIG.A. 76 SURFACE TEMPERATURE OF FUEL ROD C33

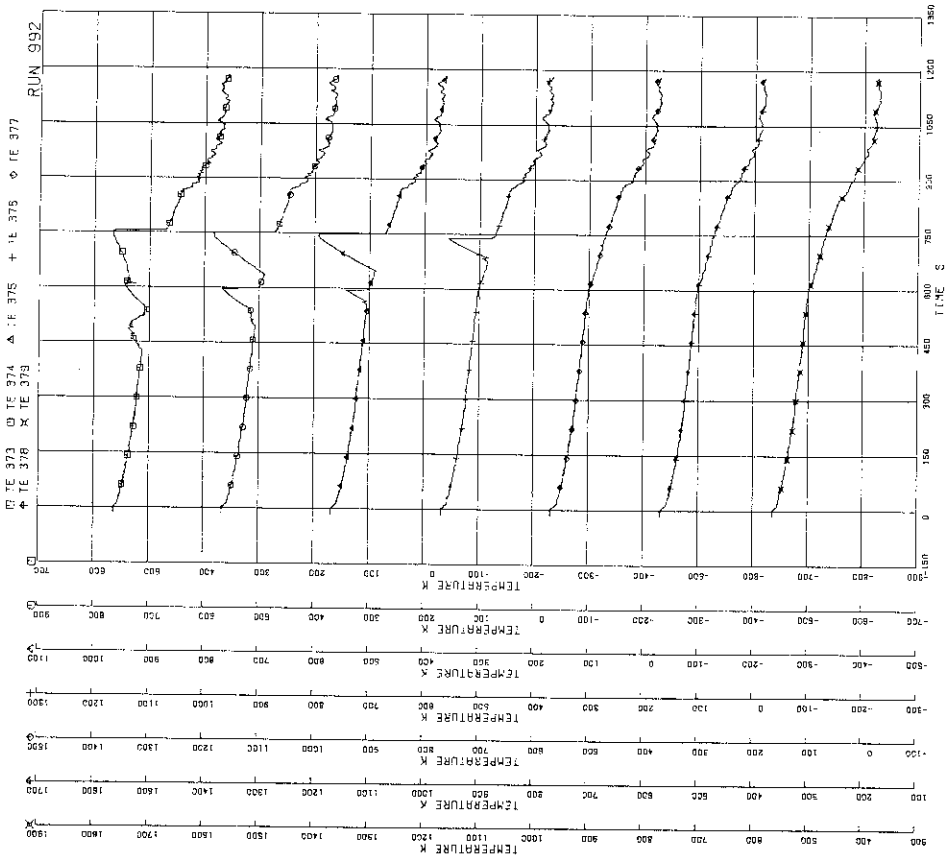

FIG.A. 75 SURFACE TEMPERATURE OF FUEL ROD C22

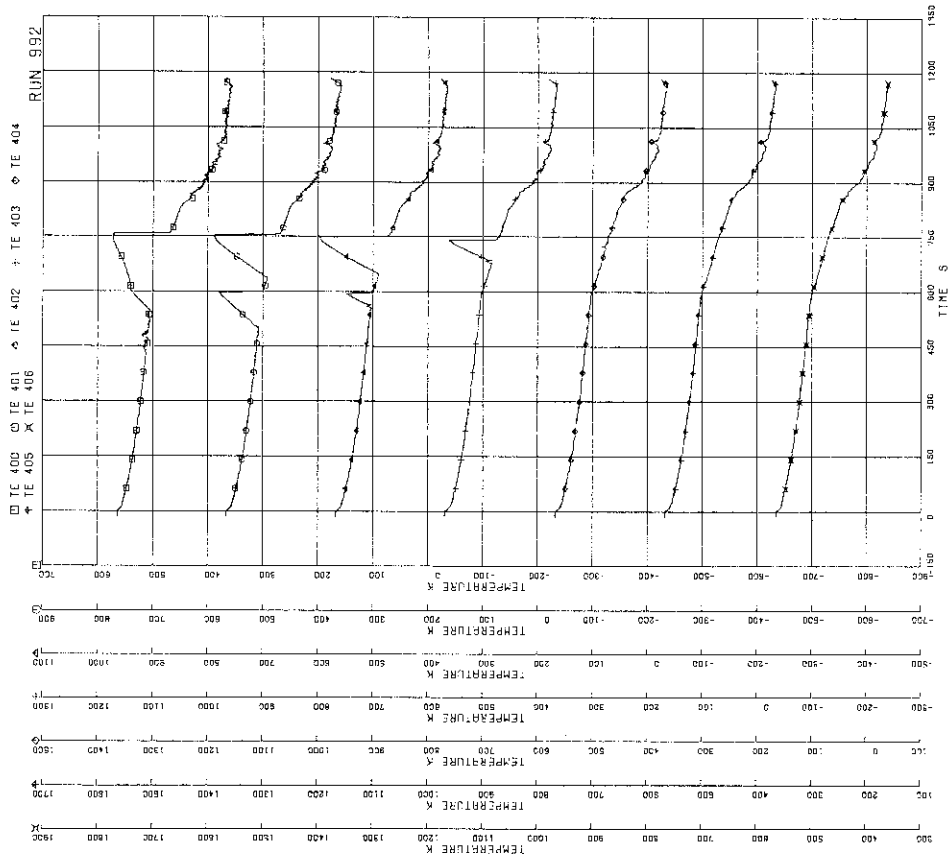

FIG.A. 78 SURFACE TEMPERATURE OF FUEL ROD 022

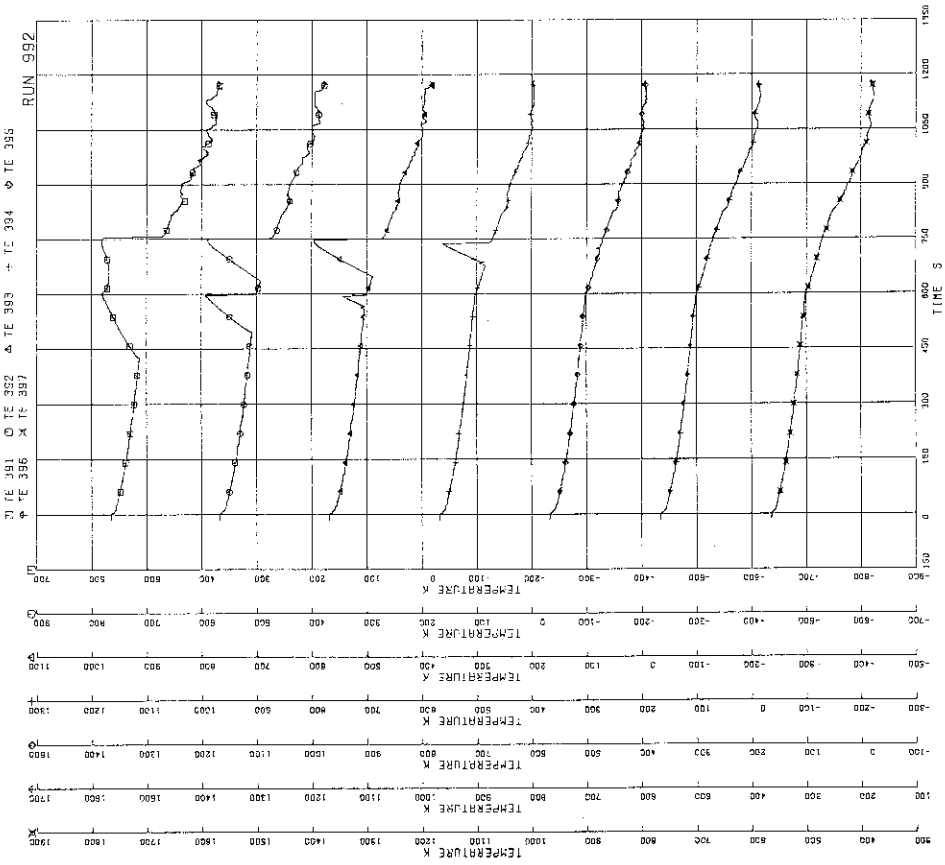

FIG.A. 77 SURFACE TEMPERATURE OF FUEL ROD C77

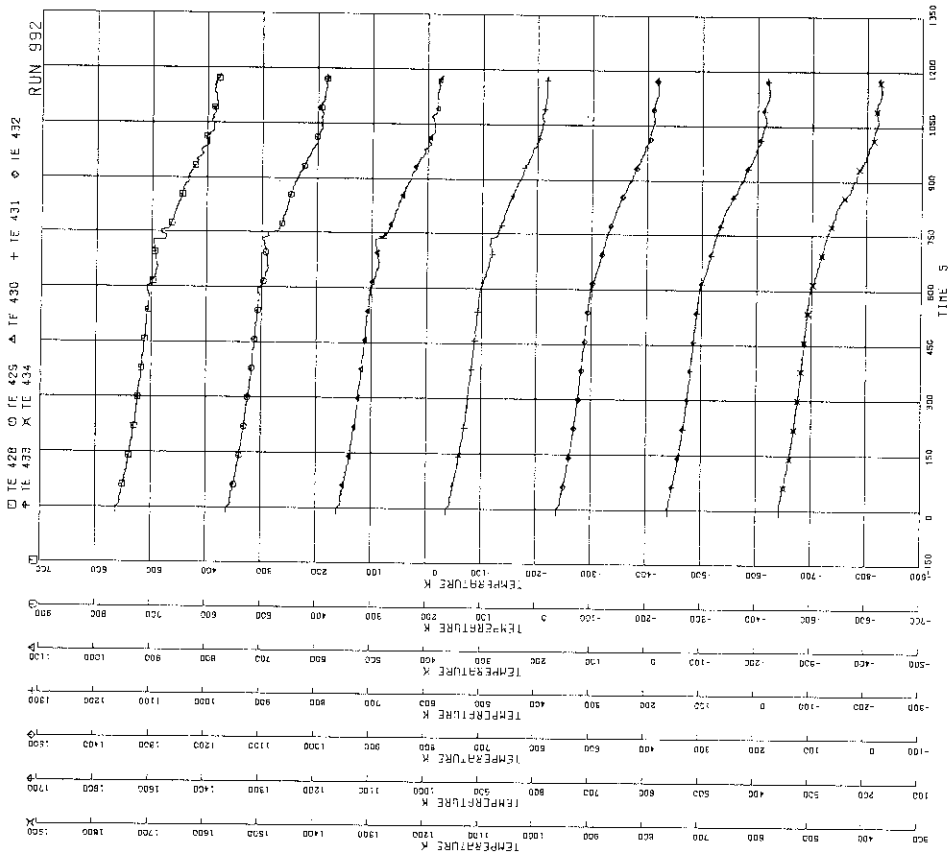

FIG.A. 80 SURFACE TEMPERATURE OF WATER ROD SIMULATOR C45

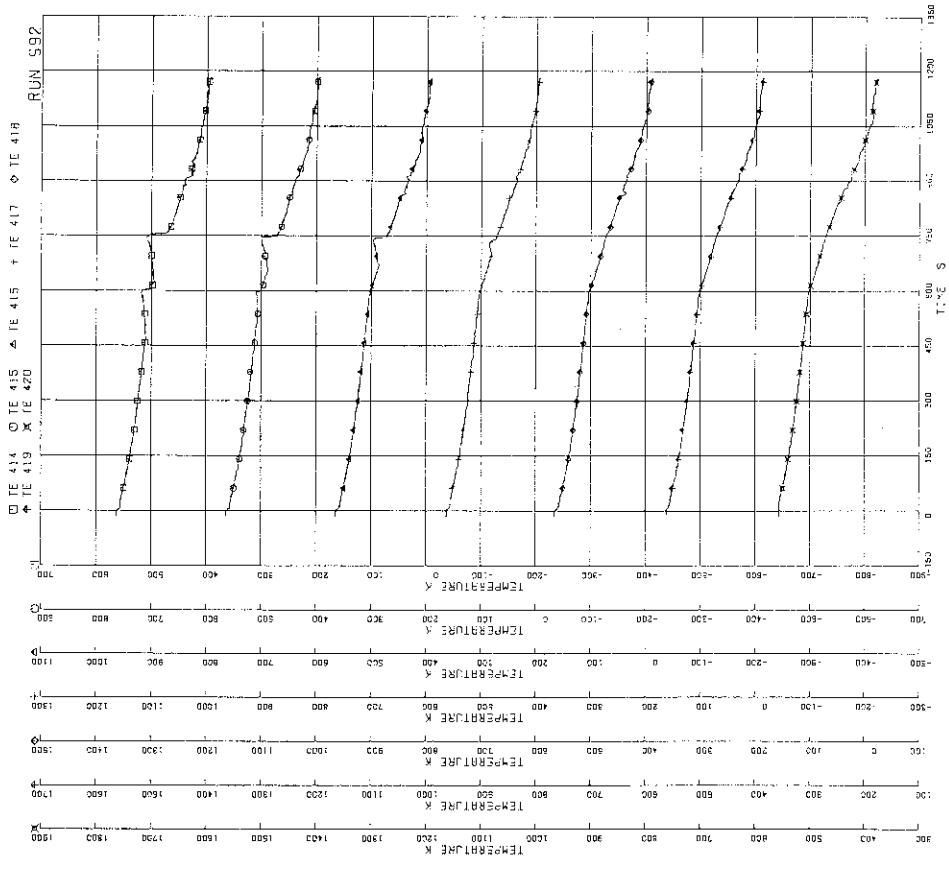

FIG.A. 79 SURFACE TEMPERATURE OF WATER ROD SIMULATOR C45

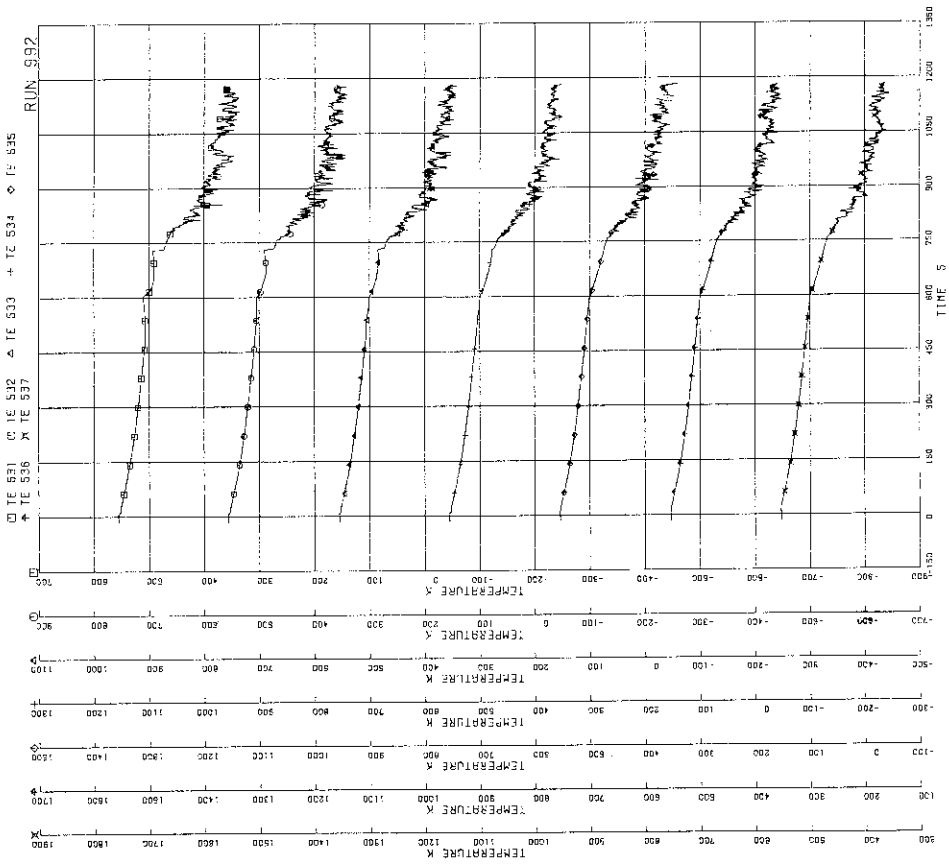

FIG.4.C1 OUTER SURFACE TEMPERATURE OF CHANNEL BOX D

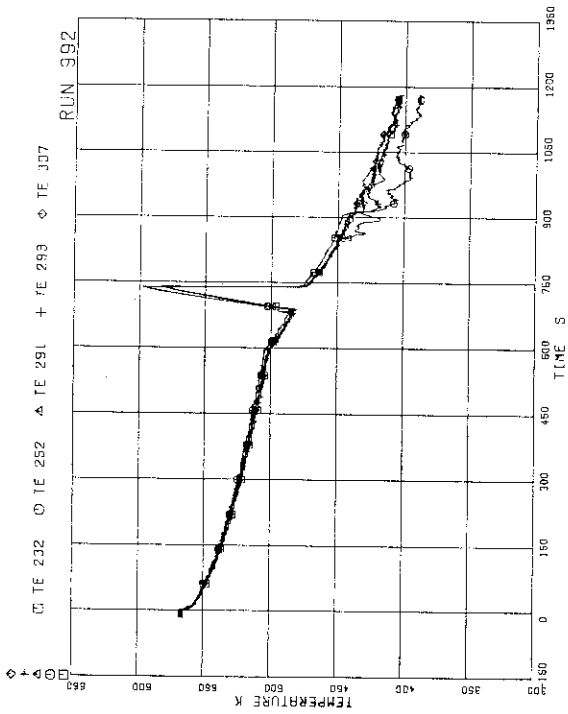

FIG.A. 82 SURFACE TEMPERATURES OF FUEL RODS A17,A31,A68,A71,A82 AT POSITION 4

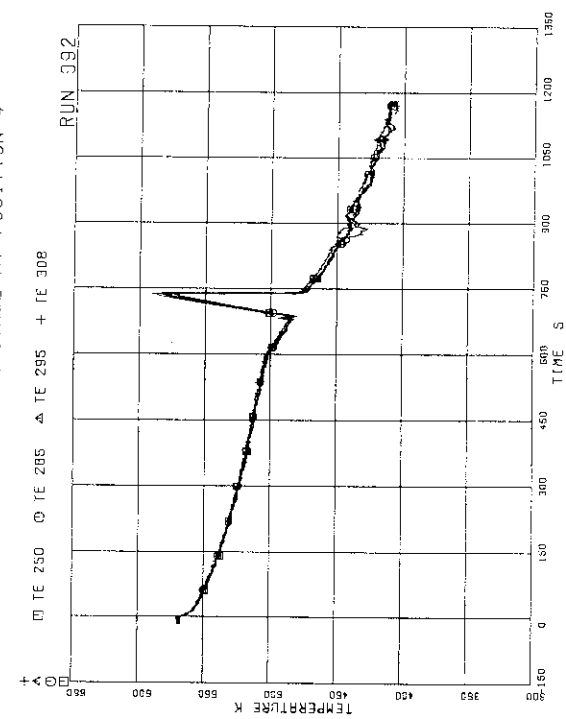

FIG.A. 83 SURFACE TEMPERATURES OF FUEL RODS A28,A57,A73,A84 AT POSITION 4

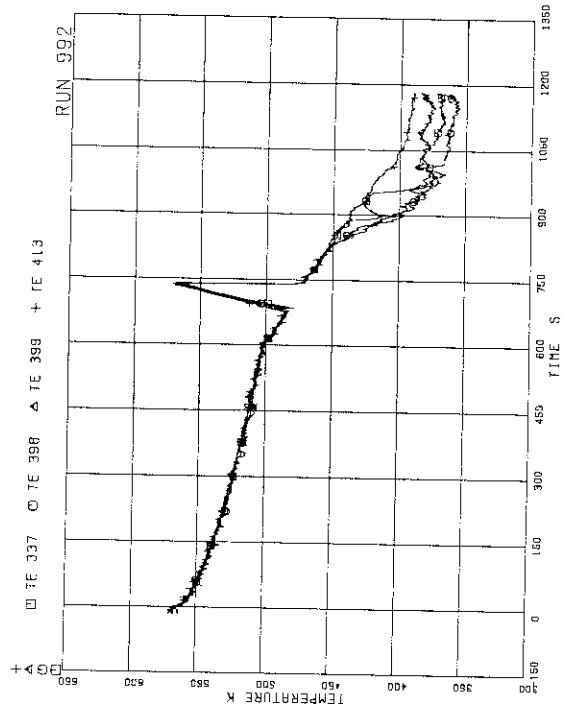

FIG.A. 84 SURFACE TEMPERATURES OF FUEL RODS B13,D11,D13,D86 AT POSITION 4

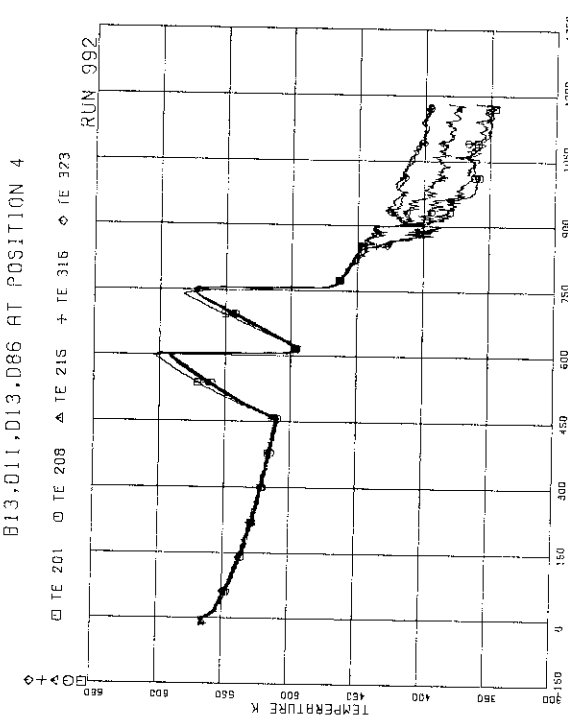

FIG.A. 85 SURFACE TEMPERATURES OF FUEL RODS A11,A12,A13,A87,A88 AT POSITION 1

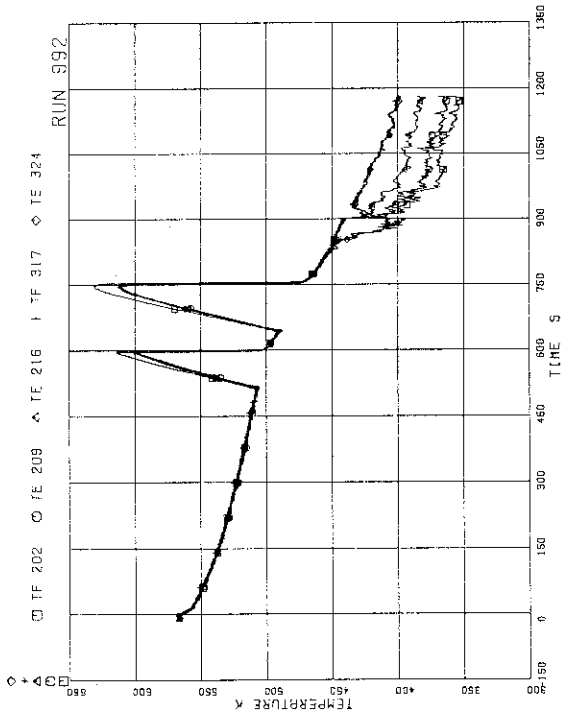

FIG.A. 86 SURFACE TEMPERATURES OF FUEL RODS A11,A12,A13,A87,A88 AT POSITION 2

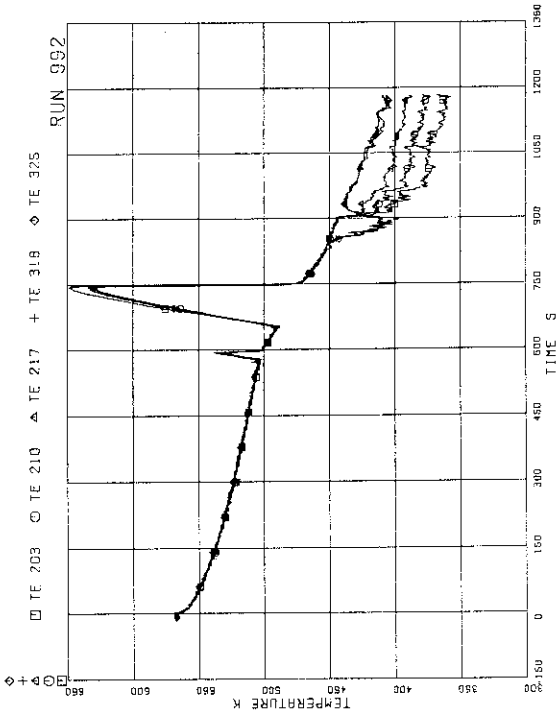

FIG.A. 87 SURFACE TEMPERATURES OF FUEL RODS A11,A12,A13,A87,A88 AT POSITION 3

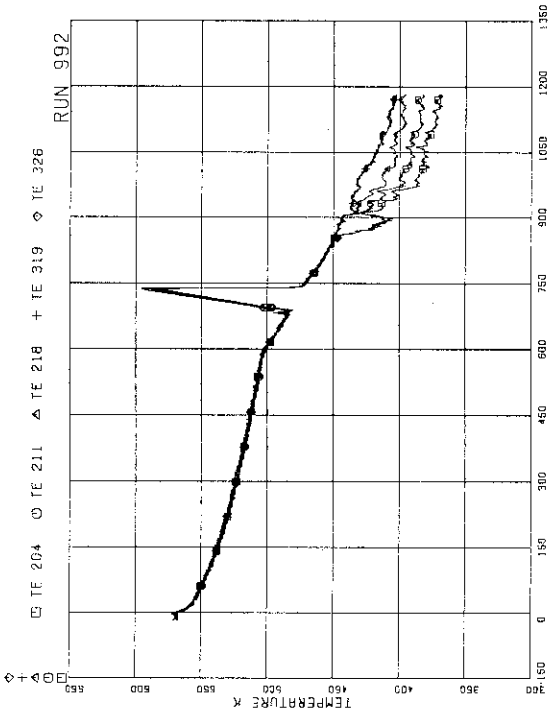

FIG.A. 88 SURFACE TEMPERATURES OF FUEL RODS A11,A12,A13,A87,A88 AT POSITION 4

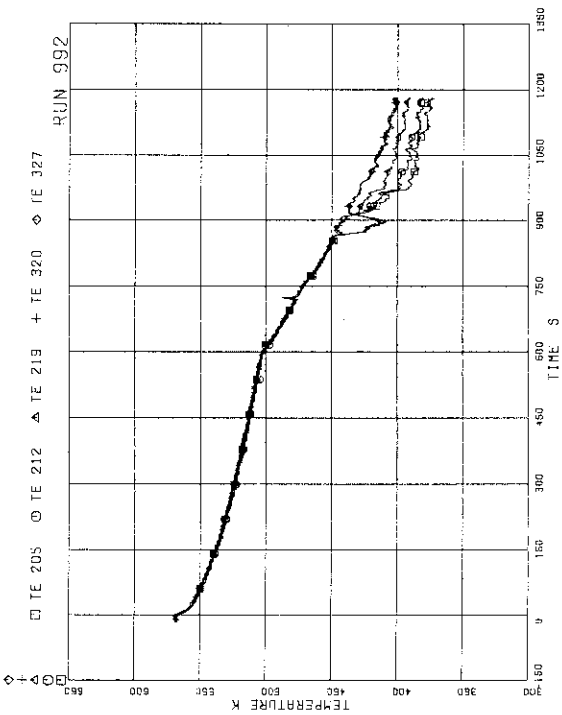

FIG.A. 89 SURFACE TEMPERATURES OF FUEL RODS A11,A12,A13,A87,A88 AT POSITION 5

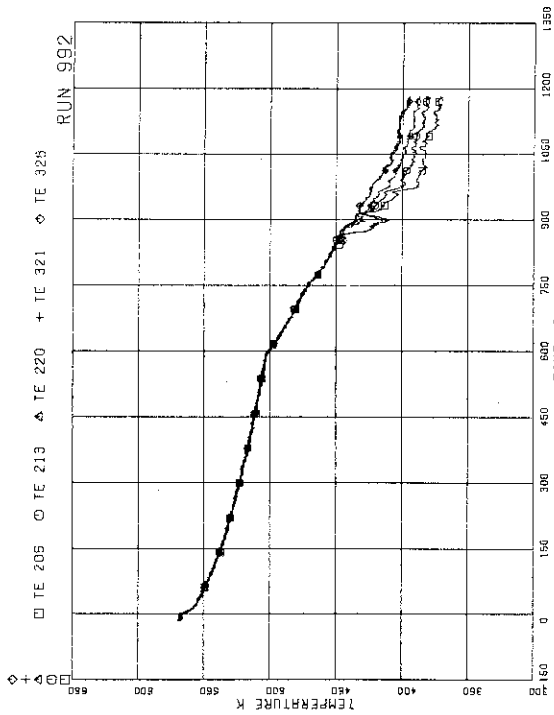

FIG.A. 90 SURFACE TEMPERATURES OF FUEL RODS A11,A12,A13,A87,A88 AT POSITION 6

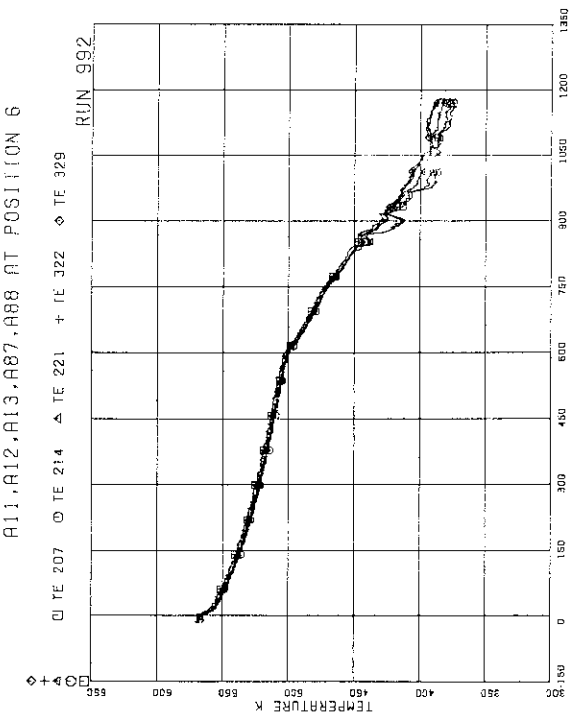

FIG.A. 91 SURFACE TEMPERATURES OF FUEL RODS A11,A12,A13,A87,A88 AT POSITION 7

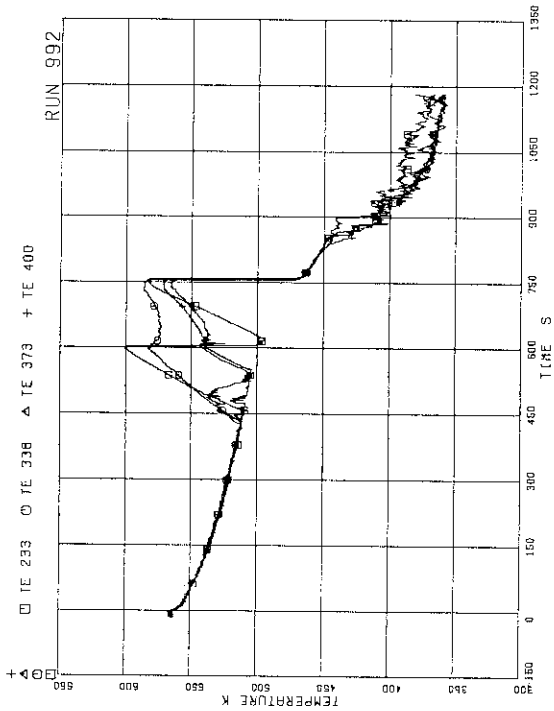

FIG.A. 92 SURFACE TEMPERATURES OF FUEL RODS A22,B22,C22,D22 AT POSITION 1

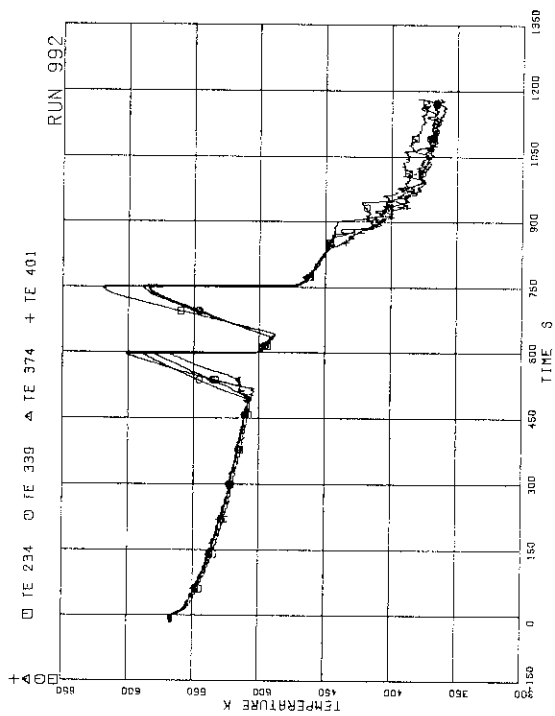

FIG.A. 93 SURFACE TEMPERATURES OF FUEL RODS A22,B22,C22,D22 AT POSITION 2

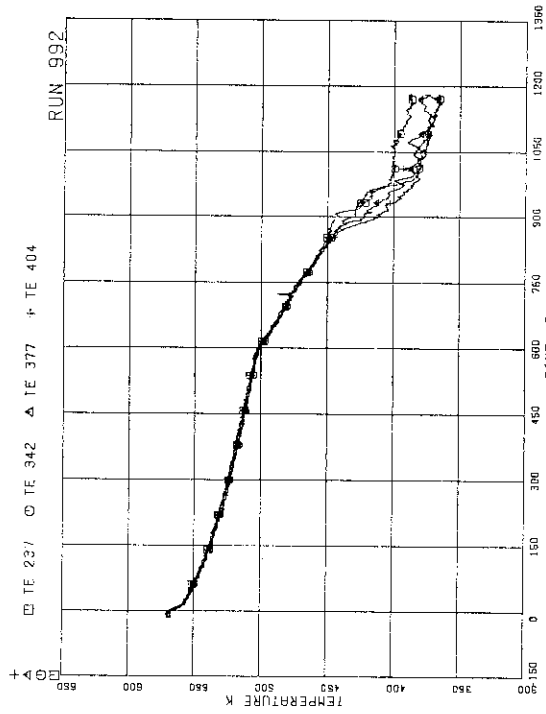

FIG.A. 94 SURFACE TEMPERATURES OF FUEL RODS A22,B22,C22,D22 AT POSITION 3

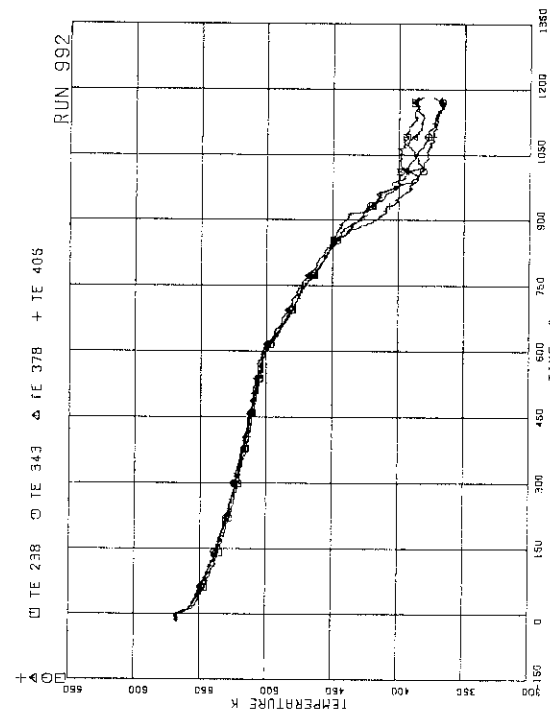

FIG.A. 95 SURFACE TEMPERATURES OF FUEL RODS A22,C22,D22 AT POSITION 4

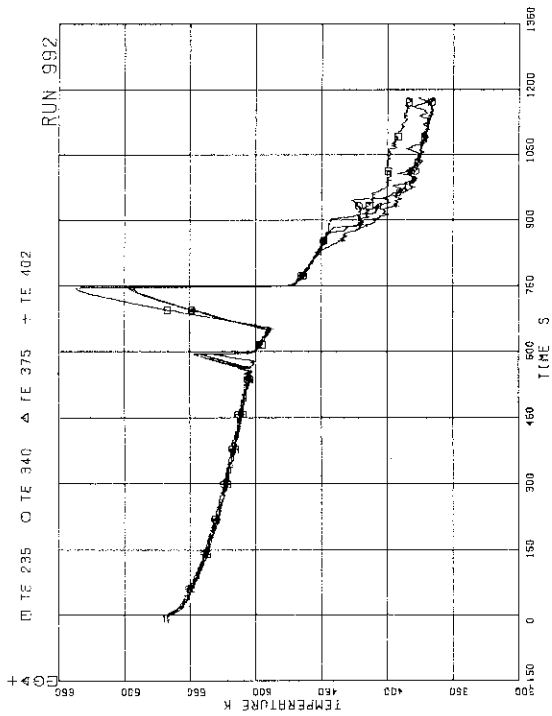

FIG.A. 96 SURFACE TEMPERATURES OF FUEL RODS A22,B22,C22,D22 AT POSITION 5

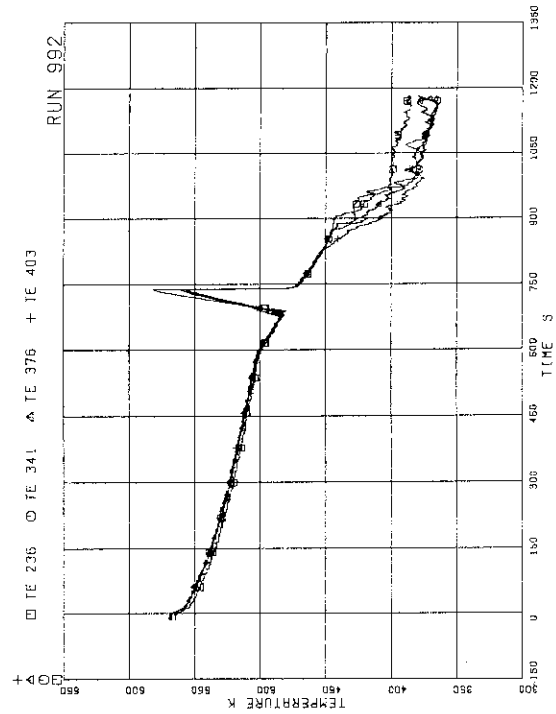

FIG.A. 97 SURFACE TEMPERATURES OF FUEL RODS A22,B22,C22,D22 AT POSITION 5

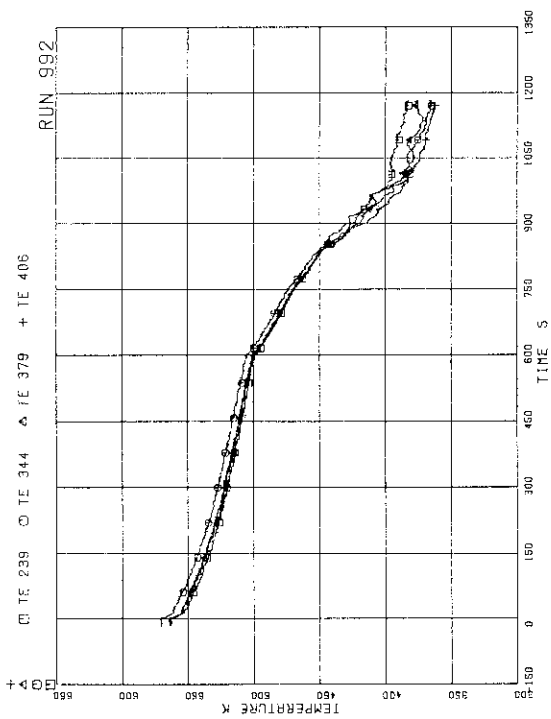

FIG.A. 98 SURFACE TEMPERATURES OF FUEL RODS A22,B22,C22,D22 AT POSITION 7

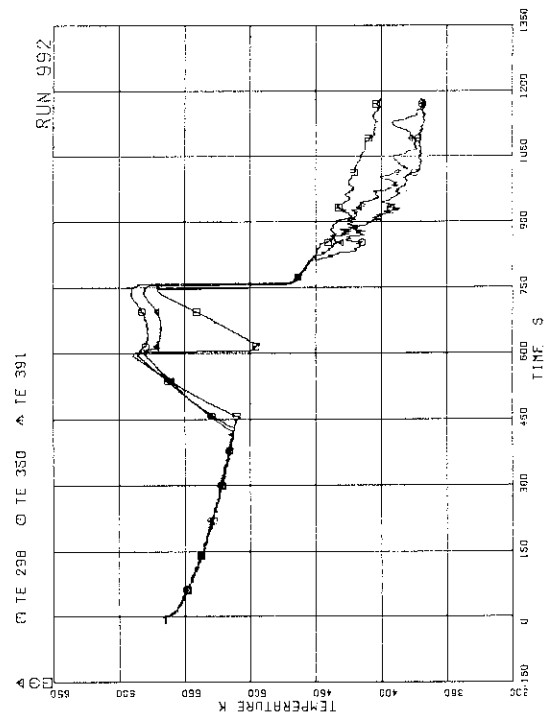

FIG.A. 99 SURFACE TEMPERATURES OF FUEL RODS A77,B77,C77 AT POSITION 1

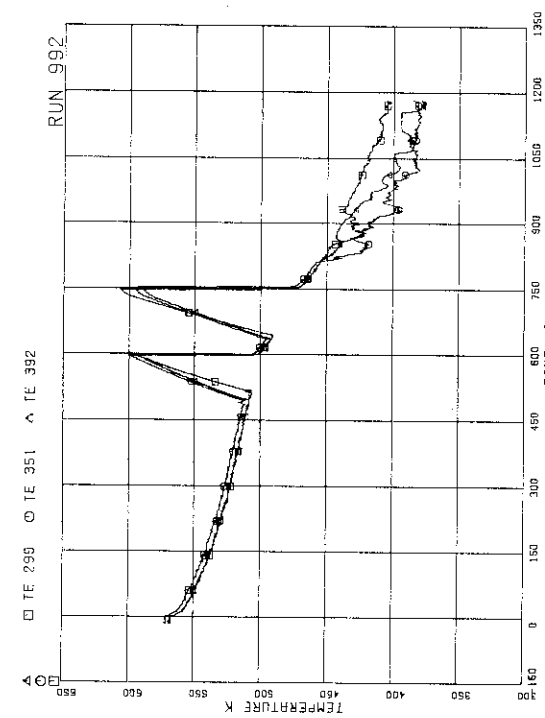

FIG.A.100 SURFACE TEMPERATURES OF FUEL RODS A77,B77,C77 AT POSITION 2

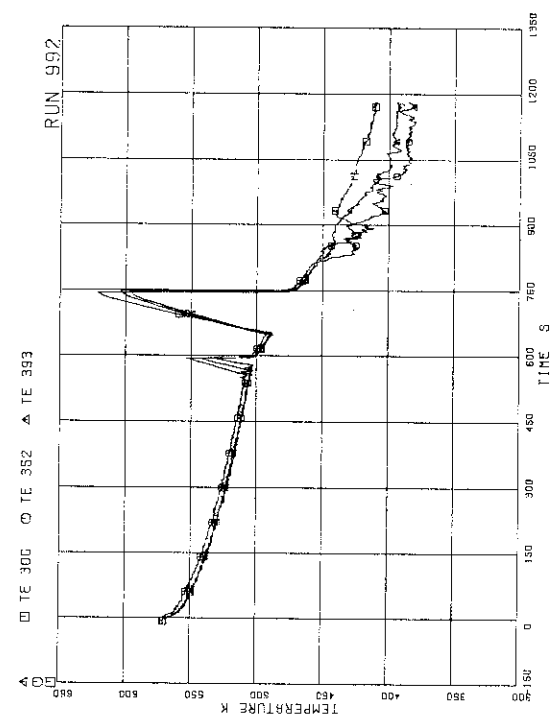

FIG.A.101 SURFACE TEMPERATURES OF FUEL RODS A77,B77,C77 AT POSITION 3

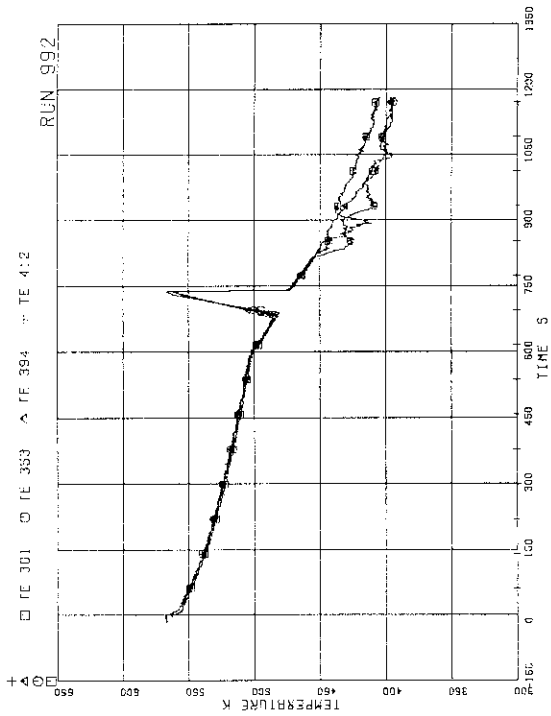

FIG.A.102 SURFACE TEMPERATURES OF FUEL RODS A77,B77,C77 AT POSITION 4

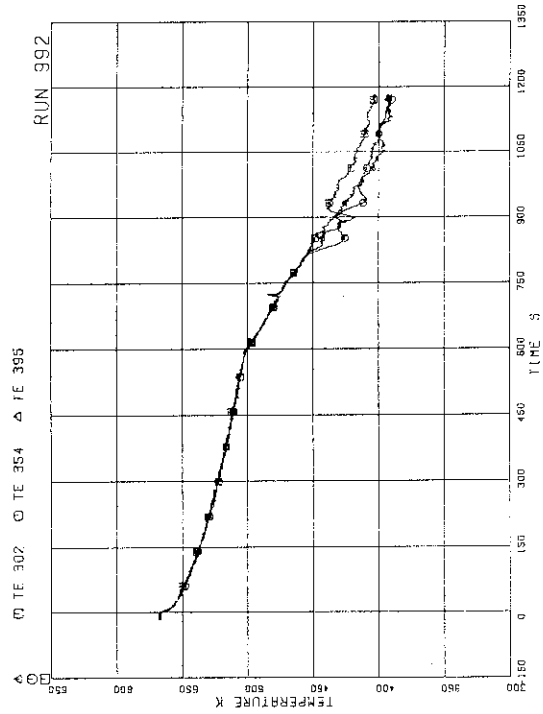

FIG.A.103 SURFACE TEMPERATURES OF FUEL RODS A77,B77,C77 AT POSITION 5

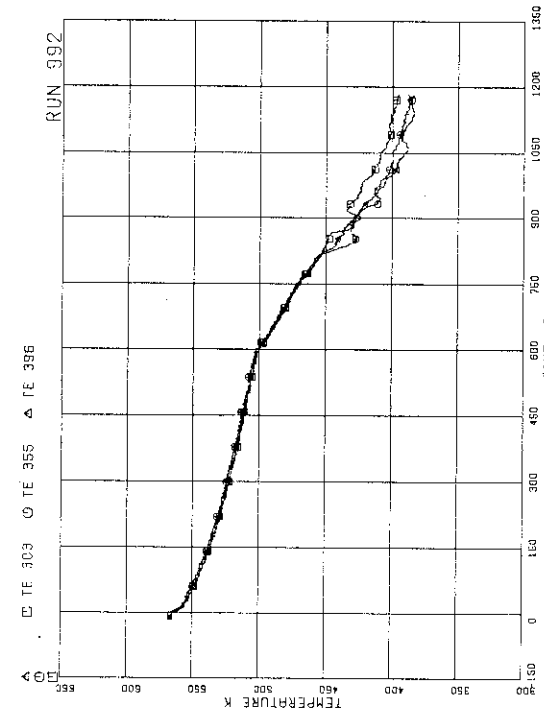

FIG.A.104 SURFACE TEMPERATURES OF FUEL RODS A77,B77,C77 AT POSITION 6

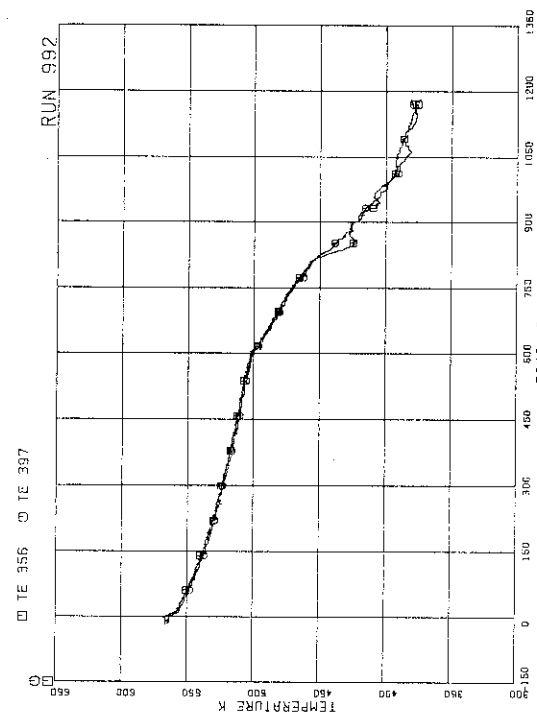

FIG.A.105 SURFACE TEMPERATURES OF FUEL RODS A77,C77 RODS AT POSITION 7

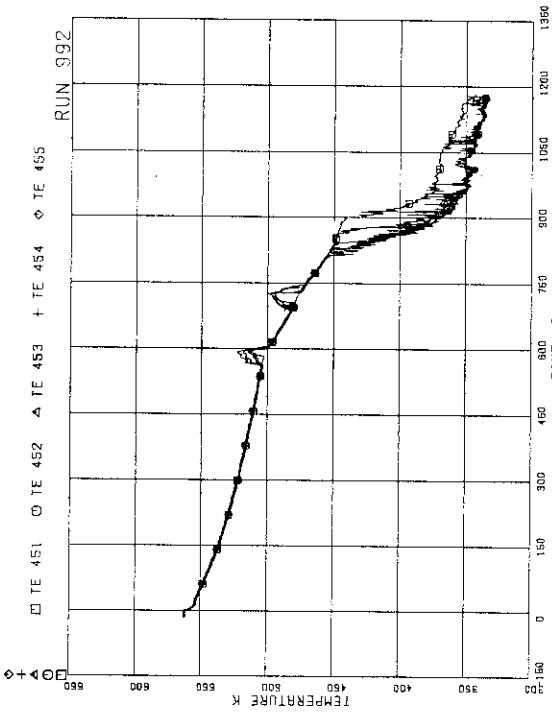

FIG.A.108 FLUID TEMPERATURES AT CHANNEL C OUTLET

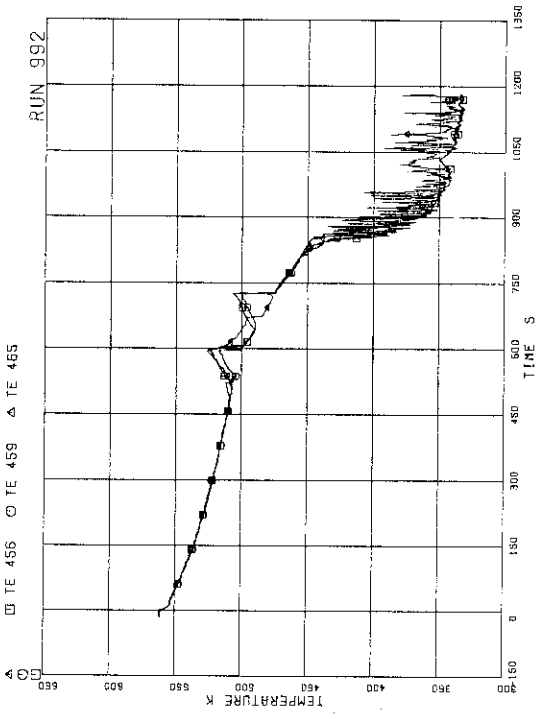

FIG.A.109 FLUID TEMPERATURES ABOVE UTP OF CHANNEL A, OPENINGS 1,4,10

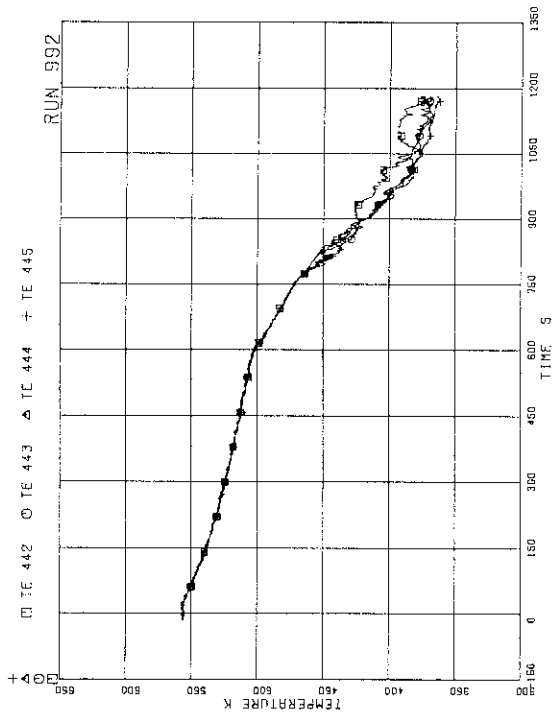

FIG.A.106 FLUID TEMPERATURES AT CHANNEL INLET

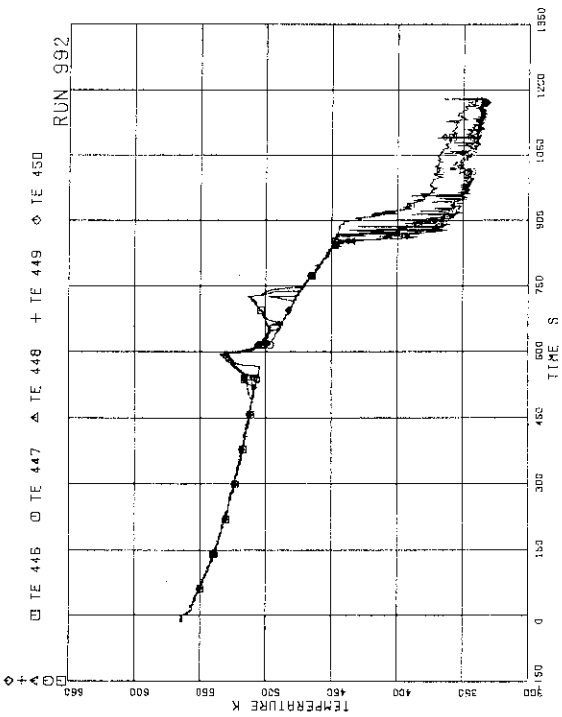

FIG.A.107 FLUID TEMPERATURES AT CHANNEL A OUTLET

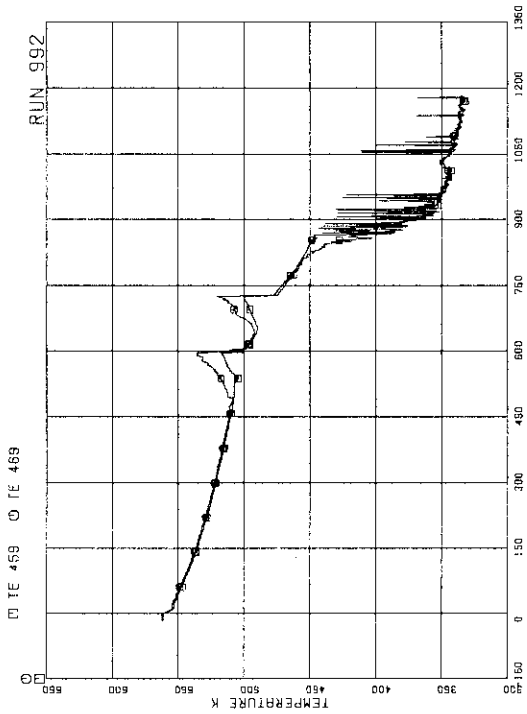

FIG.A.110 FLUID TEMPERATURES BELOW UTP OF CHANNEL A, OPENINGS 1,4,10

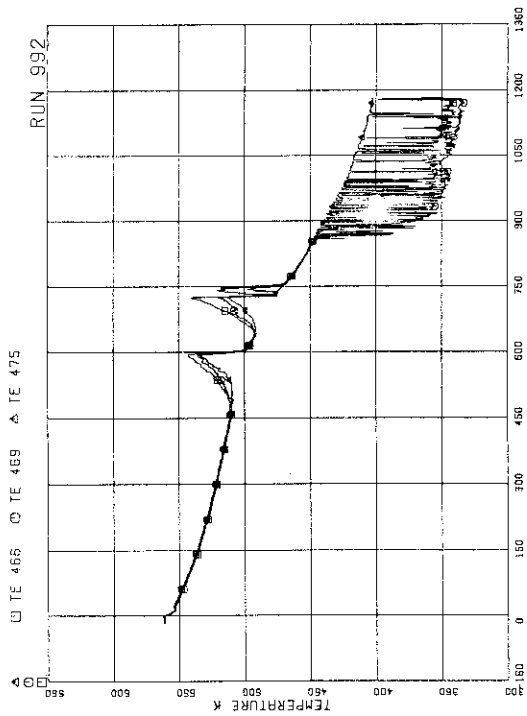

FIG.A.111 FLUID TEMPERATURES AT UTP IN CHANNEL A, OPENING 1

FIG.A.112 FLUID TEMPERATURES AT UTP IN CHANNEL A, OPENING 4

FIG.A.113 FLUID TEMPERATURES AT UTP IN CHANNEL A, OPENING 10

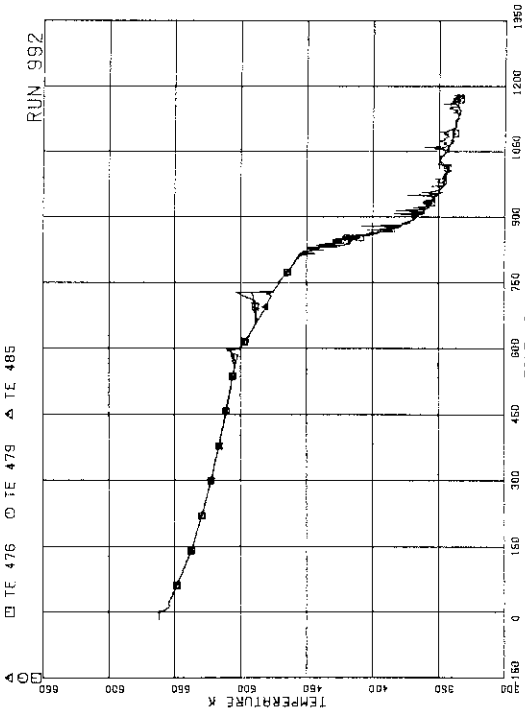

FIG.A.114 FLUID TEMPERATURES ABOVE UTP OF CHANNEL C, OPENINGS 1,4,10

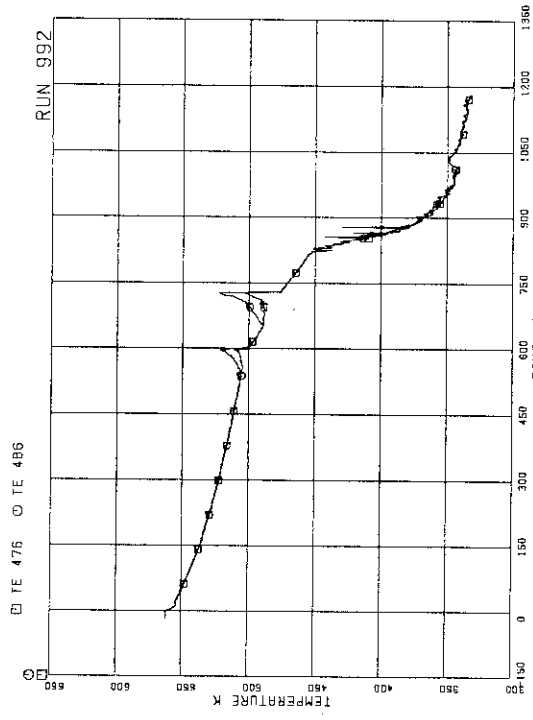

FIG.A.116 FLUID TEMPERATURES AT UTP IN CHANNEL C, OPENINGS 1

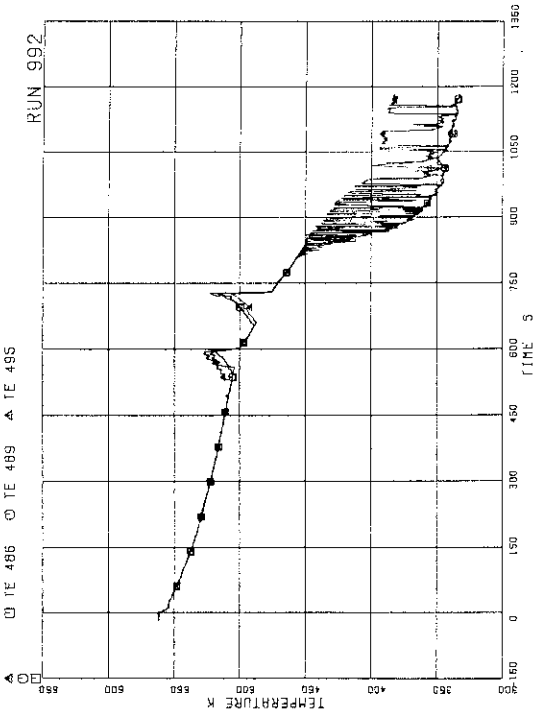

FIG.A.115 FLUID TEMPERATURES BELOW UTP OF CHANNEL C, OPENINGS 1,4,10

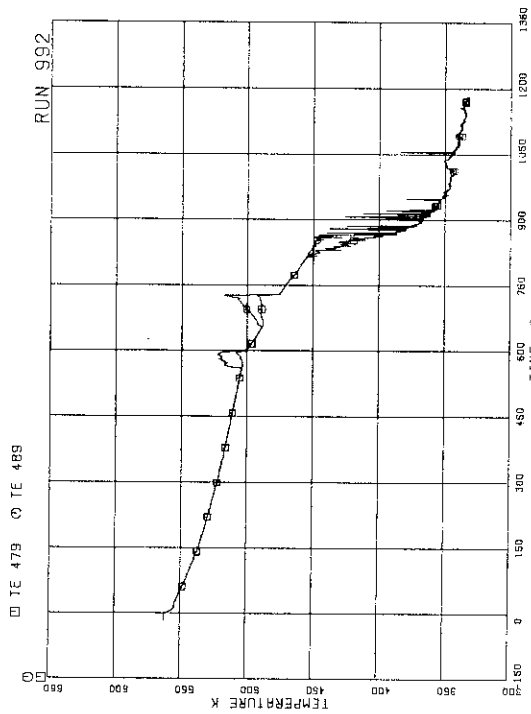

FIG.A.117 FLUID TEMPERATURES AT UTP IN CHANNEL C, OPENING 4

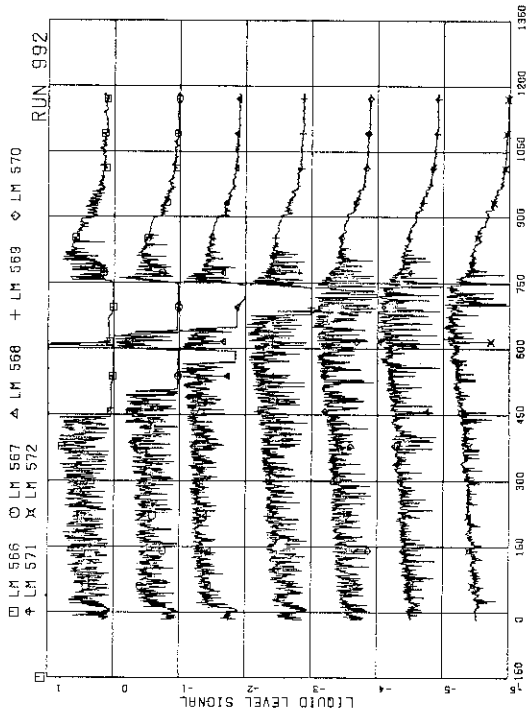

FIG.A.120 LIQUID LEVEL SIGNALS IN CHANNEL BOX A, LOCATION A2

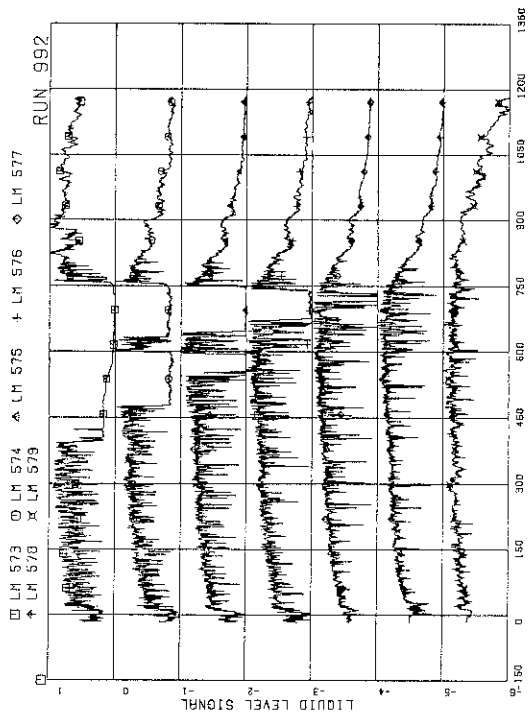

FIG.A.121 LIQUID LEVEL SIGNALS IN CHANNEL BOX B

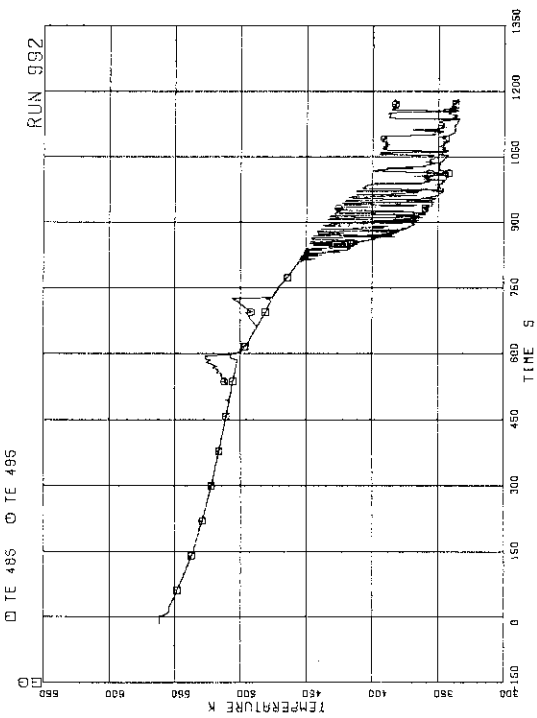

FIG.A.118 FLUID TEMPERATURES AT UTP IN CHANNEL C, OPENING 10

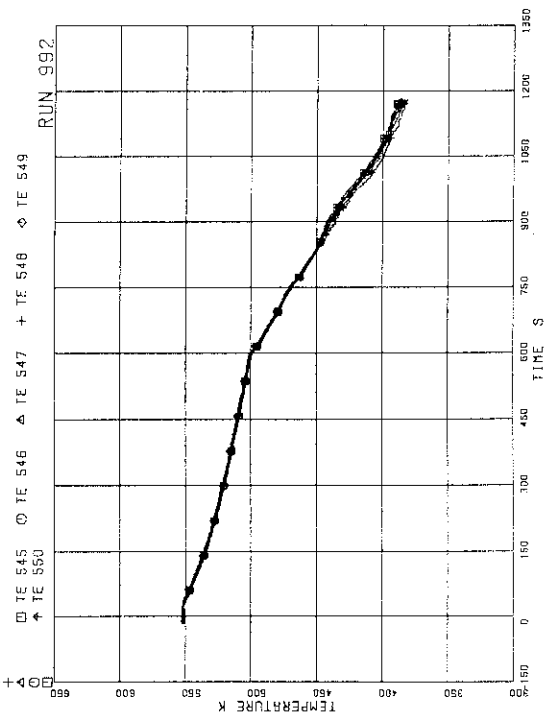

FIG.A.119 FLUID TEMPERATURE IN L.PLENUM

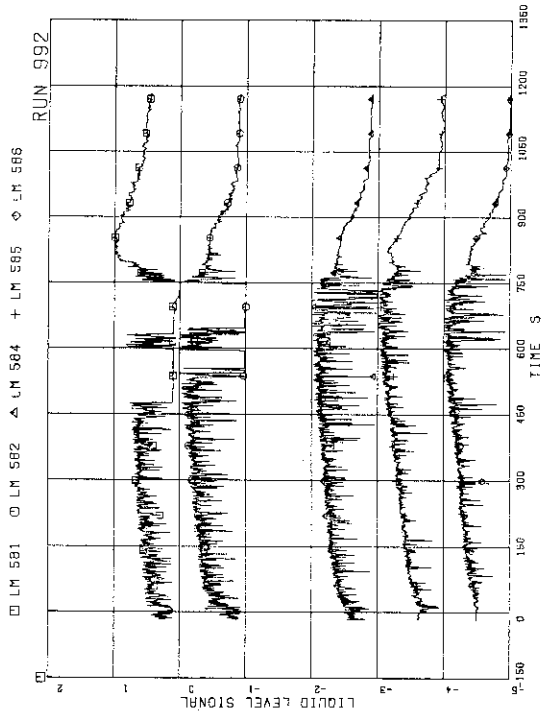

FIG.A.122 LIQUID LEVEL SIGNALS IN CHANNEL BOX C

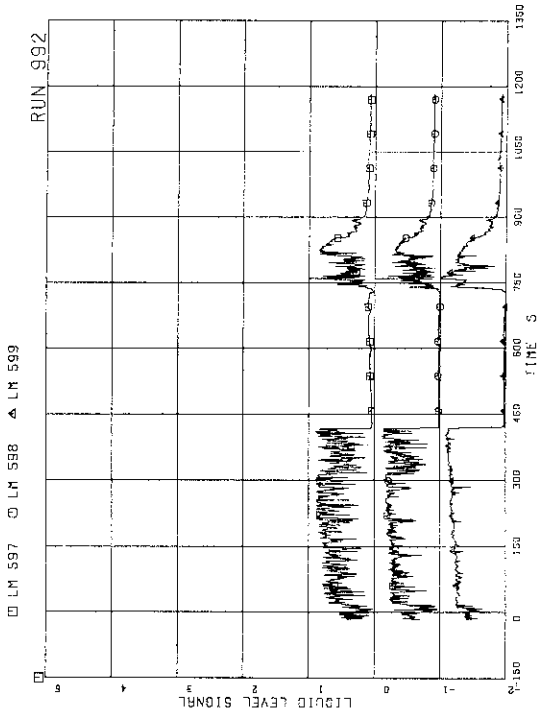

FIG.A.123 LIQUID LEVEL SIGNALS IN CHANNEL A OUTLET LOCATION A2

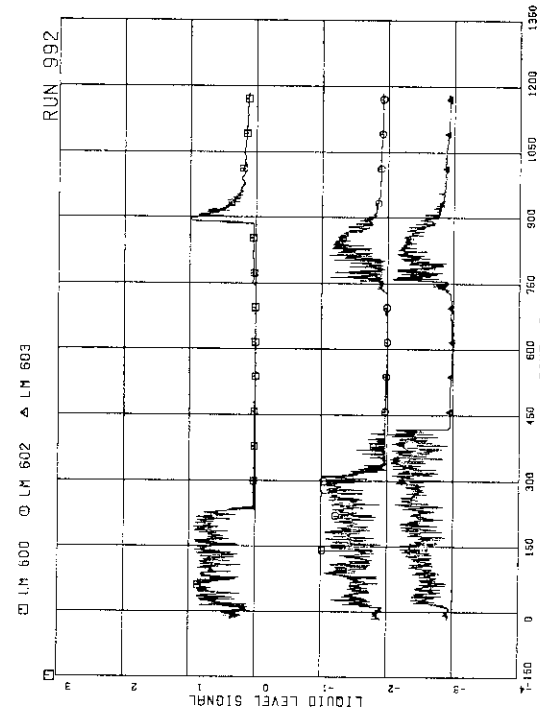

FIG.A.124 LIQUID LEVEL SIGNALS IN CHANNEL A OUTLET CENTER

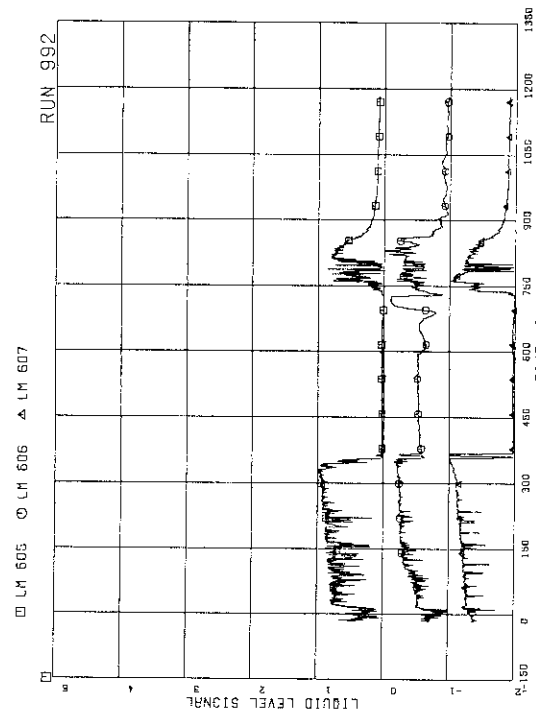

FIG.A.125 LIQUID LEVEL SIGNALS IN CHANNEL C OUTLET LOCATION C1

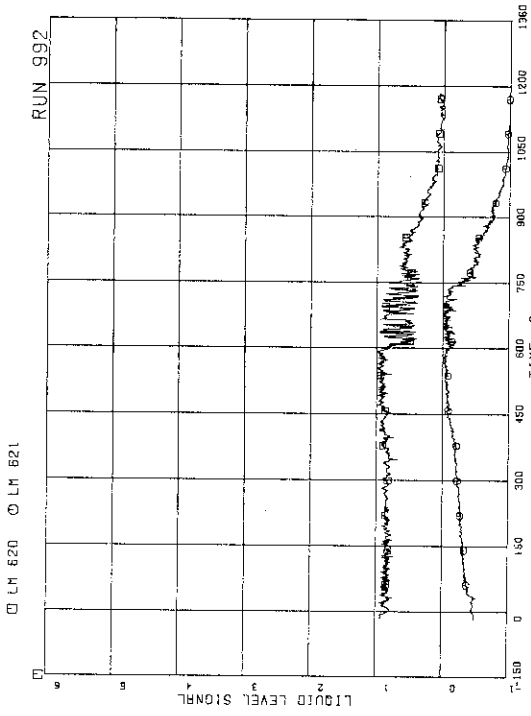

FIG.A.126 LIQUID LEVEL SIGNALS IN CHANNEL C OUTLET CENTER

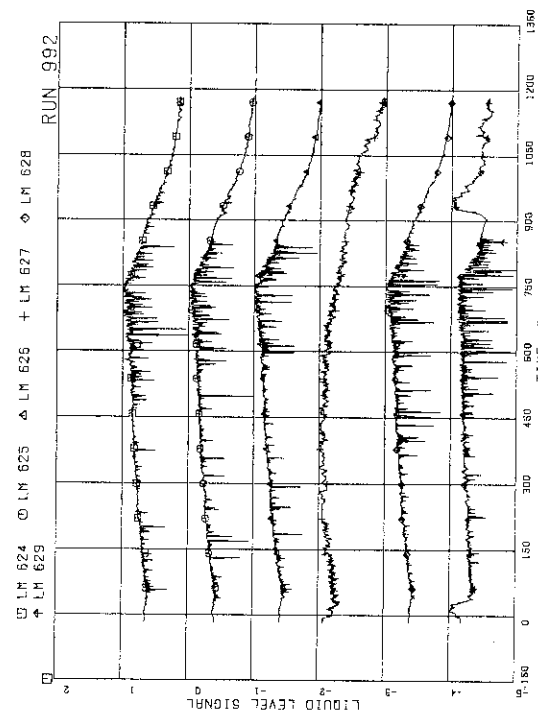

FIG.A.127 LIQUID LEVEL SIGNALS IN CHANNEL A INLET

FIG.A.128 LIQUID LEVEL SIGNALS IN CHANNEL C INLET

FIG.A.129 LIQUID LEVEL SIGNALS IN LOWER PLENUM, NORTH

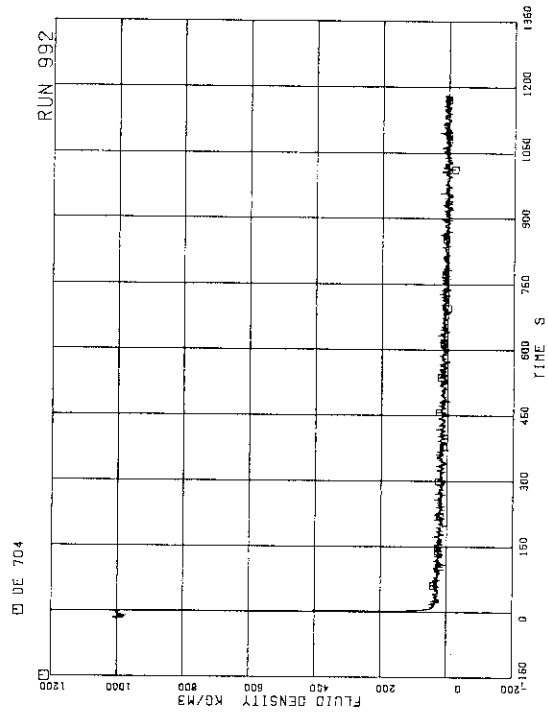

FIG.A.132 AVERAGE DENSITY AT PV SIDE OF BREAK

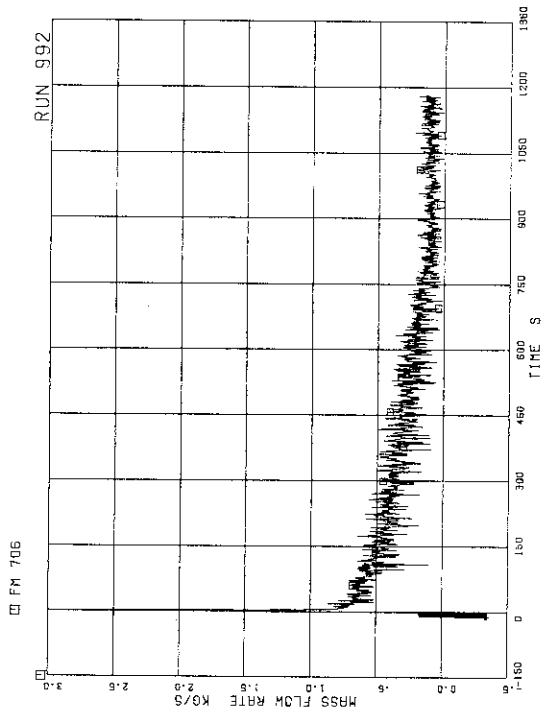

FIG.A.133 FLOW RATE AT PV SIDE OF BREAK (BASED ON LOW RANGE DRAG DISK DATA)

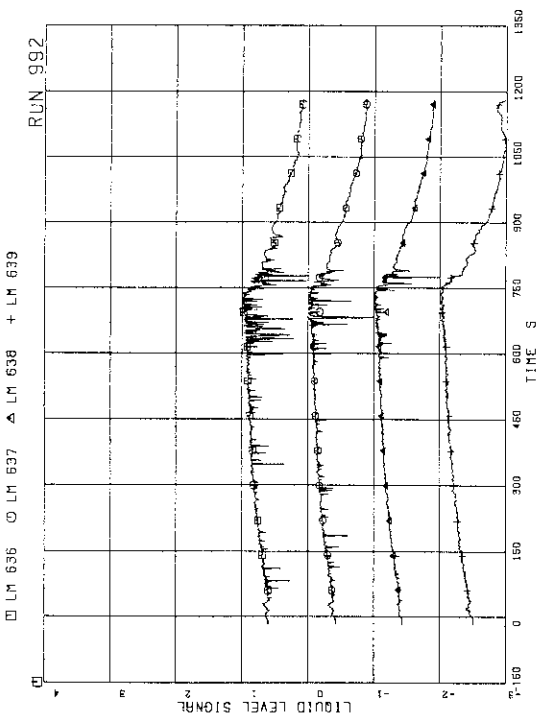

FIG.A.130 LIQUID LEVEL SIGNALS IN GUIDE TUBE, NORTH

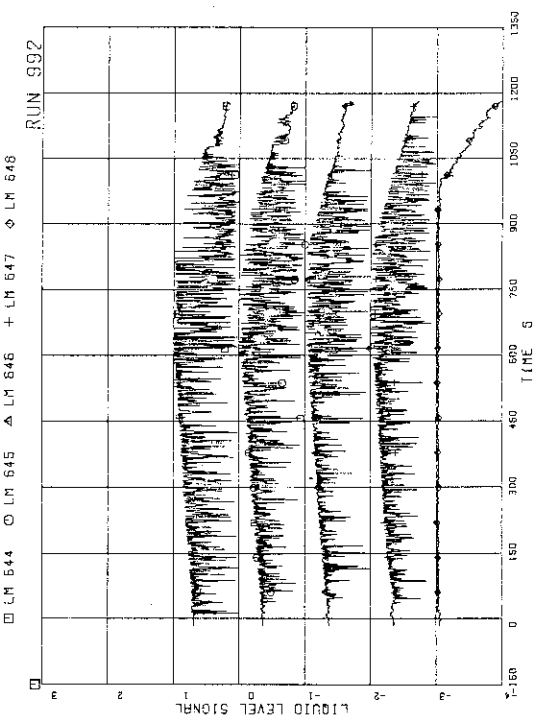

FIG.A.131 LIQUID LEVEL SIGNALS IN DOWNCOMER, D SIDE

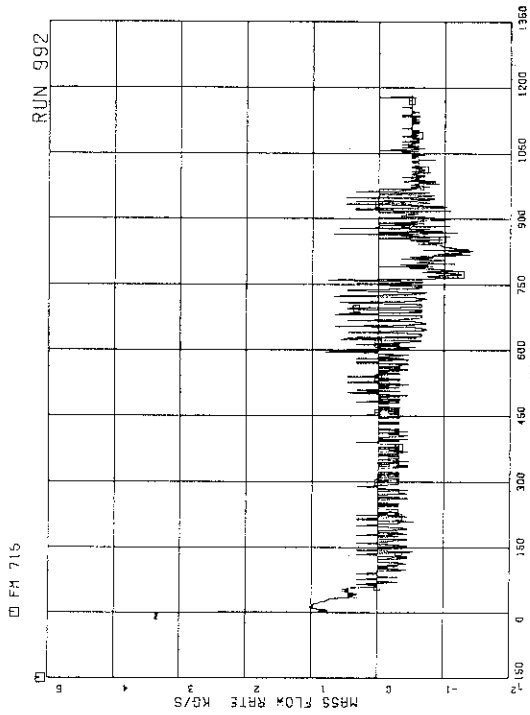

FIG.A.136 FLOW RATE AT CHANNEL B INLET

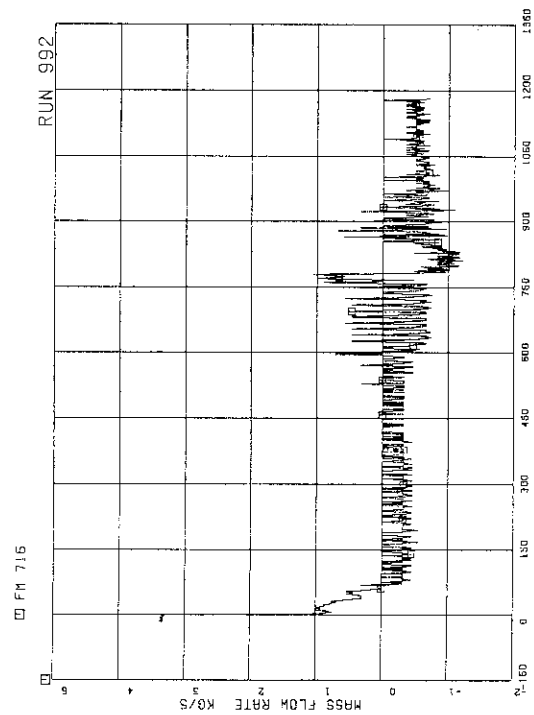

FIG.A.137 FLOW RATE AT CHANNEL C INLET

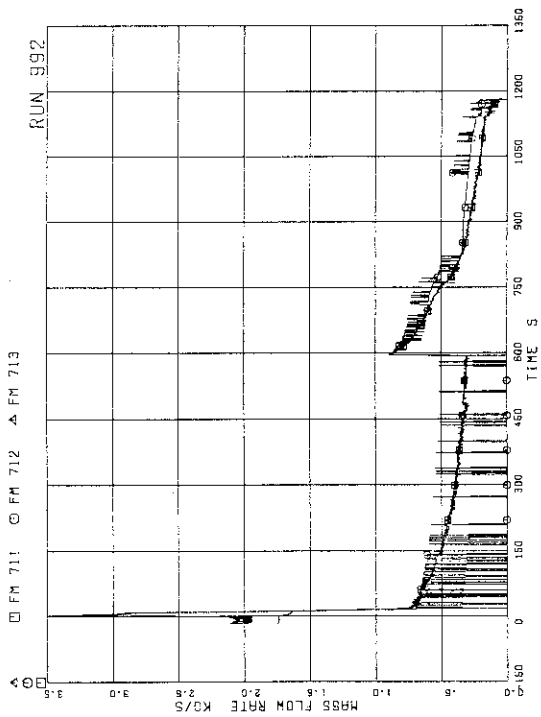

FIG.A.134 STEAM DISCHARGE FLOW RATE THROUGH MSL

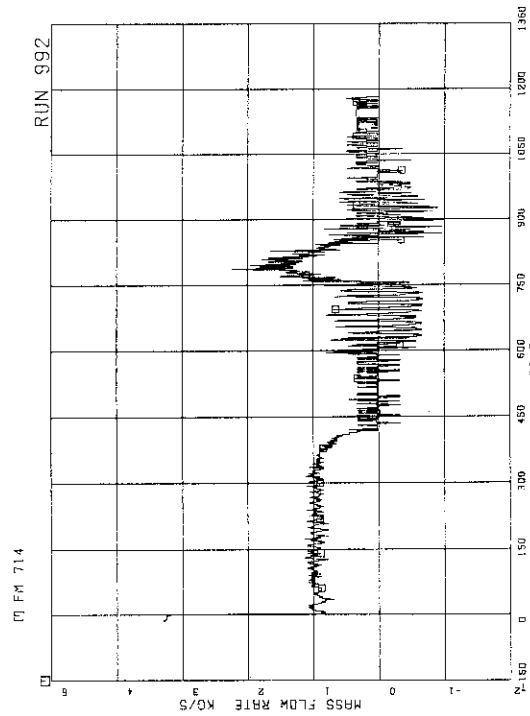

FIG.A.135 FLOW RATE AT CHANNEL A INLET

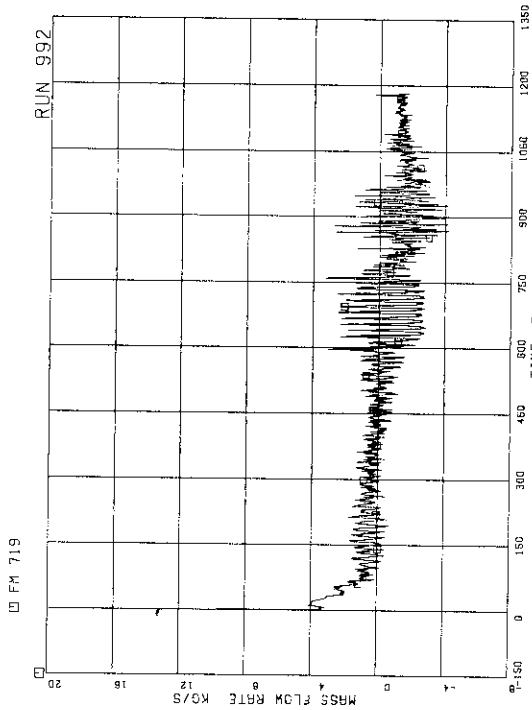

FIG.A.140 TOTAL CHANNEL INLET FLOW RATE

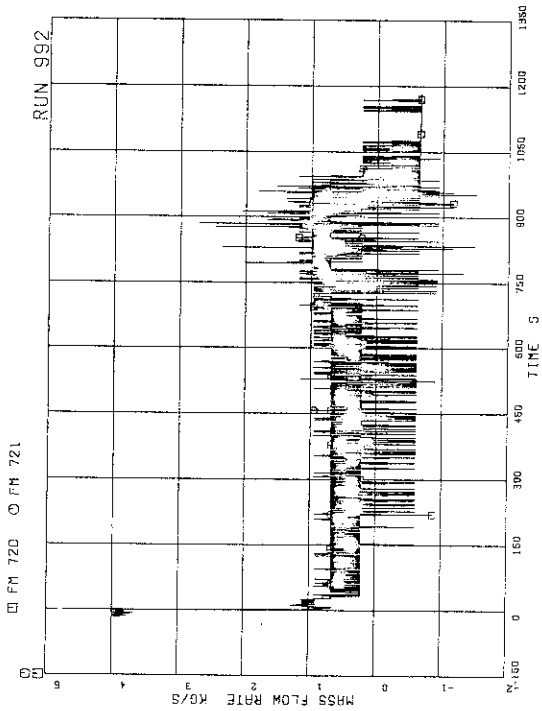

FIG.A.141 FLOW RATE AT JP-1.2 OUTLET

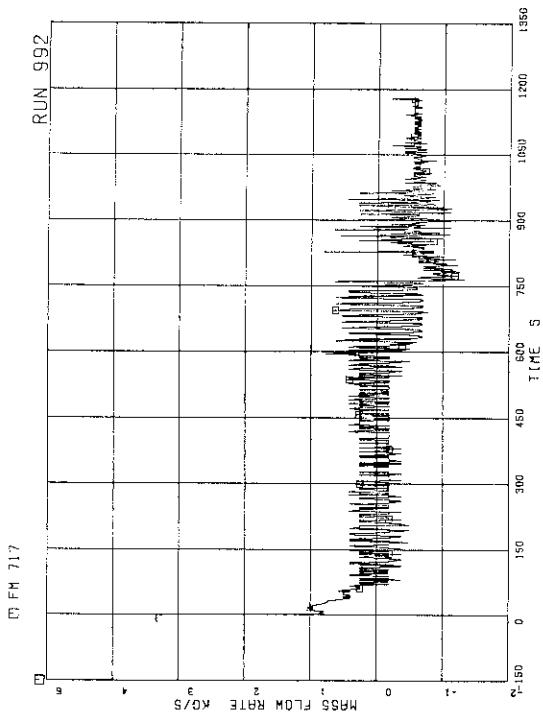

FIG.A.138 FLOW RATE AT CHANNEL 0 INLET

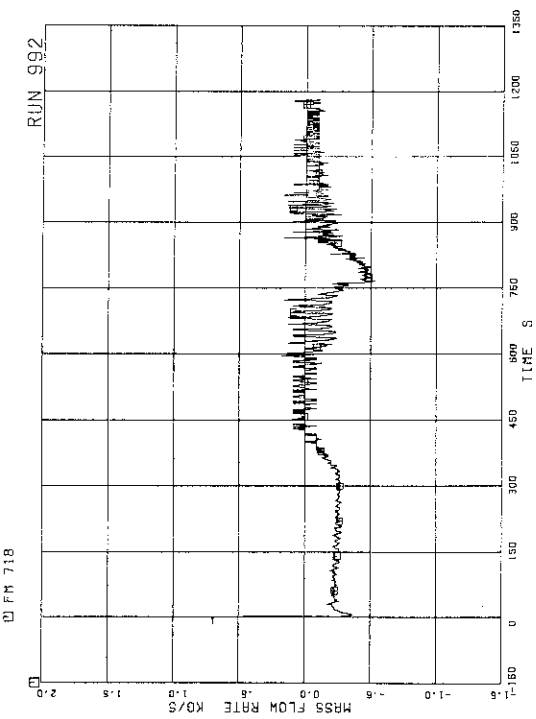

FIG.A.139 FLOW RATE AT BYPASS HOLE

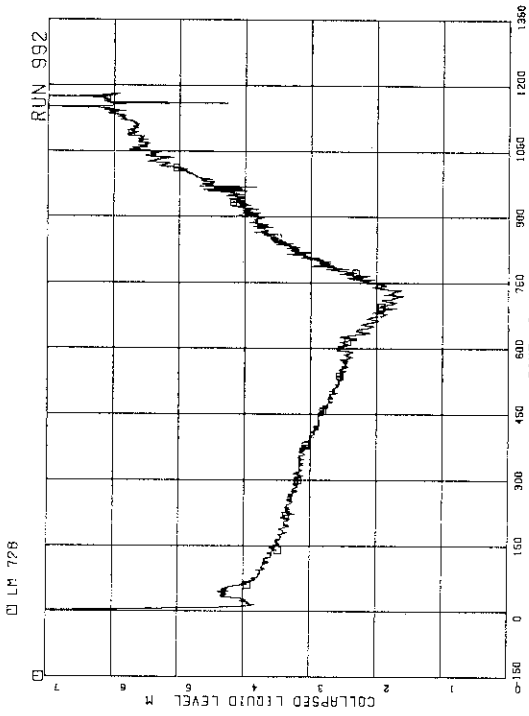

FIG.A.144 COLLAPSED LIQUID LEVEL INSIDE CORE SHROUD

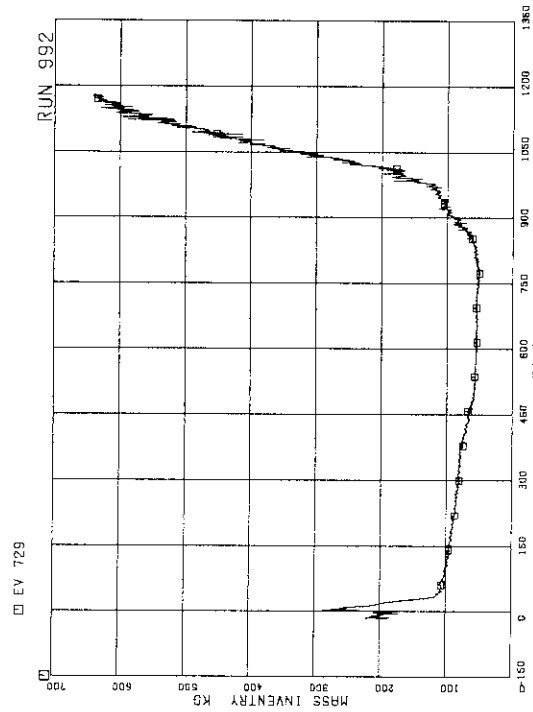

FIG.A.145 FLUID INVENTORY IN DOWNCOMER

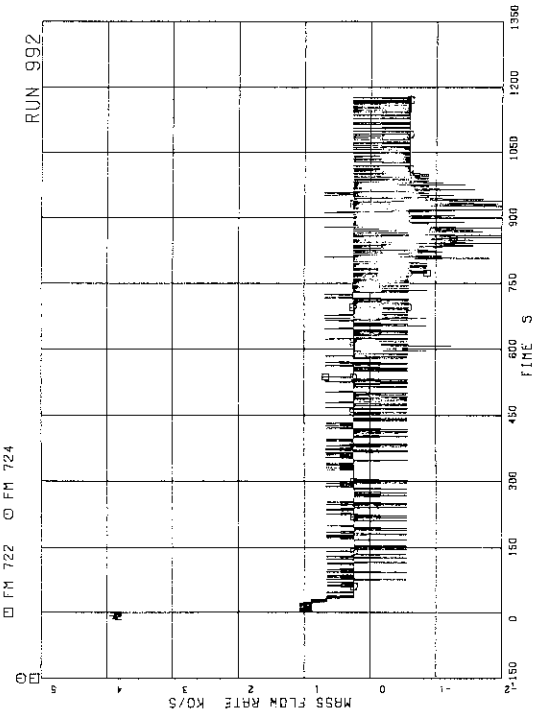

FIG.A.142 FLOW RATE AT JP-3,4 OUTLET

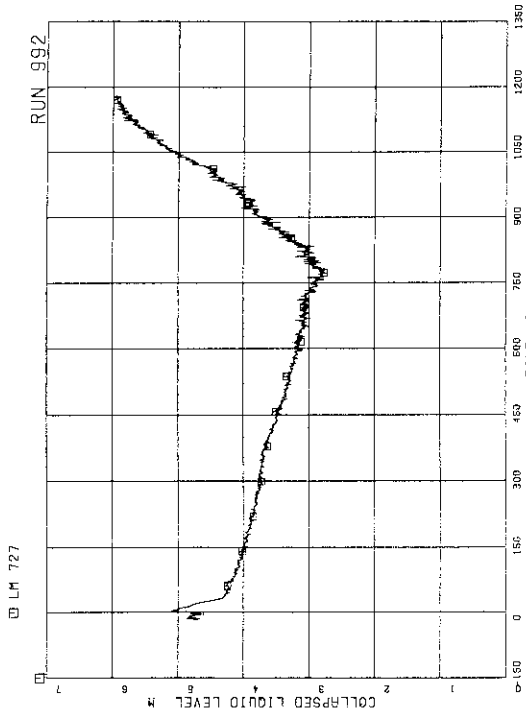

FIG.A.143 COLLAPSED LIQUID LEVEL IN DOWNCOMER

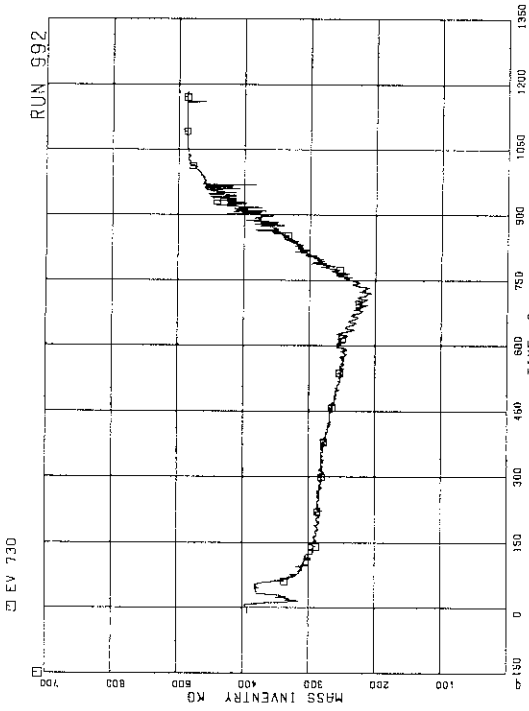

FIG.A.146 FLUID INVENTORY INSIDE CORE SHROUD

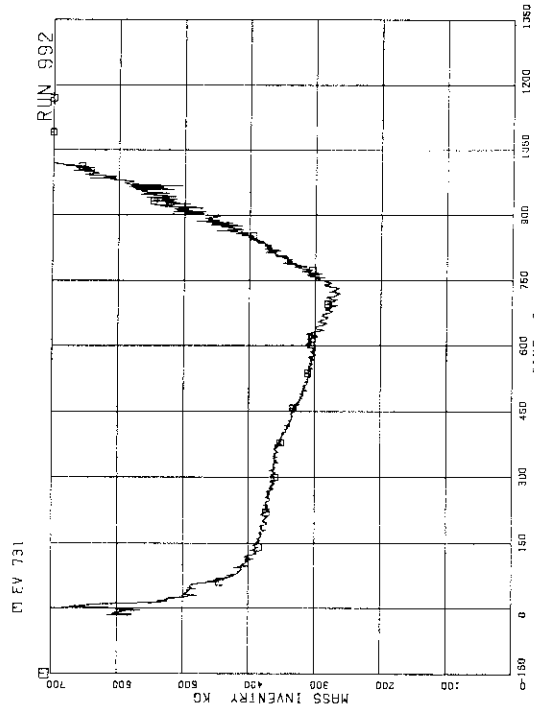

FIG.A.147 TOTAL FLUID INVENTORY IN PRESSURE VESSEL

Appendix III Maximum Cladding Temperature Distribution of RUN 992

Maximum surface temperature at each thermo-couple is searched during a time period after the break and data plotting time, and is recorded with its observation time as shown in Table A.5.

Table A.5 Maximum temperature distribution for RUN 992

Table A.5 Maximum temperature distribution for RUN 992

	Pos.1	Pos.2	Pos.3	Pos.4	Pos.5	Pos.6	Pos.7
A-11 rod	TE 201	TE 202	TE 203	TE 204	TE 205	TE 206	TE 207
PCT (K)	604.3	631.9	648.7	595.9	568.8	567.4	569.5
Time (s)	598.8	750.0	744.0	738.0	0.0	0.0	0.0
A-12 rod	TE 208	TE 209	TE 210	TE 211	TE 212	TE 213	TE 214
PCT (K)	589.9	612.7	630.7	579.1	566.9	566.7	564.8
Time (s)	596.4	745.2	742.8	736.8	0.0	0.0	0.0
A-13 rod	TE 215	TE 216	TE 217	TE 218	TE 219	TE 220	TE 221
PCT (K)	592.3	610.5	628.3	581.5	567.1	568.4	568.6
Time (s)	600.0	744.0	740.4	738.0	0.0	0.0	0.0
A-14 rod	TE 222	TE 223	TE 224	TE 225	TE 226	TE 227	TE 228
PCT (K)	------	------	------	------	------	------	------
Time (s)	------	------	------	------	------	------	------
A-15 rod	TE 229			TE 230			
PCT (K)	------			------			
Time (s)	------			------			
A-17 rod	TE 231			TE 232			
PCT (K)	------			581.5			
Time (s)	------			738.0			
A-22 rod	TE 233	TE 234	TE 235	TE 236	TE 237	TE 238	TE 239
PCT (K)	600.7	619.9	636.7	581.5	570.3	566.7	563.2
Time (s)	595.2	746.4	742.8	738.0	0.0	0.0	0.0
A-24 rod	TE 240	TE 241	TE 242	TE 243	TE 244	TE 245	TE 246
PCT (K)	------	------	------	------	------	------	------
Time (s)	------	------	------	------	------	------	------

	Pos.1	Pos.2	Pos.3	Pos.4	Pos.5	Pos.6	Pos.7
A-26 rod	TE 247			TE 248			
PCT (K)	------			------			
Time (s)	------			------			
A-28 rod	TE 249			TE 250			
PCT (K)	------			582.8			
Time (s)	------			738.0			
A-31 rod	TE 251			TE 252			
PCT (K)	------			595.2			
Time (s)	------			736.8			
A-33 rod	TE 253	TE 254	TE 255	TE 256	TE 257	TE 258	TE 259
PCT (K)	572.4	585.0	597.5	563.5	565.9	568.1	565.4
Time (s)	595.2	744.0	744.0	0.0	0.0	0.0	0.0
A-34 rod	TE 260	TE 261	TE 262	TE 263	TE 264	TE 265	TE 266
PCT (K)	------	------	------	------	------	------	------
Time (s)	------	------	------	------	------	------	------
A-37 rod	TE 267			TE 268			
PCT (K)	------			------			
Time (s)	------			------			
A-42 rod	TE 269			TE 270			
PCT (K)	------			------			
Time (s)	------			------			
A-44 rod	TE 271	TE 272	TE 273	TE 274	TE 275	TE 276	TE 277
PCT (K)	------	------	------	------	------	------	------
Time (s)	------	------	------	------	------	------	------

Table A.5 Maximum temperature distribution for RUN 992 (Cont'd)

	Pos.1	Pos.2	Pos.3	Pos.4	Pos.5	Pos.6	Pos.7
A-48 rod	TE 278			TE 279			
PCT (K)	------			------			
Time (s)	------			------			
A-51 rod	TE 280			TE 281			
PCT (K)	------			------			
Time (s)	------			------			
A-53 rod	TE 282			TE 283			
PCT (K)	------			------			
Time (s)	------			------			
A-57 rod	TE 284			TE 285			
PCT (K)	------			574.9			
Time (s)	------			736.8			
A-62 rod	TE 286			TE 287			
PCT (K)	------			------			
Time (s)	------			------			
A-66 rod	TE 288			TE 289			
PCT (K)	------			------			
Time (s)	------			------			
A-68 rod	TE 290			TE 291			
PCT (K)	------			581.6			
Time (s)	------			738.0			
A-71 rod	TE 292			TE 293			
PCT (K)	------			598.0			
Time (s)	------			738.0			

	Pos.1	Pos.2	Pos.3	Pos.4	Pos.5	Pos.6	Pos.7
A-73 rod	TE 294			TE 295			
PCT (K)	------			582.6			
Time (s)	------			736.8			
A-75 rod	TE 296			TE 297			
PCT (K)	------			------			
Time (s)	------			------			
A-77 rod	TE 298	TE 299	TE 300	TE 301	TE 302	TE 303	TE 304
PCT (K)	589.3	606.6	620.9	567.2	566.5	566.0	------
Time (s)	592.8	746.4	742.8	736.8	0.0	0.0	------
A-82 rod	TE 305			TE 306			
PCT (K)	------			------			
Time (s)	------			------			
A-84 rod	TE 307			TE 308			
PCT (K)	598.0			590.3			
Time (s)	738.0			736.8			
A-85 rod	TE 309	TE 310	TE 311	TE 312	TE 313	TE 314	TE 315
PCT (K)	------	------	------	------	------	------	------
Time (s)	------	------	------	------	------	------	------
A-87 rod	TE 316	TE 317	TE 318	TE 319	TE 320	TE 321	TE 322
PCT (K)	592.2	610.4	632.4	584.5	569.1	567.8	566.8
Time (s)	594.0	745.2	740.4	738.0	0.0	0.0	0.0
A-88 rod	TE 323	TE 324	TE 325	TE 326	TE 327	TE 328	TE 329
PCT (K)	592.2	611.4	634.3	588.4	569.0	567.2	567.3
Time (s)	594.0	744.0	744.0	736.8	0.0	0.0	0.0

Table A.5 Maximum temperature distribution for RUN 992 (Cont'd)

	Pos.1	Pos.2	Pos.3	Pos.4	Pos.5	Pos.6	Pos.7
B-11 rod	TE 330	TE 331	TE 332	TE 333	TE 334	TE 335	TE 336
PCT (K)	593.2	596.1	606.6	566.3	567.2	567.2	------
Time (s)	735.6	595.2	745.2	0.0	0.0	0.0	------
B-13 rod				TE 337			
PCT (K)				567.4			
Time (s)				0.0			
B-22 rod	TE 338	TE 339	TE 340	TE 341	TE 342	TE 343	TE 344
PCT (K)	586.4	588.4	598.0	568.3	568.4	567.1	570.7
Time (s)	729.6	594.0	746.4	0.0	0.0	0.0	0.0
B-31 rod				TE 345			
PCT (K)				------			
Time (s)				------			
B-33 rod				TE 346			
PCT (K)				------			
Time (s)				------			
B-51 rod				TE 347			
PCT (K)				------			
Time (s)				------			
B-53 rod				TE 348			
PCT (K)				------			
Time (s)				------			
B-66 rod				TE 349			
PCT (K)				------			
Time (s)				------			

	Pos.1	Pos.2	Pos.3	Pos.4	Pos.5	Pos.6	Pos.7
B-77 rod	TE 350	TE 351	TE 352	TE 353	TE 354	TE 355	TE 356
PCT (K)	591.3	598.9	603.7	567.2	567.6	567.9	566.2
Time (s)	732.0	595.2	745.2	0.0	0.0	0.0	0.0
B-86 rod				TE 357			
PCT (K)				------			
Time (s)				------			
C-11 rod	TE 358	TE 359	TE 360	TE 361	TE 362	TE 363	TE 364
PCT (K)	572.5	588.4	601.8	565.8	563.2	569.0	561.5
Time (s)	0.0	745.2	741.6	0.0	0.0	0.0	0.0
C-13 rod	TE 365	TE 366	TE 367	TE 368	TE 369	TE 370	TE 371
PCT (K)	562.3	581.6	598.0	567.4	568.1	568.1	565.3
Time (s)	0.0	747.6	742.8	0.0	0.0	0.0	0.0
C-15 rod				TE 372			
PCT (K)				------			
Time (s)				------			
C-22 rod	TE 373	TE 374	TE 375	TE 376	TE 377	TE 378	TE 379
PCT (K)	566.2	584.5	593.2	567.2	568.4	568.4	563.3
Time (s)	738.0	746.4	742.8	0.0	0.0	0.0	0.0
C-31 rod				TE 380			
PCT (K)				------			
Time (s)				------			
C-33 rod	TE 381	TE 382	TE 383	TE 384	TE 385	TE 386	TE 387
PCT (K)	563.7	566.8	569.1	566.5	566.2	564.5	561.2
Time (s)	0.0	0.0	742.8	0.0	0.0	0.0	0.0

Table A.5 Maximum temperature distribution for RUN 992 (Cont'd)

	Pos.1	Pos.2	Pos.3	Pos.4	Pos.5	Pos.6	Pos.7
C-35 rod				TE 388			
PCT (K)				------			
Time (s)				------			
C-66 rod				TE 389			
PCT (K)				------			
Time (s)				------			
C-68 rod				TE 390			
PCT (K)				------			
Time (s)				------			
C-77 rod	TE 391	TE 392	TE 393	TE 394	TE 395	TE 396	TE 397
PCT (K)	581.6	592.2	597.0	567.2	567.5	565.4	563.8
Time (s)	735.6	592.8	745.2	0.0	0.0	0.0	0.0
D-11 rod				TE 398			
PCT (K)				568.1			
Time (s)				736.8			
D-13 rod				TE 399			
PCT (K)				568.9			
Time (s)				0.0			
D-22 rod	TE 400	TE 401	TE 402	TE 403	TE 404	TE 405	TE 406
PCT (K)	572.0	588.4	598.0	568.9	567.7	568.1	564.3
Time (s)	745.2	745.2	747.6	0.0	0.0	0.0	0.0
D-31 rod				TE 407			
PCT (K)				------			
Time (s)				------			

	Pos.1	Pos.2	Pos.3	Pos.4	Pos.5	Pos.6	Pos.7
D-33 rod				TE 408			
PCT (K)				------			
Time (s)				------			
D-51 rod				TE 409			
PCT (K)				------			
Time (s)				------			
D-53 rod				TE 410			
PCT (K)				------			
Time (s)				------			
D-66 rod				TE 411			
PCT (K)				------			
Time (s)				------			
D-77 rod				TE 412			
PCT (K)				------			
Time (s)				------			
D-86 rod				TE 413			
PCT (K)				567.8			
Time (s)				0.0			